Functional characterization of the FLCN-AMPK-TFE3 Signaling Pathway

Leeanna El-Houjeiri

Department of Biochemistry Goodman Cancer Research Center McGill University Montreal, Québec, Canada

December 2021

A thesis submitted to McGill University in partial fulfillment of the requirements of the degree of Doctor of Philosophy

TABLE OF CONTENTS

TABLE OF CONTENTS	II
ABSTRACT	<i>V</i>
RÉSUMÉ	VII
ACKNOWLEDGEMENTS	IX
PUBLICATIONS	XI
CONTRIBUTION OF AUTHORS	<i>XIII</i>
ORIGINAL CONTRIBUTION TO KNOWLEDGE	XIV
LIST OF ABBREVIATIONS	XV
LIST OF FIGURES	XXII
CHAPTER 1 – Literature Review	1
1.1. Birt-Hogg-Dubé Syndrome	2
1.2 FLCN and its interacting proteins FNIP1 and FNIP2	
1.2.1. Human folliculin (FLCN) gene and protein	3
1.2.2. FLCN/FNIP complex	
1.2.3. FLCN/FNIP structure	
1.3. The mammalian target of Rapamycin (mTOR) and FLCN/FNIP complex	
1.3.1. The mammalian target of Rapamycin (mTOR)	6
1.4. The AMP-activated protein kinase (AMPK) and FLCN/FNIP complex:	9 0
1.4.2. AMPK and FLCN/FNIP complex	
1.5. Other FLCN functions	
1.6. Microphthalmia Family of bHLH-zip Transcription Factors (MiT Family)	
1.6.1. MiT Family: genes and domains	
1.6.2. MiT Family: expression and interactions	
1.6.3. MiT Family members: isoforms	13
1.7. Role of MiT/TFE family in lysosomes and autophagy	14
1.7.1. Role of MiT/TFE family in lysosomal biogenesis	
1.7.2. Role of MiT/TFE family in Autophagy	
1.8. Autophagy, lysosomes, and Immune response	16
1.9. TFEB and TFE3 link cellular stress to the immune response	16
1.10. TFEB and TFE3 as metabolic regulators	18
1.11. Physiological roles of TFEB and TFE3	19
1.12 Regulation of TFEB and TFE3	20
1.12.1 Regulation of TFEB and TFE3 by mTOR	

	21
1.12.3 Regulation of TFEB and TFE3 by AMPK	
1.12.4 Regulation of TFEB and TFE3 by phosphatases	
1.13. Cancer	
1.14. TFEB and TFE3 in cancer	24
1.15. Autophagy and Cancer	26
1.16. Breast cancer	
1.16.1. Breast cancer: Statistics and subtypes	
1.16.2. Triple negative breast cancer	
1.17. Angiogenesis and Metastasis	
1.17.1. Angiogenesis enables Metastasis	
1.18. Hypoxia and HIF-1 pathways	32
1.18.1. Hypoxia	32
1.18.2. Hypoxia Inducible Factor (HIF)	
1.19. TFEB, TFE3 and angiogenesis	
1.20. FLCN/TFE/AMPK and angiogenic pathways	
1.21. Research rationale and objectives	
1.22. References associated with Chapter 1	37
CHAPTER 2 – The transcription factors TFEB and TFE3 link the FLCN-AMPK signal axis to innate immune response and pathogen resistance	_
2.1. ABSTRACT	
2.1. ABSTRACT 2.2. INTRODUCTION	54
	54 54
2.2. INTRODUCTION	54 54 58
2.2. INTRODUCTION	54 54 58
2.2. INTRODUCTION 2.3. RESULTS 2.4. DISCUSSION 2.5. STAR METHODS	54 54 58 66
2.2. INTRODUCTION	54 58 66 71
2.2. INTRODUCTION	54 58 66 71 73
2.2. INTRODUCTION	54 58 66 71 73 82
2.2. INTRODUCTION	54 58 66 71 73 82 82
2.2. INTRODUCTION	54 58 66 71 82 82 83
2.2. INTRODUCTION	54 58 66 71 82 82 83 95
2.2. INTRODUCTION	54 58 66 71 82 82 83 95 100

3.2. INTRODUCTION	108
3.3. RESULTS	110
3.4. DISCUSSION	122
3.5. METHODS	125
3.7. AUTHORS' CONTRIBUTIONS	136
3.8. FIGURES AND FIGURE LEGENDS	137
3.9. SUPPLEMENTARY FIGURES AND TABLES WITH LEGENDS	153
4.0. REFERENCES ASSOCIATED WITH CHAPTER 3	163
CHAPTER 4 – Identification and functional characterization of the two TFE3 isoform	ns 167
4.1. ABSTRACT	169
4.2. INTRODUCTION	170
4.3. RESULTS	173
4.4. DISCUSSION	184
4.5. METHODS	186
4.7. AUTHORS' CONTRIBUTIONS	191
4.8. FIGURES AND FIGURE LEGENDS	192
4.9. SUPPLEMENTAL FIGURES AND LEGENDS	206
4.10. REFERENCES ASSOCIATED WITH CHAPTER 4	208
CHAPTER 5 – General Discussion	212
5.1. Potential roles for FLCN in regulating important metabolic and cellular pro	
5.1.1. TFEB and TFE3 link the FLCN-AMPK signaling axis to innate immune resp	
5.1.1. TEB and TES link the FLCN-AMPK signating axis to inhate infinding resp	
5.1.1.2 BHD disease and inflammation	
5.1.2 Role of the FLCN-TFE3-AMPK signaling pathway in Breast Cancer tumor g	
5.1.2.1. Autophagy, angiogenesis and cancer: is TFE3 the link?	216 ory
phenotype	217 218
5.2. Controversial role of FLCN/FNIP complex on mTORC1-explained	
5.3. Lysosomal and autophagy disfunction as a recurrent feature in cancer	
5.4. Therapeutic Implications	
5.5. Concluding remarks	
5.6. References associated with Chapter 5	
S.V. INICIONEUS ASSUCIANU WITH CHAPTEL S	443

ABSTRACT

The FLCN tumor suppressor complex (FLCN, FNIP1, FNIP2) has been implicated in the regulation of energy homeostasis *via* two metabolic master kinases: AMPK and mTORC1. These kinases have been linked transcriptionally to autophagy and lysosomal biogenesis through the the transcription factors TFEB and TFE3. These transcription factors regulate a panel of genes involved in autophagy, lipid metabolism and innate immune response response pathways, but the mechanisms regulating their activation upon pathogen infection are poorly elucidated. Herein, we report, using *C. elegans* and mammalian models, that AMPK and its negative regulator FLCN act upstream of TFEB/TFE3 in the innate immune response, independently of the mTORC1 signaling pathway. We show that loss of FLCN or pharmacological activation of AMPK induces TFEB/TFE3-dependent pro-inflammatory cytokine expression and confers resistance to pathogen infection. These results uncover an ancient, highly conserved, and pharmacologically actionable mechanism coupling energy status with innate immunity.

Given that loss-of-function mutations of the FLCN-FNIP complex have only been reported in renal tumors in patients with the rare Birt-Hogg-Dube syndrome, we wanted to investigate the involvement of the FLCN/AMPK/TFE3 pathway in cancer. We reveal that FLCN, FNIP1, and FNIP2 are downregulated in many human cancers including poor prognosis invasive basal-like breast carcinomas where AMPK and TFE3 targets are activated compared to the luminal, less aggressive subtypes. We demonstrate that FLCN loss in luminal subtypes promotes tumor growth through TFE3 activation and subsequent induction of several pathways including aerobic glycolysis, and angiogenesis which we reveal to be dictated by the activation of PGC- 1α /HIF- 1α pathway. Thus, FLCN loss induces TFE3-dependent breast tumor growth through activation of

multiple mechanisms which could point to a general role of a deregulated FLCN/TFE3 tumor suppressor pathway in human cancers.

Interestingly, to date, two isoforms of human TFE3 protein have been identified: the full length TFE3 (TFE3-L) and the alternatively spliced, N-terminal truncated, variant (missing exon 1 and 2, TFE3-S). However, the function of each isoform is not described to date. Here, we provide evidence that both TFE3 isoforms have different stabilities and gene activation potentials, and we explore the mechanisms controlling TFE3-L stability in cancer cells which can provide a new insight for their aberrant expression in human cancers.

Collectively, we have identified novel roles of the FLCN-TFE-AMPK pathway in immune response and tumor growth through activation of several pathways that provide a survival advantage to the cells. Additionally, we characterized two different TFE3 isoforms which adds another layer of tight regulation of these transcription factors through proteasomal degradation. Better understanding of the FLCN-TFE-AMPK can lead to the discovery of new modalities of targeted therapies in diseases where this pathway is disrupted to ultimately open horizons toward more promising drug targets.

RÉSUMÉ

Le complexe suppresseur de tumeur FLCN (FLCN, FNIP1, FNIP2) a été impliqué dans la régulation de l'homéostasie énergétique via deux maîtres kinases métaboliques : AMPK et mTORC1. Ces kinases ont été liées transcriptionnellement à l'autophagie et à la biogenèse lysosomale par le biais des facteurs de transcription TFEB et TFE3. Ces facteurs de transcription régulent un panel de gènes impliqués dans l'autophagie, le métabolisme lipidique et les voies de réponse immunitaire innée, mais les mécanismes régulant leur activation lors d'une infection pathogène sont mal élucidés. Nous rapportons ici, en utilisant C. elegans et des modèles de mammifères, que l'AMPK et son régulateur négatif FLCN agissent en amont de TFEB/TFE3 dans la réponse immunitaire innée, indépendamment de la voie de signalisation mTORC1. Nous montrons que la perte de FLCN ou l'activation pharmacologique de l'AMPK induit l'expression de cytokines pro-inflammatoires dépendantes de TFEB/TFE3 et confère une résistance à l'infection pathogène. Ces résultats révèlent un mécanisme ancien, hautement conservé et pharmacologiquement actionnable, couplant le statut énergétique à l'immunité innée.

Étant donné que des mutations de perte de fonction du complexe FLCN-FNIP n'ont été rapportées que dans des tumeurs rénales chez des patients atteints du rare syndrome de Birt-Hogg-Dube, nous avons voulu étudier l'implication de la voie FLCN/AMPK/TFE3 dans le cancer. Nous révélons que FLCN, FNIP1 et FNIP2 sont régulés à la baisse dans de nombreux cancers humains, y compris les carcinomes mammaires invasifs de type basal de mauvais pronostic où les cibles AMPK et TFE3 sont activées par rapport aux sous-types luminaux moins agressifs. Nous démontrons que la perte de FLCN dans les sous-types luminaux favorise la croissance tumorale par l'activation de TFE3 et l'induction subséquente de plusieurs voies, y compris la glycolyse aérobie et l'angiogenèse qui, selon nous, sont dictées par l'activation de la voie PGC-1α/HIF-1α.

Ainsi, la perte de FLCN induit une croissance tumorale mammaire dépendante de TFE3 par l'activation de plusieurs mécanismes qui pourraient indiquer un rôle général d'une voie de suppression de tumeur FLCN/TFE3 dérégulée dans les cancers humains.

Il est intéressant de noter qu'à ce jour, deux isoformes de la protéine TFE3 humaine ont été identifiées : la TFE3 pleine longueur (TFE3-L) et la variante alternativement épissée, N-terminale tronquée (exons manquants 1 et 2, TFE3-S). Cependant, la fonction de chaque isoforme n'est pas décrite à ce jour. Ici, nous fournissons la preuve que les deux isoformes de TFE3 ont des stabilités et des potentiels d'activation génique différents, et nous explorons les mécanismes contrôlant la stabilité de TFE3-L dans les cellules cancéreuses, ce qui peut fournir un nouvel aperçu de leur expression aberrante dans les cancers humains.

Collectivement, nous avons identifié de nouveaux rôles de la voie FLCN-TFE-AMPK dans la réponse immunitaire et la croissance tumorale grâce à l'activation de plusieurs voies qui offrent un avantage de survie aux cellules. De plus, nous avons caractérisé deux isoformes différentes de TFE3 qui ajoutent une autre couche de régulation stricte de ces facteurs de transcription par dégradation protéasomale. Une meilleure compréhension du FLCN-TFE-AMPK peut conduire à la découverte de nouvelles modalités de thérapies ciblées dans des maladies où cette voie est perturbée pour finalement ouvrir des horizons vers des cibles médicamenteuses plus prometteuses.

ACKNOWLEDGEMENTS

My entire Ph.D project was a collaborative effort, with numerous people involved from the start to the finish and I am honored to have had the opportunity to work with and learn from all of them.

First and foremost, I would like to express my heartfelt gratitude and appreciation to my supervisors Dr. Arnim Pause and Dr. Peter Siegel for their continuous support throughout my Ph.D years. Thank you for your patience, motivation, enthusiasm, and immense complimentary knowledge in the field. You have truly shaped the scientist who I am today, and for that I will forever be grateful.

I would like to express the deepest appreciation to my research committee members Dr. Sidong Huang and Dr. Jean-Francois Côté for their time, guidance, and constructive feedback throughout the years.

I couldn't have done this without the invaluable support from my colleagues at Pause and Siegel Labs. Marco, you are a great example of what a collaborative work should be like. I am grateful for all our fruitful discussions and teamwork. Your work was so critical to the success of the breast cancer project, and I couldn't have done it without you. Mathieu, you were always there to help out and to listen to my trials and tribulations; it was truly a pleasure to with you. I am very grateful for our cooperative effort that resulted in many great papers! I look forward to more of your friendship and colleagueship in the world of science in the years to come!

I would like to further extend my gratitude to all the present and former members of both labs specifically Dr. Paola Blanchette, Dr. Rafael Cuesta Sanchez, Jalal Kazan, Josué Ramírez-Reyes, and Hyeonju Jeong. I can't thank you enough for all your support, advice, and good times. Dr. Matthew Annis and Dr. Sebastien Tabaries, I deeply appreciate all your advice and help with the animal work.

I would like to acknowledge the funding agencies that provided stipend support throughout my Ph.D., including Dr. Victor K.S. Lui and Dr. Michael D'Avirro and Canderel fellowships in Oncology from Goodman Institute Research Centre and FRQS doctoral fellowship.

I also acknowledge the funding agencies that supported Dr. Arnim Pause and Dr. Peter Siegel labs including Terry Fox New Frontiers Program Project and the CIHR. I would like to acknowledge McGill University Life Sciences Complex Advanced BioImaging Facility (ABIF) though which the microscopy image processing and analysis for this thesis were performed. I would also like to thank the McGill Core Flow Cytometry Facility (McGill University) for their technical support and expertise. Further appreciation goes to the Canadian Centre for Computational Genomics and the Histology Core Facility (McGill University) for their services. I further acknowledge the Goodman Cancer Research Institute Metabolomics Core Facility (McGill University), which is supported by the Canada Foundation for Innovation, the Terry Fox Research Institute, and the Quebec Breast Cancer Foundation. Further appreciation goes to Helen from the Park lab for her help in patient derived xenograft data analysis. Patient derived xenograft banking was performed by the BCFGG breast tissue and data bank at the Goodman Cancer Research Institute-RI- MUHC

in collaboration with the Réseau de Recherche sur le cancer (Fonds de la Recherche du Québec-Santé), which is affiliated with the Canadian Tumor Repository Network (CTRNet).

I would like to extend my sincere thanks to my friends Rola and Martin for their endless support and encouragement throughout the years.

My deep and sincere gratitude to my family for their continuous and unparalleled love, help and support (Loubna, Lama, and Mohammad). I am forever indebted to my parents (Ali and Lina) for giving me the opportunities and experiences that have made me who I am today.

Finally, I'd like to extend my gratitude to my Nadim for his unconditional love and constant support throughout this journey. Thank you for believing in me.

PUBLICATIONS

This thesis is written in manuscript format and resulted in one published review paper, one published article, one manuscript under revision, one paper under preparation, and four papers/manuscripts in collaboration.

Sections of Chapter 1 are published in the following review article:

El-Houjeiri, L., Paquette, M. & Pause, A. (2018). mTOR pathways in cancer and autophagy. *Cancers*, 10(1), 18.

Chapter 2 is published as the following peer-reviewed original research article:

El-Houjeiri, L., Possik, E., Vijayaraghavan, T., Paquette, M., Martina, J.A., Kazan, J.M., Ma, E.H., Jones, R., Blanchette, P., Puertollano, R. and Pause, A., 2019. The transcription factors TFEB and TFE3 link the FLCN-AMPK signaling axis to innate immune response and pathogen resistance. *Cell reports*, 26(13), pp.3613-3628.

Chapter 3 is published as the following peer-reviewed original research article:

El-Houjeiri, L., Biondini, M., Paquette, M., Kuasne, H., Pacis, A., Park, M., Siegel, P.M. and Pause, A., 2021. Folliculin impairs breast tumor growth by repressing TFE3-dependent induction of the Warburg effect and angiogenesis. *Journal of Clinical Investigation*, *131*(22), p.e144871.

Chapter 4 is a manuscript in preparation:

El-Houjeiri, L., Cuesta R., Jeong, H., Biondini, M., Paquette M., Siegel, PM., and Pause, A. The Regulation and Functional Characterization of the Two TFE3 Isoforms. 2021. *Manuscript in preparation*

Additional collaborations that transpired from work performed during my Ph.D. studies but not included in this thesis:

Paquette, M., Yan, M., Ramírez-Reyes, J.M., <u>El-Houjeiri, L.</u>, Biondini, M., Dufour, C.R., Jeong, H., Pacis, A., Giguère, V., Estall, J.L. and Siegel, P.M., 2021. Loss of hepatic Flcn protects against fibrosis and inflammation by activating autophagy pathways. *Scientific reports*, 11(1), pp.1-13.

Paquette, M., <u>El-Houjeiri, L.</u>, C. Zirden, L., Puustinen, P., Blanchette, P., Jeong, H., ... & Pause, A. (2021). AMPK-dependent phosphorylation is required for transcriptional activation of TFEB and TFE3. Autophagy, 1-19.

Paquette, M., **El-Houjeiri**, L., Blanchette, P., Ramírez-Reyes, J. M. J., Zirden, L. C., Jeong, H., Siegel, P. M., & Pause, A. AMPK-mediated FLCN phosphorylation inhibits its GAP activity, representing a novel mTORC1 inhibitory pathway. 2021. *Manuscript in preparation*.

Biondini M.^{1,2}, Kiepas A.^{1,2}, <u>El-Houjeiri L</u>.^{1,2}, ... and Siegel P.M. HSP90 inhibitors induce GPNMB cell surface expression by modulating lysosomal positioning and sensitize breast cancer cells to Glembatumumab Vedotin. 2021. *Accepted. Oncogene*.

CONTRIBUTION OF AUTHORS

Chapter 1

L.E.-H, M.P. and A.P. designed and drafted the review.

Chapter 2

L.E.-H., E.P., and A.P. conceived and designed the experiments. L.E.-H., E.P., T.V., M.P., J.K., J.M, R.P., P.B., R.J., and E.M., performed the experiments. Specifically, the *C.elegans* experiments were performed by E.P. and T.V (Figure 1, Figure 2, and Figure 5 and supplemental documents). I performed almost all experiments involving mammalian cells -except for Figure 3A, D, and G which were performed by M.P., and Figure 6A was performed by J.M from P. B.'s lab. Figure 4I was done in collaboration with J.K. L.E.-H., E.P., and A.P. wrote and revised the manuscript.

Chapter 3

I was part of conceiving and designed the experiments. In addition, I performed, collected, and assembled most of the experiments. Specifically, all immunohistochemistry experiments and quantifications were performed by M.B. M.B and I performed, collected data, and analyzed the results from the *in vivo* mice experiments. Al.P. performed the bioinformatics analysis of the RNA-sequencing data. H.K. from Mo.P. lab analyzed the patient derived xenograft data which resulted in Figure 1B, Figure S1B, C, D, and F. L.E.-H., M.B, P.M.S., and Ar.P., wrote and revised the manuscript critically for important intellectual content.

Chapter 4

L.E.-H., R.C., P.M.S., and A.P. conceived and designed the experiments. L.E.-H., R.C., H.J., M.P, performed, collected, and assembled the experiments. Specifically, R.C. performed experiments corresponding to Figure 1B, C, and F, Figure 2D, and F. All immunoprecipitation experiments were performed by R.C. and H.J. Figure 3, 4, 5, 6, and 7 was a collaborative work between R.C. and L.E.-H. L.E.-H., R.C., P.M.S., and A.P., wrote the manuscript.

ORIGINAL CONTRIBUTION TO KNOWLEDGE

- 1. In this work we identified a novel role for FLCN in the innate immune response and pathogen infection through modulation of AMPK and TFEB/TFE3 activity.
- 2. We placed AMPK upstream of TFEB and TFE3 in the immune response and showed that it is essential for their optimal activity.
- 3. We are the first to link "energy levels" to inflammation through acute AMPK response.
- 4. We are the first to assess FLCN levels across different types to cancers and proposed that downregulation -and not deletion- of tumor suppressors in cancer models can be sufficient to activate oncogenic pathways.
- 5. We reveal for the first time that FLCN, FNIP1, and FNIP2 are downregulated in the poor prognosis invasive basal-like breast carcinomas where AMPK and TFE3 targets are activated compared to the luminal, less aggressive subtypes.
- 6. We introduced a novel role of FLCN-AMPK-TFE3 pathway in breast tumor growth
- 7. We demonstrate that TFE3 has important roles in the induction of PGC-1α/HIF-1α, directly linking TFE3 to Warburg metabolic reprogramming and angiogenesis
- 8. We are the first to characterize the two TFE3 isoforms
- 9. We are the first to prove that TFE3 activity is not only controlled by nuclear localization, but also by proteasomal degradation, where we identified Skp2 as a potential E3 ligase.
- 10. We are the first to show that the levels of TFE3 isoforms are controlled post-translationally by many cellular environmental factors.

LIST OF ABBREVIATIONS

AA Amino acids

ACC1/2 Acetyl-CoA carboxylase 1 or 2

ADP Adenosine diphosphate

AICAR 5-Aminoimidazole-4-carboxamide ribonucleotide

AML Acute myeloid leukemia

AMP Adenosine monophosphate

AMPK AMP-activated protein kinase

ASAH1 N-Acylsphingosine Amidohydrolase 1

ASPS Alveolar soft part sarcoma

ASPSCR1 Alveolar soft part sarcoma critical region 1

ATCC American Type Culture Collection

ATG Autophagy related

ATM Ataxia-telangiectasia-mutated

ATP Adenosine triphosphate

ATP6 ATPase H+ Transporting Subunit

B2M Beta-2-Microglobulin

BC Breast cancer

bFGF Basic fibroblast growth factor

BHD Birt-Hogg-Dubé

BHLH Basic helix-loop-helix

BL Basal-like

BMDM Bone marrow derived macrophages

BSA Bovine serum albumin
C.elegans Caenorhabditis elegans

CA Constitutively active

CaMKK2 Calcium/calmodulin-dependent protein kinase kinase 2

CARM1 Coactivator-Associated Arginine Methyltransferase

CC3 Caspase-3

CCL5 C-C Motif Chemokine Ligand 5

CD Cluster differentiation

CD31 Cluster of differentiation 31

CDH1 Cadherin-1

CDK Cyclin-dependent Kinase

CLEAR Coordinated Lysosomal Expression and Regulation

CLTC Clathrin Heavy Chain

CO₂ Carbon Dioxide

CRISPR Clustered Regularly Interspaced Short Palindromic Repeats

CSF Colony-stimulating factor

CTS Cathepsin

DAPI 4',6-diamidino-2-phenylindole

DC Dendritic cells

DENN Differentially Expressed in Normal and Neoplastic cells

DKO Double Knock-out

DMEM Dulbecco's modified Eagle's medium

DMSO Dimethyl sulfoxide

DNA Deoxyribonucleic acid

DQ-BSA Self-Quenched BODIPY Dye Conjugates of Bovine Serum Albumin

DTT Dithiothreitol

E.coli Escherichia coli

EBSS Earle's Balanced Salt Solution

ECAR Extracellular acidification rate

EGF Epidermal growth factor

EGLN1 Egl-9 Family Hypoxia Inducible Factor 1

EGTA Ethylene glycol-bis(β-aminoethyl ether)-N,N,N',N'-tetraacetic acid

ELISA Enzyme-linked immunosorbent assay

EMT Epithelial—mesenchymal transition

ENO1 Enolase 1

EPHA2 Ephrin Receptor A2

ErbB2 Epidermal growth factor receptor

ERK Extracellular signal-regulated kinase

ESC Embryonic stem cells

EV Empty vector

FBS Fetal Bovine Serum

FLCN Folliculin

FNIP1/2 Folliculin Interacting Protein 1 and 2

FOXO3 Forkhead box O3

GABARAP Gamma-aminobutyric acid receptor-associated protein

GAP GTPase-activating proteins

GATOR1 GAP activity toward RAGs 1

GCRC Goodman cancer research center

GDP Guanosine diphosphate

GEF Guanine nucleotide exchange factor

GEO Gene expression omnibus
GFP Green fluorescent protein

GM Granulocyte-macrophage

GPNMB Transmembrane glycoprotein non-metastatic breast

GSK621 AMPK activator

GST Glutathione S-transferases

GTP Guanosine triphosphate

H&E Hematoxylin and eosin

HA Hemagglutinin

HCQ. Hydroxychloroquine

HER2+ Human epidermal growth factor receptor 2-positive

HIF- 1α Hypoxia induced factor $1-\alpha$

HK2 Hexokinase 2

IFNγ Interferon gamma

IHC Immunohistochemistry

IL Interleukin

IM Immunomodulatory

IP Immunoprecipitation

IRF-3 Interferon Regulatory Factor 3

KC keratinocytes-derived chemokine

kDa Kilo dalton KO Knock-out

KRAS Kirsten rat sarcoma virus

LAMP1 Lysosomal-associated membrane protein 1

LAMTOR Late endosomal/lysosomal adaptor and mitogen activated protein kinase

and mechanistic target of rapamycin activator

LAR Luminal androgen receptor

LDHA Lactate dehydrogenase A

LIF Leukemia inhibitory factor

LIX LPS-induced CXC chemokine

LKB1 Liver kinase B1

LOVD Leiden Open Variation Data Base

LPS Lipopolysaccharide

LZ Leucine zipper M Mesenchymal

M-CSF Macrophage colony stimulating factor

MCD Methionine/Choline Deficient diet

MCOLN1 Mucolipin TRP Cation Channel 1

MCP-1 Monocyte Chemoattractant Protein-1

MEF Mouse Embryonic Fibroblasts

MG-132 Proteosome inhibitor

MIP2 Macrophage inflammatory protein-2

MiT/TFE Microphthalmia/transcription factors E

MITF Melanocyte Inducing Transcription Factor

mRNA Messenger RNA

MSL Mesenchymal stem-like

mTORC1 Mammalian Target of Rapamycin Complex 1 mTORC2 Mammalian Target of Rapamycin Complex 2

NAC N-Acetyl-L-cysteine

NaCl Sodium chloride

NaPPi Sodium pyrophosphate

NASH Non-alcoholic steatohepatitis

NCBI National Center for Biotechnology Information

NF-κB Nuclear factor-kappa B

NLR Nucleotide-binding leucine-rich repeat containing

NLS Nuclear Localization Signal

NOD Non-obese diabetic

NONO Non-POU Domain Containing Octamer Binding

NOS3 Nitric Oxide Synthase 3

NSG NOD SCID gamma

O₂ Oxygen

OCR Oxygen consumption rate

OXPHOS Oxidative phosphorylation

P Phosphorylated

P. aeruginosa Pseudomonas aeruginosa

P300 Histone acetyltransferase p300

P62 Ubiquitin-binding protein p62

PBS Phosphate-buffered saline

PDA Pancreatic ductal adenocarcinoma

PDGF Platelet-derived growth factor

PDX Patient derived xenografts

PEI Polyethylenimine

PGC1α Peroxisome proliferator-activated receptor gamma coactivator 1-α

PI3P Phosphatidylinositol 3-phosphate

PIK3CA Phosphatidylinositol-4,5-Bisphosphate 3-Kinase Catalytic Subunit Alpha

PJS Peutz-Jeghers syndrome

PKA Protein kinase A
PKB Protein kinase B
PKD Protein kinase D
PLC Phospholipase C

PR Progesterone receptor

PRCC Proline Rich Mitotic Checkpoint Control Factor

PTEN Phosphatase and TENsin homolog

Ras Related GTP Binding

RANTES Regulated upon Activation, Normal T cell Expressed, and Secreted

Raptor Regulatory-associated protein of mTOR

RCC Renal cell carcinoma

RHEB Ras homolog enriched in brain

RNA Ribonucleic acid

RNA-sequencing

ROS Reactive oxygen species

RPLP0 Ribosomal Protein Lateral Stalk Subunit P0

RPMI Roswell Park Memorial Institute Medium

RSK Ribosomal S6 kinase

RT-PCR Reverse transcription quantitative polymerase chain reaction

RTK Receptor tyrosine kinases

S. aureus Staphylococcus aureus

S6 Ribosomal Protein S6

SCID Severe combined immunodeficient mice

SDS-PAGE Sodium dodecyl sulfate polyacrylamide gel electrophoresis

SEM Standard error of the mean

SEMA3A Semaphorin-3A

Ser/S Serine

SFPQ Splicing factor proline- and glutamine-rich

shRNA Short hairpin RNA

siRNA Small interfering RNA

Skp2 S-Phase Kinase Associated Protein 2

SLC2A1 Solute carrier family 2 member 1

SOCS3 Suppressor of cytokine signaling 3

SQSTM1 Sequestosome 1

STAT Signal Transducers and Activators of Transcription

TF Transcription factor

TFE3 Transcription Factor E3

TFE3-L Transcription Factor E3-Long isoform
TFE3-S Transcription Factor E3-short isoform

TFEB Transcription Factor EB
TFEC Transcription factor EC
TGF Tumor growth factor

TGF-β Transforming growth factor beta

Thr/T Threonine

TILs Tumor-infiltrating lymphocytes

TKO Triple Knock-out
TLR Toll-like receptor

TMEM2 Tansmembrane protein 2

TN Triple-negative

TNBC Triple negative breast cancer

TNF Tumor necrosis factor

TNF-α Tumour necrosis factor αTPP1 Tripeptidyl Peptidase 1

TRAIL Tumour necrosis factor (TNF)-related apoptosis-inducing ligand

TRCC Translocation renal cell carcinoma

TSC1/2 Tuberous Sclerosis Complex 1/2

ULK1 Unc-51-Like Kinase 1

UNS Unstable

UVRAG UV Radiation Resistance Associated
UVRAG UV Radiation Resistance Associated
VEGF Vascular endothelial growth factor

VHL Von Hippel-Lindau

WT Wild-type

LIST OF FIGURES

Chapter 1	
Figure 1. Clinical manifestations of Birt-Hogg-Dubé.	3
Figure 2. Interaction between FLCN/FNIP complex and mTORC1 at the lysosome	8
Figure 3. Structure of the four MiT family members: MiTF, TFEB, TFE3, TFEC, and TFE3	13
Figure 4. Regulation of TFEB/TFE3 at the lysosome	
Chapter 2	
Figure 1: Loss of flcn-1 increases the expression of antimicrobial genes and confers resistance	
bacterial	
Figure 2: Loss of flcn-1 increases pathogen resistance via HLH-30 activation	
independent mechanisms	
Figure 4: FLCN depletion in macrophages enhances their energy metabolism and phagocytic potential.	
Figure 5: AMPK regulates HLH-30 activation and antimicrobial response upon infection wit	h
bacterial pathogens	
Figure 6: AMPK regulates TFEB/TFE3-mediated innate immune response	
Supplemental Figure S1 Supplemental Figure S2	
Supplemental Figure 52	91
Figure 1. FLCN and its binding partners FNIP1 and FNIP2 are downregulated in basal-like breast cancer compared to luminal subtypes. Figure 2. Loss of FLCN in luminal breast cancer cell lines activates AMPK and induces TFE nuclear localization and transcriptional activation. Figure 3. Loss of FLCN in MCF7 enhances cellular metabolism in a TFE3-dependent manner.	E3 . 139
rigure 3. Loss of r Lety in Wer 7 chilanees centual metabolism in a 11 L3-dependent manne	
Figure 4. Loss of FLCN in luminal breast cancer cells enhances tumor growth	
Figure 5. Loss of FLCN in luminal breast cancer cells promotes an angiogenic profile	
Figure 6. Loss of FLCN in luminal breast cancer cells enhances tumor growth and promotes	
angiogenesis in a TFE3-dependent manner.	
Figure 7. Loss of FLCN in luminal breast cancer cells activates a HIF-1α-dependent angioge	
program in a TFE3-dependent manner.	
Figure 8. FLCN overexpression in basal-like breast cancer cells restores TFE3 cytoplasmic	
localization and attenuates tumor growth.	. 151
Supplemental Figure 1 (related to Figure 1). FLCN, FNIP1 and FNIP2 are downregulated in	
basal-like breast cancer models compared to luminal subtypes.	
Supplemental Figure 2 (related to Figure 4). Loss of FLCN in luminal breast cancer cells	
enhances tumor growth.	. 156
Supplemental Figure 3 (related to Figure 5). Loss of FLCN in luminal breast cancer cells ind	uces
an angiogenic response.	. 158
Supplemental Figure 4 (related to Figure 6). Validation of TFE3 and FLCN levels in MCF7	
breast cancer cells prior to injection.	. 159

Supplemental Figure 5 (related to Figure 8). FLCN overexpression in basal-like breast cancer	
cells.	160
Chapter 4	
Figure 1. TFE3 exists as two different isoforms with distinct expression patterns	192
Figure 2. TFE3-L expression is post-translationally regulated	194
Figure 3. Expression of TFE3-L is dependent on cellular nutrient status	196
Figure 4. Expression of TFE3-L is regulated through its binding to active Rag GTPases	198
Figure 5. Identification of Skp2 as a potential E3 ligase regulating TFE3-L stability	200
Figure 6. Contribution of mTORC1 and AMPK signaling pathways to Skp2-mediated TFE3-I	
degradation	203
Figure 7. Functional characterization of TFE3-L	205
Supplemental Figure S1 (related to Figure 3). Expression of TFE3-L is dependent on cellular	
nutrient status	206
Supplemental Figure S2 (related to Figure 6). Amino acid sequence of the N-terminal region of	of
TFE3-L and Binding of TFE3-L mutants to Skp2	207

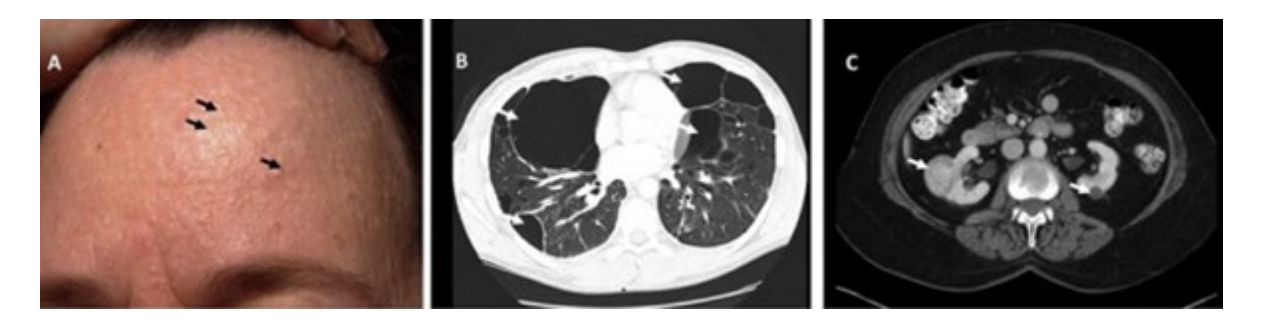
CHAPTER 1 – Literature Review

1.1. Birt-Hogg-Dubé Syndrome

Birt-Hogg-Dubé syndrome (also known as BHD) is a hereditary condition named after the three Canadian doctors that first described it in 1977 – Arthur R. Birt, Georgina R. Hogg, and William J. Dubé (Birt et al., 1977). BHD syndrome was first characterized as a rare skin condition, where patients presented with face and neck skin lesions; however, it was subsequently found to predispose individuals to the development of benign cysts in the lungs, repeated episodes of a collapsed lung (pneumothorax), and increased risk for developing kidney neoplasia (Birt et al., 1977; Zbar et al., 2002) (Figure 1). After almost 20 years following its discovery, germline mutations in a novel gene, *folliculin* (*FLCN*), were identified as causative for BHD syndrome (Nickerson et al., 2002). BHD patients typically inherit one germline FLCN mutation, and somatic second hit mutations that result in the complete loss of FLCN function in the cells that give rise to disease pathology (Baba et al., 2006; Choyke et al., 2003).

To date, most FLCN mutations found in BHD patients result in frameshifts (insertion/deletion), nonsense open reading frames, or the loss of proper mRNA splicing, and are reported in the Leiden Open Variation Data Base (LOVD) (Lim et al., 2010). The predominant result of these mutations is the truncation of the protein, and therefore loss of its function, which is typical for a tumor suppressor (Birt et al., 1977; Vocke et al., 2005). The diversity of symptoms presented in BHD patients raise important questions about the cellular functions of the FLCN protein. Although loss-of-function mutations in human FLCN predominantly affect specific tissues, FLCN gene orthologs have been characterized in yeast (Péli-Gulli et al., 2015; Roberg et al., 1997) nematode (Gharbi et al., 2013; Possik et al., 2014), fruit fly (Liu et al., 2013; Singh et al., 2006), zebrafish (Kenyon et al., 2016), and mouse (Baba et al., 2006; Chen et al., 2008),

implying that FLCN controls certain fundamental cellular processes that are not unique to higher organisms.



¹Figure 1. Clinical manifestations of Birt-Hogg-Dubé.

A) Fibrofolliculomas on the face of a BHD patient. B) Bilateral lung cysts in a BHD patient with pneumothorax on the right. C) computerized tomography scan showing multifocal kidney tumors in a BHD patient. Adapted from (Schmidt and Linehan, 2015).

1.2 FLCN and its interacting proteins FNIP1 and FNIP2

1.2.1. Human folliculin (FLCN) gene and protein

The human folliculin (*FLCN*) gene encodes a 579 amino acid protein with a molecular weight of 64 kDa and no sequence homology to other known proteins. Northern blot analysis revealed that FLCN is expressed in a wide range of human adult tissues, including brain, heart, skin, lung, liver, and kidney (Nickerson et al., 2002). Moreover, homozygous loss of FLCN causes early embryonic lethality, suggesting that FLCN has an important biological role (Hasumi et al., 2009).

1.2.2. FLCN/FNIP complex

Through protein interaction studies, FLCN was shown to form heterodimeric complexes with either FLCN-interacting protein (FNIP) 1 or 2 (Baba et al., 2006; Hasumi et al., 2008; Takagi

et al., 2008). Similar to FLCN, FNIP1 and FNIP2 are widely expressed in cells and conserved through Xenopus (Baba et al., 2006). Considering the close relationship between FLCN and FNIPs, it is not surprising that they have also been suggested to function as tumor suppressors. Mice deficient in FNIP1 and/or FNIP2 were shown to develop tumors in several different organs (Hasumi et al., 2015). FNIP1 and FNIP2 were also found to be critical for the tumor-suppressive function of FLCN in kidney tissue, suggesting that tumor formation in BHD patients may be caused by the disruption of crucial FLCN-FNIP interactions (Hasumi et al., 2015). Additionally, frameshift mutations causing premature stop codons in both FNIP1 and FNIP2 have been reported in gastric and colorectal malignancies, supporting a role for FNIP1 and FNIP2 in the development of these cancers (Mo et al., 2019); however, further studies are required to understand the roles of FLCN interacting partners in tumorigenesis (Cancer is introduced later in section 1.13). Of relevance to BHD syndrome, mice with kidney-targeted FNIP1 and FNIP2 combined inactivation (but not with inactivation of either FNIP1 or FNIP2 alone) developed highly cystic kidneys with increased mitochondrial biogenesis (Hasumi et al., 2015) mimicking the phenotype of kidneytargeted FLCN knockout mice (Baba et al., 2008; Chen et al., 2008). Furthermore, mice with FNIP1 heterozygous and FNIP2 homozygous inactivation developed kidney tumors, suggesting that these proteins are somewhat redundant and function in cooperation with FLCN to regulate normal cell growth in the kidney, whereas loss of FNIP1/2 expression abrogates the tumor suppressive properties of FLCN (Hasumi et al., 2015).

1.2.3. FLCN/FNIP structure

Binding studies demonstrated that FNIP1 and FNIP2 bind to the carboxy-terminus of FLCN (Baba et al., 2006; Hasumi et al., 2008). Computational and three-dimensional studies of

FLCN identified structural similarity with DENN1B protein, predicting a differentially expressed in normal and neoplasia (DENN) domain at its C-terminus and an N-terminal Longin domain (Nookala et al., 2012; Wu et al., 2011). Similarly, bioinformatic analyses predicted that FNIP proteins also contain a DENN domain as their major structural feature (Levine et al., 2013; Zhang et al., 2012). These predictions were supported by a crystal structure of the N-terminus region of the yeast FNIP1/2 orthologue, Lst4, which contains a Longin module, the first element of the full DENN domain (Pacitto, 2015). The DENN and Longin domain family of proteins have been shown to be guanine nucleotide exchange factors (GEF) for Rab GTPases (Yoshimura et al., 2010), facilitating GDP-GTP exchange to activate the vesicular transport function of these small GTPases. Thus, these sequence homologies suggest that the FLCN/FNIP complex may possess GEF activity towards Rab GTPases and function in membrane trafficking processes (Allaire et al., 2010; Marat et al., 2011; Wu et al., 2011; Yoshimura et al., 2010). However, contrary to such expectations, the FLCN-FNIP complex was shown to modulate the mammalian target of Rapamycin (mTOR) activity at the lysosome by its interaction with Rag GTPases by serving as a GTPase-activating protein (GAP) for the lysosome-localized RagC/D GTPases (explained in more details in section 1.3) (Péli-Gulli et al., 2015; Tsun et al., 2013). Even though one group has suggested that FLCN may act as a GEF for RagA at the lysosome (Petit et al., 2013), no followup studies have confirmed this possibility.

More recently, two groups concurrently published the cryo-EM structures of the human FLCN-FNIP2-RagA-RagC-Ragulator complex (Lawrence et al., 2019; Shen et al., 2019). Both studies confirm the previous computational studies implying that both FLCN and FNIP contain a DENN module formed by a N-terminal Longin domain and a C-terminal DENN domain.

1.3. The mammalian target of Rapamycin (mTOR) and FLCN/FNIP complex

1.3.1. The mammalian target of Rapamycin (mTOR)

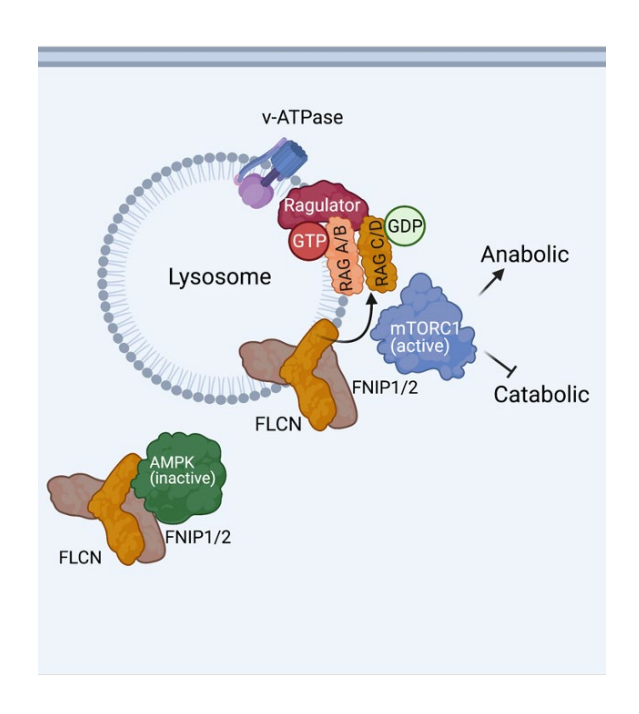
mTOR is a serine-threonine protein kinase that can be divided into two functionally and biochemically distinct complexes, mTORC1 and mTORC2. Whereas mTORC2 regulates cell survival, metabolism and cytoskeletal structure (Oh and Jacinto, 2011), mTORC1 functions as a central regulator of metabolism, ensuring that the cell grows only under favorable conditions (Rabanal-Ruiz and Korolchuk, 2018). The dysregulation of the mTORC1 signaling pathway is thus associated with many forms of cancer and metabolic disorders (Guertin and Sabatini, 2007; Mossmann et al., 2018; Saxton and Sabatini, 2017). "Growth factors act upstream of mTORC1. Binding of growth factors to their specific receptors triggers a cascade of events leading to increased activity of kinases, such as protein kinase B (PKB or AKT), extracellular signalregulated kinase (ERK) and ribosomal S6 kinase (RSK), which all ultimately feed into the tuberous sclerosis complex 1 and 2 (TSC1 and TSC2) signaling pathway (Laplante and Sabatini, 2009). The inputs detected by mTORC1 are not limited to growth factors. In addition, information on nutrient abundance, more specifically the amino acid abundance, is relayed to mTORC1. The major proteins regulating mTORC1 activity in regard to amino acid levels are the Ras-related GTPases (Rags) (Sancak et al., 2008). There are four members (RagA/B/C/D) in mammals, which assemble in heterodimers (A/B with C/D) at the lysosomal surface (Sancak et al., 2010; Sekiguchi et al., 2001). Their activity is regulated by their guanine nucleotide state; fully activated Rags harbour GTP-bound RagA/RagB and GDP-bound RagC/RagD (Sancak et al., 2008). Activated Rags are necessary to anchor mTORC1 at the lysosomes and to permit amino acid sensing (Sancak et al., 2010). However, even though Rags were not shown to directly stimulate mTORC1 kinase activity, they seem to modulate mTORC1 localization to other components, such as Rheb, to regulate its

activity (Avruch et al., 2009). Overexpression of constitutively active Rag mutants increased mTORC1 localization to the lysosomes and increased mTORC1 activity even in the absence of amino acids (Kim et al., 2008; Sancak et al., 2008). Fully activated Rags and mTORC1 require GTP-bound RagA/B, which is achieved by Ragulator-associated GEF activity, and GDP-bound RagC/D" (El-Houjeiri & Paquette et al., 2018).

1.3.2. FLCN/FNIP complex as mTOR regulators at the lysosome:

"Importantly, FLCN has been identified as a GTPase activating protein (GAP) for RagC/D (Péli-Gulli et al., 2015; Tsun et al., 2013). The FLCN/FNIP complex binds to the lysosomal surface after amino acid depletion, where it interacts with the Rag GTPases, and was shown to be necessary for mTORC1 activation by amino acids (Petit et al., 2013) (Figure 2).

Nutrient Rich Conditons



²Figure 2. Interaction between FLCN/FNIP complex and mTORC1 at the lysosome

Under nutrient rich conditions, mTOR is recruited to the lysosome through the interaction with the Ras-related GTP-binding protein RAG GTPases, which are themselves anchored to the lysosome. These RAGs function as heterotetramers consisting of two heterodimers. The active complex consists of RAGA/B bound to GTP RAG C/D bound to GDP. FLCN acts as a GTPase-activating protein (GAP) for RagC/D, which activates mTOR promoting anabolic processes and inhibiting catabolic ones. Illustration generated by Biorender (https://biorender.com/).

However, the FLCN-mTOR relationship remains unclear with respect to mTORC1 activity. Indeed, various groups have reported mTORC1 activation as well as mTORC1 inhibition in FLCN-deficient cells, suggesting context-dependent regulation (Baba et al., 2006; El-Houjeiri et al., 2019; Hasumi et al., 2014; Hudon et al., 2010; Paquette et al., 2021; Possik et al., 2014, 2015; Wada et al., 2016; Wu et al., 2015; Yan et al., 2014, 2016). More studies will be needed to

clarify the different roles of FLCN in amino acid sensing and mTORC1 regulation. In addition, FLCN plays a role in lysosome positioning. Following serum or amino acid withdrawal, FLCN promotes the peri-nuclear clustering of the lysosomes by promoting the association of Ras-related protein Rab-34 (Rab-34) to the lysosomes (Starling et al., 2016). Reciprocally, in nutrient replete conditions and high mTORC1 activity, lysosomes disperse and accumulate at the cell periphery. The exact mechanism leading to cancer progression and the possible role of FLCN-driven mTORC1 regulation still requires further investigation." (El-Houjeiri & Paquette et al., 2018).

1.4. The AMP-activated protein kinase (AMPK) and FLCN/FNIP complex:

1.4.1. The AMP-activated protein kinase (AMPK)

While mTORC1 is highly sensitive to nutrient availability, it also responds indirectly to other stimuli, including energy availability through its interaction with other kinases. Low energy conditions are normally characterized by high AMP:ATP ratios, which allosterically activates another master metabolic regulator, the AMP-activated protein kinase (AMPK) (Carling, 2004; Shackelford and Shaw, 2009). AMPK is a heterotrimeric enzyme formed by a catalytic α subunit, and two regulatory subunits: β and γ . The α subunit contains a typical serine/threonine protein kinase catalytic domain (Hanks et al., 1988), while the β subunit allows glycogen binding. The γ subunit contains four domains that each allow binding to an adenine nucleotide (Mihaylova and Shaw, 2011). In mammals, α and β subunits exist in two isoforms, while the γ has three isoforms (Kim et al., 2016; Mihaylova and Shaw, 2011). Given that all the combinations are possible, mammalian cells can form 12 distinct AMPK complexes. However, the physiological significance of the different isoform complexes remains to be elucidated (Mihaylova and Shaw, 2011). Two upstream kinases, Liver kinase B1 (LKB1) and calmodulin kinase kinase (CAMKK), were shown

to phosphorylate and activate AMPK by phosphorylation at Thr172/174, depending on the cellular context (Shaw et al., 2004; Woods et al., 2003). When activated, AMPK increases ATP production by promoting catabolic pathways and inhibiting anabolic pathways that consume ATP, in a manner antagonistic to mTORC1 activity. Additionally, AMPK inhibits mTORC1 both directly, through the phosphorylation of its component Raptor (Gwinn et al., 2008), and indirectly, by phosphorylation and activation of TSC2 (Inoki et al., 2002). Crosstalk between mTORC1 and AMPK provides a more specific mechanism by which cell growth may be coordinated according to environmental conditions.

1.4.2. AMPK and FLCN/FNIP complex

Interestingly, early co-immunoprecipitation experiments demonstrated an interaction of FNIP1 with the γ subunit of AMPK (Baba et al., 2006). Moreover, FLCN was shown to interact with the FNIP1-AMPK complex but was not essential for their interaction. FNIP1 preferentially bound the active phosphorylated form of AMPK and both FLCN and FNIP1 were shown to be phosphorylated by AMPK (Baba et al., 2006). However, the significance of this phosphorylation is still poorly understood.

Given the interaction between AMPK and the FLCN/FNIP complex, multiple efforts have focused on the functional consequences of this association. Loss of *FLCN* expression or loss of FLCN-AMPK binding was shown to induce chronic AMPK activation in nematodes and various cellular models, leading to increased energy reserves, enhanced metabolic and osmotic stress resistance, and metabolic transformation (Possik et al., 2014; Preston et al., 2011; Yan et al., 2014). Moreover, mutations in FNIP1 were shown to be associated with higher AMPK activity (Siggs et al., 2016), and phosphorylated FNIP1 was shown to bind to chaperone Hsp90, which regulates the

proper folding of AMPK subunits, mTORC1, and its pathway components, such as Raptor, suggesting another function for FNIP1 in the regulation of AMPK and mTORC1 pathways (Sager et al., 2018, 2019; Woodford et al., 2016). All this data strongly suggests a role for the FLCN/FNIP complex in coordinating major cellular metabolic pathways through modulation of mTORC1 and AMPK.

1.5. Other FLCN functions

In addition to its role in mTOR and AMPK pathways, a number of published studies support roles for FLCN in many signaling pathways and cellular processes including: TGF-β signaling (Cash et al., 2011; Chen et al., 2015; Hong et al., 2010a; Khabibullin et al., 2014; Singh et al., 2006), regulation of rRNA synthesis, cell cycle progression (Kenyon et al., 2016; Laviolette et al., 2013), and interaction with HSP90 (Woodford et al., 2016), reviewed in (Schmidt and Linehan, 2018)

FLCN has also been reported to control the cellular localization and activation of a family of oncogenic transcription factors, wherein FLCN-deficient cells consistently display nuclear translocation of the MiT/TFE family members TFEB and TFE3 in various cellular models (El-Houjeiri et al., 2019; Hong et al., 2010b; Napolitano et al., 2020; Petit et al., 2013; Wada et al., 2016).

1.6. Microphthalmia Family of bHLH-zip Transcription Factors (MiT Family)

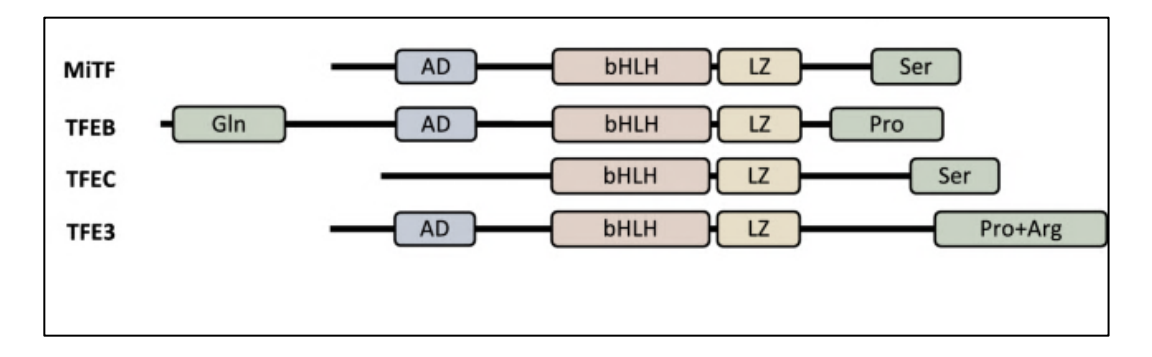
1.6.1. MiT Family: genes and domains

The microphthalmia/transcription factor E (MiT/TFE) family of transcription factors (TFs) encodes four distinct genes: *MITF*, *TFEB*, TFE3, and *TFEC* (Hemesath et al., 1994). All MiT

family members share structural similarities, consisting of a basic helix-loop-helix (bHLH) leucine zipper (LZ) dimerization motif, a transactivation domain, and an identical basic region that binds specific DNA regions (Beckmann et al., 1990; Sato et al., 1997; Steingrímsson et al., 2004) (Figure 3). The functional overlap between MiT family members is expected, as lower organisms, including *Caenorhabditis elegans* (*C.elegans*) contain a single MiT ortholog capable of functioning similarly to several mammalian MiT members known as *HLH-30* (Hallsson et al., 2004). *HLH-30* contain the conserved basic regions and HLH-zip domains seen in mammalian MiT members – suggesting similar mechanisms of DNA binding (Hallsson et al., 2004).

1.6.2. MiT Family: expression and interactions

All four MiT/TFE members are conserved in vertebrates (Bouché et al., 2016). While TFEC expression is restricted to cells of myeloid origin (Martina et al., 2016), the *MITF* gene is predominantly expressed in melanocytes, retinal pigment epithelium (RPE), macrophages, mast cells, osteoclasts, natural killer cells (Martina et al., 2014). In contrast, TFE3 and TFEB show a more ubiquitous pattern of expression and have been detected in multiple cell types (Jebbink et al., 2015). Structural and biochemical data suggest that these transcription factors can form homoor hetero-dimers through their HLH-LZ motif with members within the family, but not with other related bHLH proteins such as c-Myc and Max (Hemesath et al., 1994; Pogenberg et al., 2012), due to a unique three-residue shift within the ZIP domain of MiT family members that introduces an abnormal leucine zipper kink (Pogenberg et al., 2012).



³Figure 3. Structure of the four MiT family members: MiTF, TFEB, TFE3, TFEC, and TFE3

AD, acidic domain; bHLH, basic helix-loop-helix; LZ, leucine zipper; Ser, serine-rich region; Gln, glutamine-rich region; Pro, proline-rich segment; Pro + Arg, proline- and arginine-rich region. Adapted from: (Nabar et al., 2017).

1.6.3. MiT Family members: isoforms

The *MiTF* gene is expressed as different isoforms that are under the control of distinct promoters (Hallsson et al., 2000; Udono et al., 2000). Currently, at least nine major MiTF isoforms have been identified that are differentially expressed in a variety of tissues (Amae et al., 1998; Fuse et al., 1999; Hershey and Fisher, 2005; Oboki et al., 2002; Takeda et al., 2002; Takemoto et al., 2002). These isoforms share the important functional domains, including the transactivation and DNA binding domains, helix–loop–helix and leucine zipper, but differ in their N-termini. These N-termini may contribute to the cell type-specific properties of the various isoforms, but their functional significance remains to be elucidated. To date, little is known about the different isoforms of the other three MiTF/TFE family members TFE3, TFEB and TFEC.

1.7. Role of MiT/TFE family in lysosomes and autophagy

1.7.1. Role of MiT/TFE family in lysosomal biogenesis

Lysosomes were discovered in the early 1950s as membrane-bound organelles containing more than 50 types of acid hydrolases for a wide variety of macromolecules including lipids, carbohydrates, nucleic acids, and proteins (De Duve et al., 1955). Lysosomes have long been considered as static organelles whose main function is the terminal degradation of waste material; however, this concept has been challenged by subsequent discoveries highlighting their critical role in cellular homeostasis (Ballabio, 2016). These roles include cellular recycling, cholesterol homeostasis, endocytosis, autophagy, regulation of surface receptors, lysosomal exocytosis, membrane trafficking, antigen presentation, and inactivation of pathogenic organisms (Saftig and Haas, 2016). More recently, lysosomal biogenesis and function were shown to be tightly controlled by transcriptional regulation (Napolitano and Ballabio, 2016).

The promoter analysis of lysosomal genes revealed that they share a 10-base E-box-like palindromic sequence (GTCACGTGAC) usually found within 500 base pairs of the transcription initiation site. This motif was termed Coordinated Lysosomal Expression and Regulation (CLEAR) element (Sardiello et al., 2009). Interestingly, genome wide chromatin immunoprecipitation sequencing (ChIP-seq) of CLEAR elements showed direct TFEB binding (Palmieri et al., 2011). Subsequently, TFEB and TFE3 were shown to directly bind to CLEAR elements on the promoters of several lysosomal genes to promote their expression including those encoding lysosomal membrane permeases, hydrolases, permeases, and lysosome-associated proteins in different cell types (Martina et al., 2014; Palmieri et al., 2011; Ploper et al., 2015; Settembre et al., 2011, 2012). Importantly, TFEB and TFE3 overexpression was shown to increase the number of lysosomes and levels of lysosomal enzymes (including lysosomal hydrolases, V-

ATPases, and lysosomal transmembrane proteins), thus promoting lysosomal catabolic activity (Martina et al., 2014; Sardiello et al., 2009), whereas downregulation of these genes abolished the enhanced transcriptional response (Li et al., 2016; Martina et al., 2014), confirming TFEB and TFE3 as a bona-fide master regulators of lysosome function.

1.7.2. Role of MiT/TFE family in Autophagy

In addition to regulating lysosomal genes, TFEB and TFE3 were shown to regulate the expression of several genes involved in macroautophagy. "Macroautophagy (referred to as autophagy hereafter), the cellular self-degradation process, plays an important role in energy supply, particularly during development and in response to nutrient stress. It is a process through which cargo is delivered to double-membrane vesicles, termed autophagosomes, which fuse with the lytic compartment and release the inner vesicle into the lumen, leading to the degradation of cell components and the recycling of cellular building blocks (Klionsky, 2005; Mizushima, 2007). This intracellular mechanism is conserved in eukaryotes from yeast to complex multicellular organisms, and its dysfunction has been implicated in many human diseases, including myopathy, neurodegeneration, and cancer, as well as resistance to pathogen infection (Cadwell et al., 2009; Huang and Klionsky, 2007; Liang and Jung, 2010; Scott et al., 2004)" (El-Houjeiri & Paquette et al., 2018). For this reason, increasing the transcription of autophagy genes plays a pivotal role in cells under certain conditions, such as nutrient scarcity.

TFEB and TFE3 were shown to induce the expression of genes involved in substrate capture (*SQSTM1*), autophagosome initiation (*BECN1*, *WIPI1*, *ATG9B*, and *NRBF2*), elongation (*GABARAP*, *MAP1LC3B*, and *ATG5*), and autophagosome trafficking and fusion with lysosomes

(*UVRAG* and *RAB7*), all of which harbor CLEAR elements in their promoters (Palmieri et al., 2011; Settembre et al., 2011).

1.8. Autophagy, lysosomes, and Immune response

Interestingly, autophagy and lysosomal genes have been tightly linked to the regulation of the immune response, where they have been shown to participate in the defense against intracellular pathogens (Deretic, 2011; Deretic et al., 2013; Schmid and Münz, 2005; Yordy and Iwasaki, 2011). For example, autophagy is activated by innate immune receptors like toll-like receptors (TLRs) and can directly eliminate intracellular pathogens (Shi and Kehrl, 2010). Autophagy can also control the immune response by direct elimination of active inflammasomes and decreasing inflammation (Shi et al., 2012), where the autophagic machinery was shown to be essential in the secretion of chemokines and cytokines (Deretic et al., 2013; Jiang et al., 2013). Furthermore, autophagy and the lysosomal pathways play a pivotal role in antigen presentation, which is a key function of certain adaptive immune cells including dendritic cells (DCs), B cells, and CD4+ helper T cells (Crotzer and Blum, 2009). Hence, given the firmly established transcriptional role of TFEB and TFE3 in autophagy and lysosomal biogenesis, it wasn't surprising when several subsequent studies reported their crucial transcriptional role in the modulation of the immune response and inflammation.

1.9. TFEB and TFE3 link cellular stress to the immune response

The first evidence alluding to a role for TFEB and TFE3 in the immune response came from studies on their ortholog HLH-30 in *C. elegans* (Tiller and Garsin, 2014; Visvikis et al., 2014). The immune system of *C. elegans*, which is mediated in its gut, precedes the highly complex

immunity of vertebrates, as it contains the most ancestral signaling networks, and hence can be experimentally advantageous in terms of detailed characterization of the immune signaling cascades (Ermolaeva and Schumacher, 2014). For example, *C. elegans* does not contain a functional orthologue of the NFkB gene (Lawrence, 2009), a critical proinflammatory mediator in vertebrates, and hence this organism was used for genetically dissecting non-NF-kB immune responses that might be relevant to human immunity (Irazoqui et al., 2010).

Importantly, infection of worms with bacterial pathogens resulted in HLH-30 activation, and worms lacking functional HLH-30 were shown to be more prone to death following infection (Visvikis et al., 2014). Interestingly, RNA-seq analysis of wildtype and HLH-30-deficient worms indicates that HLH-30 is responsible for upregulation of ~80 percent of the genes involved in infection, and gene-ontology analysis reported enrichment in several pathways including cytoprotective, antimicrobial, and signaling categories. Importantly, the authors showed that HLH-30-dependent autophagy activation is critical in mediating the increased resistance to infection (Visvikis et al., 2014). The authors then extended their study to human models and reported a similar phenotype where knockdown of TFEB in murine macrophages decreased the transcription of several cytokines and chemokines after infection, including IL-1β, IL-6, TNF-α, and CCL5, indicating that TFEB likely directly controls the transcriptional regulation of immune genes.

Following this study, several reports identified upstream regulation of TFEB and TFE3 innate immune cells including phagocytosis (Di Paola et al., 2018; Gray et al., 2016), lysosome damage (Chauhan et al., 2016), IFN-γ (Singh et al., 2018; Wu et al., 2017), lipopolysaccharide (LPS) (Brubaker et al., 2015; El-Houjeiri et al., 2019; Li et al., 2019; Pastore et al., 2016; Vural et al., 2016) and extracellular ATP (Adinolfi et al., 2018). In addition, several other downstream functions of TFEB and/or TFE3 in innate immune cells were identified including autophagy and

lysosomal biogenesis (Emanuel et al., 2014), bacterial killing (Kim et al., 2017; Visvikis et al., 2014), proinflammatory cytokine production (El-Houjeiri et al., 2019; Hayama et al., 2018; Pastore et al., 2016; Tseng et al., 2017; Visvikis et al., 2014), macrophage classical activation (Chen et al., 2018; Fang et al., 2017), antiviral responses (Campbell et al., 2015; Popp et al., 2017) and dendritic cell migration (Bretou et al., 2017). Collectively, these studies support the idea that TFEB and TFE3 can induce an immune response either by direct mechanisms, controlling the transcription of inflammatory mediators, or by indirect mechanisms, through regulation of autophagy and lysosomal function that impact microbial infection, organismal metabolism, and inflammatory signaling both locally and systemically.

1.10. TFEB and TFE3 as metabolic regulators

Being known as important regulators of lysosomal biogenesis and autophagic processes, TFEB and TFE3 have recently emerged as master metabolic coordinators. Interestingly, overexpression of TFEB in mouse liver results in major expression changes of genes involved in cellular lipid metabolic processes through direct transcriptional control of Pparge1a (encoding PGC-1α)(Settembre et al., 2013a). In fact, genes related to lipid catabolism and oxidation were reported to be upregulated by TFEB overexpression whereas genes responsible for lipid biosynthesis such as steroid, fatty acid, and isoprenoid biosynthetic processes are downregulated. In skeletal muscles, TFEB was reported to regulate mitochondria biogenesis and control energy balance during exercise (Mansueto et al., 2017). Interestingly, unlike in the liver, the effects of TFEB on cellular metabolism in skeletal muscles do not require the presence of PGC-1α, and neither TFEB activation nor depletion affects autophagy flux in the muscle. Moreover, liverspecific overexpression of TFEB in mice prevents development of metabolic syndrome in high fat

diet-fed animals and ameliorates ethanol-induced liver injury (Chao et al., 2018; Settembre et al., 2013a).

Similar to TFEB, TFE3 overexpression in the liver has been shown to enhance insulin receptor signaling, and have protective effects in mouse diabetes models by increasing liver glycogen synthesis and decreasing liver triglyceride and blood glucose levels (Nakagawa et al., 2006). Additionally, TFE3 knockout mice show defects in mitochondria dynamics, abnormalities in systemic glucose and lipid metabolism, and enhance high fat diet-induced obesity and diabetes (Pastore et al., 2017). Notably, TFEB overexpression in TFE3 knockout mice as well as TFE3 overexpression in liver-specific TFEB knockout mice rescues the diet-induced obesity, demonstrating that TFEB and TFE3 can compensate for deficiency of each other.

1.11. Physiological roles of TFEB and TFE3

To further study the physiological roles of TFEB and TFE3 genes, loss-of-function approaches based on knock-out (KO) mice and cell lines have been deployed. Interestingly, TFEB KO mice were embryonically lethal due to defect in placental vascularization (Steingrimsson et al., 1998). However, follow up experiments in tissue specific TFEB KO mice and cell lines have shown an important role for TFEB in lipid metabolism, fatty acid oxidation, lipophagy, osteoclast differentiation, dendritic cell function, and in endodermal lineage differentiation in embryonic stem cells (ESCs) (Ferron et al., 2013; Pastore et al., 2017; Samie and Cresswell, 2015; Settembre et al., 2013b; Young et al., 2016). Even though the physiological roles of TFEB and TFE3 have been thought of as redundant (Pastore et al., 2016), remarkably, TFE3 KO mice are viable and appear "healthy". However, closer examination of these mice revealed several cellular and metabolic phenotypes that are very similar to TFEB liver-, muscle-, and macrophage-specific

conditional KO mice, and such effects are significantly augmented by the loss of both TFEB/TFE3 in these tissues (Pastore et al., 2016, 2017). Similar to TFEB, TFE3 has also been implicated in development as it restricts ESC differentiation, thus retaining ESC pluripotency and self-renewal capability (Betschinger et al., 2013). These data suggest that TFEB and TFE3 regulate similar sets of genes involved in different pathways depending on the tissue type, and play a cooperative, rather than redundant role. However, more studies are required to understand the exact role of each MiT transcription factor and their contribution to human disorders.

1.12 Regulation of TFEB and TFE3

1.12.1 Regulation of TFEB and TFE3 by mTOR

Given the important and diverse cellular functions that TFEB and TFE3 mediate, it is not surprising that their activity is tightly regulated *via* posttranslational modifications, protein-protein interactions, and spatial organization (Napolitano and Ballabio, 2016; Puertollano et al., 2018). (Figure 4). Several studies have reported similar mechanisms underlying TFEB/TFE3 activation in response to nutrient deprivation and metabolic stress. Nucleo-cytoplasmic shuttling of transcription factors is utilized by the cell to control gene expression programs in response to the environment. "Under nutrient rich conditions, mTORC1 was shown to phosphorylate TFEB/TFE3 on specific serine residues and retain them in the cytoplasm in an inactive state (Martina et al., 2012, Martina et al., 2014, Roczniak-Ferguson et al., 2012, Settembre et al., 2011, Settembre et al., 2012). The mTORC1-dependent phosphorylation of TFEB (S211) and TFE3 (S321) promotes binding to 14-3-3. It has been suggested that this interaction masks the Nuclear Localization Signal (NLS), thus inhibiting TFEB and TFE3 nuclear translocation (Roczniak-Ferguson et al., 2012, Martina et al., 2012). Conversely, under starvation, this repressive phosphorylation is lifted,

resulting in their translocation to the nucleus and activation of their downstream transcriptional targets (Martina et al., 2012, Roczniak-Ferguson et al., 2012, Settembre et al., 2011, Settembre et al., 2012). Despite these remarkable similarities between TFEB and TFE3, it is still unclear whether these transcription factors have cooperative, complementary, or partially redundant roles under different environmental conditions" (El-Houjeiri et al., 2019) (Figure 4).

1.12.2 Regulation of TFEB and TFE3 by other Kinases

In addition to mTORC1, TFEB was shown to be phosphorylated at Ser 142 by extracellular signal-regulated kinase 2 (ERK2) (Settembre et al., 2012), and it has been suggested that S142 dephosphorylation mediates TFEB nuclear translocation by reducing S211 phosphorylation, although the mechanism is unknown (Vega-Rubin-de-Celis et al., 2017). More recently, Protein kinase B (also known as Akt) and Glycogen synthase kinase 3 beta (GSK3β) were reported to regulate TFEB activity, where they phosphorylate and inhibit TFEB nuclear localization at S467 and S138, respectively (Palmieri et al., 2017; Zhang et al., 2018).

Notably, TFEB and TFE3 were shown to both possess Rag binding sites that permit binding to active Rag C/D (GDP-bound) at the lysosome (Martina and Puertollano, 2013). Under nutrient rich conditions, Rag C/D are in a GDP-bound/active state and can bind and sequester TFEB and TFE3 at the lysosomal surface, which places them in close proximity with the activated mTORC1, facilitating their phosphorylation and inhibiting their activity (Martina and Puertollano, 2013; Napolitano et al., 2020). Conversely, in RagC/D or FLCN deficient cells, TFEB is constitutively nuclear and activated regardless of nutrient availability (Kim et al., 2014) (Figure 4), further supporting the role of FLCN in activating the Rags at the lysosome through its GAP activity.

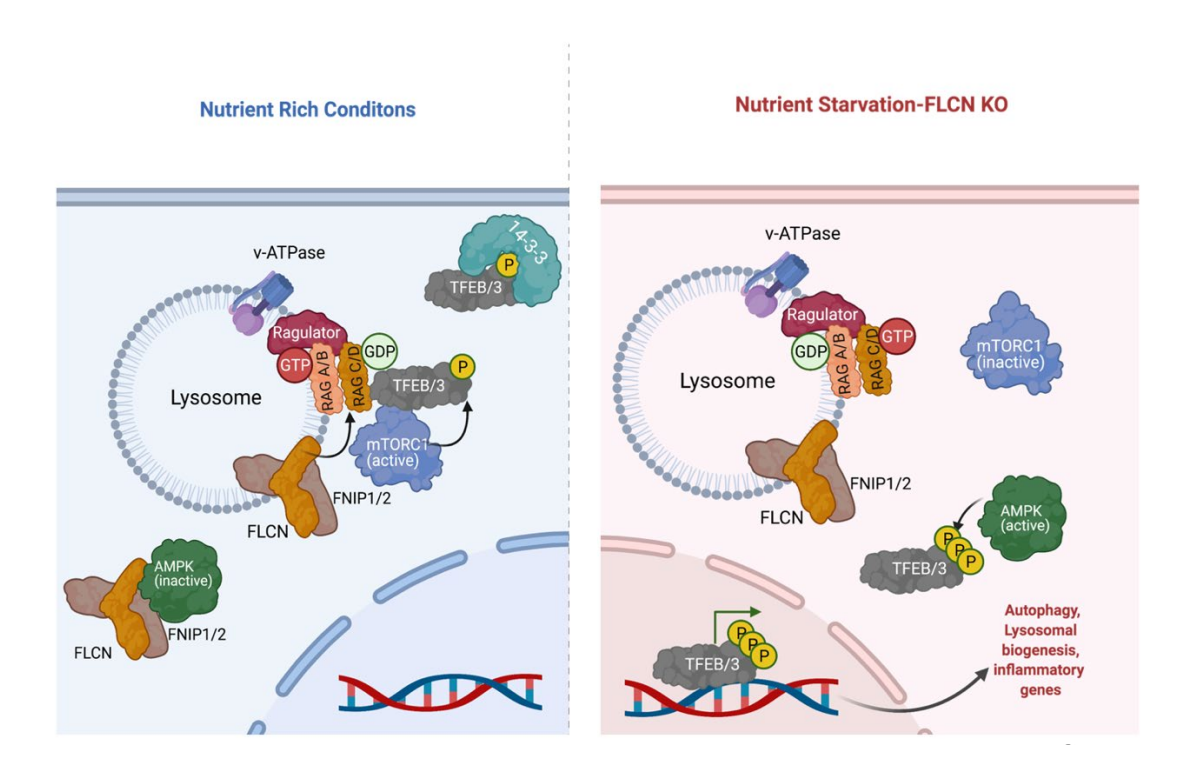
1.12.3 Regulation of TFEB and TFE3 by AMPK

Importantly, TFEB and TFE3 mediated gene transcription was shown to be epigenetically activated during starvation through AMPK. Indeed, AMPK activation under starvation conditions increased levels of the TFEB/TFE3 transcriptional co-activator CARM1 (Coactivator Associated Arginine Methyltransferase 1) and a subsequent increase in histone H3 Arg17 dimethylation (Shin et al., 2016). Interestingly, AMPK was shown to induce nuclear localization and activation of TFEB/TFE3 under nutrient starvation conditions or in FLCN deficient cells (Eichner et al., 2019; El-Houjeiri et al., 2019; Paquette et al., 2021). More recently, AMPK was reported to directly regulate TFEB and TFE3 activity through phosphorylation on C-terminal serine residues (S466, S467 and S469 in TFEB); however, the exact mechanism of how these phosphorylation events promote transcriptional activation remains to be elucidated (Paquette et al., 2021).

1.12.4 Regulation of TFEB and TFE3 by phosphatases

Although the regulation of TFEB and TFE3 phosphorylation mediated by mTORC1 and other kinases have been well reported, the regulation of the phosphatase(s) involved in their dephosphorylation remains elusive. However, through high-content screening of hundreds of phosphatases followed by cellular validation studies, the Ca²⁺- and calmodulin-dependent Ser/Thr protein phosphatase calcineurin was identified as a potential TFEB phosphatase (Medina et al., 2015). Two concurrent studies supported this idea by reporting that starvation and cellular stress induce lysosomal Ca²⁺ release, activating calcineurin, and thus leading to dephosphorylation, nuclear localization and activation of TFEB (Martina et al., 2016; Tong and Song, 2015). Collectively, it appears that TFEB/TFE3 transcription factors are tightly controlled by a panel of kinases and phosphatases that, depending on the environmental cues, exhibit different downstream

responses, and hence, it is not surprising that their deregulation has been implicated in many human disorders including cancer.



⁴Figure 4. Regulation of TFEB/TFE3 at the lysosome

To put it all into perspective, under nutrient rich condition, FLCN acts as a GAP on RAG C, activating it, which in turn activates mTOR at the lysosome. TFEB and TFE3 were shown to bind active RAG C, and when this is interaction happens, mTOR phosphorylates TFEB and TFE3 at specific serine residues, which promotes their binding to 14-3-3, rendering them inactive in the cytoplasm. However, under starvation conditions, or in FLCN-deficient cases, RAG C is in an inactive state and stuck in the GTP bound form which can no longer recruit and activate mTOR or bind to TFEB/3, hence this inhibitory phosphorylation is lifted and TFE3 now can translocate to the nucleus where it activates its downstream targets including autophagy, lysosomal biogenesis, and immune response. TFEB and TFE3 can be further phosphorylated by AMPK at the C-terminus

region which further enhances their transcriptional activity. Illustration generated by Biorender (https://biorender.com/)

1.13. Cancer

Cancer encapsulates a broad group of diseases in which cells have acquired several capabilities including sustaining proliferative signaling, evading growth suppressors, resisting cell death, enabling replicative immortality, inducing angiogenesis, and activating invasion and metastasis programs (Hanahan and Weinberg, 2011). Currently, cancer ranks as a leading cause of death and an important barrier to increasing life expectancy in every country of the world (Siegel et al., 2020). Most cancers arise as a consequence of genetic alterations to essential cellular genes, which may be inherited or arise spontaneously (Soussi and Wiman, 2007). These alterations confer a selective advantage to the cells, which together with changes in the microenvironment, promote tumor growth and progression. Gain-of-function mutations in these genes, produce so-called oncogenes that drive tumor formation (Lee and Muller, 2010). Others inactivate tumor suppressor genes that normally ensure that cells do not proliferate inappropriately or survive outside their normal niche or in response to specific environmental cues (Lee and Muller, 2010). Interestingly, chromosomal rearrangements resulting in the fusion of two different genes are the most common type of mutation found in human cancer (Futreal et al., 2004).

1.14. TFEB and TFE3 in cancer

MiT/TFE proteins have established roles in promoting tumorigenesis (Haq and Fisher, 2011; Kauffman et al., 2014). While genomic amplifications of MITF are found in 5–20% of melanomas (Cancer Genome Atlas Network, 2015), translocations and rearrangements of TFE3

and, less commonly, TFEB were found in pediatric renal cell carcinoma (RCC) and alveolar soft part sarcoma (ASPS). Only 5% of sporadic RCC tumors manifest a rare subgroup termed translocation-RCC (tRCC), which involves the MiT/TFE genes. *TFE3* gene fusions can occur with several partners including *PRCC*, *ASPSCR1*, *SFPQ*, *NONO* and *CLTC* (Kauffman et al., 2014; Linehan et al., 2010). In these studies, chromosomal translocations were reported to prompt gene fusions placing them under a control of a more active promoter resulting in their over-expression. Importantly, the resulting gene fusions maintained the helix-loop-helix domains and nuclear localization signals, keeping their transcriptional activation functions intact (Kauffman et al., 2014). These gene fusions were reported to eliminate exon 1 (containing the Rag binding site) from the resulting protein variant, preventing their binding to the lysosome and interaction with mTORC1, leading to their constitutive nuclear localization and activation (Kauffman et al., 2014).

In addition to chromosomal translocations, more recently, TFEB was shown to induce renal cancers through gene amplification (Durinck et al., 2015). Interestingly, the *TFEB* gene resides in the proximity of vascular endothelial growth factor receptor A gene (*VEGFA*), and both genes may be amplified together (Gupta et al., 2017). Subsequently, a conditional, kidney-specific, TFEB-overexpressing mouse line was generated, which recapitulates some features of human TFEB/TFE3-associated RCC such as cysts, clear cells, fibrosis, and multilayered basement membranes (Calcagnì et al., 2016). In this mouse model, severe kidney enlargement with multiple cysts developed followed by liver metastases. Interestingly, these mice had elevated levels of several genes involved in the cell cycle promotion (Calcagnì et al., 2016). Given that RCCs are characterized by metabolic dysregulation (Hakimi et al., 2016; Linehan et al., 2010), researchers have speculated that TFE-upregulated proteins promote stress response programs and enhance resistance to metabolic crisis. Interestingly, these TFEB-overexpressing mice showed TFEB-

/TFE3-dependent induction of both the Wnt-beta-catenin and mTORC1 pathways (Calcagnì et al., 2016; Di Malta et al., 2017). In addition to RCC, a recent study reported upregulated expression of MITF, TFEB, and TFE3 in pancreatic ductal adenocarcinoma (PDA), where they appear to support tumor growth through the induction of autophagy pathways (Perera et al., 2015).

The role of these transcription factors in other human cancers has been poorly studied to date, however many cancers including melanoma, prostate, and breast show a context and stage-specific dependence on activation of autophagy and lysosomal pathways during tumor initiation and progression (Huo et al., 2013; Lock et al., 2011; Santanam et al., 2016; Wei et al., 2011; Xie et al., 2015). These studies collectively highlight the importance of nutrient scavenging in cancer and establish lysosomal catabolism as essential for removing damaged organelles and supplying the building blocks for tumor growth (Guo and White, 2016). Given the firmly established roles of TFEB and TFE3 in the transcription of autophagy, lysosomal, and metabolic genes, one might speculate the important functions these transcription factors play in diverse types of cancer and the signaling pathways that control their function in different contexts.

1.15. Autophagy and Cancer

"Autophagy dysfunction is increasingly emerging as a modulator of cancer onset and progression, where it causes the accumulation of damaged macromolecules and organelles such as the mitochondria, and hence inducing oxidative stress, DNA damage and chromatin instability (Chen and Karantza, 2011; Levine and Klionsky, 2004). However, the exact role of autophagy in cancer seems ambivalent as both the induction and inhibition of autophagy have been reported to be both pro-and anti-tumorigenic (White and DiPaola, 2009). As such, the emergence of autophagy pathways as novel targets for drug development in anticancer therapy have been extensively

reviewed (Apel et al., 2009; Brech et al., 2009; Dalby et al., 2010; Levine, 2007; Mathew et al., 2007). From these reviews, it seems that, while the inhibition of autophagy may sensitize the tumor cells to conventional anticancer drugs, the induction of autophagy may also promote cell death in tumor cells with apoptotic resistance. In parallel, since cancer cells experience higher metabolic demands and stresses than normal cells (White and DiPaola, 2009), they may depend more heavily on autophagy for survival (Amaravadi et al., 2011) and thus induction of autophagy may activate several pathways promoting cell survival, tumor growth and progression. Accordingly, autophagy induction could be beneficial or detrimental depending on the type or stage of the disease (Choi et al., 2013), and subsequently more studies are required to elucidate the precise function of autophagy in different cancer types before a therapeutic approach can be considered.

To date, pharmacological induction of autophagy through mTOR inhibition or AMPK activation has been shown to have some therapeutic and prevention potential in cancer (Evans et al., 2005; Harrison et al., 2009; Kim and Guan, 2015). For example, rapamycin, selectively inhibits mTORC1 and, subsequently, activates autophagy through a mechanism that has not yet been fully elucidated, but is known to require binding to the FKBP12 protein (Shimobayashi and Hall, 2014). Following the potential success of rapamycin, several analogues have been developed to inhibit mTORC1 and are utilized in anti-cancer therapy in different types of cancer (Chagin, 2016). However, multiple concerns and limitations emerge from such therapeutic strategies, especially when mutations in key downstream autophagy genes have occurred. For instance, using a mouse model of TSC, autophagy was shown to have prosurvival effects for tumorigenesis, suggesting that autophagy inhibition and not activation is effective as a treatment (Parkhitko et al., 2014). Additionally, depending on the stage and type of cancer, inducing autophagy could activate several

transcription factors involved in stress response such as TFEB and TFE3 which might give these tumor cells potential survival advantage and resistance to therapy.

Given the potential double-edged functions of autophagy in tumor suppression and promotion, a better understanding of the different autophagy players and their interplay might provide insights to novel combinatorial therapies aimed at modulating autophagy pathways in cancer to achieve optimal therapeutic benefit. "(El-Houjeiri & Paquette et al., 2018).

1.16. Breast cancer

1.16.1. Breast cancer: Statistics and subtypes

Breast cancer (BC) is the most commonly diagnosed cancer and the second leading cause of cancer mortality among women worldwide (Siegel et al., 2020), accounting for nearly 50,000 deaths in the Canada in 2020 (Canadian Cancer Society, 2020). Gene expression profiling classifies human BCs into different subtypes, including luminal A, luminal B, human epidermal growth factor receptor 2-positive (HER2+), and triple-negative (TN) subtypes according to estrogen receptor (ER), progesterone receptor (PR), and epidermal growth factor receptor ErbB2/HER2 (HER2) expression status (Perou et al., 2000; Sørlie et al., 2001; Sorlie et al., 2003). Expression of these receptors is routinely used to select treatments for breast cancer patients and predict prognosis (Perou et al., 2000; Zhu et al., 2014). BC molecular and behavioral heterogeneity requires the application of different therapeutic methods for each subtype (Cancer Genome Atlas Network, 2012; Dai et al., 2015; Prat et al., 2015). Despite recent treatment advances, breast cancer is still associated with a poor 5-year survival rate (Chia et al., 2007; Prat et al., 2015). Subtypes vary in prognosis, with worse outcomes traditionally seen among the three-hormone receptor negative subgroups compared to luminal subgroups.

1.16.2. Triple negative breast cancer

Of all the subtypes, TNBC is extremely heterogenous and represents 15-20% of breast cancers and is associated with the worst prognostic outcome (Dawson et al., 2009). Hence it was necessary to establish a more detailed classification of lesions belonging to this subtype. Besides histopathological differences, multiple effort was put to subclassify TNBC subtypes at the transcriptomic level. The landmark study by Lehmann et al. (Lehmann et al., 2011) identified seven clusters of TNBC, namely basal-like 1 (BL1), basal-like 2 (BL2), immunomodulatory (IM), mesenchymal (M), mesenchymal stem-like (MSL), luminal androgen receptor (LAR), and unstable (UNS). Specifically, 75–80% of tumors were classified as the BL breast cancer group; where BL1 is enriched in cell cycle regulator and DNA damage response pathways, and the BL2 demonstrates high levels of growth factor and metabolic pathways, as well as an increased myoepithelial marker expression. The IM subtype is characterized by immune cell processes and signaling cascades. The M and MS subtypes both show enrichment in genes implicated in cell motility and in epithelial-mesenchymal transition (EMT), however, the MSL subtype shows lower expression of genes associated with cellular proliferation. Lastly, the LAR subtype has luminallike gene expression pattern, despite ER negativity.

TNBC can further characterized by the degree of genetic instability and intricate patterns of copy number alterations and chromosomal rearrangements. Recent studies by Bareche et al. (Bareche et al., 2018) reported the genomic alterations characteristic of each TNBC molecular subtype. BL1 tumors demonstrated high levels of chromosomal instability, high rate of TP53 mutations, copy-number gains and amplifications of PI3KCA and AKT2, and deletions in genes involved in DNA repair mechanisms. The LAR subtype is characterized by higher mutational

burden and enrichment in mutations of PI3KCA, AKT1 and CDH1 genes. Mesenchymal and MSL subtypes are associated with higher signature score for angiogenesis. Expectedly, the IM group displayed high expression levels of immune response-associated signatures.

Despite multiple efforts to stratify TNBC into different subtypes to provide accurate cell model for their clinical treatment, to date, all TNBC subtypes have limited treatment options, are prone to recurrence and metastasis, and has a poor prognosis. The main reason is that the expression of ER, PR, and HER2 are all negative, making specific endocrine therapies and targeted therapies ineffective. Hence, chemotherapy remains the only systemic therapeutic option in the adjuvant and metastatic setting of this disease. Importantly, one of the important reasons associated with this subtype's worse prognosis is the high neovascularization level caused by VEGF-A overexpression (Linderholm et al., 2009). Interestingly, VEGF-A, a member of the VEGF platelet-derived growth factor (PDGF) family of structurally related mitogen, is one of the key mediators in angiogenesis (Carmeliet, 2005).

1.17. Angiogenesis and Metastasis

1.17.1. Angiogenesis

Angiogenesis is a processes whereby new blood vessels form from pre-existing blood vessels to supply nutrients, oxygen and immune cells, and to remove waste products (Folkman, 1971). Several proteins have been identified as angiogenic activators, the prototypic factor being VEGF-A. Other factors include basic fibroblast growth factor (bFGF), angiogenin, transforming growth factor (TGF)-α, TGF-β, tumor necrosis factor (TNF)-α, platelet-derived endothelial growth factor, granulocyte colony-stimulating factor, placental growth factor, interleukin-8, hepatocyte growth factor, and epidermal growth factor (Jeong et al., 2021). In addition to the tumor cells,

many cells within the tumor microenvironment, including tumor-associated fibroblasts and macrophages, can secrete angiogenic factors that cause increased vascularization and dramatically increase tumor angiogenesis and tumor growth rates (Orimo and Weinberg, 2006; Watnick, 2012). The initiation of tumor angiogenesis is a crucial point in tumor progression and has been referred to as the "angiogenic switch" (Hanahan and Folkman, 1996). This hallmark of cancer represents the shift from dormancy to progressive growth (Hanahan and Weinberg, 2011). Angiogenesis has been strongly linked to metastasis as tumor microvessel density was shown to correlate with increased metastatic potential and poor survival in nearly all forms of malignancy (Zetter, 1998).

1.17.1. Angiogenesis enables Metastasis

Metastasis is the general term used to describe the spread of cancer cells from the primary tumor site to surrounding tissues and to distant organs, and is currently the leading cause of cancer morbidity and mortality (Chaffer and Weinberg, 2011). Metastasis involves a series of sequential and interrelated steps including detachment from the primary tumor, intravasation into the circulatory and lymphatic systems, evading the immune system, extravasating at distant capillary beds, and invading and proliferate in distant organs (Welch and Hurst, 2019). Many of these rate limiting steps in the metastatic process involve angiogenesis, which can be triggered by hypoxia resulting from the increasing distance between the proliferating tumor cells and the capillaries or from the inefficiency of new vessels (Chaudary and Hill, 2007).

1.18. Hypoxia and HIF-1 pathways

1.18.1. Hypoxia

Mammalian cells need to maintain proper oxygen hemostasis to execute their aerobic metabolism and energy production. In many disorders including cancer, heart diseases, or chronic obstructive pulmonary disorders, the cellular oxygen balance is highly impaired, and cells become hypoxic (having low oxygen (O₂) levels) (Semenza, 2000). Hypoxia is a common phenotype observed in proliferating solid tumors that suffer from poor O₂ supply, especially to the center tumor regions (Powis and Kirkpatrick, 2004). Reciprocally, cancer itself induces hypoxia due to inflammatory processes, which activates a cascade of cytokines and chemokines (Aggarwal et al., 2006; Balkwill and Mantovani, 2001).

1.18.2. Hypoxia Inducible Factor (HIF)

Tumor cells in hypoxic environments usually adapt to low oxygen conditions by activating several survival pathways including Hypoxia Inducible Factor -1 Subunit Alpha (HIF-1 α). HIF-1 is a heterodimeric transcription factor, composed of two subunits, the HIF-1 α (or its analogs HIF-2 α and HIF-3 α) and HIF-1 β subunits (Wang et al., 1995). HIF-1 α is the functional subunit determining the activity of the complex (Zhang et al., 2015), where under low cellular oxygen levels, HIF-1 α is stabilized via a block of its degradation (Iwai et al., 1999).

Interest in HIF-1 α in cancer research has been substantially increasing over the past decade, where it has been shown to regulate the transcription of hundred target genes, including those involved in glycolysis, metabolic adaptation and angiogenesis (Shaw, 2006). Importantly, HIF-1 α induces the transcription of several pro-angiogenic factors including VEGF-A, which in turn promotes the formation of new blood vessels to enrich tumor cells with oxygen for their growth

(Conway et al., 2001). In addition, HIF-1 promotes tumor metastasis through the transcriptional activation of several oncogenic growth factors such (TGF- β 3), epidermal growth factor (EGF) and others (Conway et al., 2001; Laderoute et al., 2002). In breast cancer, studies have shown that high HIF-1 α levels is correlated with more aggressive cancer characteristics and poor prognosis (Gruber et al., 2004). High HIF-1 α levels are associated with proliferation and angiogenesis stimulated by VEGF (Bos et al., 2001), and a shorter survival in lymph node negative breast cancer patients (Bos et al., 2003).

1.18.1. Peroxisome proliferator-activated receptor gamma coactivator 1-alpha (PGC-1a)

Another important player in hypoxia and metabolic flexibility is the peroxisome proliferator-activated receptor gamma coactivator 1-alpha (PGC-1 α) (Puigserver, 2005). PGC-1 α is a co-activator for steroid and nuclear receptors involved in several energy metabolic pathways including: mitochondrial function, endurance, induction of angiogenesis, glucose and lipid metabolism (Handschin and Spiegelman, 2008). Relation between PGC-1 α and HIF-1 α has been studied extensively and it seems that in angiogenesis, PGC-1 α can indirectly stimulate VEGF-A transcription in a HIF-1 α -dependent manner, where PGC-1 α induces mitochondrial respiration and this lowers the oxygen levels and increases ROS production, inducing HIF-1 α activation (Puigserver, 2005).

1.19. TFEB, TFE3 and angiogenesis

A role for MiT/TFE factors in the regulation of angiogenesis was first hypothesized following the observation that *Tfeb* knockout mice are lethal due to a defect in placental vascularization (Steingrímsson et al., 1998). In addition, ASPSCR1-TFE3-driven ASPS is a highly

vascularized tumor, which was shown to respond to anti-angiogenic therapy (Lazar et al., 2007; Zhou et al., 2017). However, the mechanism and the direct role for these transcription factors in the regulation of angiogenesis remains poorly understood.

1.20. FLCN/TFE/AMPK and angiogenic pathways

AMPK is a well-known regulator of PGC-1α that tightly controls its expression and activity. AMPK was shown to directly regulate PGC-1a activity through phosphorylation and subsequent activation of a metabolic transcriptional program in skeletal muscle (Jager et al., 2007). Additionally, exercise or direct activation of AMPK induces the transcriptional upregulation of PGC-1α cofactors in skeletal muscle (Lee et al., 2006; Terada and Tabata, 2004). Remarkably, TFEB and TFE3 were recently shown to induce the transcription of PGC-1α and PGC-1β in different cellular settings by directly binding their promoters (Baba et al., 2018; Salma et al., 2015; Settembre et al., 2013a; Wada et al., 2016). However, no direct link to HIF1-α was made in these studies. Interestingly, in addition to TFEB and TFE3, HIF-1α is another transcriptional factor whose activity increases in the absence of FLCN. Increased transcriptional activity, but not elevated HIF-1α levels, was reported in BHD-derived renal tumor cell line UOK257 and in renal carcinomas from BHD patients (Preston et al., 2011; Yan et al., 2014). These studies report an increase in HIF-1\alpha target genes including those involved in angiogenesis (e.g., VEGF-A) and glycolysis (e.g., HK2). Interestingly, rapamycin-mediated inhibition of mTORC1 suppresses upregulation of HIF-1α target genes under hypoxic conditions (Preston et al., 2011). Under normoxia, AMPK activation in FLCN-deficient cells was shown to induce the expression of PGC-1α, which enhances mitochondrial biogenesis and ATP production, resulting in reactive oxygen

species (ROS)-dependent activation of HIF-1 α and a metabolic switch to aerobic glycolysis (Yan et al., 2014).

1.21. Research rationale and objectives

FLCN has been shown to interact with AMPK and mTORC1 pathways, both being central regulators of cellular metabolism. Interestingly, these metabolic kinases were shown to antagonistically regulate the MiTF family members: TFEB and TFE3. These transcription factors have been involved in the transcription of genes involved in metabolism, stress response, and more recently the immune response. The general objective of this thesis is to characterize functional role of the FLCN-AMPK-TFE3 pathway in diverse biological processes.

Specifically, in chapter two, we aimed to link the FLCN-AMPK signaling axis to innate immune response and pathogen resistance through the modulation of TFEB and TFE3. We utilized *c.elegans* and mammalian models to investigate the conservation of this pathway through evolution.

Given that our previous and current data suggested the existence of a novel metabolic checkpoint governed by AMPK, FLCN, and TFEB/3 that provides metabolic advantage to cells through resistance to several energy depleting stress, highlighting a possible involvement of this pathway in cancer, in the third chapter of this thesis, we aimed to explore the role of FLCN-AMPK-TFE3 pathway in the context of breast cancer. We analyze FLCN, FNIP1 and FNIP2 expression levels across breast cancer subtypes and compare them to AMPK and TFE3 targets expression. We examine the consequences of FLCN loss in luminal breast cancer and its over-expression in the more aggressive triple negative subtypes. Subsequently we analyzed the involvement of several

metabolic pathways that can pinpoint to a general role of FLCN-AMPK-TFE3 pathway in human cancers.

TFE3 acts downstream of FLCN-AMPK pathway and orchestrates several cellular processes that are important in cellular hemostasis and disease. TFE3 exists in two different isoforms, the full length TFE3 (575aa) and an alternatively spliced, N-terminally truncated, variant (470aa). The resulting proteins possess distinct amino termini, but share transactivation, DNA binding, and dimerization motifs. However, to date, these two isoforms have not been functionally characterized. cells and their implications. In the fourth chapter of this thesis, we aim to explore the mechanisms controlling their stability and gene activating potential in regulating various cancer-associated processes, which can provide a new insight for their aberrant expression in human cancers.

Collectively, we have identified novel roles of the FLCN-TFE-AMPK pathway in immune response and tumor growth through activation of several pathways that provide a survival advantage to the cells. Additionally, the characterization of the different TFE3 isoforms adds another layer of tight regulation of these transcription factors through proteasomal degradation. Better understanding of the FLCN-TFE-AMPK can lead to the discovery of new modalities of targeted therapies in diseases where this pathway is disrupted to ultimately open horizons toward more promising drug targets.

1.22. References associated with Chapter 1

- [1] Adinolfi, E., Giuliani, A.L., De Marchi, E., Pegoraro, A., Orioli, E., and Di Virgilio, F. (2018). The P2X7 receptor: A main player in inflammation. Biochem. Pharmacol. *151*, 234–244.
- [2] Aggarwal, B.B., Shishodia, S., Sandur, S.K., Pandey, M.K., and Sethi, G. (2006). Inflammation and cancer: how hot is the link? Biochem. Pharmacol. 72, 1605–1621.
- [3] Allaire, P.D., Marat, A.L., Dall'Armi, C., Di Paolo, G., McPherson, P.S., and Ritter, B. (2010). The Connecdenn DENN domain: a GEF for Rab35 mediating cargo-specific exit from early endosomes. Mol. Cell *37*, 370–382.
- [4] Amae, S., Fuse, N., Yasumoto, K., Sato, S., Yajima, I., Yamamoto, H., Udono, T., Durlu, Y.K., Tamai, M., Takahashi, K., et al. (1998). Identification of a novel isoform of microphthalmia-associated transcription factor that is enriched in retinal pigment epithelium. Biochem. Biophys. Res. Commun. 247, 710–715.
- [5] Amaravadi, R.K., Lippincott-Schwartz, J., Yin, X.-M., Weiss, W.A., Takebe, N., Timmer, W., DiPaola, R.S., Lotze, M.T., and White, E. (2011). Principles and current strategies for targeting autophagy for cancer treatment. Clin. Cancer Res. *17*, 654–666.
- [6] Apel, A., Zentgraf, H., Büchler, M.W., and Herr, I. (2009). Autophagy-A double-edged sword in oncology. Int. J. Cancer *125*, 991–995.
- [7] Avruch, J., Long, X., Ortiz-Vega, S., Rapley, J., Papageorgiou, A., and Dai, N. (2009). Amino acid regulation of TOR complex 1. Am. J. Physiol. Endocrinol. Metab. *296*, E592-602.
- [8] Baba, M., Hong, S.-B., Sharma, N., Warren, M.B., Nickerson, M.L., Iwamatsu, A., Esposito, D., Gillette, W.K., Hopkins, R.F., Hartley, J.L., et al. (2006). Folliculin encoded by the BHD gene interacts with a binding protein, FNIP1, and AMPK, and is involved in AMPK and mTOR signaling. Proc. Natl. Acad. Sci. USA *103*, 15552–15557.
- [9] Baba, M., Furihata, M., Hong, S.-B., Tessarollo, L., Haines, D.C., Southon, E., Patel, V., Igarashi, P., Alvord, W.G., Leighty, R., et al. (2008). Kidney-targeted Birt-Hogg-Dube gene inactivation in a mouse model: Erk1/2 and Akt-mTOR activation, cell hyperproliferation, and polycystic kidneys. J. Natl. Cancer Inst. *100*, 140–154.
- [10] Baba, M., Endoh, M., Ma, W., Toyama, H., Hirayama, A., Nishikawa, K., Takubo, K., Hano, H., Hasumi, H., Umemoto, T., et al. (2018). Folliculin regulates osteoclastogenesis through metabolic regulation. J. Bone Miner. Res. *33*, 1785–1798.
- [11] Balkwill, F., and Mantovani, A. (2001). Inflammation and cancer: back to Virchow? Lancet 357, 539–545.
- [12] Ballabio, A. (2016). The awesome lysosome. EMBO Mol. Med. 8, 73–76.
- [13] Bareche, Y., Venet, D., Ignatiadis, M., Aftimos, P., Piccart, M., Rothe, F., and Sotiriou, C. (2018). Unravelling triple-negative breast cancer molecular heterogeneity using an integrative multiomic analysis. Ann. Oncol. 29, 895–902.
- [14] Beckmann, H., Su, L.K., and Kadesch, T. (1990). TFE3: a helix-loop-helix protein that activates transcription through the immunoglobulin enhancer muE3 motif. Genes Dev. 4, 167–179.
- [15] Betschinger, J., Nichols, J., Dietmann, S., Corrin, P.D., Paddison, P.J., and Smith, A. (2013). Exit from pluripotency is gated by intracellular redistribution of the bHLH transcription factor Tfe3. Cell *153*, 335–347.
- [16] Birt, A.R., Hogg, G.R., and Dubé, W.J. (1977). Hereditary multiple fibrofolliculomas with trichodiscomas and acrochordons. Arch. Dermatol. *113*, 1674–1677.

- [17] Bos, R., Zhong, H., Hanrahan, C.F., Mommers, E.C., Semenza, G.L., Pinedo, H.M., Abeloff, M.D., Simons, J.W., van Diest, P.J., and van der Wall, E. (2001). Levels of hypoxia-inducible factor-1 alpha during breast carcinogenesis. J. Natl. Cancer Inst. *93*, 309–314.
- [18] Bos, R., van der Groep, P., Greijer, A.E., Shvarts, A., Meijer, S., Pinedo, H.M., Semenza, G.L., van Diest, P.J., and van der Wall, E. (2003). Levels of hypoxia-inducible factor-1alpha independently predict prognosis in patients with lymph node negative breast carcinoma. Cancer 97, 1573–1581.
- [19] Bouché, V., Espinosa, A.P., Leone, L., Sardiello, M., Ballabio, A., and Botas, J. (2016). Drosophila Mitf regulates the V-ATPase and the lysosomal-autophagic pathway. Autophagy *12*, 484–498.
- [20] Brech, A., Ahlquist, T., Lothe, R.A., and Stenmark, H. (2009). Autophagy in tumour suppression and promotion. Mol. Oncol. *3*, 366–375.
- [21] Bretou, M., Sáez, P.J., Sanséau, D., Maurin, M., Lankar, D., Chabaud, M., Spampanato, C., Malbec, O., Barbier, L., Muallem, S., et al. (2017). Lysosome signaling controls the migration of dendritic cells. Sci. Immunol. 2.
- [22] Brubaker, S.W., Bonham, K.S., Zanoni, I., and Kagan, J.C. (2015). Innate immune pattern recognition: a cell biological perspective. Annu. Rev. Immunol. *33*, 257–290.
- [23] Cadwell, K., Stappenbeck, T.S., and Virgin, H.W. (2009). Role of autophagy and autophagy genes in inflammatory bowel disease. Curr. Top. Microbiol. Immunol. *335*, 141–167.
- [24] Calcagnì, A., Kors, L., Verschuren, E., De Cegli, R., Zampelli, N., Nusco, E., Confalonieri, S., Bertalot, G., Pece, S., Settembre, C., et al. (2016). Modelling TFE renal cell carcinoma in mice reveals a critical role of WNT signaling. Elife 5.
- [25] Campbell, G.R., Rawat, P., Bruckman, R.S., and Spector, S.A. (2015). Human Immunodeficiency Virus Type 1 Nef Inhibits Autophagy through Transcription Factor EB Sequestration. PLoS Pathog. *11*, e1005018.
- [26] Cancer Genome Atlas Network (2012). Comprehensive molecular portraits of human breast tumours. Nature 490, 61–70.
- [27] Cancer Genome Atlas Network (2015). Genomic classification of cutaneous melanoma. Cell *161*, 1681–1696.
- [28] Carling, D. (2004). The AMP-activated protein kinase cascade--a unifying system for energy control. Trends Biochem. Sci. 29, 18–24.
- [29] Carmeliet, P. (2005). VEGF as a key mediator of angiogenesis in cancer. Oncology 69 Suppl 3, 4–10.
- [30] Cash, T.P., Gruber, J.J., Hartman, T.R., Henske, E.P., and Simon, M.C. (2011). Loss of the Birt-Hogg-Dubé tumor suppressor results in apoptotic resistance due to aberrant TGFβ-mediated transcription. Oncogene *30*, 2534–2546.
- [31] Chaffer, C.L., and Weinberg, R.A. (2011). A perspective on cancer cell metastasis. Science 331, 1559–1564.
- [32] Chagin, A.S. (2016). Effectors of mTOR-autophagy pathway: targeting cancer, affecting the skeleton. Curr. Opin. Pharmacol. 28, 1–7.
- [33] Chao, X., Wang, S., Zhao, K., Li, Y., Williams, J.A., Li, T., Chavan, H., Krishnamurthy, P., He, X.C., Li, L., et al. (2018). Impaired TFEB-Mediated Lysosome Biogenesis and Autophagy Promote Chronic Ethanol-Induced Liver Injury and Steatosis in Mice. Gastroenterology *155*, 865–879.e12.
- [34] Chaudary, N., and Hill, R.P. (2007). Hypoxia and metastasis. Clin. Cancer Res. 13, 1947–1949.

- [35] Chauhan, S., Kumar, S., Jain, A., Ponpuak, M., Mudd, M.H., Kimura, T., Choi, S.W., Peters, R., Mandell, M., Bruun, J.-A., et al. (2016). TRIMs and Galectins Globally Cooperate and TRIM16 and Galectin-3 Co-direct Autophagy in Endomembrane Damage Homeostasis. Dev. Cell *39*, 13–27.
- [36] Chen, N., and Karantza, V. (2011). Autophagy as a therapeutic target in cancer. Cancer Biol. Ther. 11, 157–168.
- [37] Chen, D., Xie, J., Fiskesund, R., Dong, W., Liang, X., Lv, J., Jin, X., Liu, J., Mo, S., Zhang, T., et al. (2018). Chloroquine modulates antitumor immune response by resetting tumor-associated macrophages toward M1 phenotype. Nat. Commun. *9*, 873.
- [38] Chen, J., Futami, K., Petillo, D., Peng, J., Wang, P., Knol, J., Li, Y., Khoo, S.-K., Huang, D., Qian, C.-N., et al. (2008). Deficiency of FLCN in mouse kidney led to development of polycystic kidneys and renal neoplasia. PLoS One *3*, e3581.
- [39] Chen, J., Huang, D., Rubera, I., Futami, K., Wang, P., Zickert, P., Khoo, S.-K., Dykema, K., Zhao, P., Petillo, D., et al. (2015). Disruption of tubular Flcn expression as a mouse model for renal tumor induction. Kidney Int. 88, 1057–1069.
- [40] Chia, S.K., Speers, C.H., D'yachkova, Y., Kang, A., Malfair-Taylor, S., Barnett, J., Coldman, A., Gelmon, K.A., O'reilly, S.E., and Olivotto, I.A. (2007). The impact of new chemotherapeutic and hormone agents on survival in a population-based cohort of women with metastatic breast cancer. Cancer *110*, 973–979.
- [41] Choi, A.M.K., Ryter, S.W., and Levine, B. (2013). Autophagy in human health and disease. N. Engl. J. Med. *368*, 651–662.
- [42] Choyke, P.L., Glenn, G.M., Walther, M.M., Zbar, B., and Linehan, W.M. (2003). Hereditary renal cancers. Radiology 226, 33–46.
- [43] Conway, E.M., Collen, D., and Carmeliet, P. (2001). Molecular mechanisms of blood vessel growth. Cardiovasc. Res. 49, 507–521.
- [44] Crotzer, V.L., and Blum, J.S. (2009). Autophagy and its role in MHC-mediated antigen presentation. J. Immunol. *182*, 3335–3341.
- [45] Dai, X., Li, T., Bai, Z., Yang, Y., Liu, X., Zhan, J., and Shi, B. (2015). Breast cancer intrinsic subtype classification, clinical use and future trends. Am. J. Cancer Res. 5, 2929–2943.
- [46] Dalby, K.N., Tekedereli, I., Lopez-Berestein, G., and Ozpolat, B. (2010). Targeting the prodeath and prosurvival functions of autophagy as novel therapeutic strategies in cancer. Autophagy 6, 322–329.
- [47] Dawson, S.J., Provenzano, E., and Caldas, C. (2009). Triple negative breast cancers: clinical and prognostic implications. Eur. J. Cancer 45 Suppl 1, 27–40.
- [48] De Duve, C., Pressman, B.C., Gianetto, R., Wattiaux, R., and Appelmans, F. (1955). Tissue fractionation studies. 6. Intracellular distribution patterns of enzymes in rat-liver tissue. Biochem. J. 60, 604–617.
- [49] Deretic, V. (2011). Autophagy in immunity and cell-autonomous defense against intracellular microbes. Immunol. Rev. 240, 92–104.
- [50] Deretic, V., Saitoh, T., and Akira, S. (2013). Autophagy in infection, inflammation and immunity. Nat. Rev. Immunol. *13*, 722–737.
- [51] Di Malta, C., Siciliano, D., Calcagni, A., Monfregola, J., Punzi, S., Pastore, N., Eastes, A.N., Davis, O., De Cegli, R., Zampelli, A., et al. (2017). Transcriptional activation of RagD GTPase controls mTORC1 and promotes cancer growth. Science *356*, 1188–1192.
- [52] Di Paola, S., Scotto-Rosato, A., and Medina, D.L. (2018). TRPML1: The Ca(2+)retaker of the lysosome. Cell Calcium *69*, 112–121.

- [53] Durinck, S., Stawiski, E.W., Pavía-Jiménez, A., Modrusan, Z., Kapur, P., Jaiswal, B.S., Zhang, N., Toffessi-Tcheuyap, V., Nguyen, T.T., Pahuja, K.B., et al. (2015). Spectrum of diverse genomic alterations define non-clear cell renal carcinoma subtypes. Nat. Genet. 47, 13–21.
- [54] Eichner, L.J., Brun, S.N., Herzig, S., Young, N.P., Curtis, S.D., Shackelford, D.B., Shokhirev, M.N., Leblanc, M., Vera, L.I., Hutchins, A., et al. (2019). Genetic Analysis Reveals AMPK Is Required to Support Tumor Growth in Murine Kras-Dependent Lung Cancer Models. Cell Metab. *29*, 285–302.e7.
- [55] El-Houjeiri, L., Possik, E., Vijayaraghavan, T., Paquette, M., Martina, J.A., Kazan, J.M., Ma, E.H., Jones, R., Blanchette, P., Puertollano, R., et al. (2019). The Transcription Factors TFEB and TFE3 Link the FLCN-AMPK Signaling Axis to Innate Immune Response and Pathogen Resistance. Cell Rep. 26, 3613–3628.e6.
- [56] Emanuel, R., Sergin, I., Bhattacharya, S., Turner, J., Epelman, S., Settembre, C., Diwan, A., Ballabio, A., and Razani, B. (2014). Induction of lysosomal biogenesis in atherosclerotic macrophages can rescue lipid-induced lysosomal dysfunction and downstream sequelae. Arterioscler. Thromb. Vasc. Biol. *34*, 1942–1952.
- [57] Ermolaeva, M.A., and Schumacher, B. (2014). Insights from the worm: the C. elegans model for innate immunity. Semin. Immunol. 26, 303–309.
- [58] Evans, J.M.M., Donnelly, L.A., Emslie-Smith, A.M., Alessi, D.R., and Morris, A.D. (2005). Metformin and reduced risk of cancer in diabetic patients. BMJ *330*, 1304–1305.
- [59] Fang, L., Hodge, J., Saaoud, F., Wang, J., Iwanowycz, S., Wang, Y., Hui, Y., Evans, T.D., Razani, B., and Fan, D. (2017). Transcriptional factor EB regulates macrophage polarization in the tumor microenvironment. Oncoimmunology *6*, e1312042.
- [60] Ferron, M., Settembre, C., Shimazu, J., Lacombe, J., Kato, S., Rawlings, D.J., Ballabio, A., and Karsenty, G. (2013). A RANKL-PKCβ-TFEB signaling cascade is necessary for lysosomal biogenesis in osteoclasts. Genes Dev. *27*, 955–969.
- [61] Folkman, J. (1971). Tumor angiogenesis: therapeutic implications. N. Engl. J. Med. 285, 1182–1186.
- [62] Fuse, N., Yasumoto, K. i, Takeda, K., Amae, S., Yoshizawa, M., Udono, T., Takahashi, K., Tamai, M., Tomita, Y., Tachibana, M., et al. (1999). Molecular cloning of cDNA encoding a novel microphthalmia-associated transcription factor isoform with a distinct amino-terminus. J. Biochem. *126*, 1043–1051.
- [63] Futreal, P.A., Coin, L., Marshall, M., Down, T., Hubbard, T., Wooster, R., Rahman, N., and Stratton, M.R. (2004). A census of human cancer genes. Nat. Rev. Cancer 4, 177–183.
- [64] Gharbi, H., Fabretti, F., Bharill, P., Rinschen, M.M., Brinkkötter, S., Frommolt, P., Burst, V., Schermer, B., Benzing, T., and Müller, R.-U. (2013). Loss of the Birt-Hogg-Dubé gene product folliculin induces longevity in a hypoxia-inducible factor-dependent manner. Aging Cell *12*, 593–603.
- [65] Gray, M.A., Choy, C.H., Dayam, R.M., Ospina-Escobar, E., Somerville, A., Xiao, X., Ferguson, S.M., and Botelho, R.J. (2016). Phagocytosis enhances lysosomal and bactericidal properties by activating the transcription factor TFEB. Curr. Biol. *26*, 1955–1964.
- [66] Gruber, G., Greiner, R.H., Hlushchuk, R., Aebersold, D.M., Altermatt, H.J., Berclaz, G., and Djonov, V. (2004). Hypoxia-inducible factor 1 alpha in high-risk breast cancer: an independent prognostic parameter? Breast Cancer Res. 6, R191-8.
- [67] Guertin, D.A., and Sabatini, D.M. (2007). Defining the role of mTOR in cancer. Cancer Cell 12, 9–22.
- [68] Guo, J.Y., and White, E. (2016). Autophagy, metabolism, and cancer. Cold Spring Harb.

- Symp. Quant. Biol. *81*, 73–78.
- [69] Gupta, S., Johnson, S.H., Vasmatzis, G., Porath, B., Rustin, J.G., Rao, P., Costello, B.A., Leibovich, B.C., Thompson, R.H., Cheville, J.C., et al. (2017). TFEB-VEGFA (6p21.1) coamplified renal cell carcinoma: a distinct entity with potential implications for clinical management. Mod. Pathol. *30*, 998–1012.
- [70] Gwinn, D.M., Shackelford, D.B., Egan, D.F., Mihaylova, M.M., Mery, A., Vasquez, D.S., Turk, B.E., and Shaw, R.J. (2008). AMPK phosphorylation of raptor mediates a metabolic checkpoint. Mol. Cell *30*, 214–226.
- [71] Hakimi, A.A., Reznik, E., Lee, C.-H., Creighton, C.J., Brannon, A.R., Luna, A., Aksoy, B.A., Liu, E.M., Shen, R., Lee, W., et al. (2016). An integrated metabolic atlas of clear cell renal cell carcinoma. Cancer Cell *29*, 104–116.
- [72] Hallsson, J.H., Favor, J., Hodgkinson, C., Glaser, T., Lamoreux, M.L., Magnúsdóttir, R., Gunnarsson, G.J., Sweet, H.O., Copeland, N.G., Jenkins, N.A., et al. (2000). Genomic, transcriptional and mutational analysis of the mouse microphthalmia locus. Genetics *155*, 291–300.
- [73] Hallsson, J.H., Haflidadóttir, B.S., Stivers, C., Odenwald, W., Arnheiter, H., Pignoni, F., and Steingrímsson, E. (2004). The basic helix-loop-helix leucine zipper transcription factor Mitf is conserved in Drosophila and functions in eye development. Genetics *167*, 233–241.
- [74] Hanahan, D., and Folkman, J. (1996). Patterns and emerging mechanisms of the angiogenic switch during tumorigenesis. Cell *86*, 353–364.
- [75] Hanahan, D., and Weinberg, R.A. (2011). Hallmarks of cancer: the next generation. Cell 144, 646–674.
- [76] Handschin, C., and Spiegelman, B.M. (2008). The role of exercise and PGC1alpha in inflammation and chronic disease. Nature 454, 463–469.
- [77] Hanks, S.K., Quinn, A.M., and Hunter, T. (1988). The protein kinase family: conserved features and deduced phylogeny of the catalytic domains. Science 241, 42–52.
- [78] Haq, R., and Fisher, D.E. (2011). Biology and clinical relevance of the micropthalmia family of transcription factors in human cancer. JCO 29, 3474–3482.
- [79] Harrison, D.E., Strong, R., Sharp, Z.D., Nelson, J.F., Astle, C.M., Flurkey, K., Nadon, N.L., Wilkinson, J.E., Frenkel, K., Carter, C.S., et al. (2009). Rapamycin fed late in life extends lifespan in genetically heterogeneous mice. Nature *460*, 392–395.
- [80] Hasumi, H., Baba, M., Hong, S.-B., Hasumi, Y., Huang, Y., Yao, M., Valera, V.A., Linehan, W.M., and Schmidt, L.S. (2008). Identification and characterization of a novel folliculin-interacting protein FNIP2. Gene *415*, 60–67.
- [81] Hasumi, H., Baba, M., Hasumi, Y., Lang, M., Huang, Y., Oh, H.F., Matsuo, M., Merino, M.J., Yao, M., Ito, Y., et al. (2015). Folliculin-interacting proteins Fnip1 and Fnip2 play critical roles in kidney tumor suppression in cooperation with Flcn. Proc. Natl. Acad. Sci. USA *112*, E1624-31.
- [82] Hasumi, Y., Baba, M., Ajima, R., Hasumi, H., Valera, V.A., Klein, M.E., Haines, D.C., Merino, M.J., Hong, S.-B., Yamaguchi, T.P., et al. (2009). Homozygous loss of BHD causes early embryonic lethality and kidney tumor development with activation of mTORC1 and mTORC2. Proc. Natl. Acad. Sci. USA *106*, 18722–18727.
- [83] Hasumi, Y., Baba, M., Hasumi, H., Huang, Y., Lang, M., Reindorf, R., Oh, H., Sciarretta, S., Nagashima, K., Haines, D.C., et al. (2014). Folliculin (Flcn) inactivation leads to murine cardiac hypertrophy through mTORC1 deregulation. Hum. Mol. Genet. *23*, 5706–5719.
- [84] Hayama, Y., Kimura, T., Takeda, Y., Nada, S., Koyama, S., Takamatsu, H., Kang, S., Ito,

- D., Maeda, Y., Nishide, M., et al. (2018). Lysosomal protein lamtor1 controls innate immune responses via nuclear translocation of transcription factor EB. J. Immunol. 200, 3790–3800.
- [85] Hemesath, T.J., Steingrímsson, E., McGill, G., Hansen, M.J., Vaught, J., Hodgkinson, C.A., Arnheiter, H., Copeland, N.G., Jenkins, N.A., and Fisher, D.E. (1994). microphthalmia, a critical factor in melanocyte development, defines a discrete transcription factor family. Genes Dev. *8*, 2770–2780.
- [86] Hershey, C.L., and Fisher, D.E. (2005). Genomic analysis of the Microphthalmia locus and identification of the MITF-J/Mitf-J isoform. Gene *347*, 73–82.
- [87] Hong, S.-B., Oh, H., Valera, V.A., Stull, J., Ngo, D.-T., Baba, M., Merino, M.J., Linehan, W.M., and Schmidt, L.S. (2010a). Tumor suppressor FLCN inhibits tumorigenesis of a FLCN-null renal cancer cell line and regulates expression of key molecules in TGF-beta signaling. Mol. Cancer *9*, 160.
- [88] Hong, S.-B., Oh, H., Valera, V.A., Baba, M., Schmidt, L.S., and Linehan, W.M. (2010b). Inactivation of the FLCN tumor suppressor gene induces TFE3 transcriptional activity by increasing its nuclear localization. PLoS One *5*, e15793.
- [89] Huang, J., and Klionsky, D.J. (2007). Autophagy and human disease. Cell Cycle 6, 1837–1849.
- [90] Hudon, V., Sabourin, S., Dydensborg, A.B., Kottis, V., Ghazi, A., Paquet, M., Crosby, K., Pomerleau, V., Uetani, N., and Pause, A. (2010). Renal tumour suppressor function of the Birt-Hogg-Dubé syndrome gene product folliculin. J. Med. Genet. 47, 182–189.
- [91] Huo, Y., Cai, H., Teplova, I., Bowman-Colin, C., Chen, G., Price, S., Barnard, N., Ganesan, S., Karantza, V., White, E., et al. (2013). Autophagy opposes p53-mediated tumor barrier to facilitate tumorigenesis in a model of PALB2-associated hereditary breast cancer. Cancer Discov. 3, 894–907.
- [92] Inoki, K., Li, Y., Zhu, T., Wu, J., and Guan, K.-L. (2002). TSC2 is phosphorylated and inhibited by Akt and suppresses mTOR signalling. Nat. Cell Biol. 4, 648–657.
- [93] Irazoqui, J.E., Troemel, E.R., Feinbaum, R.L., Luhachack, L.G., Cezairliyan, B.O., and Ausubel, F.M. (2010). Distinct pathogenesis and host responses during infection of C. elegans by P. aeruginosa and S. aureus. PLoS Pathog. *6*, e1000982.
- [94] Iwai, K., Yamanaka, K., Kamura, T., Minato, N., Conaway, R.C., Conaway, J.W., Klausner, R.D., and Pause, A. (1999). Identification of the von Hippel-lindau tumor-suppressor protein as part of an active E3 ubiquitin ligase complex. Proc. Natl. Acad. Sci. USA *96*, 12436–12441.
- [95] Jager, S., Handschin, C., St-Pierre, J., and Spiegelman, B.M. (2007). AMP activated protein kinase (AMPK) action in skeletal muscle via direct phosphorylation of PGC-1alpha. Proc. Natl. Acad. Sci. USA, V. 104, P. 12017-12022.
- [96] Jebbink, J.M., Boot, R.G., Keijser, R., Moerland, P.D., Aten, J., Veenboer, G.J.M., van Wely, M., Buimer, M., Ver Loren van Themaat, E., Aerts, J.M.F.G., et al. (2015). Increased glucocerebrosidase expression and activity in preeclamptic placenta. Placenta *36*, 160–169.
- [97] Jeong, J.-H., Ojha, U., and Lee, Y.M. (2021). Pathological angiogenesis and inflammation in tissues. Arch. Pharm. Res. 44, 1–15.
- [98] Jiang, S., Dupont, N., Castillo, E.F., and Deretic, V. (2013). Secretory versus degradative autophagy: unconventional secretion of inflammatory mediators. J Innate Immun *5*, 471–479.
- [99] Kauffman, E.C., Ricketts, C.J., Rais-Bahrami, S., Yang, Y., Merino, M.J., Bottaro, D.P., Srinivasan, R., and Linehan, W.M. (2014). Molecular genetics and cellular features of TFE3 and TFEB fusion kidney cancers. Nat. Rev. Urol. *11*, 465–475.

- [100] Kenyon, E.J., Luijten, M.N.H., Gill, H., Li, N., Rawlings, M., Bull, J.C., Hadzhiev, Y., van Steensel, M.A.M., Maher, E., and Mueller, F. (2016). Expression and knockdown of zebrafish folliculin suggests requirement for embryonic brain morphogenesis. BMC Dev. Biol. *16*, 23.
- [101] Khabibullin, D., Medvetz, D.A., Pinilla, M., Hariharan, V., Li, C., Hergrueter, A., Laucho Contreras, M., Zhang, E., Parkhitko, A., Yu, J.J., et al. (2014). Folliculin regulates cell-cell adhesion, AMPK, and mTORC1 in a cell-type-specific manner in lung-derived cells. Physiol. Rep. 2.
- [102] Kim, Y.C., and Guan, K.-L. (2015). mTOR: a pharmacologic target for autophagy regulation. J. Clin. Invest. 125, 25–32.
- [103] Kim, E., Goraksha-Hicks, P., Li, L., Neufeld, T.P., and Guan, K.-L. (2008). Regulation of TORC1 by Rag GTPases in nutrient response. Nat. Cell Biol. *10*, 935–945.
- [104] Kim, J., Yang, G., Kim, Y., Kim, J., and Ha, J. (2016). AMPK activators: mechanisms of action and physiological activities. Exp Mol Med 48, e224.
- [105] Kim, Y.C., Park, H.W., Sciarretta, S., Mo, J.-S., Jewell, J.L., Russell, R.C., Wu, X., Sadoshima, J., and Guan, K.-L. (2014). Rag GTPases are cardioprotective by regulating lysosomal function. Nat. Commun. *5*, 4241.
- [106] Kim, Y.S., Lee, H.-M., Kim, J.K., Yang, C.-S., Kim, T.S., Jung, M., Jin, H.S., Kim, S., Jang, J., Oh, G.T., et al. (2017). PPAR-α Activation Mediates Innate Host Defense through Induction of TFEB and Lipid Catabolism. J. Immunol. *198*, 3283–3295.
- [107] Klionsky, D.J. (2005). The molecular machinery of autophagy: unanswered questions. J. Cell Sci. 118, 7–18.
- [108] Laderoute, K.R., Calaoagan, J.M., Gustafson-Brown, C., Knapp, A.M., Li, G.-C., Mendonca, H.L., Ryan, H.E., Wang, Z., and Johnson, R.S. (2002). The response of c-jun/AP-1 to chronic hypoxia is hypoxia-inducible factor 1 alpha dependent. Mol. Cell. Biol. *22*, 2515–2523.
- [109] Laplante, M., and Sabatini, D.M. (2009). mTOR signaling at a glance. J. Cell Sci. 122, 3589–3594.
- [110] Laviolette, L.A., Wilson, J., Koller, J., Neil, C., Hulick, P., Rejtar, T., Karger, B., Teh, B.T., and Iliopoulos, O. (2013). Human folliculin delays cell cycle progression through late S and G2/M-phases: effect of phosphorylation and tumor associated mutations. PLoS One *8*, e66775.
- [111] Lawrence, T. (2009). The nuclear factor NF-kappaB pathway in inflammation. Cold Spring Harb. Perspect. Biol. *1*, a001651.
- [112] Lawrence, R.E., Fromm, S.A., Fu, Y., Yokom, A.L., Kim, D.J., Thelen, A.M., Young, L.N., Lim, C.-Y., Samelson, A.J., Hurley, J.H., et al. (2019). Structural mechanism of a Rag GTPase activation checkpoint by the lysosomal folliculin complex. Science *366*, 971–977.
- [113] Lazar, A.J.F., Das, P., Tuvin, D., Korchin, B., Zhu, Q., Jin, Z., Warneke, C.L., Zhang, P.S., Hernandez, V., Lopez-Terrada, D., et al. (2007). Angiogenesis-promoting gene patterns in alveolar soft part sarcoma. Clin. Cancer Res. *13*, 7314–7321.
- [114] Lee, E.Y.H.P., and Muller, W.J. (2010). Oncogenes and tumor suppressor genes. Cold Spring Harb. Perspect. Biol. 2, a003236.
- [115] Lee, W.J., Kim, M., Park, H.-S., Kim, H.S., Jeon, M.J., Oh, K.S., Koh, E.H., Won, J.C., Kim, M.-S., Oh, G.T., et al. (2006). AMPK activation increases fatty acid oxidation in skeletal muscle by activating PPARalpha and PGC-1. Biochem. Biophys. Res. Commun. *340*, 291–295.
- [116] Lehmann, B.D., Bauer, J.A., Chen, X., Sanders, M.E., Chakravarthy, A.B., Shyr, Y., and Pietenpol, J.A. (2011). Identification of human triple-negative breast cancer subtypes and preclinical models for selection of targeted therapies. J. Clin. Invest. *121*, 2750–2767.
- [117] Levine, B. (2007). Cell biology: autophagy and cancer. Nature 446, 745–747.

- [118] Levine, B., and Klionsky, D.J. (2004). Development by self-digestion: molecular mechanisms and biological functions of autophagy. Dev. Cell *6*, 463–477.
- [119] Levine, T.P., Daniels, R.D., Gatta, A.T., Wong, L.H., and Hayes, M.J. (2013). The product of C9orf72, a gene strongly implicated in neurodegeneration, is structurally related to DENN Rab-GEFs. Bioinformatics *29*, 499–503.
- [120] Li, J., Wada, S., Weaver, L.K., Biswas, C., Behrens, E.M., and Arany, Z. (2019). Myeloid Folliculin balances mTOR activation to maintain innate immunity homeostasis. JCI Insight 5.
- [121] Li, M., Pi, H., Yang, Z., Reiter, R.J., Xu, S., Chen, X., Chen, C., Zhang, L., Yang, M., Li, Y., et al. (2016). Melatonin antagonizes cadmium-induced neurotoxicity by activating the transcription factor EB-dependent autophagy-lysosome machinery in mouse neuroblastoma cells. J Pineal Res *61*, 353–369.
- [122] Liang, C., and Jung, J.U. (2010). Autophagy genes as tumor suppressors. Curr. Opin. Cell Biol. 22, 226–233.
- [123] Lim, D.H.K., Rehal, P.K., Nahorski, M.S., Macdonald, F., Claessens, T., Van Geel, M., Gijezen, L., Gille, J.J.P., Giraud, S., Richard, S., et al. (2010). A new locus-specific database (LSDB) for mutations in the folliculin (FLCN) gene. Hum. Mutat. 31, E1043-51.
- [124] Linderholm, B.K., Hellborg, H., Johansson, U., Elmberger, G., Skoog, L., Lehtiö, J., and Lewensohn, R. (2009). Significantly higher levels of vascular endothelial growth factor (VEGF) and shorter survival times for patients with primary operable triple-negative breast cancer. Ann. Oncol. 20, 1639–1646.
- [125] Linehan, W.M., Srinivasan, R., and Schmidt, L.S. (2010). The genetic basis of kidney cancer: a metabolic disease. Nat. Rev. Urol. 7, 277–285.
- [126] Liu, W., Chen, Z., Ma, Y., Wu, X., Jin, Y., and Hou, S. (2013). Genetic characterization of the Drosophila birt-hogg-dubé syndrome gene. PLoS One 8, e65869.
- [127] Lock, R., Roy, S., Kenific, C.M., Su, J.S., Salas, E., Ronen, S.M., and Debnath, J. (2011). Autophagy facilitates glycolysis during Ras-mediated oncogenic transformation. Mol. Biol. Cell 22, 165–178.
- [128] Mansueto, G., Armani, A., Viscomi, C., D'Orsi, L., De Cegli, R., Polishchuk, E.V., Lamperti, C., Di Meo, I., Romanello, V., Marchet, S., et al. (2017). Transcription Factor EB Controls Metabolic Flexibility during Exercise. Cell Metab. *25*, 182–196.
- [129] Marat, A.L., Dokainish, H., and McPherson, P.S. (2011). DENN domain proteins: regulators of Rab GTPases. J. Biol. Chem. 286, 13791–13800.
- [130] Martina, J.A., and Puertollano, R. (2013). Rag GTPases mediate amino acid-dependent recruitment of TFEB and MITF to lysosomes. J. Cell Biol. 200, 475–491.
- [131] Martina, J.A., Diab, H.I., Lishu, L., Jeong-A, L., Patange, S., Raben, N., and Puertollano, R. (2014). The nutrient-responsive transcription factor TFE3 promotes autophagy, lysosomal biogenesis, and clearance of cellular debris. Sci. Signal. 7, ra9.
- [132] Martina, J.A., Diab, H.I., Brady, O.A., and Puertollano, R. (2016). TFEB and TFE3 are novel components of the integrated stress response. EMBO J. 35, 479–495.
- [133] Mathew, R., Karantza-Wadsworth, V., and White, E. (2007). Role of autophagy in cancer. Nat. Rev. Cancer *7*, 961–967.
- [134] Medina, D.L., Di Paola, S., Peluso, I., Armani, A., De Stefani, D., Venditti, R., Montefusco, S., Scotto-Rosato, A., Prezioso, C., Forrester, A., et al. (2015). Lysosomal calcium signalling regulates autophagy through calcineurin and TFEB. Nat. Cell Biol. *17*, 288–299.
- [135] Mihaylova, M.M., and Shaw, R.J. (2011). The AMPK signalling pathway coordinates cell growth, autophagy and metabolism. Nat. Cell Biol. *13*, 1016–1023.

- [136] Mizushima, N. (2007). Autophagy: process and function. Genes Dev. 21, 2861–2873.
- [137] Mo, H.Y., Son, H.J., Choi, E.J., Yoo, N.J., An, C.H., and Lee, S.H. (2019). Somatic mutations of candidate tumor suppressor genes folliculin-interacting proteins FNIP1 and FNIP2 in gastric and colon cancers. Pathol Res Pract *215*, 152646.
- [138] Mossmann, D., Park, S., and Hall, M.N. (2018). mTOR signalling and cellular metabolism are mutual determinants in cancer. Nat. Rev. Cancer 18, 744–757.
- [139] Nakagawa, Y., Shimano, H., Yoshikawa, T., Ide, T., Tamura, M., Furusawa, M., Yamamoto, T., Inoue, N., Matsuzaka, T., Takahashi, A., et al. (2006). TFE3 transcriptionally activates hepatic IRS-2, participates in insulin signaling and ameliorates diabetes. Nat. Med. *12*, 107–113.
- [140] Napolitano, G., and Ballabio, A. (2016). TFEB at a glance. J. Cell Sci. 129, 2475–2481.
- [141] Napolitano, G., Di Malta, C., Esposito, A., de Araujo, M.E.G., Pece, S., Bertalot, G., Matarese, M., Benedetti, V., Zampelli, A., Stasyk, T., et al. (2020). A substrate-specific mTORC1 pathway underlies Birt-Hogg-Dubé syndrome. Nature *585*, 597–602.
- [142] Nickerson, M.L., Warren, M.B., Toro, J.R., Matrosova, V., Glenn, G., Turner, M.L., Duray, P., Merino, M., Choyke, P., Pavlovich, C.P., et al. (2002). Mutations in a novel gene lead to kidney tumors, lung wall defects, and benign tumors of the hair follicle in patients with the Birt-Hogg-Dubé syndrome. Cancer Cell *2*, 157–164.
- [143] Nookala, R.K., Langemeyer, L., Pacitto, A., Ochoa-Montaño, B., Donaldson, J.C., Blaszczyk, B.K., Chirgadze, D.Y., Barr, F.A., Bazan, J.F., and Blundell, T.L. (2012). Crystal structure of folliculin reveals a hidDENN function in genetically inherited renal cancer. Open Biol *2*, 120071.
- [144] Oboki, K., Morii, E., Kataoka, T.R., Jippo, T., and Kitamura, Y. (2002). Isoforms of mi transcription factor preferentially expressed in cultured mast cells of mice. Biochem. Biophys. Res. Commun. 290, 1250–1254.
- [145] Oh, W.J., and Jacinto, E. (2011). mTOR complex 2 signaling and functions. Cell Cycle 10, 2305–2316.
- [146] Orimo, A., and Weinberg, R.A. (2006). Stromal fibroblasts in cancer: a novel tumor-promoting cell type. Cell Cycle 5, 1597–1601.
- [147] Pacitto, A. (2015). Towards structural and functional understanding of the Flcn/Fnip complex through its yeast orthologue Lst7/Lst4. Undergraduate thesis.
- [148] Palmieri, M., Impey, S., Kang, H., di Ronza, A., Pelz, C., Sardiello, M., and Ballabio, A. (2011). Characterization of the CLEAR network reveals an integrated control of cellular clearance pathways. Hum. Mol. Genet. 20, 3852–3866.
- [149] Palmieri, M., Pal, R., Nelvagal, H.R., Lotfi, P., Stinnett, G.R., Seymour, M.L., Chaudhury, A., Bajaj, L., Bondar, V.V., Bremner, L., et al. (2017). mTORC1-independent TFEB activation via Akt inhibition promotes cellular clearance in neurodegenerative storage diseases. Nat. Commun. 8, 14338.
- [150] Paquette, M., El-Houjeiri, L., and Pause, A. (2018). mTOR Pathways in Cancer and Autophagy. Cancers (Basel) 10.
- [151] Paquette, M., El-Houjeiri, L., C Zirden, L., Puustinen, P., Blanchette, P., Jeong, H., Dejgaard, K., Siegel, P.M., and Pause, A. (2021). AMPK-dependent phosphorylation is required for transcriptional activation of TFEB and TFE3. Autophagy 1–19.
- [152] Parkhitko, A.A., Priolo, C., Coloff, J.L., Yun, J., Wu, J.J., Mizumura, K., Xu, W., Malinowska, I.A., Yu, J., Kwiatkowski, D.J., et al. (2014). Autophagy-dependent metabolic reprogramming sensitizes TSC2-deficient cells to the antimetabolite 6-aminonicotinamide. Mol.

- Cancer Res. 12, 48–57.
- [153] Pastore, N., Brady, O.A., Diab, H.I., Martina, J.A., Sun, L., Huynh, T., Lim, J.-A., Zare, H., Raben, N., Ballabio, A., et al. (2016). TFEB and TFE3 cooperate in the regulation of the innate immune response in activated macrophages. Autophagy *12*, 1240–1258.
- [154] Pastore, N., Vainshtein, A., Klisch, T.J., Armani, A., Huynh, T., Herz, N.J., Polishchuk, E.V., Sandri, M., and Ballabio, A. (2017). TFE3 regulates whole-body energy metabolism in cooperation with TFEB. EMBO Mol. Med. 9, 605–621.
- [155] Péli-Gulli, M.-P., Sardu, A., Panchaud, N., Raucci, S., and De Virgilio, C. (2015). Amino Acids Stimulate TORC1 through Lst4-Lst7, a GTPase-Activating Protein Complex for the Rag Family GTPase Gtr2. Cell Rep. 13, 1–7.
- [156] Perera, R.M., Stoykova, S., Nicolay, B.N., Ross, K.N., Fitamant, J., Boukhali, M., Lengrand, J., Deshpande, V., Selig, M.K., Ferrone, C.R., et al. (2015). Transcriptional control of autophagy-lysosome function drives pancreatic cancer metabolism. Nature *524*, 361–365.
- [157] Perou, C.M., Sørlie, T., Eisen, M.B., van de Rijn, M., Jeffrey, S.S., Rees, C.A., Pollack, J.R., Ross, D.T., Johnsen, H., Akslen, L.A., et al. (2000). Molecular portraits of human breast tumours. Nature 406, 747–752.
- [158] Petit, C.S., Roczniak-Ferguson, A., and Ferguson, S.M. (2013). Recruitment of folliculin to lysosomes supports the amino acid-dependent activation of Rag GTPases. J. Cell Biol. 202, 1107–1122.
- [159] Ploper, D., Taelman, V.F., Robert, L., Perez, B.S., Titz, B., Chen, H.-W., Graeber, T.G., von Euw, E., Ribas, A., and De Robertis, E.M. (2015). MITF drives endolysosomal biogenesis and potentiates Wnt signaling in melanoma cells. Proc. Natl. Acad. Sci. USA *112*, E420-9.
- [160] Pogenberg, V., Ogmundsdóttir, M.H., Bergsteinsdóttir, K., Schepsky, A., Phung, B., Deineko, V., Milewski, M., Steingrímsson, E., and Wilmanns, M. (2012). Restricted leucine zipper dimerization and specificity of DNA recognition of the melanocyte master regulator MITF. Genes Dev. 26, 2647–2658.
- [161] Popp, L., Gomez, E., Orji, W., Ho, M., Suh, J., and Segatori, L. (2017). TFEB-mediated activation of the lysosome-autophagy system affects the transduction efficiency of adenoassociated virus 2. Virology 510, 1–8.
- [162] Possik, E., Jalali, Z., Nouët, Y., Yan, M., Gingras, M.-C., Schmeisser, K., Panaite, L., Dupuy, F., Kharitidi, D., Chotard, L., et al. (2014). Folliculin regulates ampk-dependent autophagy and metabolic stress survival. PLoS Genet. *10*, e1004273.
- [163] Possik, E., Ajisebutu, A., Manteghi, S., Gingras, M.-C., Vijayaraghavan, T., Flamand, M., Coull, B., Schmeisser, K., Duchaine, T., van Steensel, M., et al. (2015). FLCN and AMPK confer resistance to hyperosmotic stress via remodeling of glycogen stores. PLoS Genet. 11, e1005520.
- [164] Powis, G., and Kirkpatrick, L. (2004). Hypoxia inducible factor-1alpha as a cancer drug target. Mol. Cancer Ther. *3*, 647–654.
- [165] Prat, A., Pineda, E., Adamo, B., Galván, P., Fernández, A., Gaba, L., Díez, M., Viladot, M., Arance, A., and Muñoz, M. (2015). Clinical implications of the intrinsic molecular subtypes of breast cancer. Breast *24 Suppl 2*, S26-35.
- [166] Preston, R.S., Philp, A., Claessens, T., Gijezen, L., Dydensborg, A.B., Dunlop, E.A., Harper, K.T., Brinkhuizen, T., Menko, F.H., Davies, D.M., et al. (2011). Absence of the Birt-Hogg-Dubé gene product is associated with increased hypoxia-inducible factor transcriptional activity and a loss of metabolic flexibility. Oncogene *30*, 1159–1173.
- [167] Puertollano, R., Ferguson, S.M., Brugarolas, J., and Ballabio, A. (2018). The complex relationship between TFEB transcription factor phosphorylation and subcellular localization.

- EMBO J. 37.
- [168] Puigserver, P. (2005). Tissue-specific regulation of metabolic pathways through the transcriptional coactivator PGC1-alpha. Int. J. Obes. 29 Suppl 1, S5-9.
- [169] Rabanal-Ruiz, Y., and Korolchuk, V.I. (2018). mTORC1 and Nutrient Homeostasis: The Central Role of the Lysosome. Int. J. Mol. Sci. 19.
- [170] Roberg, K.J., Bickel, S., Rowley, N., and Kaiser, C.A. (1997). Control of amino acid permease sorting in the late secretory pathway of Saccharomyces cerevisiae by SEC13, LST4, LST7 and LST8. Genetics *147*, 1569–1584.
- [171] Saftig, P., and Haas, A. (2016). Turn up the lysosome. Nat. Cell Biol. 18, 1025–1027.
- [172] Sager, R.A., Woodford, M.R., and Mollapour, M. (2018). The mTOR Independent Function of Tsc1 and FNIPs. Trends Biochem. Sci. 43, 935–937.
- [173] Sager, R.A., Woodford, M.R., Backe, S.J., Makedon, A.M., Baker-Williams, A.J., DiGregorio, B.T., Loiselle, D.R., Haystead, T.A., Zachara, N.E., Prodromou, C., et al. (2019). Post-translational Regulation of FNIP1 Creates a Rheostat for the Molecular Chaperone Hsp90. Cell Rep. 26, 1344–1356.e5.
- [174] Salma, N., Song, J.S., Arany, Z., and Fisher, D.E. (2015). Transcription Factor Tfe3 Directly Regulates Pgc-1alpha in Muscle. J. Cell Physiol. 230, 2330–2336.
- [175] Samie, M., and Cresswell, P. (2015). The transcription factor TFEB acts as a molecular switch that regulates exogenous antigen-presentation pathways. Nat. Immunol. *16*, 729–736.
- [176] Sancak, Y., Peterson, T.R., Shaul, Y.D., Lindquist, R.A., Thoreen, C.C., Bar-Peled, L., and Sabatini, D.M. (2008). The Rag GTPases bind raptor and mediate amino acid signaling to mTORC1. Science 320, 1496–1501.
- [177] Sancak, Y., Bar-Peled, L., Zoncu, R., Markhard, A.L., Nada, S., and Sabatini, D.M. (2010). Ragulator-Rag complex targets mTORC1 to the lysosomal surface and is necessary for its activation by amino acids. Cell *141*, 290–303.
- [178] Santanam, U., Banach-Petrosky, W., Abate-Shen, C., Shen, M.M., White, E., and DiPaola, R.S. (2016). Atg7 cooperates with Pten loss to drive prostate cancer tumor growth. Genes Dev. *30*, 399–407.
- [179] Sardiello, M., Palmieri, M., di Ronza, A., Medina, D.L., Valenza, M., Gennarino, V.A., Di Malta, C., Donaudy, F., Embrione, V., Polishchuk, R.S., et al. (2009). A gene network regulating lysosomal biogenesis and function. Science *325*, 473–477.
- [180] Sato, S., Roberts, K., Gambino, G., Cook, A., Kouzarides, T., and Goding, C.R. (1997). CBP/p300 as a co-factor for the Microphthalmia transcription factor. Oncogene *14*, 3083–3092.
- [181] Saxton, R.A., and Sabatini, D.M. (2017). mTOR Signaling in Growth, Metabolism, and Disease. Cell.
- [182] Schmid, D., and Münz, C. (2005). Immune surveillance of intracellular pathogens via autophagy. Cell Death Differ. *12 Suppl 2*, 1519–1527.
- [183] Schmidt, L.S., and Linehan, W.M. (2015). Molecular genetics and clinical features of Birt-Hogg-Dubé syndrome. Nat. Rev. Urol. *12*, 558–569.
- [184] Schmidt, L.S., and Linehan, W.M. (2018). FLCN: The causative gene for Birt-Hogg-Dubé syndrome. Gene *640*, 28–42.
- [185] Scott, R.C., Schuldiner, O., and Neufeld, T.P. (2004). Role and regulation of starvation-induced autophagy in the Drosophila fat body. Dev. Cell 7, 167–178.
- [186] Sekiguchi, T., Hirose, E., Nakashima, N., Ii, M., and Nishimoto, T. (2001). Novel G proteins, Rag C and Rag D, interact with GTP-binding proteins, Rag A and Rag B. J. Biol. Chem. 276, 7246–7257.

- [187] Semenza, G.L. (2000). HIF-1 and human disease: one highly involved factor. Genes Dev. 14, 1983–1991.
- [188] Settembre, C., Di Malta, C., Polito, V.A., Garcia Arencibia, M., Vetrini, F., Erdin, S., Erdin, S.U., Huynh, T., Medina, D., Colella, P., et al. (2011). TFEB links autophagy to lysosomal biogenesis. Science *332*, 1429–1433.
- [189] Settembre, C., Zoncu, R., Medina, D.L., Vetrini, F., Erdin, S., Erdin, S., Huynh, T., Ferron, M., Karsenty, G., Vellard, M.C., et al. (2012). A lysosome-to-nucleus signalling mechanism senses and regulates the lysosome via mTOR and TFEB. EMBO J. 31, 1095–1108.
- [190] Settembre, C., De Cegli, R., Mansueto, G., Saha, P.K., Vetrini, F., Visvikis, O., Huynh, T., Carissimo, A., Palmer, D., Klisch, T.J., et al. (2013a). TFEB controls cellular lipid metabolism through a starvation-induced autoregulatory loop. Nat. Cell Biol. *15*, 647–658.
- [191] Settembre, C., Fraldi, A., Medina, D.L., and Ballabio, A. (2013b). Signals from the lysosome: a control centre for cellular clearance and energy metabolism. Nat. Rev. Mol. Cell Biol. 14, 283–296.
- [192] Shackelford, D.B., and Shaw, R.J. (2009). The LKB1-AMPK pathway: metabolism and growth control in tumour suppression. Nat. Rev. Cancer *9*, 563–575.
- [193] Shaw, R.J. (2006). Glucose metabolism and cancer. Curr. Opin. Cell Biol. 18, 598–608.
- [194] Shaw, R.J., Kosmatka, M., Bardeesy, N., Hurley, R.L., Witters, L.A., DePinho, R.A., and Cantley, L.C. (2004). The tumor suppressor LKB1 kinase directly activates AMP-activated kinase and regulates apoptosis in response to energy stress. Proc. Natl. Acad. Sci. USA *101*, 3329–3335.
- [195] Shen, K., Rogala, K.B., Chou, H.-T., Huang, R.K., Yu, Z., and Sabatini, D.M. (2019). Cryo-EM Structure of the Human FLCN-FNIP2-Rag-Ragulator Complex. Cell *179*, 1319–1329.e8.
- [196] Shi, C.-S., and Kehrl, J.H. (2010). TRAF6 and A20 regulate lysine 63-linked ubiquitination of Beclin-1 to control TLR4-induced autophagy. Sci. Signal. 3, ra42.
- [197] Shi, C.-S., Shenderov, K., Huang, N.-N., Kabat, J., Abu-Asab, M., Fitzgerald, K.A., Sher, A., and Kehrl, J.H. (2012). Activation of autophagy by inflammatory signals limits IL-1 β production by targeting ubiquitinated inflammasomes for destruction. Nat. Immunol. 13, 255–263.
- [198] Shimobayashi, M., and Hall, M.N. (2014). Making new contacts: the mTOR network in metabolism and signalling crosstalk. Nat. Rev. Mol. Cell Biol. *15*, 155–162.
- [199] Shin, H.-J.R., Kim, H., Oh, S., Lee, J.-G., Kee, M., Ko, H.-J., Kweon, M.-N., Won, K.-J., and Baek, S.H. (2016). AMPK-SKP2-CARM1 signalling cascade in transcriptional regulation of autophagy. Nature *534*, 553–557.
- [200] Siegel, R.L., Miller, K.D., Goding Sauer, A., Fedewa, S.A., Butterly, L.F., Anderson, J.C., Cercek, A., Smith, R.A., and Jemal, A. (2020). Colorectal cancer statistics, 2020. CA Cancer J Clin 70, 145–164.
- [201] Siggs, O.M., Stockenhuber, A., Deobagkar-Lele, M., Bull, K.R., Crockford, T.L., Kingston, B.L., Crawford, G., Anzilotti, C., Steeples, V., Ghaffari, S., et al. (2016). Mutation of Fnip1 is associated with B-cell deficiency, cardiomyopathy, and elevated AMPK activity. Proc. Natl. Acad. Sci. USA *113*, E3706-15.
- [202] Singh, N., Kansal, P., Ahmad, Z., Baid, N., Kushwaha, H., Khatri, N., and Kumar, A. (2018). Antimycobacterial effect of IFNG (interferon gamma)-induced autophagy depends on HMOX1 (heme oxygenase 1)-mediated increase in intracellular calcium levels and modulation of PPP3/calcineurin-TFEB (transcription factor EB) axis. Autophagy *14*, 972–991.
- [203] Singh, S.R., Zhen, W., Zheng, Z., Wang, H., Oh, S.W., Liu, W., Zbar, B., Schmidt, L.S., and Hou, S.X. (2006). The Drosophila homolog of the human tumor suppressor gene BHD

- interacts with the JAK-STAT and Dpp signaling pathways in regulating male germline stem cell maintenance. Oncogene 25, 5933–5941.
- [204] Sørlie, T., Perou, C.M., Tibshirani, R., Aas, T., Geisler, S., Johnsen, H., Hastie, T., Eisen, M.B., van de Rijn, M., Jeffrey, S.S., et al. (2001). Gene expression patterns of breast carcinomas distinguish tumor subclasses with clinical implications. Proc. Natl. Acad. Sci. USA *98*, 10869–10874.
- [205] Sorlie, T., Tibshirani, R., Parker, J., Hastie, T., Marron, J.S., Nobel, A., Deng, S., Johnsen, H., Pesich, R., Geisler, S., et al. (2003). Repeated observation of breast tumor subtypes in independent gene expression data sets. Proc. Natl. Acad. Sci. USA *100*, 8418–8423.
- [206] Soussi, T., and Wiman, K.G. (2007). Shaping genetic alterations in human cancer: the p53 mutation paradigm. Cancer Cell 12, 303–312.
- [207] Starling, G.P., Yip, Y.Y., Sanger, A., Morton, P.E., Eden, E.R., and Dodding, M.P. (2016). Folliculin directs the formation of a Rab34-RILP complex to control the nutrient-dependent dynamic distribution of lysosomes. EMBO Rep. 17, 823–841.
- [208] Steingrímsson, E., Tessarollo, L., Reid, S.W., Jenkins, N.A., and Copeland, N.G. (1998). The bHLH-Zip transcription factor Tfeb is essential for placental vascularization. Development *125*, 4607–4616.
- [209] Steingrímsson, E., Copeland, N.G., and Jenkins, N.A. (2004). Melanocytes and the microphthalmia transcription factor network. Annu. Rev. Genet. 38, 365–411.
- [210] Takagi, Y., Kobayashi, T., Shiono, M., Wang, L., Piao, X., Sun, G., Zhang, D., Abe, M., Hagiwara, Y., Takahashi, K., et al. (2008). Interaction of folliculin (Birt-Hogg-Dubé gene product) with a novel Fnip1-like (FnipL/Fnip2) protein. Oncogene *27*, 5339–5347.
- [211] Takeda, K., Yasumoto, K., Kawaguchi, N., Udono, T., Watanabe, K., Saito, H., Takahashi, K., Noda, M., and Shibahara, S. (2002). Mitf-D, a newly identified isoform, expressed in the retinal pigment epithelium and monocyte-lineage cells affected by Mitf mutations. Biochimica et Biophysica Acta (BBA) Gene Structure and Expression *1574*, 15–23.
- [212] Takemoto, C.M., Yoon, Y.-J., and Fisher, D.E. (2002). The identification and functional characterization of a novel mast cell isoform of the microphthalmia-associated transcription factor. J. Biol. Chem. 277, 30244–30252.
- [213] Terada, S., and Tabata, I. (2004). Effects of acute bouts of running and swimming exercise on PGC-1alpha protein expression in rat epitrochlearis and soleus muscle. Am. J. Physiol. Endocrinol. Metab. 286, E208-16.
- [214] Tiller, G.R., and Garsin, D.A. (2014). Of worms and men: HLH-30 and TFEB regulate tolerance to infection. Immunity 40, 857–858.
- [215] Tong, Y., and Song, F. (2015). Intracellular calcium signaling regulates autophagy via calcineurin-mediated TFEB dephosphorylation. Autophagy 11, 1192–1195.
- [216] Tseng, H.H.L., Vong, C.T., Kwan, Y.W., Lee, S.M.-Y., and Hoi, M.P.M. (2017). Lysosomal Ca2+ Signaling Regulates High Glucose-Mediated Interleukin-1 β Secretion via Transcription Factor EB in Human Monocytic Cells. Front. Immunol. δ , 1161.
- [217] Tsun, Z.-Y., Bar-Peled, L., Chantranupong, L., Zoncu, R., Wang, T., Kim, C., Spooner, E., and Sabatini, D.M. (2013). The folliculin tumor suppressor is a GAP for the RagC/D GTPases that signal amino acid levels to mTORC1. Mol. Cell *52*, 495–505.
- [218] Udono, T., Yasumoto, K., Takeda, K., Amae, S., Watanabe, K., Saito, H., Fuse, N., Tachibana, M., Takahashi, K., Tamai, M., et al. (2000). Structural organization of the human microphthalmia-associated transcription factor gene containing four alternative promoters. Biochimica et Biophysica Acta (BBA) Gene Structure and Expression *1491*, 205–219.

- [219] Vega-Rubin-de-Celis, S., Peña-Llopis, S., Konda, M., and Brugarolas, J. (2017). Multistep regulation of TFEB by MTORC1. Autophagy *13*, 464–472.
- [220] Visvikis, O., Ihuegbu, N., Labed, S.A., Luhachack, L.G., Alves, A.-M.F., Wollenberg, A.C., Stuart, L.M., Stormo, G.D., and Irazoqui, J.E. (2014). Innate host defense requires TFEB-mediated transcription of cytoprotective and antimicrobial genes. Immunity *40*, 896–909.
- [221] Vocke, C.D., Yang, Y., Pavlovich, C.P., Schmidt, L.S., Nickerson, M.L., Torres-Cabala, C.A., Merino, M.J., Walther, M.M., Zbar, B., and Linehan, W.M. (2005). High frequency of somatic frameshift BHD gene mutations in Birt-Hogg-Dubé-associated renal tumors. J. Natl. Cancer Inst. *97*, 931–935.
- [222] Vural, A., Al-Khodor, S., Cheung, G.Y.C., Shi, C.-S., Srinivasan, L., McQuiston, T.J., Hwang, I.-Y., Yeh, A.J., Blumer, J.B., Briken, V., et al. (2016). Activator of G-Protein Signaling 3-Induced Lysosomal Biogenesis Limits Macrophage Intracellular Bacterial Infection. J. Immunol. *196*, 846–856.
- [223] Wada, S., Neinast, M., Jang, C., Ibrahim, Y.H., Lee, G., Babu, A., Li, J., Hoshino, A., Rowe, G.C., Rhee, J., et al. (2016). The tumor suppressor FLCN mediates an alternate mTOR pathway to regulate browning of adipose tissue. Genes Dev. 30, 2551–2564.
- [224] Wang, G.L., Jiang, B.H., Rue, E.A., and Semenza, G.L. (1995). Hypoxia-inducible factor 1 is a basic-helix-loop-helix-PAS heterodimer regulated by cellular O2 tension. Proc. Natl. Acad. Sci. USA *92*, 5510–5514.
- [225] Watnick, R.S. (2012). The role of the tumor microenvironment in regulating angiogenesis. Cold Spring Harb. Perspect. Med. 2, a006676.
- [226] Wei, H., Wei, S., Gan, B., Peng, X., Zou, W., and Guan, J.-L. (2011). Suppression of autophagy by FIP200 deletion inhibits mammary tumorigenesis. Genes Dev. 25, 1510–1527.
- [227] Welch, D.R., and Hurst, D.R. (2019). Defining the hallmarks of metastasis. Cancer Res. 79, 3011–3027.
- [228] White, E., and DiPaola, R.S. (2009). The double-edged sword of autophagy modulation in cancer. Clin. Cancer Res. *15*, 5308–5316.
- [229] Woodford, M.R., Dunn, D.M., Blanden, A.R., Capriotti, D., Loiselle, D., Prodromou, C., Panaretou, B., Hughes, P.F., Smith, A., Ackerman, W., et al. (2016). The FNIP co-chaperones decelerate the Hsp90 chaperone cycle and enhance drug binding. Nat. Commun. 7, 12037.
- [230] Woods, A., Johnstone, S.R., Dickerson, K., Leiper, F.C., Fryer, L.G.D., Neumann, D., Schlattner, U., Wallimann, T., Carlson, M., and Carling, D. (2003). LKB1 is the upstream kinase in the AMP-activated protein kinase cascade. Curr. Biol. *13*, 2004–2008.
- [231] Wu, M., Si, S., Li, Y., Schoen, S., Xiao, G.-Q., Li, X., Teh, B.T., Wu, G., and Chen, J. (2015). Flcn-deficient renal cells are tumorigenic and sensitive to mTOR suppression. Oncotarget *6*, 32761–32773.
- [232] Wu, M., Gibbons, J.G., DeLoid, G.M., Bedugnis, A.S., Thimmulappa, R.K., Biswal, S., and Kobzik, L. (2017). Immunomodulators targeting MARCO expression improve resistance to postinfluenza bacterial pneumonia. Am. J. Physiol. Lung Cell Mol. Physiol. *313*, L138–L153.
- [233] Wu, X., Bradley, M.J., Cai, Y., Kümmel, D., De La Cruz, E.M., Barr, F.A., and Reinisch, K.M. (2011). Insights regarding guanine nucleotide exchange from the structure of a DENN-domain protein complexed with its Rab GTPase substrate. Proc. Natl. Acad. Sci. USA *108*, 18672–18677.
- [234] Xie, X., Koh, J.Y., Price, S., White, E., and Mehnert, J.M. (2015). Atg7 Overcomes Senescence and Promotes Growth of BrafV600E-Driven Melanoma. Cancer Discov. 5, 410–423.
- [235] Yan, M., Gingras, M.-C., Dunlop, E.A., Nouët, Y., Dupuy, F., Jalali, Z., Possik, E., Coull,

- B.J., Kharitidi, D., Dydensborg, A.B., et al. (2014). The tumor suppressor folliculin regulates AMPK-dependent metabolic transformation. J. Clin. Invest. *124*, 2640–2650.
- [236] Yan, M., Audet-Walsh, É., Manteghi, S., Dufour, C.R., Walker, B., Baba, M., St-Pierre, J., Giguère, V., and Pause, A. (2016). Chronic AMPK activation via loss of FLCN induces functional beige adipose tissue through PGC-1α/ERRα. Genes Dev. 30, 1034–1046.
- [237] Yordy, B., and Iwasaki, A. (2011). Autophagy in the control and pathogenesis of viral infection. Curr Opin Virol *I*, 196–203.
- [238] Yoshimura, S., Gerondopoulos, A., Linford, A., Rigden, D.J., and Barr, F.A. (2010). Family-wide characterization of the DENN domain Rab GDP-GTP exchange factors. J. Cell Biol. 191, 367–381.
- [239] Young, N.P., Kamireddy, A., Van Nostrand, J.L., Eichner, L.J., Shokhirev, M.N., Dayn, Y., and Shaw, R.J. (2016). AMPK governs lineage specification through Tfeb-dependent regulation of lysosomes. Genes Dev. *30*, 535–552.
- [240] Zbar, B., Alvord, W.G., Glenn, G., Turner, M., Pavlovich, C.P., Schmidt, L., Walther, M., Choyke, P., Weirich, G., Hewitt, S.M., et al. (2002). Risk of renal and colonic neoplasms and spontaneous pneumothorax in the Birt-Hogg-Dubé syndrome. Cancer Epidemiol. Biomarkers Prev. 11, 393–400.
- [241] Zetter, B.R. (1998). Angiogenesis and tumor metastasis. Annu. Rev. Med. 49, 407–424.
- [242] Zhang, D., Iyer, L.M., He, F., and Aravind, L. (2012). Discovery of Novel DENN Proteins: Implications for the Evolution of Eukaryotic Intracellular Membrane Structures and Human Disease. Front. Genet. *3*, 283.
- [243] Zhang, N., Liu, X., Liu, L., Deng, Z., Zeng, Q., Pang, W., Liu, Y., Song, D., and Deng, H. (2018). Glycogen synthase kinase-3β inhibition promotes lysosome-dependent degradation of c-FLIP L in hepatocellular carcinoma. Cell Death Dis. *9*, 1–13.
- [244] Zhang, W., Shi, X., Peng, Y., Wu, M., Zhang, P., Xie, R., Wu, Y., Yan, Q., Liu, S., and Wang, J. (2015). HIF-1α Promotes Epithelial-Mesenchymal Transition and Metastasis through Direct Regulation of ZEB1 in Colorectal Cancer. PLoS One *10*, e0129603.
- [245] Zhou, Y., Tang, F., Wang, Y., Min, L., Luo, Y., Zhang, W., Shi, R., Duan, H., and Tu, C. (2017). Advanced alveolar soft part sarcoma responds to apatinib. Oncotarget *8*, 50314–50322.
- [246] Zhu, X., Ying, J., Wang, F., Wang, J., and Yang, H. (2014). Estrogen receptor, progesterone receptor, and human epidermal growth factor receptor 2 status in invasive breast cancer: a 3,198 cases study at National Cancer Center, China. Breast Cancer Res. Treat. *147*, 551–555.

CHAPTER 2 – The AMPK signaling as		FE3 link the FLCN- pathogen resistance

The transcription factors TFEB and TFE3 link the FLCN-AMPK signaling axis to innate immune response and pathogen resistance

Authors/Affiliation

Leeanna El-Houjeiri^{1,2,5}, Elite Possik^{1,2,5}, Tarika Vijayaraghavan^{1,2}, Mathieu Paquette^{1,2}, José A Martina³, Jalal M. Kazan^{1,2}, Eric H. Ma^{1,4}, Russell Jones^{1,4}, Paola Blanchette^{1,2}, Rosa Puertollano³ and Arnim Pause^{1,2}

¹Goodman Cancer Research Center, McGill University, Montréal, Québec, Canada. ²Department of Biochemistry, McGill University, Montréal, Québec, Canada. ³Cell Biology and Physiology Center, National Heart, Lung, and Blood Institute, National Institutes of Health, Bethesda MD, USA ⁴Department of Physiology, McGill University, Montréal, Québec, Canada. ⁵Equal contribution

Published: Cell reports 26.13 (2019): 3613-3628.

Correspondence and Lead contact

Arnim Pause; arnim.pause@mcgill.ca, Phone: 1-514-398-1521; Fax: 1-514-398-6769

Running Head

FLCN/AMPK/TFEB-TFE3 signaling axis regulates innate immune response

2.1. ABSTRACT

TFEB and TFE3 are transcriptional regulators of the innate immune response, but the mechanisms regulating their activation upon pathogen infection are poorly elucidated. Using *C. elegans* and mammalian models, we report that the master metabolic modulator 5'-AMP-activated protein kinase (AMPK) and its negative regulator Folliculin (FLCN) act upstream of TFEB/TFE3 in the innate immune response, independently of the mTORC1 signaling pathway. In nematodes, loss of FLCN or overexpression of AMPK confers pathogen resistance *via* activation of TFEB/TFE3-dependent antimicrobial genes, while ablation of total AMPK activity abolishes this phenotype. Similarly, in mammalian cells, loss of FLCN or pharmacological activation of AMPK induces TFEB/TFE3-dependent pro-inflammatory cytokine expression. Importantly, a rapid reduction in cellular ATP levels in murine macrophages is observed upon lipopolysaccharide (LPS) treatment accompanied by an acute AMPK activation and TFEB nuclear localization. These results uncover an ancient, highly conserved and pharmacologically actionable mechanism coupling energy status with innate immunity.

2.2. INTRODUCTION

Innate immune responses constitute the first line of defense against pathogenic infections in simple metazoans, invertebrates, and mammals (Akira et al., 2006, Hoffmann, 2003, Irazoqui et al., 2010b, Medzhitov, 2007). While much effort has been put into elucidating the functions of downstream mediators of immune response including antimicrobial peptides, C-type lectins, cytokines and chemokines, less is known regarding how host cells recognize foreign infections and trigger the activation of transcription factors that coordinate the anti-microbial response. Among the few well-characterized transcription factors, NF-κB, was shown to be an important

factor in controlling host defense gene expression, mediated through toll like receptor (TLR) and nucleotide-binding leucine-rich repeat containing (NLR) ligand pathways (Medzhitov, 2009). However, another under-appreciated host-defense transcription factor was recently identified in Caenorhabditis elegans (C. elegans), which lacks the NF-kB pathway (Visvikis et al., 2014). Using this model, HLH-30, the *C. elegans* ortholog of TFEB and TFE3, was identified as an important evolutionarily conserved transcriptional regulator of the host response to infection (Lapierre et al., 2013, Visvikis et al., 2014, Rehli et al., 1999). TFEB and TFE3 are basic helixloop-helix leucine zipper transcription factors that multi-task in regulating a similar set of genes involved in lipid metabolism, autophagy, lysosomal biogenesis and stress response genes (David, 2011, Raben and Puertollano, 2016, Sardiello, 2016, Settembre et al., 2013, Settembre et al., 2011). Several studies have reported a similar mechanisms underlying TFEB/TFE3 activation in response to nutrient deprivation and metabolic stress. In nutrient-rich environments, the kinases ERK2 and mTORC1 phosphorylate TFEB/TFE3 on specific serine residues and retain them in the cytoplasm in an inactive state (Martina et al., 2012, Martina et al., 2014, Roczniak-Ferguson et al., 2012, Settembre et al., 2011, Settembre et al., 2012). The mTORC1-dependent phosphorylation of TFEB (S211) and TFE3 (S321) promotes binding to 14-3-3. It has been suggested that this interaction masks the Nuclear Localization Signal (NLS), thus inhibiting TFEB and TFE3 nuclear translocation (Roczniak-Ferguson et al., 2012, Martina et al., 2012). Conversely, under starvation, this repressive phosphorylation is lifted, resulting in their translocation to the nucleus and activation of their downstream transcriptional targets that encode components of the lysosomal biogenesis and autophagy pathways (Martina et al., 2012, Roczniak-Ferguson et al., 2012, Settembre et al., 2011, Settembre et al., 2012). Despite these remarkable similarities between TFEB and TFE3, it is still unclear whether these transcription factors have cooperative,

complementary, or partially redundant roles under different environmental conditions. Importantly, in murine macrophages, both TFEB and TFE3 were shown to be activated and translocated to the nucleus upon pathogen infection or stimulation with TLR ligands, where they collaborate in mediating the transcriptional upregulation of several cytokines and chemokines involved in antimicrobial immune response (Pastore et al., 2016, Samie and Cresswell, 2015, Visvikis et al., 2014). This functional conservation of the TFEB/TFE3 pathway is further supported by a recent study showing that bacterial membrane pore-forming toxin induces cellular autophagy in an HLH-30-dependent manner in C. elegans (Chen et al., 2017). However, the mechanisms by which nematode and mammalian TFEB/TFE3 are activated during infection are still poorly understood. Recently, TFEB activation was found to involve phospholipase C and protein kinase D pathways both in C. elegans and mammals upon pathogen infection (Najibi et al., 2016). Subsequent studies showed that lipopolysaccharide (LPS)-stimulated TFEB/TFE3 activation in murine macrophages induced cytokine production and secretion independent of mTORC1, but the specific pathway by which their activation was mediated was not elucidated (Pastore et al., 2016).

Folliculin (FLCN) is a binding partner and negative regulator of 5'-AMP-activated protein kinase (AMPK) (Baba et al., 2006, Takagi et al., 2008), which was identified as a tumor suppressor protein responsible for the Birt-Hogg-Dubé (BHD) neoplastic syndrome in humans (Tee and Pause, 2013). Importantly, the interaction of FLCN with AMPK is mediated by two homologous FLCN-binding proteins FNIP1 and 2 [22,23]. Pathogenic mutations from BHD patients lead to a loss of FNIP/AMPK binding pointing to the functional significance of this interaction in tumor suppression [22]. AMPK is a heterotrimeric enzyme, which monitors the energy status and maintains energy homeostasis under metabolic stress by activating catabolic processes and

inhibiting anabolic pathways (Hardie, 2015, Hardie and Ashford, 2014, Hardie et al., 2012). We have previously shown that loss of FLCN or expression of a FLCN mutant unable to bind FNIP/AMPK led to chronic AMPK activation, resulting in increased ATP levels through an elevated glycolytic flux, oxidative phosphorylation and autophagy (Possik et al., 2015, Possik et al., 2014, Possik and Pause, 2016). Importantly, we have shown that loss of FLCN mediates resistance to oxidative stress, heat, anoxia, obesity, and hyperosmotic stresses *via* AMPK activation in *C. elegans* and mammalian models (Possik et al., 2015, Possik et al., 2014, Possik and Pause, 2016, Yan et al., 2014).

While a role for FLCN in regulating immune responses has not been reported, the functional role for AMPK in innate immunity seems to be context and cell-type dependent (Blagih et al., 2015, Prantner et al., 2017). In this study, we demonstrate an evolutionarily conserved pathogen resistance mechanism mediated by FLCN and AMPK via TFEB/TFE3. Specifically, we show that loss of flcn-1 in C. elegans, which leads to chronic AMPK activation, enhances the HLH-30 nuclear translocation and induces the expression of hlh-30-dependent antimicrobial genes upon infection, mediating resistance to bacterial pathogens. Using RNA-seq, we show that many hlh-30-dependent antimicrobial genes are regulated by AMPK upon S. aureus infection. AMPK loss reduces HLH-30 nuclear translocation and abrogates the increased resistance of *flcn-1(ok975)* mutant animals to pathogens. Furthermore, we show that constitutive activation of AMPK C. elegans nematodes leads to an HLH-30-dependent increase in pathogen resistance, similar to what we observe upon loss of flcn-1. Importantly, we show that this pathway of regulation is evolutionarily conserved and that FLCN and AMPK regulate TFEB/TFE3-driven cytokine and inflammatory genes in mouse embryonic fibroblasts and macrophages. Overall, our data suggest an essential role of the FLCN/AMPK axis in the regulation of host-defense response via TFEB/TFE3, highlighting a possible mechanism likely to contribute to tumor formation in BHD patients. Our findings also shed light on the potential use of AMPK activators in the stimulation of the innate immune response and defense against pathogens.

2.3. RESULTS

Loss of flcn-1 in C. elegans increases the expression of anti-microbial genes and confers resistance to bacterial pathogens

To understand the physiological role of FLCN-1, we compared gene expression profiles of wild-type and flcn-1(ok975) mutant animals. Among differentially expressed genes, 243 transcripts were up-regulated in *flcn-1(ok975)* mutant animals compared to wild-type animals at basal level (Table S3-Sheet 1) and were classified based on their biological functions (Table 1 and Table S3-Sheets 1 and 2). Genes associated with stress response, innate immune response, defense mechanisms and response to stimulus processes, including heat shock proteins, C-type lectins, lysozymes and cytochrome P450 genes, were induced in *flcn-1(ok975)* unstressed mutant animals compared to wild-type animals (Table 1, S1-3, Figure 1A). Selected genes were validated using RT-qPCR (Figure 1B and Table S3-Sheet 3). On the other hand, 704 genes were shown to be downregulated in *flcn-1(ok975)* mutant animals (Table S3-Sheet 4) and are involved in various processes that control proliferation and growth (Table S3-Sheet 5). These results indicate that a differential gene expression might be providing advantage to the flcn-1 mutant worms prior to stress or pathogen attacks. This is in accordance with our previously reported results where loss of flcn-1(ok975) conferred resistance to oxidative stress, heat stress, anoxia and hyperosmotic stress in C. elegans (Possik et al., 2015, Possik et al., 2014, Possik and Pause, 2015, Possik and Pause, 2016, Yan et al., 2014). Since it was demonstrated that the osmo-sensitive gene expression mimics the transcriptional profiles of pathogen infection (Rohlfing et al., 2010), we compared the overlap between genes upregulated in flcn-1(ok975) mutant animals and genes induced by infection of C.

elegans nematodes with pathogens (Irazoqui et al., 2010a, Troemel et al., 2006). Indeed, we found a significant overlap of the transcriptome especially upon *Staphylococcus aureus* (*S. aureus*) (Figure S1A and Table S3-Sheet 6) and *Pseudomonas aeruginosa* (*P. aeruginosa*) infection (Figure S1B and Table S3-Sheet 7).

Next, we asked whether *flcn-1(ok975)* mutant animals display enhanced resistance to pathogens. Strikingly, we found that the *flcn-1(ok975)* mutant animals are more resistant than wild-type animals to *S. aureus* and *P. aeruginosa* infection (Figure 1C-D, Table S1). These phenotypes were rescued using a transgenic *flcn-1* mutant animal re-expressing *flcn-1* (Figure 1E, Table S1). These results demonstrate an important role for *flcn-1* in the induction of antimicrobial peptides and stress response genes mediating the resistance to infection with bacterial pathogens.

Loss of flcn-1 increases pathogen resistance via HLH-30 activation

HLH-30, the worm ortholog of TFEB/TFE3, has been reported to modulate longevity and pathogen resistance in *C. elegans* through activation of autophagy and expression of antimicrobial genes (Lapierre et al., 2013, Settembre et al., 2013). Importantly, we found a significant overlap between genes that were upregulated in *flcn-1(ok975)* mutant animals and downregulated in *hlh-30(tm1978)* mutant animals (Table S3-Sheet 8) (Visvikis et al., 2014). Thus, we asked whether HLH-30 is induced in *flcn-1* mutants using an *hlh-30*::GFP transgenic reporter strain (Lapierre et al., 2013, Visvikis et al., 2014). Upon infection with *S. aureus*, as shown in this study and others (Visvikis et al., 2014), HLH-30 translocated to the nucleus (Figure 2A). In particular, about 40% of the wild-type animals displayed an HLH-30 nuclear localization after 20 min of infection with *S. aureus*. Importantly, we observed that the percentage of animals displaying a constitutive nuclear HLH-30 translocation in uninfected worms was significantly higher upon loss of *flcn-1* (Figure 2B, time 0). Strikingly, we show that upon *S. aureus* infection, the percentage of animals

with HLH-30 nuclear translocation increased further in *flcn-1* mutant animals. Specifically, we found that after 20 min of infection with *S. aureus*, more than 80% of the *flcn-1* mutant animals displayed an HLH-30 nuclear localization in comparison to less than 40% for wild-type animals. Overall, this highlights an important role for HLH-30 in the increased pathogen resistance conferred by loss of *flcn-1* (Figure 2B).

To determine whether *hlh-30* is required for the increased survival of *flcn-1* mutant animals to pathogens, we generated a *flcn-1(ok975); hlh-30(tm1978)* double mutant strain. Importantly, loss of *hlh-30* significantly impaired the survival advantage upon both *S. aureus* (Figure 2C) and *P. aeruginosa* infections (Figure 2D) that was conferred by loss of *flcn-1*, demonstrating its involvement in pathogen resistance (Table S1). Accordingly, loss of *hlh-30* also suppressed the increased resistance of *flcn-1* to hyperosmotic stress (Possik et al., 2015) supporting that the adaptation to the two stresses requires a similar transcriptional profile dictated by HLH-30 (Figure S2).

To further assess the involvement of HLH-30 in the transcriptional response downstream of FLCN-1, we measured the gene expression of known HLH-30 target genes (Visvikis et al., 2014). Using RT-qPCR, we found a significant upregulation in many *hlh-30*-dependent antimicrobial and infection-associated genes in uninfected *flcn-1* mutant worms (Figures 2E-K). Furthermore, after 4 h of infection with *S. aureus*, we show that loss of *hlh-30* strongly reduced the expression of antimicrobial peptide genes and infection-related genes in both wild-type and *flcn-1* mutant animals (Figures 2E-K), supporting a role for HLH-30 in the pathogen transcriptional signature downstream of *flcn-1*. Collectively, we found that loss of *flcn-1* activates the transcription of HLH-30 antimicrobial peptide genes at basal level, which is further induced upon *S. aureus* infection.

The regulation of TFEB/TFE3 by FLCN is evolutionarily conserved through an mTOR independent mechanism

Because the role of HLH-30 in host defense is evolutionarily conserved (Visvikis et al., 2014), we tested whether the FLCN-HLH-30 axis that we uncovered in C. elegans is conserved from worms to mammals. Indeed, we observed that Flcn deletion in mouse embryonic fibroblasts (MEFs) promoted TFEB and TFE3 nuclear localization at basal levels compared to wild-type MEFs as detected by subcellular fractionation and immunofluorescence assays (Figure 3A-C). The difference in the cytosolic TFEB molecular weight can be attributed to the phosphorylation forms of TFEB [17]. Consequently, known TFEB and TFE3 targets were upregulated at the mRNA level upon Flcn deletion (Figure 3B), including genes involved in innate host response, such as IL-6. Addition of Torin1, a specific inhibitor of mTORC1 and mTORC2, induced TFEB nuclear localization in *Flcn* knockout (KO) MEFs to a higher extent than wild-type MEFs (Figure 3C), evoking an mTOR independent pathway. Moreover, loss of Flcn did not affect mTOR signaling, as measured by immunoblotting for the phosphorylated form of the S6 ribosomal protein (S6), a well-described mTORC1 downstream target (Figure 3D). In line with this, in C. elegans, inhibition of let-363, the C. elegans TOR homolog, increased the HLH-30 nuclear translocation at basal level similar to what has been previously reported (Lapierre et al., 2013) (Figure 3E). Importantly, loss of flcn-1 further increased the HLH-30 nuclear translocation upon inhibition of let-363 at basal level supporting a TOR-independent pathway governing HLH-30 regulation (Figure 3E). Moreover, infection with S. aureus increased to a similar extent the HLH-30 nuclear localization both in wild-type and flcn-1 (ok975) animals fed with let-363 RNAi, presumably because the infection happens rapidly masking the effects of let-363 RNAi on HLH-30 translocation (Figure 3E). These findings suggest that loss of FLCN drives HLH-30/TFEB/TFE3 nuclear localization through a mechanism distinct from the canonical mTOR pathway both in nematodes and mammalian cells.

To further assess whether the transcriptional up-regulation of cytokines and chemokines upon loss of Flcn was mediated by TFEB and TFE3, we knocked down their endogenous expression simultaneously using shTFEB and shTFE3 in wild-type and Flcn KO MEFs and determined the expression of IL-6 following TNFa stimulation (Figure 3F-G). Notably, we found that the significant induction of IL-6 mRNA levels upon TNF-α stimulation in both wild-type and Flcn KO MEFs was abrogated to levels observed in unstimulated cells upon knockdown of TFEB/TFE3 (Figure 3F). To confirm the observed effects in a relevant cellular system for innate immune response, we used RAW264.7 murine macrophages and reduced the endogenous expression of Flcn using shRNA-mediated knockdown approaches. Importantly, we show a significant increase in IL-6 production, at both mRNA (Figure 3H) and protein levels (Figure 3I), in FLCN KD macrophages compared to empty vector (EV) in response to LPS stimulation. To further assess the role of FLCN in inflammation and innate immune response, we determined the cytokine and chemokine secretion profiles in wild-type and shFLCN macrophages after 3h and 24h of LPS stimulation using mouse protein cytokine arrays. Notably, we show a significant and prominent increase in many cytokines in FLCN KD macrophages as compared to EV upon LPS stimulation (Figures 3J-K). These cytokines encompass key mediators of the inflammatory response.

FLCN depletion in macrophages enhances their energy metabolism and phagocytic potential

Next, we investigated the metabolic consequences of FLCN depletion in RAW264.7 macrophages. We found that glucose consumption and lactate production were increased in FLCN KD macrophages compared to control macrophages (Figure 4A-B), and this was accompanied by

an augmented extracellular acidification rate (ECAR) (Figure 4C-D) and oxygen consumption rate (OCR) (Figure 4E-F) at basal level and upon the sequential addition of oligomycin (an ATP synthase inhibitor), Carbonyl cyanide-p-trifluoromethoxyphenylhydrazone (FCCP) (for maximum respiratory capacity), followed by rotenone/antimycin A (to block mitochondrial electron transport). In line with these results, we also report an increase in ATP production in FLCN KD macrophages compared to controls (Figure 4G). Next, we investigated whether FLCN depletion enhances the phagocytic potential in macrophages (Figure 4I). Using pHrodo Red S. aureus Bioparticles, we report a 30% increase in phagocytic capacity of FLCN KD macrophages compared to control cells, as shown by the fold change in the mean florescence intensity (Figure 4I). To test whether this increase in phagocytic activity in FLCN KD macrophages is dependent on TFEB/TFE3 activation, we knocked down FLCN in TFEB/TFE3 DKO RAW macrophages (Figure 4H) and showed that the phagocytic activity of these cells decreased by almost 50% compared to FLCN depleted macrophages, upon stimulation with pHrodo Red S. aureus Bioparticles (Figure 4I). Taken together, we show that depletion of FLCN in macrophages prompts a metabolic transformation toward increased cellular bioenergetics, accompanied by an augmented TFEB/TFE3-dependent phagocytic capacity, which might further enhance the innate immune response.

AMPK regulates HLH-30 activation and antimicrobial response upon infection with bacterial pathogens.

Given that we have previously reported that loss of *flcn-1* leads to chronic AMPK activation, which increases resistance to energy (Possik et al., 2014) and hyperosmotic stresses (Possik and Pause, 2015) in nematodes, we tested whether *flcn-1* mutant animals confer pathogen resistance via AMPK-mediated regulation of HLH-30. Importantly, simultaneous loss of *aak*-

1 and aak-2 (C. elegans orthologs of AMPK $\alpha 1/\alpha 2$) completely abolished the increased survival to both S. aureus and P. aeruginosa in wild-type and flcn-1 mutant animals, demonstrating that this phenotype requires AMPK (Figures 5A-B and Table S1). Furthermore, transgenic overexpression of a constitutively active catalytic subunit of AMPK (aak-2 oe) in nematodes confers pathogen resistance similar to flcn-1(ok975) mutants, which is mostly dependent on HLH-30 (Figure 5C and Table S1). Moreover, loss of both AMPK catalytic subunits significantly reduced the nuclear translocation of HLH-30 upon S. aureus infection (Figure 5D). Additionally, we found that loss of aak-2(ok524) alone was insufficient to reduce the nuclear translocation of HLH-30 upon S. aureus infection, suggesting that complete abrogation of both AMPK catalytic activities is required for this phenotype (Figure S3B). To further elaborate the role of AMPK in pathogen response and specifically in the transcription of antimicrobial and stress response genes upon infection, we used RNA-seq technology to measure differential gene expression in wild-type and aak-1(tm1944); aak-2(ok524) mutant animals at basal level and after 4 h infection with S. aureus (Figure S3A, Table S3-Sheets 9-13). We identified more than 800 genes induced upon S. aureus infection that are dependent on AMPK (Figure 5E and S3A, Table S3-Sheets 15 and 15). Furthermore, we found a significant overlap of 112 genes down-regulated in aak-1(tm1944); aak-2(ok524) mutant animals and genes regulated by hlh-30 upon S. aureus infection (Visvikis et al., 2014) (Figure 5F, Table S3-Sheet 16). Gene ontology classification highlights important pathways regulated by AMPK during S. aureus infection, including defense response and stress response pathways (Figure 5G and Table S3-Sheets 14-17). Using RT-qPCR, we validated several genes obtained by RNA-seq (Figures 5H-R), all of which have been reported to be involved in defense mechanisms against bacterial pathogens (Irazoqui et al., 2010a, Irazoqui et al., 2010b). Overall,

these results indicate that AMPK regulates the nuclear translocation of HLH-30 and the HLH-30 driven antimicrobial response upon infection with bacterial pathogens.

AMPK regulates TFEB/TFE3-mediated innate immune response

Based on our previous and current data, we tested whether the transcriptional innate immune response observed upon loss of FLCN is similar to a gain in AMPK activity in mammalian cells using GSK-621, a specific AMPK activator (Chen et al., 2016, Jiang et al., 2016). In MEFs, we show that GSK-621 activated AMPK, as shown by increased downstream target p-ACC, without inhibiting mTOR signaling as measured by immunoblotting for the phosphorylated forms of p70S6K and 4EBP1 (Figure 6A). Such activation was accompanied by a significant increase in the nuclear translocation of TFEB and TFE3 (Figures 6B-C), which was lost in AMPKα1/α2 double knock out (DKO) MEFs (Figures 6B-C), confirming the specific activation of AMPK by GSK-621. Additionally, we show that IL-6, a TFEB/TFE3 target, was transcriptionally upregulated when treated with GSK-621 and its expression was abrogated upon down-regulation of TFEB/TFE3 using shTFEB/TFE3 (Figure 6D) implying that AMPK impinges on TFEB/TFE3mediated transcription in mammalian cells similarly to what we have observed in C. elegans. Moreover, treatment of RAW264.7 macrophages with GSK-621 activated AMPK without affecting mTOR signaling (Figure 6E), promoted the nuclear translocation of TFEB (Figure 6F), and led to a strong increase in production and secretion of various cytokines and chemokines even in the absence of LPS treatment or pathogen infection (Figure 6G). To substantiate our findings in a more physiological context, we tested whether acute LPS treatment of macrophages could affect cellular bioenergetics, which could be sensed by AMPK. Indeed, we observed an acute reduction in cellular ATP levels (Figure 6H), accompanied by AMPK activation (Figure 6I), and a significant

increase in TFEB nuclear localization (Figure 6J) as early as 30 minutes after addition of LPS in RAW macrophages.

Collectively, both the mammalian and worm results demonstrate an important role for AMPK in the regulation of the innate host immune response through TFEB/TFE3 activation.

2.4. DISCUSSION

We have previously shown that loss of FLCN activates AMPK, increasing the resistance to oxidative stress, heat, anoxia, hyperosmotic stresses, and obesity in *C. elegans* and mammalian models (Possik et al., 2015, Possik et al., 2014, Possik and Pause, 2016, Yan et al., 2016, Yan et al., 2014). Here, we report evidence supporting an evolutionary conserved role of FLCN in innate host defense mediated through AMPK and TFEB/TFE3 activation.

Given that the gene profile upon osmotic stress mimics that of pathogen infection (Irazoqui et al., 2010a), we found a significant overlap in the transcriptional profile in *flcn-1* mutant animals when compared to wild-type animals infected with pathogens. We report that *flcn-1* mutant animals confer resistance to pathogen infection through nuclear localization and activation of HLH-30. Increased nuclear localization and activation of TFE3 were previously reported in renal tumors from Birt Hogg-Dubé syndrome patients, a syndrome associated with a germline mutation of the FLCN gene (Hong et al., 2010). Subsequent studies further supported a role for FLCN in the cytoplasmic retention of TFE3 and TFEB (Betschinger et al., 2013, Martina and Puertollano, 2013, Petit et al., 2013, Wada et al., 2016). The mechanisms through which TFEB and TFE3 are regulated in response to nutrient status have been characterized. Most studies to date suggested that mTORC1-dependent phosphorylation of TFEB causes cytoplasmic retention of this transcription factor under nutrient-rich conditions. Inhibition of mTORC1 activity upon nutrient starvation has been associated with hypo-phosphorylated forms and nuclear accumulation of TFEB

and TFE3 inducing the up-regulation of genes involved in autophagy and lysosomal biogenesis, and thus favoring cell survival and adaption to stress (Efeyan et al., 2013, Martina et al., 2012, Martina and Puertollano, 2013, Petit et al., 2013, Roczniak-Ferguson et al., 2012, Settembre et al., 2012). The link between FLCN and mTOR has been previously proposed, where FLCN was identified as a GTP-Activating Protein (GAP) for Ras-related GTPase (Rag)C/D, and a Guanine Exchange Factor (GEF) for RagA/B, which ultimately activates mTOR (Petit et al., 2013, Tsun et al., 2013). The yeast ortholog of FLCN, Lst7, also acts as a GAP for yeast RagC/D ortholog Gtr2 (Peli-Gulli et al., 2017). Conversely, FLCN-deficient tumors were shown to exhibit activated mTOR while acute loss of FLCN in cellular systems led to mTOR inhibition (Baba et al., 2006, Hasumi et al., 2014, Peli-Gulli et al., 2017, Petit et al., 2013, Tsun et al., 2013), suggesting that FLCN's role in this process is cell and context-dependent, and might vary in response to different environmental signals.

Our current work reveals that pathogen-induced regulation of TFEB and TFE3 activation appears to have different dynamics than that of starvation-induced regulation. Using both *C. elegans* and mammalian models, we show that the FLCN/AMPK axis and the mTOR axis impinge differently and independently on TFEB and TFE3 activation status. We show in nematodes that AMPK regulated the nuclear localization of HLH-30 and the transcription of anti-microbial genes. In mammalian cells, we show that AMPK activation led to the transcriptional up-regulation of proinflammatory cytokines through the nuclear translocation and activation of TFEB/TFE3. AMPK has been shown to govern lineage specification by promoting autophagy and lysosomal biogenesis through transcriptional mechanisms including TFEB (Young et al., 2016). Although no direct link between AMPK and TFEB has been reported, AMPK was thought to activate TFEB through inhibition of mTORC1 (Young et al., 2016). Conversely, and in support of our observed results

herein, it has been shown that while starvation-mediated activation of TFEB/TFE3 involved mTORC1, their pathogen-induced activation appeared to be mTORC1 independent (Pastore et al., 2016).

Bacterivorous nematodes, such as C. elegans induce the expression of transcriptional hostdefense responses including the HLH-30/TFEB pathway that promote organismal survival (Engelmann et al., 2011, O'Rourke et al., 2006, Sinha et al., 2012, Troemel et al., 2006, Visvikis et al., 2014). However, these invertebrates appear to lack the NLR and TLR pathogen sensing pathways as well as NF-κB and other transcription factor pathways that regulate innate immunity in higher organisms (Irazoqui et al., 2010b, Ishii et al., 2008). Our findings shed light on an ancient, highly conserved pathogen sensing and signal transduction mechanism, which involves AMPK and the transcription factor TFEB/TFE3. LPS, which is part of the outer membrane of Gramnegative bacteria, was shown to inhibit respiration and energy production in cells and isolated mitochondria (Frisard et al., 2015, Hansen et al., 2015, Kato, 1972, McGivney and Bradley, 1980). We show here, that LPS treatment of macrophages leads to an acute reduction of cellular energy levels resulting in AMPK activation, induction of TFEB/TFE3 and inflammatory cytokines (Figure 6H-K; Figure 3H, I). Therefore, this ancient pathogen-sensing pathway may have evolved by the fact that pathogen infection leads to an energy shortage, which is sensed by cellular AMPK. Activated AMPK will in turn promote TFEB/TFE3 nuclear translocation and induction of an innate host defense.

It remains to be elucidated how exactly loss of FLCN leads to AMPK activation on a mechanistic level. FLCN is a GAP for RagC/D, which ultimately activates mTOR (Petit et al., 2013, Tsun et al., 2013). Loss of FLCN leads to permanent mTOR inhibition with respect to activation of lysosomal biogenesis and autophagy via TFEB/TFE3, whereas mTOR-mediated

signaling towards protein synthesis appears not to be affected (Wada et al., 2016). We showed previously that loss of binding of FLCN to FNIP/AMPK via introduction of a phospho-mutant of FLCN as well as knockdown or complete loss of FLCN leads to permanent activation of AMPK with respect to autophagy via ULK-1, mitochondrial biogenesis via PGC-1α, glycolysis and angiogenesis via HIF-1α, glycogen metabolism upon osmotic stress, and resistance to obesity via induction of functional beige adipose tissue (Possik et al., 2015, Possik et al., 2014, Yan et al., 2016, Yan et al., 2014). However, more detailed work needs to be performed to fully understand the role of FLCN binding to FNIP and AMPK and its regulation in the role of AMPK activation.

How AMPK activates TFEB and TFE3 upon depletion of FLCN remains unknown. However, it is likely that AMPK activation under pathogen-induced conditions regulates TFEB and TFE3 activation distinctly from the mTOR pathway. Recent studies have shown that the kinases PLC-1 and DKF-1, the *C. elegans* orthologs of mammalian PLC and PRKD1/PKD, respectively, are required for HLH-30 activation during infection of nematodes with *S. aureus* (Najibi et al., 2016). A similar mechanism of TFEB activation in mouse macrophages infected with pathogens involved the PRKCA/PKCa axis demonstrating that TFEB activation in response to pathogen infection is conserved throughout evolution (Najibi et al., 2016). It appears that TFEB/TFE3 are controlled by a panel of kinases and phosphatases that depending on the environmental cues exhibit different downstream responses. Quantitative proteomics have identified over 20 phosphorylation sites on TFEB and TFE3, and although not directly tested in this current study, assessing their direct phosphorylation by AMPK could provide information about the contribution of AMPK in TFEB regulation.

The mechanisms through which TFEB and TFE3 confer pathogen resistance are still being deciphered. While TFEB/TFE3 activation were previously reported not to affect pathogen burden

over the course of infection, they appear to regulate the mechanisms of tolerance to infection through autophagy/lysosomal pathways that enhance ability of the host to survive upon pathogen invasion (Visvikis et al., 2014). Moreover, induction of lysosomal pathways have been demonstrated to enhance the phagocytic capacity of innate immune effector cells (Gordon, 2016). In this study, we show that down-regulation of FLCN in murine macrophages enhances their phagocytic activity and prompts a metabolic transformation toward increased cellular bioenergetics, which might further enhance the innate immune response. FLCN/AMPK-mediated increase in autophagic flux and AMPK/TFEB-mediated increase in lysosomal biogenesis are likely to contribute to metabolic fitness of infected cells and increased phagocytosis in macrophages. Interestingly, and in line with our results, it was recently proposed that the activation of the Fcy receptor in macrophages enhances lysosome-based proteolysis and killing of phagocytosed E. coli and this activation induces the nuclear translocation of TFEB accompanied by an increase the expression of specific lysosomal proteins. Notably, TFEB silencing represses the Fcy-receptormediated enhancements in degradation and bacterial killing (Gray et al., 2016). Hence, further studies are required to elucidate precisely how TFEB/TFE3 regulation through FLCN/AMPK axis affects host tolerance of infection in nematodes and in mammals.

Patients affected with BHD syndrome are at risk of developing bilateral, multifocal renal tumors, skin tumors and lung cysts (Schmidt and Linehan, 2015). In addition, chromosomal translocations leading to TFE3 or TFEB over-activation were reported in sporadic juvenile and advanced renal cell carcinoma (RCC) (Kauffman et al., 2014). Hence, it is tempting to speculate whether loss of FLCN and AMPK activation in humans induce a chronic inflammatory response and thereby promoting cancer progression, similar to reported cancer cases where innate immune response pathway such as NF-κB is over-activated (Karin, 2009).

Furthermore, in this study we place AMPK at the center of FLCN-TFEB/TFE3 axis. Several direct AMPK activators are being developed for treatment of type-2 diabetes, obesity, and metabolic syndrome (Zhang et al., 2009). We propose that some of these specific AMPK activating compounds could be repurposed to enhance host defense against pathogens or treat other immunodeficiency syndromes through AMPK-mediated activation of TFEB/TFE3, providing druggable strategies in innate immune modulation and therapy of bacterial infections. To this end, pharmacological inhibition of mTOR is currently being investigated in human clinical trials to treat age-associated immune dysfunction, also dubbed "immune senescence" (resTORbio, Inc).

2.5. STAR METHODS

Contact for Reagent and Resource Sharing

Further information and requests for resources and reagents should be directed to and will be fulfilled by the Lead Contact, Arnim Pause (arnim.pause@mcgill.ca).

EXPERIMENTAL MODEL AND SUBJECT DETAILS

Mice

C57BL/6 Flcn floxed mice (generously provided by Dr. Laura S. Schmidt, NCI, Bethesda, MD, USA) were used in to generate primary MEFs used in this study. Mice were housed in the McGill Animal Care Facility in standard cages with food and water ad libidum. Mice were maintained at 22-24°C on a 12-hr light/12-hr dark cycle. All studies were approved by the Animal Resource Centre at McGill University and comply with guidelines set by the Canadian Council of Animal Care. To generate the MEFs, pregnant mice were sacrificed at day 12.5 of the pregnancy by cervical dislocation to prevent embryos death. The embryos were then dissected out, sacrificed by cutting the head using standard procedures and isolated MEFs were then cultured for *in vitro*

analysis. The sex of the cell lines was not determined as they were isolated from mice at embryonic stage.

C. elegans strains, maintenance, and RNAi treatments

Strains used in this study: Wild-type Bristol (N2), flcn-1(ok975) II, aak-1(tm1944)III; aak-2(ok524)X, flcn-1(ok975)II; aak-1(tm1944)III; aak-2(ok524)X, hlh-30(tm1978)IV, flcn-1(ok975)II; hlh-30(tm1978)IV, sqIs19[hlh-30p::hlh-30::gfp, rol-6(su1006), N2; uthIs202 [Paak-2c:: aak2 (aa1-321)::Tomato::unc-54 3'UTR, rol6], flcn-1(ok975); flcn-1::GFP. Nematodes were maintained and synchronized using standard culture methods (Brenner, 1974). The RNAi feeding experiments were performed, and bacteria transformed with empty vector were used as control. Briefly, young adult animals were placed on NGM plated containing seeded bacteria expressing dsRNA against indicated genes and L4 / young adult F1 progeny was used for phenotypic scoring in all RNAi experiments. Plates were incubated at 20°C.

Bacterial strains

The bacterial strains used in this study are: Escherichia coli OP50; Staphylococcus aureus (MW2); and Pseudomonas aeruginosa (PA14).

Cell Lines and Cell Culture

Primary MEFs were isolated from C57BL/6 E12.5 *Flcn* floxed mice and were maintained in Dulbecco's modified Eagle's medium (DMEM) supplemented with 10% fetal bovine serum (FBS), 100 U/ml penicillin and 100 μg/ml streptomycin (Invitrogen). Flcn wild-type and knockout MEFs were generated after immortalization of primary Flcn Flox/Flox MEFs with retroviral infection of SV40 large T (hygromycin B) and retroviral infection of CD8 or CD8-Cre recombinase, followed by FACS sorting of CD8 positive cells. AMPK DKO MEFs and their wild-

type counterpart cells were generously provided by Dr. Benoit Viollet (Institut Cochin INSERM, Paris, France). RAW 264.7 cells (termed RAW cells), a murine macrophage cell line (ATCC CRL-24) were generously provided by Dr. C. Krawczyk (McGill University, Montreal, Canada). RAW 264.7 TFEB/TFE3 DKO cells and their EV counterpart cells were generously provided by Dr. Rosa Puertollano (National Institutes of Health, Bethesda, MD, USA). Cell lines were maintained in Dulbecco's modified Eagle's medium (DMEM) supplemented with 10% fetal bovine serum (FBS) (Wisent), 100 U/ml penicillin and 100 μg/ml streptomycin (Invitrogen) in 5% CO₂ at 37°C. MEFs and RAW cells were stably downregulated for TFEB/TFE3 or FLCN, respectively, using the Mission lentivirus shRNA empty vector (shEV), shTFEB (TRCN0000013110; Sigma-Aldrich), shTFE3 (TRCN0000232151; Sigma-Aldrich), or shFLCN (TRCN00000301434; Sigma-Aldrich).

2.6. METHODS DETAILS

Pathogen resistance assay

To measure pathogen stress resistance, synchronized L4 worms were transferred to Tryptic Soya Agar (TSA) plates with 8 μg/ml Nalidixic acid that were seeded with 1:50 *S. aureus* MW2 bacteria incubated at 37°C for 3 h (Powell and Ausubel, 2008). Survival was measured daily by transferring worms onto new plates. To measure stress resistance to *P. aeruginosa* PA14, synchronized L4 worms were transferred to Slow Killing (SK) plates (Powell and Ausubel, 2008). Worms were transferred to new plates every 24 h to monitor survival. Worms that responded with movement upon being touched by a platinum wire were considered alive. Assays were performed in triplicate plates per condition with 30 animals per plate, in three independent experiments.

HLH-30 nuclear translocation assay

The *hlh-30p::hlh-30::GFP* was kindly provided by Malene Hansen's Lab. The *flcn-1(ok975); hlh-30p::hlh-30::GFP* and *aak-1(tm1944);aak-2(gt-33); hlh-30p::hlh-30::GFP* and *aak-1(tm1944);aak-2(gt-33); hlh-30p::hlh-30::GFP* strains, respectively, were obtained using standard genetic crossing strategies. 30-40 worm eggs were transferred to 35 mm regular NGM plates seeded with OP50. Synchronized young adult animals expressing the HLH-30:GFP transgene were transferred to TSA plates seeded with 1:20 *S. aureus* MW2 bacteria on the day of the experiment. Worms displaying HLH-30 translocation were scored. For the *let-363* RNAi based experiments, synchronized animals were grown on RNAi plates and were used at the young adult stage for infection with *S. aureus* MW2 bacteria. Translocation was counted using a fluorescent dissecting microscope at indicated timepoints and imaged using Zeiss confocal laser scanning microscope. Images were taken within the first 5 min because mounting stress also induces HLH-30 nuclear translocation.

RNA extraction and real-time PCR in C. elegans

Synchronized young adult nematodes were exposed to pathogenic *S. aureus* bacteria or OP50 seeded plates for 4 h, harvested and washed with M9 buffer. Pellets were flash frozen in liquid nitrogen. Total RNA was extracted with Trizol. iScript Supermix from Bio-Rad was used to reverse transcribe 1 µg RNA samples. Bio-Rad SYBR Green mix was used and qPCRs were performed on the Roche LightCycler 480 machine. Three housekeeping genes were used to confirm changes in gene expression, *cdc-42*, *pmp-3* and Y45FD10.4 (Hoogewijs et al., 2008). Primers are available upon request.

Microarray experiment and gene overlap analysis

Synchronized L4/young adult wild-type and *flcn-1(ok975)* animals were harvested and RNA was extracted using Trizol and purified on Qiagen RNeasy columns. Total RNA samples were then hybridized onto Agilent gene chips. Fold change values were calculated using the mean of both data sets. Agilent files were uploaded into the FlexArray software at Genome Quebec for analysis. Three replicates were normalized and analyzed for each condition. Fold change was determined and p-value was obtained using a standard student's t-test. Differentially expressed genes were compared to other studies; hyperosmotic stress (Rohlfing et al., 2010) and pathogen infection (Irazoqui et al., 2010a, Troemel et al., 2006) using the "compare two lists" online tool at http://www.nemates.org/MA/progs/Compare.html. The significance of the overlap and enrichment scores was determined via hypergeometric distribution method using http://nemates.org/MA/progs/overlap_stats.html. The number of genes in the *C. elegans* genome was considered 19,735.

RNA sequencing method

Synchronized wild-type and *aak-1(tm1944); aak-2(ok524)* animals were harvested at the late L4 stage, washed with M9, and flash frozen in liquid nitrogen. RNA was extracted using Trizol and purified using Qiagen RNeasy columns. RNA samples were processed for RNA-seq analysis at Novogene Inc.

RNA sequencing analysis

RNA samples were processed for RNA sequencing analysis at Novogene Inc. Briefly, the clustering of the index-coded samples was performed on a cBot Cluster Generation System using HiSeq PE Cluster Kit cBot-HS (Illumina). Quality control Raw data of fastq format were firstly

processed through in-house perl scripts. In this step, clean data (clean reads) were obtained by removing reads containing adapter, reads containing ploy-N and low quality reads from raw data. At the same time, Q20, Q30 and GC content the clean data were calculated. All the downstream analyses were based on the clean data with high quality. Reads mapping to the reference genome. Index of the reference genome was built using Bowtie v2.2.3 and paired-end clean reads were aligned to the reference genome using TopHat v2.0.12. TopHat was selected as the mapping tool. Quantification of gene expression level HTSeq v0.6.1 was used to count the reads numbers mapped to each gene. And then FPKM of each gene was calculated based on the length of the gene and reads count mapped to this gene. For DESeq with biological replicates, differential expression analysis of two conditions/groups (two biological replicates per condition) was performed using the DESeq R package (1.18.0). The resulting P-values were adjusted using the Benjamini and Hochberg's approach for controlling the false discovery rate. Gene Ontology (GO) enrichment analysis of differentially expressed genes was implemented by the GOseq R package, in which gene length bias wascorrected. GO terms with corrected Pvalue less than 0.05 were considered significantly enriched by differential expressed genes. KOBAS software was used to test the statistical enrichment of differential expression genes in KEGG pathways. PPI analysis of differentially expressed genes was based on the STRING database, which known and predicted Protein-Protein Interactions. For the species existing in the database, the networks were constructed by extracting the target gene list from the database; Otherwise, Blastx (v2.2.28) was used to align the target gene sequences to the selected reference protein sequences, and then the networks were built according to the known interaction of selected reference species.

Reagents, chemicals, and antibodies

LPS derived from Escherichia Coli endotoxin (0111:B4, InvivoGen, San Diego, CA, USA) was dissolved in PBS (5 mg/ml) by sonication for 2 min, aliquoted and stored at -80°C until use. All LPS preparations were free of protein or lipoprotein contaminants. LPS was used at a final concentration of 1 μg/ml. Recombinant mouse TNF-α was obtained from Biolegend (#575206) with a stock concentration of 0.2 mg/ml and was used at a final concentration of 10 ng/ml dissolved in 10% DMEM. GSK-621 was obtained from APExBIO or Selleckchem (Houston, Texas, USA) and dissolved in DMSO to a stock concentration of 30 mM and used at a final concentration of 30 μM for MEFs. Torin1 was obtained from Tocris Bioscience (Bristol, UK) and dissolved in DMSO to a stock concentration of 1 mM and used at a final concentration of 1 μM. The final DMSO concentration never exceeded 0.1% and this concentration was shown to have no detrimental effect on all the studied cells.

The mouse FLCN polyclonal antibody was generated by the McGill animal resource center services through injecting purified GST-FLCN recombinant protein in rabbits. β-Actin (SC-47778; Santa Cruz Biotechnology), Tubulin (T9026; Sigma-Aldrich), LaminA (SC-71481; Santa Cruz Biotechnology), AMPKα (2532; Cell Signaling Technology), human FLCN 3697; Cell Signaling Technology), p-AMPKα (Thr172) (2531; Cell Signaling Technology), ACC (3676; Cell Signaling Technology), p-ACC (S79) (3661; Cell Signaling Technology), TFEB (A303-673A; Bethyl Laboratories), TFE3 (14779S; Cell Signaling Technology and HPA023881; Sigma-Aldrich), p70S6K (2708; Cell Signaling Technology), p-p70S6K (9205; Cell Signaling Technology), S6 (2217; Cell Signaling Technology), p-S6 (4858; Cell Signaling Technology), 4EBP1 (9644; Cell Signaling Technology), p-4EBP1 (9456; Cell Signaling Technology) antibodies are commercially available.

Quantitative real-time RT-PCR in mammalian cells

FLCN wild-type, FLCN KO MEFs, and RAW 264.7 cells were seeded in triplicates in 6-well plates at 3 × 10⁵ cells per well in DMEM medium supplemented with 10% FBS. After incubation for 24 h at 37°C, 5% CO₂, cells were treated with TNF-α, LPS, GSK-621 or vehicle for 2, 3, or 24 h. Cells were then collected, and total RNA was isolated and purified using Total RNA Mini Kit (Geneaid) according to the manufacturer's instructions. For quantitative real-time PCR analysis, 1 μg of total RNA was reverse-transcribed using the SuperScript III kit (Invitrogen). SYBR Green reactions using the SYBR Green qPCR supermix (Invitrogen) and specific primers (available upon request) were performed using an AriaMX Real-time PCR system (Agilent Technologies). Relative expression of mRNAs was determined after normalization against housekeeping gene RPLP0 or B2M.

Mouse Protein Cytokine Array

RAW 264.7 cells were seeded in triplicates in 6-well plates at 1 x 10⁶ cells per well in DMEM medium supplemented with 10% FBS. After incubation for 24 h at 37 °C, 5% CO₂, cells were treated with LPS or GSK-621 or vehicle for 3, or 24 h, and the conditioned medium was harvested and centrifuged at 1,500 × g to remove cell debris. 32 cytokine/chemokine/growth factor biomarkers were simultaneously quantified by using a Discovery Assay® called the Mouse Cytokine Array/Chemokine Array 32-Plex (Eve Technologies Corp, Calgary, AB, Canada). The multiplex assay was performed by using the Bio-PlexTM 200 system (Bio-Rad Laboratories, Inc., Hercules, CA, USA), and a Milliplex Mouse Cytokine/Chemokine kit (Millipore, St. Charles, MO, USA) according to the manufacturers protocol. The 32-plex consisted of Eotaxin, G-CSF, GM-CSF, IFNγ, IL-1α, IL-1β, IL-2, IL-3, IL-4, IL-5, IL-6, IL-7, IL-9, IL-10, IL-12 (p40), IL-12 (p70),

IL-13, IL-15, IL-17, IP-10, KC, LIF, LIX, MCP-1, M-CSF, MIG, MIP-1α, MIP-1β, MIP-2, RANTES, VEGF. The change in the cytokine levels in FLCN KO medium was normalized against their respective wild-type medium.

Protein extraction and immunoblotting

For AMPK immunoblotting, cells were washed twice with cold PBS, lysed in AMPK lysis buffer (10 mM Tris-HCl (pH 8.0), 0.5 mM CHAPS, 1.5 mM MgCl₂ 1 mM EGTA, 10% glycerol, 5 mM NaF, 0.1 mM Na₃VO₄, 1 mM benzamidine, 5 mM NaPPi), supplemented with complete protease inhibitor (Roche) and DTT (1 mM), and cell lysates were cleared by centrifugation at 13000 x g. For all other immunoblotting, cells were washed twice with cold PBS and lysed directly in Laemmli buffer (62.5 mM Tris-HCl (pH 6.8), 2% (w/v) sodium dodecyl sulphate, 10% (v/v) glycerol, 5% (v/v) β-mercaptoethanol and 0.01% (w/v) bromophenol blue). Proteins were separated on SDS-PAGE gels and revealed by western blot using the antibodies listed above.

Subcellular fractionation

Cells were washed and resuspended in PBS and pelleted 5 min at 300 x g at 4°C. The pellet was lysed in NP-40 lysis buffer (50 mM Tris-HCl (pH 7.4), 0.5 % NP-40, 5 mM MgCl₂ 140 mM KCl, 5 mM NaF, 0.1 mM Na₃VO₄, 1 mM benzamidine, 5 mM NaPPi, 1x protease inhibitors) and pelleted 5 min at 1000 x g. Supernatant was collected as the cytosolic fraction. The pellet was lysed in nuclear lysis buffer (25 mM Tris-HCl (pH 7.4), 0.5 % Triton X-100, 0.5% SDS, 5 mM MgCl₂ 140 mM KCl, 5 mM NaF, 0.1 mM Na₃VO₄, 1 mM benzamidine, 5 mM NaPPi, 1 x protease inhibitors), sonicated 15 min with 30 sec bursts and collected as the nuclear + membrane fraction.

Immunofluorescence

Cells were washed with PBS and fixed in petri dishes with 3.7% formaldehyde at room temperature for 30 min. After fixation, cells were washed twice with PBS and then permeabilized with 0.3%

Triton X-100 in PBS at room temperature for 5 min. Cells were incubated in 10% BSA in PBS for 1 h and then with TFEB or TFE3 primary antibody in 1.5% BSA in PBS for 2 h at 37°C. Cells were washed three times with PBS and incubated with the corresponding secondary antibodies conjugated to Alexa Fluor 488 in 1.5% BSA in PBS for 30 min at 37°C. Cells were washed three times with PBS and incubated with DAPI (0.1 μg/ml) in PBS for 15 min at room temperature. PBS-washed dishes were covered with cover slips and observed with Axioskop microscope (Zeiss).

Metabolic Assays

Glucose production and lactate consumption was measured using a NOVA Bioanalysis flux analyzer or the Eton Bioscience kit (Eton Bioscience, Charlestown, MA, USA). Briefly, cells were plated at 500,000 cells/well in triplicates in 6-well plates in DMEM growth medium for 24 h. Then The conditioned media was collected, spun down at 13xg for 5 mins, and transferred to new tubes were the media was analyzed using the NOVA Bioanalysis flux analyzer. OCR and the ECAR of cells were measured using an XF96 Extracellular Flux Analyzer (Seahorse Bioscience, Boston, MA, USA). In brief, EV or shFLCN RAW264.7 were plated at 100,000 cells/well in growth medium for 24 h. After 24 h, cells were incubated in non-buffered DMEM containing 25 mM glucose and 2 mM glutamine in a CO2-free incubator at 37°C for 2 h to allow for temperature and pH equilibration before loading into the XF96 apparatus. XF assays consisted of sequential mix (3 min), pause (3 min), and measurement (5 min) cycles, allowing for determination of OCR/ECAR every 10 min. After establishing a baseline, Oligomycin (10 uM), FCCP (15 μM), and Rotenone/Antimycin A (1 μM, and 10 μM, respectively) were added sequentially.

ATP quantification

Cells were plated at 4,000 cells/well in triplicates in 96-well plates. After 24 h, cells were lysed and mixed for 10 min according to manufacturer's instructions (CellTiter-Glo luminescent cell viability assay, Promaga). Luminescence was measured using Fluostar Omage (BMG Labtech) directly in plates.

Phagocytosis Assay

Phagocytosis in EV or shFLCN RAW264.7 cells was assessed using Red pHrodo *S.aureus* BioParticles conjugate assay (Thermofisher) according to the manufacturer's protocol. In brief, EV or shFLCN RAW264.7 were plated in triplicates in 96-well plates at 80,000 cells/well in growth medium for 2 h before treatment. After 2 h, cells were treated with the BioParticles (after homogenization in serum-free DMEM) at a final concentration of 1 mg/ml and incubated at 37 °C for 3 h. Subsequently, cells were collected and analyzed using FACSDiva analyzer (Becton Dickison).

Quantification and statistical analysis

Data are expressed as mean \pm SEM. Statistical analyses for all data were performed using student's t-test for comparisons between 2 groups, one-way ANOVA for comparisons between 3 or more groups, and Log-rank Mantel Cox test for survival plots, using GraphPad Prism 7 software. The data is assumed normal as tested by the Shapiro and Wilk normality test. Statistical significance is indicated in figures (*p<0.05, **p<0.01, ***p<0.001, ****p<0.0001) or included in the supplemental tables. *In vitro* studies were biologically repeated at least three times in triplicates. the numbers of animals in each experiment are indicated in the figure legends.

Data and software availability

The RNA sequencing and microarray data are deposited at Gene Expression Omnibus (GEO) accession number: GSE126656.

2.7. ACKNOWLEDGEMENTS

We thank Audrey Kapelanski-Lamoureux for technical support, Javier Irazoqui for kindly providing the hlh-30(tm1978) mutant strain, Malene Hansen for the hlh-30::GFP transgenic line, Joaquin Madrenas and Eric Deziel for providing us the MW2 S. aureus and PA14 P. aeruginosa bacterial strains, respectively. We thank Dr. Yong Chen and Dr. Marjan Gucek (Proteomic Core Facility, NHLBI, NIH) for their assistance with mass spectrometry analysis. We thank Nahum Sonenberg and Marie-Claude Gingras for the critical reading of the manuscript. We thank Ribal Abi Raad (Concordia University, Montreal, Canada) for the statistical analysis of the results, and Alain Sarabia Pacis (GCRC, McGill University, Montreal, Canada) for his bioinformatics support. We acknowledge the Caenorhabditis Genetic Center for C. elegans strains. E.P., L.E., M.P., and T. V. were supported by Rolande and Marcel Gosselin studentship and the MICRTP training grant, Dr. Victor K.S. Lui Fellowship and Dr. Michael D'Avirro from GCRC, FRQS, and Canderel studentship award, respectively. This work was supported by grants to A.P. from Myrovlytis Trust, Kidney Foundation of Canada and Terry Fox Research Institute. The Goodman Cancer Research Centre Metabolomics Core Facility is supported by the Canada Foundation of Innovation and Terry Fox Research Institute. R.J. and E.M. were supported by CIHR grant MOP-142259. J.A.M. and R.P. were supported by the Intramural Research Program of the National Institutes of Health, National Heart, Lung, and Blood Institute (NHLBI).

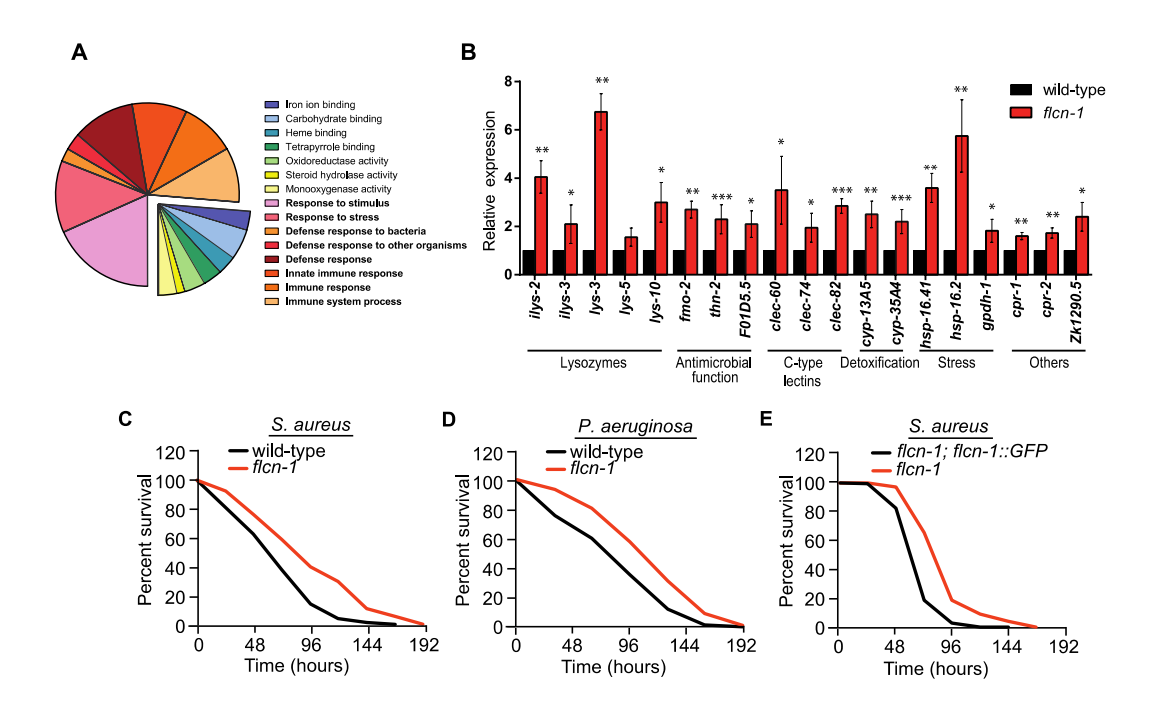
2.8. AUTHORS' CONTRIBUTIONS

LEH, EP, and AP conceived and designed the experiments, LEH, EP, TV, MP, JK, JM, RP, PB, RJ, and EM, performed the experiments, LEH, EP and AP wrote and revised the manuscript.

Declaration of interests

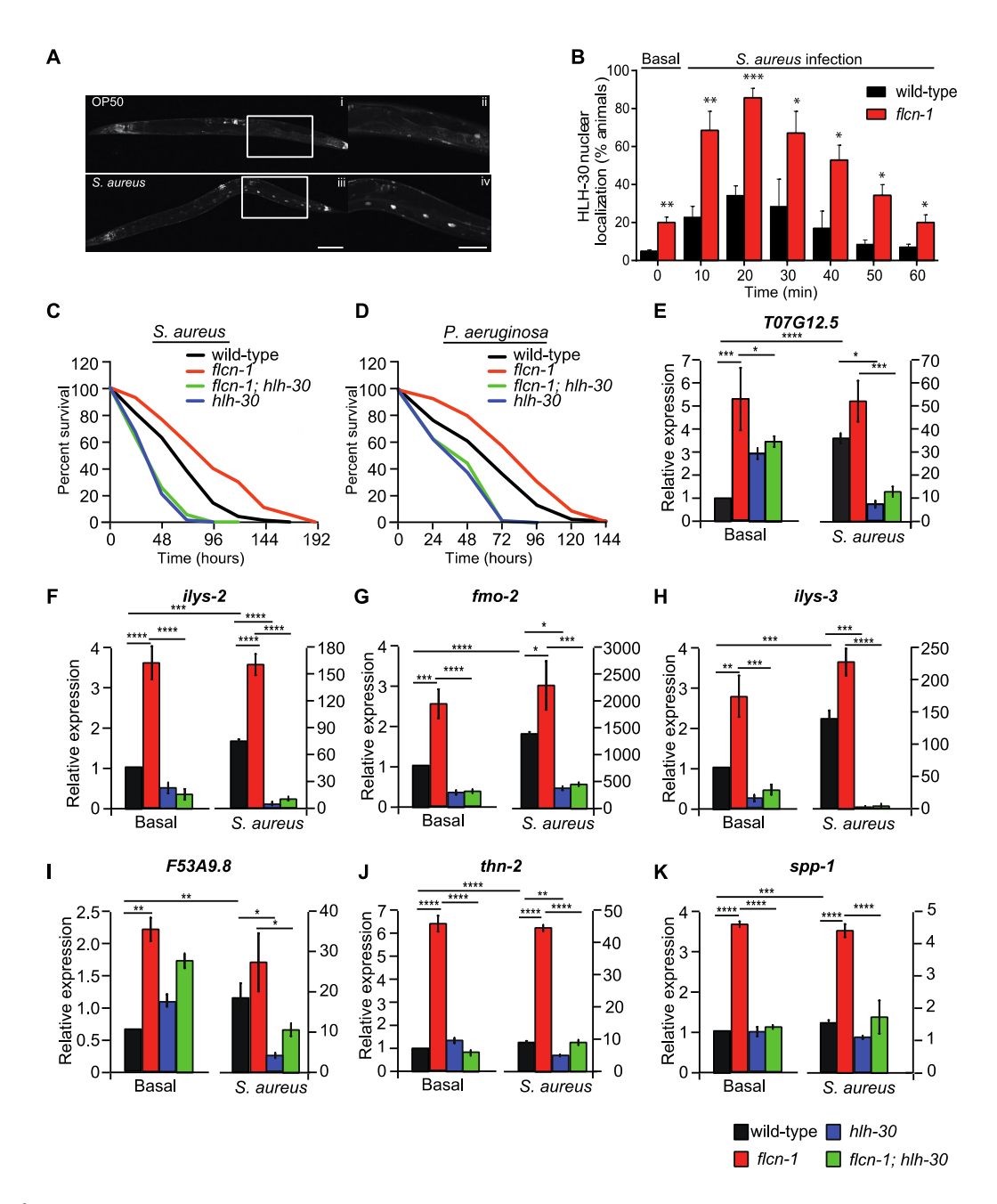
The authors declare no competing interests.

2.9. FIGURES AND FIGURE LEGENDS



⁵Figure 1: Loss of *flcn-1* increases the expression of antimicrobial genes and confers resistance to bacterial

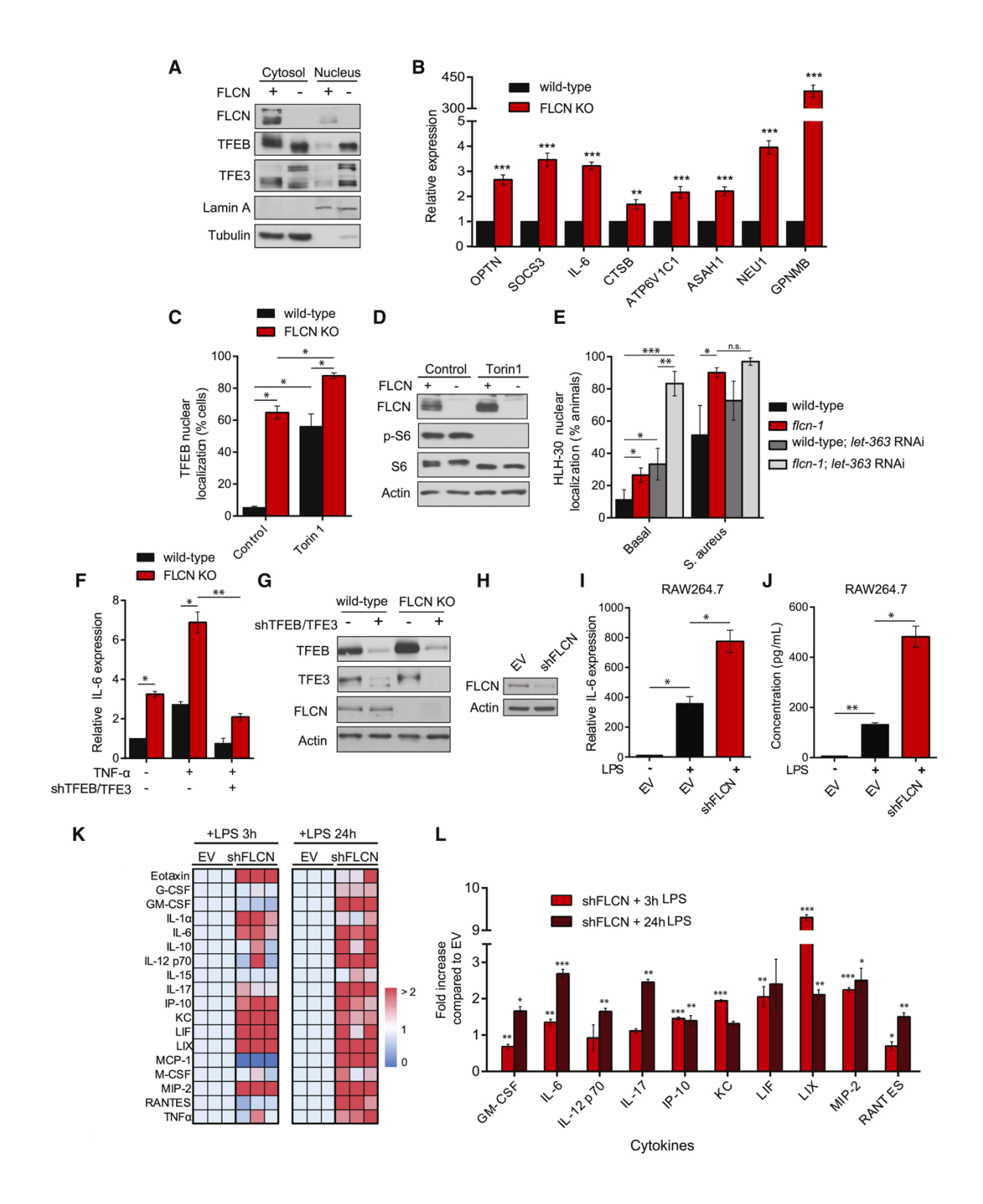
(A) Pie chart of functional gene ontology analysis of the genes upregulated in flcn-1(ok975) mutant animals at basal level. (B) Relative mRNA expression of stress response and antimicrobial peptide genes in wild-type and flcn-1 mutant animals. Data represents the average of three independent experiments, each done in triplicates \pm SEM. Significance was determined using student's t-test (*p<0.05, **p<0.01, ***p<0.001). (C-E) Percent survival of indicated strains upon infection with S. aureus and P. aeruginosa. Refer to Table S1 for details on number of animals utilized and number of repeats. The Statistical analysis was obtained using Mantel Cox test on the pooled curve.



⁶Figure 2: Loss of flcn-1 increases pathogen resistance via HLH-30 activation

(A) Representative micrographs of HLH-30::GFP at basal level or after infection with *S. aureus* for 30 min. The signal is found in the nuclei of enterocytes, a cell-type in which lipids are stored in nematodes. Scale bars in i, iii and in ii, iv represent 100 μm and 50 μm respectively. (B) Percent animals showing HLH-30 nuclear translocation in *hlh-30p::hlh-30*::GFP and *flcn-1; hlh-30p::hlh-30*::GFP worm strains upon *S. aureus* infection for indicated time points to determine HLH-30

nuclear localization upon flcn-1 loss at basal level (time 0) and upon S. aureus infection. Data represents the mean \pm SEM from three independent repeats, $n \ge 30$ animals/condition for every repeat. Significance was determined using student's t-test (*p<0.05, **p<0.01, ***p<0.001). (C, D) Percent survival of indicated worm strains upon infection with S. aureus and P. aeruginosa. Refer to Table S1 for details on number of animals utilized and number of repeats. Statistics obtained using Mantel-Cox analysis on the pooled curve. (E-K) Relative mRNA expression of indicated target genes in wild-type, flcn-1(ok975), flcn-1(ok975); hlh-30 (tm1978), and hlh-30 (tm1978) animals at basal level and after treatment with S. aureus for 4 h. Data represents the average of three independent experiments done in triplicates \pm SEM. Significance was determined using one-way ANOVA with the application of Bonferroni correction (*p<0.05, **p<0.01, ***p<0.001).

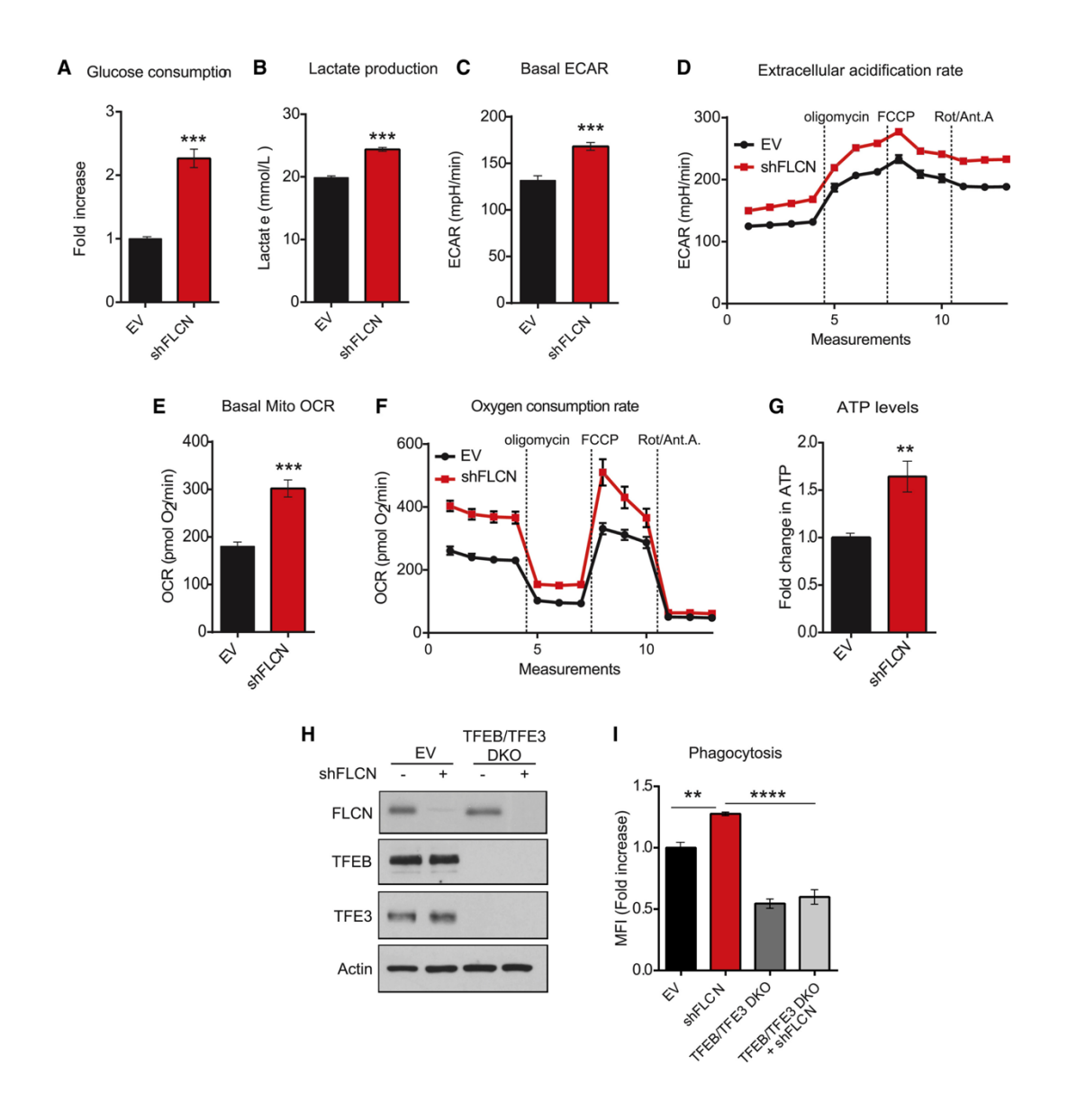


⁷Figure 3: The regulation of TFEB/TFE3 by FLCN is evolutionarily conserved through mTOR independent mechanisms

(A) Immunoblot of isolated cytosolic-soluble fractions and nuclear fractions of wild-type and FLCN KO mouse embryonic fibroblasts (MEFs). (B) Relative mRNA levels measured by qRT-

PCR of indicated genes in wild-type and FLCN KO MEFs. Data represent the average of three independent experiments done in triplicates \pm SEM. Significance was determined using student's t-test (**p<0.01, ***p<0.001). (C) Quantification of the percentage of cells showing TFEB nuclear staining treated with mTORC1 inhibitor; Torin1 (1 µM) for 2 h. Data represents the average of three independent experiments, each done in triplicates ± SEM. Significance was determined using one-way ANOVA with the application of Bonferroni correction (*p<0.05). (D) Immunoblot analysis of whole cell extracts with or without Torin1 (1 µM) for 2 h. (E) Percent animals showing HLH-30 nuclear translocation in indicated hlh-30p::hlh-30::GFP worm strains treated with or without let-363 RNAi at basal level or upon S. aureus infection. Data represent the mean \pm SEM with 3 independent repeats, n \geq 30 animals/condition for every repeat. Significance was determined using one-way ANOVA with the application of the Bonferroni correction (**p<0.01, ***p<0.001). (F) Relative IL-6 mRNA levels measured by qRT-PCR in empty vector (EV) or shTFEB/TFE3-treated wild-type or FLCN KO MEFs, stimulated with or without 10 ng/ml TNF-α for 2 h. Data represents the average of three independent experiments, each done in triplicates \pm SEM. Significance was determined using one-way ANOVA with the application of Bonferroni correction (*p<0.05, **p<0.01). (G) Immunoblot analysis of wild-type and FLCN KO MEFs transfected with EV or shTFEB/TFE3. (H) Immunoblot analysis of RAW 264.7 cells transfected with EV or shFLCN. (I) Relative IL-6 mRNA levels measured by qRT-PCR in EV or shFLCN-treated RAW264.7 cells, stimulated with or without 1 µg/ml LPS for 3 h. (J) Quantification of IL-6 levels of conditions described in (I) using Mouse Protein Cytokine Array. Data represent the average of three independent experiments \pm SEM. Significance was determined using one-way ANOVA with the application of Bonferroni correction (*p<0.05, **p<0.01). (K) Hierarchical clustering of cytokine and chemokine secretion in the supernatant using Mouse

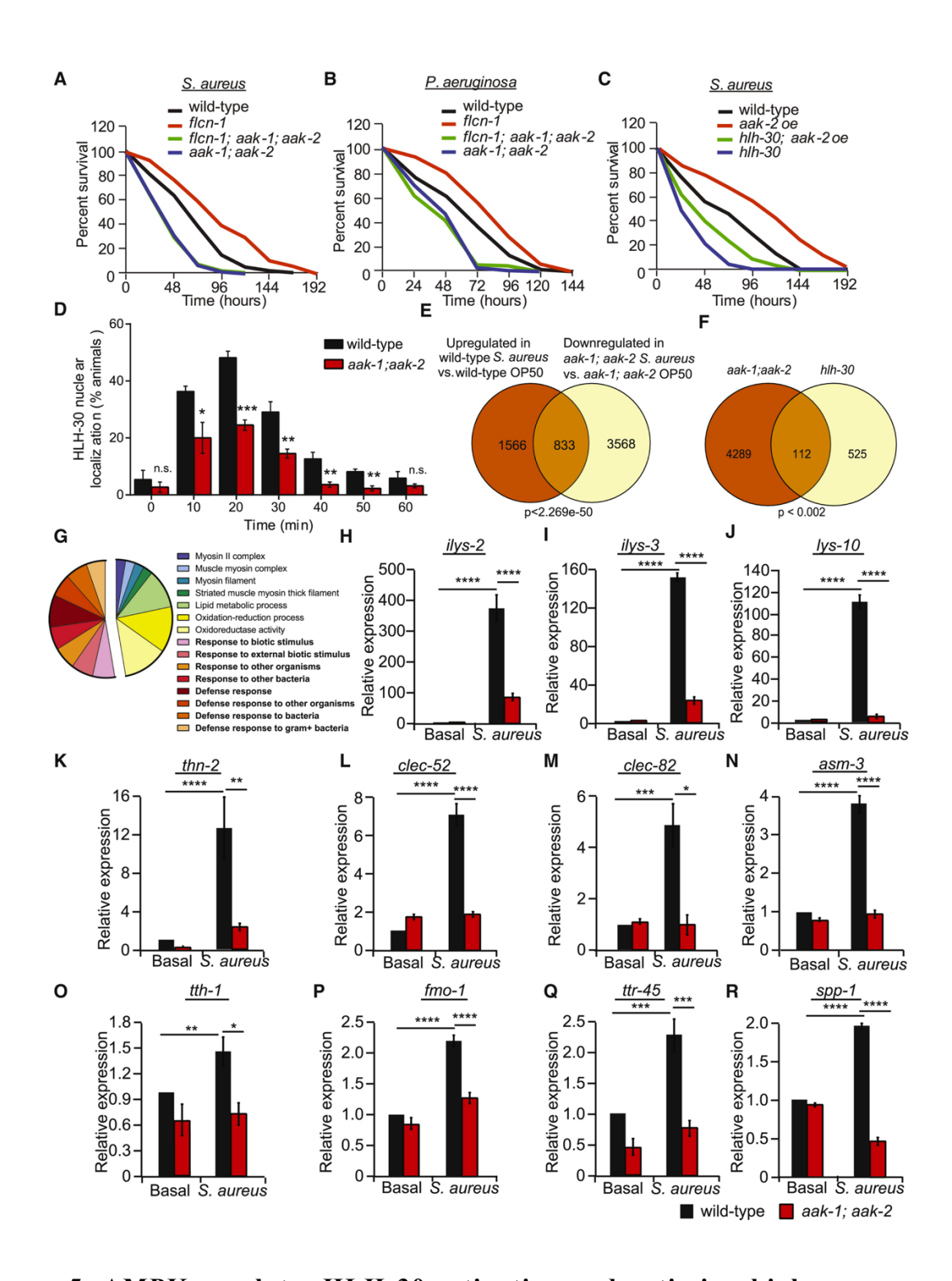
Protein Cytokine Array in EV or shFLCN-treated RAW264.7 cells stimulated with 1 μ g/ml LPS for 3 and 24 h. Each square in a column represents the average of triplicate experiments, and each column represents an independent replicate. Fold increase was normalized against EV and color-coded (dark red indicates 2 or more-fold increase, dark blue indicates no change). (L) Fold increase in cytokine and chemokine secretion levels as described in (J). Data represent the average of three independent experiments, each done in triplicates \pm SEM. Significance was determined using student's t-test in comparison to the EV stimulated with LPS for 3h and 24, respectively (*p<0.05, **p<0.01, ***p<0.001).



⁸Figure 4: FLCN depletion in macrophages enhances their energy metabolism and phagocytic potential

(A) Glucose production and (B) lactate consumption levels measured using NOVA Bioanalysis flux analyzer in empty vector (EV) or shFLCN RAW264.7 at basal level. (C, D) Extracellular acidification rate (ECAR) and (E, F) oxygen consumption rate (OCR) of EV or shFLCN RAW264.7 at basal level as measured by Seahorse Bioscience XF96 extracellular flux analyzer. After establishing a baseline, oligomycin (10 μM), FCCP (15 μM), and rotenone/antimycin A (1 μM, and 10 μM, respectively) were added. (G) Fold change in ATP levels in EV or shFLCN

RAW264.7 after 24 h of seeding as measured by CellTiter-Glo Luminescent Cell Viability Assay. Data represent the average of three independent experiments, each done in triplicates \pm SEM. Significance was determined using student's t-test (**p<0.01, ***p<0.001). (H) Immunoblot analysis of EV and TFEB/TFE3 DKO RAW264.7 cells transfected with EV or shFLCN. (I) Phagocytic activities of EV, TFEB/TFE3 DKO, and TFEB/TFE3 DKO shFLCN RAW264.7 cells measured using Red pHrodo *S.aureus* BioParticles by flow cytometry. Data represents the average of three independent experiments, each done in triplicates \pm SEM. Significance was determined using one-way ANOVA with the application of Bonferroni correction (**p<0.01, ****p<0.0001).

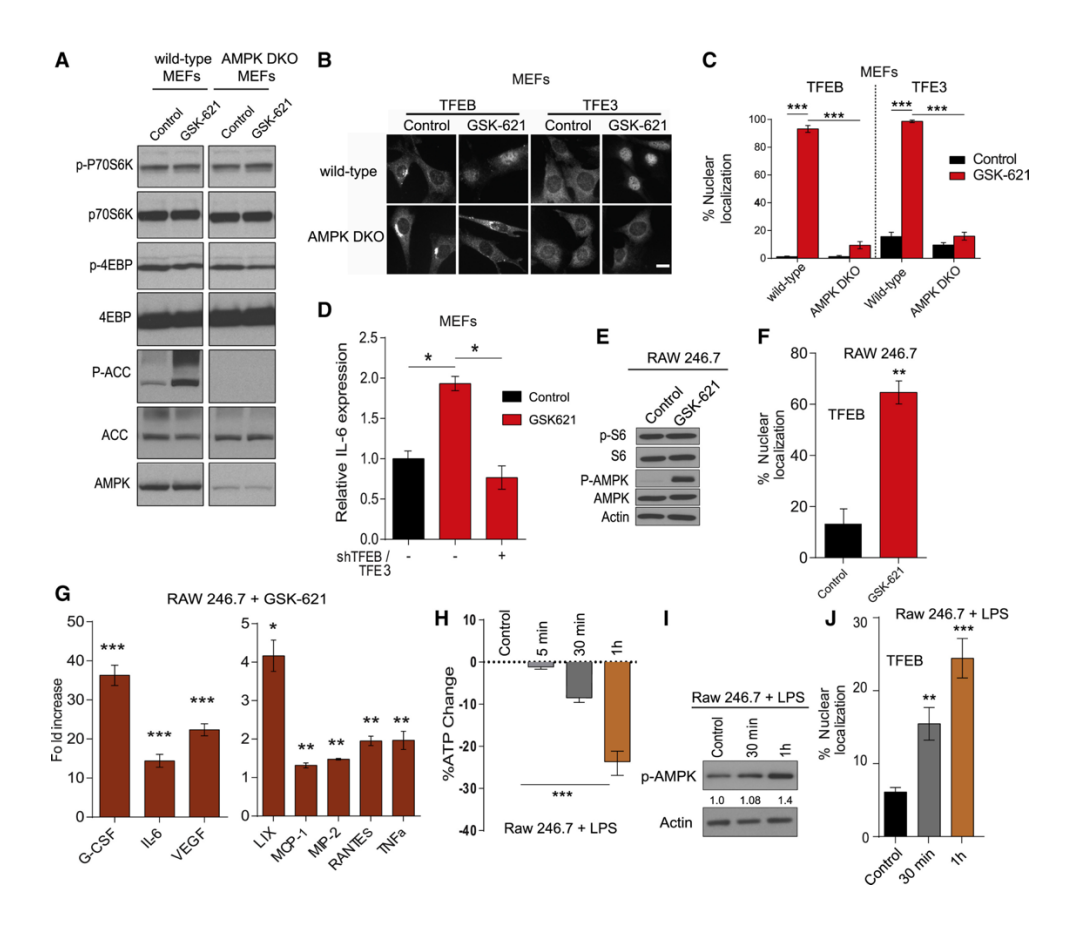


⁹Figure 5: AMPK regulates HLH-30 activation and antimicrobial response upon infection with bacterial pathogens

(A-C) Percent survival of indicated worm strains upon infection with S. aureus or P. aeruginosa.

Refer to Table S1 for details on number of animals utilized and number of repeats. Statistics

obtained by Mantel-Cox analysis on the pooled curve. (D) Percentage of animals showing HLH-30 nuclear translocation in indicated hlh-30p::hlh-30::GFP worm strains upon infection with S. aureus for the indicated amount of time. Data represent the mean \pm SEM with 3 independent repeats, $n \ge 30$ animals/condition for every repeat. Significance was determined using student's ttest (*p<0.05, **p<0.01, ***p<0.001). (E) Venn diagram of the overlapping set of genes between S. aureus-induced genes in wild-type animals and genes downregulated in aak-1(tm1944); aak-2(ok524) mutant animals upon infection. (F) Venn diagram and (G) pie chart of functional gene ontology analysis of AMPK-dependent genes obtained by the overlap analysis between genes downregulated in aak-1(tm1944); aak-2(ok524) mutant animals in comparison to wild-type animals upon S. aureus infection and the hlh-30-dependent list of genes published in (40). Comparisons were performed using the "compare two lists" online software and the significance was obtained using "nemates" software. (H-R) Relative mRNA levels measured by qRT-PCR of AMPK-dependent genes in wild-type and aak-1(tm1944); aak-2(ok524) mutant animals infected with or without S. aureus for 4 h. Results are normalized to non-treated wild-type animals. Validation of RNA-seq using three biological replicates per condition and three technical replicates per biological repeat. Significance was determined using one-way ANOVA with the application of the Bonferroni correction (*p<0.05, **p<0.01, ***p<0.001, ****p<0.001).



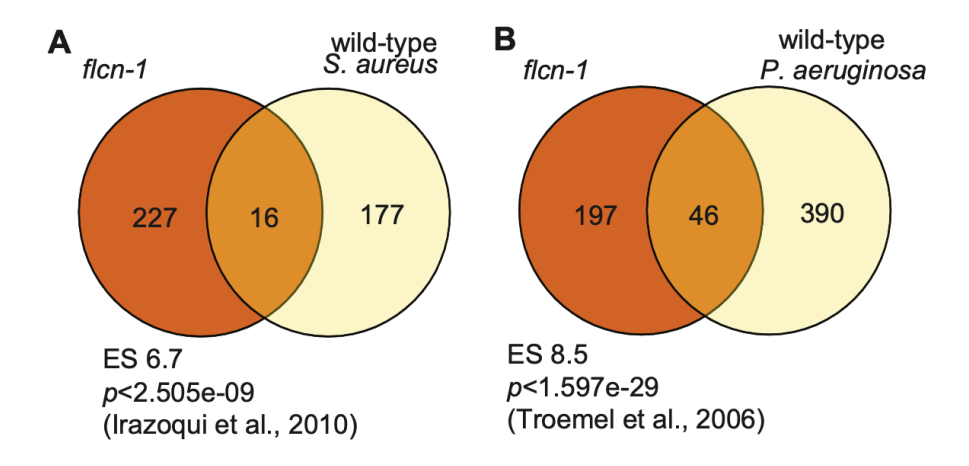
¹⁰Figure 6: AMPK regulates TFEB/TFE3-mediated innate immune response

(A) Immunoblot of wild-type or AMPK α 1/ α 2 double knock out (DKO) MEFs stimulated with the AMPK activator; GSK-621 (30 μ M) for 1 h. (B) Representative images of TFEB and TFE3 staining in wild-type and AMPK DKO MEFs before and after treatment with GSK-621 (30 μ M) for 1 h. Scale bars represent 20 μ m. (C) Quantification of the percentage of cells showing TFEB and TFE3 nuclear staining of the conditions described in (B). (D) Relative IL-6 mRNA levels measured by qRT-PCR in wild-type MEFs transfected with EV or shTFEB/TFE3, stimulated with GSK-621 for 2 h. Data represents the average of three independent experiments, each done in triplicates \pm SEM. Significance was determined using one-way ANOVA with the application of Bonferroni correction (*p<0.05, ***p<0.001). (E) Immunoblot analysis of RAW264.7 macrophages treated with GSK-621 (30 μ M) for 2 h. (F) Quantification of the percentage of

RAW264.7 cells showing TFEB nuclear staining of the conditions described in (D). (G) Quantification of the significant fold increases in cytokine and chemokine protein levels in RAW264.7 macrophages, treated with GSK-621 (30 μ M) for 2 h as compared to control. (H) Fold change in ATP levels in RAW264.7 treated with LPS (1 μ g/ml) for up to 1 h as measured by CellTiter-Glo Luminescent Cell Viability Assay. (I) Immunoblot analysis of RAW264.7 macrophages treated with LPS (1 μ g/ml) for up to 1 h. (J) Quantification of the percentage of RAW264.7 cells with TFEB nuclear localization of the conditions described in (H). Data represent the average of three independent experiments, each done in triplicates \pm SEM. Significance was determined using student's t-test (*p<0.05, **p<0.01, ***p<0.001).

Table 1: Genes classified according to family functions and upregulated in *flcn-1(ok975)* mutant animals. (attached)

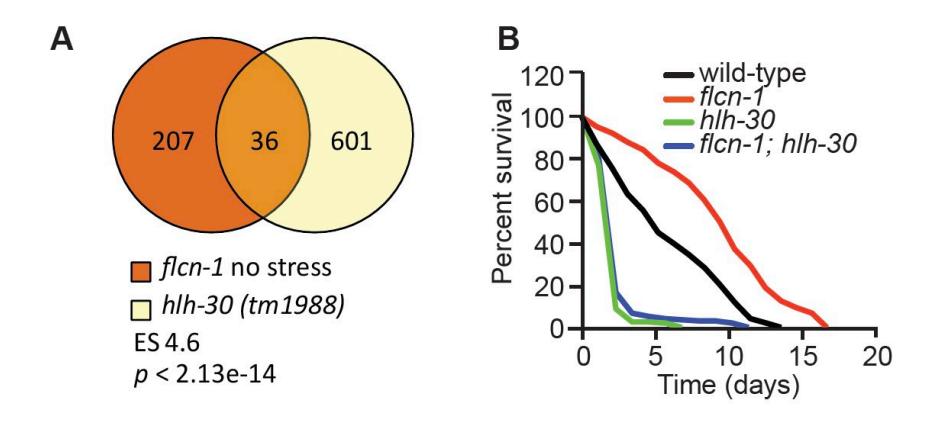
2.10. SUPPLEMENTAL DOCUMENTS AND LEGENDS:



¹¹Supplemental Figure S1

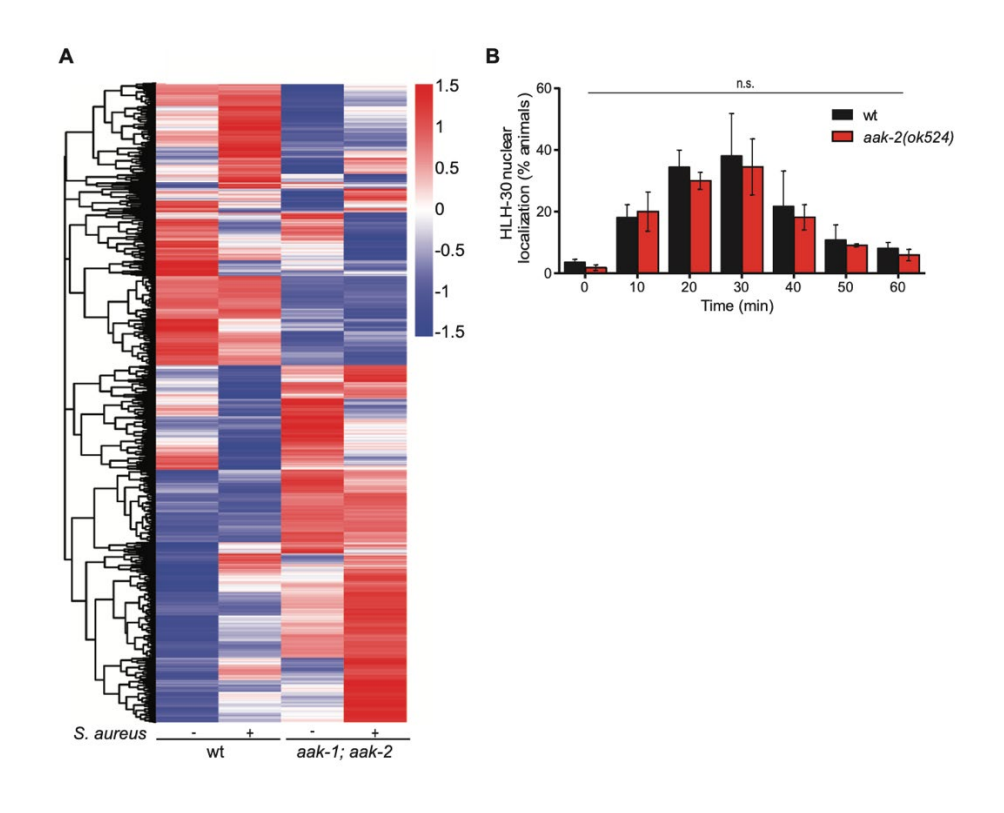
Transcriptional profile of *flcn-1* prior to stress overlaps with profiles of wild-type animals infected with pathogens and correlates with a pathogen resistance phenotype.

(A, B) Venn diagrams showing the overlap of genes upregulated in *flcn-1(ok975)* animals at basal level and genes upregulated in wild-type animals following treatment with *S. aureus* from [36] (A) or *P. aeruginosa* from [37] (B). Comparisons were performed using the "compare two lists" online software and the significance and ES (enrichment scores) were obtained using "nemates" software.



Supplemental Figure S2: Role of hlh-30 downstream of flcn-1.

(A) Venn diagrams showing the overlap of genes upregulated in *flcn-1(ok975)* animals at basal level and downregulated in *hlh-30 (tm1978)* mutant nematodes. Comparisons were performed using the "compare two lists" online software and the significance and ES (enrichment scores) were obtained using "nemates" software. (B) Percent survival of indicated strains to 400 mM NaCl stress. Refer to Table S9 for details on number of animals utilized and number of repeats Statistics obtained by Mantel-Cox analysis on the pooled curve.



¹²Supplemental Figure S2
RNA Seq heat map and gene ontology analysis in wild-type and *aak-1(tm1944); aak-2(ok524)*at basal level and upon *S. aureus* infection.

(A) Heat map showing differential gene expression in wild-type and aak-1(tm1944); aak-2(ok524) mutant animals grown on OP50 or exposed to S. aureus for 4 h. Red color indicates genes that are differentially upregulated while blue color indicates gene sets that are downregulated in comparison to untreated wild-type animals. (B) Nuclear translocation of HLH-30 in aak-2(ok524); hlh-30::GFP at basal level and upon S. aureus infection. Data represent the mean \pm SEM with 3 independent repeats, $n \ge 30$ animals/condition for every repeat. Significance was determined using student's t-test. 2

Table S1, related to Figures 1, 2, and 5: Mean survival on pathogens: results and statistical analysis (attached)

Sheet 1: Mean survival on S. aureus: results and statistical analysis.

- Sheet 2: Mean survival on *P. aeruginosa*: results and statistical analysis.
- Table S2, related to Figure 2: Mean survival on 400mM NaCl: results and statistical analysis.
- Table S3, related to Figures 1, 2, and 5: Gene expression analysis.
- Sheet 1: List of genes upregulated in *flcn-1(ok975)* mutant animals in comparison to wild-type at basal level.
- Sheet 2: GO analysis of genes upregulated in flcn-1(ok975) mutant animals at basal level.
- Sheet 3: List of genes with known antimicrobial and defense functions upregulated in *flcn-l(ok975)* at basal level; selection based on GO annotations.
- Sheet 4: List of genes downregulated in *flcn-1(ok975)* mutant animals at basal level.
- Sheet 5: GO analysis of genes downregulated in *flcn-1(ok975)* mutant animals at basal level.
- Sheet 6: Overlapping genes upregulated in *flcn-1(ok975)* animals and animals infected with *S. aureus*.
- Sheet 7: Overlapping genes upregulated in *flcn-1(ok975)* animals and animals infected with *P. aeruginosa*.
- Sheet 8: List of overlapping genes upregulated in *flcn-1(ok975)* mutant animals at basal level and *S. aureus* hlh-30-dependent genes.
- Sheet 9: Genes upregulated in wild-type animals treated with *S. aureus* for 4 h in comparison to animals grown on OP50 *E. Coli*.
- Sheet 10: List of genes downregulated in wild-type animals treated with *S. aureus* for 4 h in comparison to animals grown on OP50
- Sheet 11: List of genes upregulated in *aak-1(tm1944)*; *aak-2(ok524)* animals in comparison to wild-type animals at basal level

Sheet 12: List of genes downregulated in *aak-1(tm1944)*; *aak-2(ok524)* animals in comparison to wild-type animals at basal level

Sheet 13: List of genes downregulated in *aak-1(tm1944)*; *aak-2(ok524)* animals treated with *S. aureus* in comparison to wild-type animals treated with *S. aureus*

Sheet 14: AMPK-dependent genes determined by overlap between genes upregulated in wild-type animals upon *S. aureus* infection and downregulated in infected *aak-1(tm1944)*; *aak-2(ok524)* mutant animals

Sheet 15: GO analysis of AMPK-dependent genes obtained by overlap between genes upregulated in wild-type animals upon S. *aureus* infection and downregulated in infected *aak-1(tm1944)*; *aak-2(ok524)* mutant animals. This sheet includes a histogram of functional gene ontology analysis of genes induced by S. *aureus* in wild-type animals and downregulated in *aak-1(tm1944)*; *aak-2(ok524)* mutant animals upon infection.

Sheet 16: Genes downregulated in *aak-1(tm1944)*; *aak-2(ok524)* and *hlh-3(tm1978)* mutant animals upon *S. aureus* infection in comparison to wild-type.

Sheet 17: GO analysis of the overlap between infection genes regulated by AMPK and HLH-30.

2.11. REFERENCES ASSOCIATED WITH CHAPTER 2

- [1] Akira, S., Uematsu, S. & Takeuchi, O. 2006. Pathogen recognition and innate immunity. *Cell*, 124, 783-801.
- [2] Baba, M., Hong, S. B., Sharma, N., Warren, M. B., Nickerson, M. L., Iwamatsu, A., Esposito, D., Gillette, W. K., Hopkins, R. F., 3rd, Hartley, J. L., Furihata, M., Oishi, S., Zhen, W., Burke, T. R., Jr., Linehan, W. M., Schmidt, L. S. & Zbar, B. 2006. Folliculin encoded by the BHD gene interacts with a binding protein, FNIP1, and AMPK, and is involved in AMPK and mTOR signaling. *Proc Natl Acad Sci U S A*, 103, 15552-7.
- [3] Betschinger, J., Nichols, J., Dietmann, S., Corrin, P. D., Paddison, P. J. & Smith, A. 2013. Exit from pluripotency is gated by intracellular redistribution of the bHLH transcription factor Tfe3. *Cell*, 153, 335-47.
- [4] Blagih, J., Coulombe, F., Vincent, E. E., Dupuy, F., Galicia-Vazquez, G., Yurchenko, E., Raissi, T. C., Van Der Windt, G. J., Viollet, B., Pearce, E. L., Pelletier, J., Piccirillo, C. A., Krawczyk, C. M., Divangahi, M. & Jones, R. G. 2015. The energy sensor AMPK regulates T cell metabolic adaptation and effector responses in vivo. *Immunity*, 42, 41-54.
- [5] Brenner, S. 1974. The Genetics Of Caenorhabditis Elegans. *Genetics*, 77, 71-94.
- [6] Chen, H. D., Kao, C. Y., Liu, B. Y., Huang, S. W., Kuo, C. J., Ruan, J. W., Lin, Y. H., Huang, C. R., Chen, Y. H., Wang, H. D., Aroian, R. V. & Chen, C. S. 2017. HLH-30/TFEB-mediated autophagy functions in a cell-autonomous manner for epithelium intrinsic cellular defense against bacterial pore-forming toxin in C. elegans. *Autophagy*, 13, 371-385.
- [7] Chen, L., Chen, Q., Deng, G., Kuang, S., Lian, J., Wang, M. & Zhu, H. 2016. AMPK activation by GSK621 inhibits human melanoma cells in vitro and in vivo. *Biochem Biophys Res Commun*, 480, 515-521.
- [8] David, R. 2011. Autophagy: Tfeb Perfects Multitasking. *Nat Rev Mol Cell Biol*, 12, 404.
- [9] Efeyan, A., Zoncu, R., Chang, S., Gumper, I., Snitkin, H., Wolfson, R. L., Kirak, O., Sabatini, D. D. & Sabatini, D. M. 2013. Regulation of mTORC1 by the Rag GTPases is necessary for neonatal autophagy and survival. *Nature*, 493, 679-83.
- [10] Engelmann, I., Griffon, A., Tichit, L., Montanana-Sanchis, F., Wang, G., Reinke, V., Waterston, R. H., Hillier, L. W. & Ewbank, J. J. 2011. A comprehensive analysis of gene expression changes provoked by bacterial and fungal infection in C. elegans. *PLoS One*, 6, e19055.
- [11] Frisard, M. I., Wu, Y., Mcmillan, R. P., Voelker, K. A., Wahlberg, K. A., Anderson, A. S., Boutagy, N., Resendes, K., Ravussin, E. & Hulver, M. W. 2015. Low levels of lipopolysaccharide modulate mitochondrial oxygen consumption in skeletal muscle. *Metabolism*, 64, 416-27.
- [12] Gordon, S. 2016. Phagocytosis: An Immunobiologic Process. *Immunity*, 44, 463-475.
- [13] Gray, M. A., Choy, C. H., Dayam, R. M., Ospina-Escobar, E., Somerville, A., Xiao, X., Ferguson, S. M. & Botelho, R. J. 2016. Phagocytosis Enhances Lysosomal and Bactericidal Properties by Activating the Transcription Factor TFEB. *Curr Biol*, 26, 1955-1964.
- [14] Hansen, M. E., Simmons, K. J., Tippetts, T. S., Thatcher, M. O., Saito, R. R., Hubbard, S. T., Trumbull, A. M., Parker, B. A., Taylor, O. J. & Bikman, B. T. 2015. Lipopolysaccharide Disrupts Mitochondrial Physiology in Skeletal Muscle via Disparate Effects on Sphingolipid Metabolism. *Shock*, 44, 585-92.
 - [1] Hardie, D. G. 2015. Ampk: Positive And Negative Regulation, And Its Role In Whole-Body Energy Homeostasis. *Curr Opin Cell Biol*, 33, 1-7.
 - [2] Hardie, D. G. & Ashford, M. L. 2014. Ampk: Regulating Energy Balance At The Cellular And Whole Body Levels. *Physiology (Bethesda)*, 29, 99-107.

- [3] Hardie, D. G., Ross, F. A. & Hawley, S. A. 2012. AMPK: a nutrient and energy sensor that maintains energy homeostasis. *Nat Rev Mol Cell Biol*, 13, 251-62.
- [4] Hasumi, Y., Baba, M., Hasumi, H., Huang, Y., Lang, M., Reindorf, R., Oh, H. B., Sciarretta, S., Nagashima, K., Haines, D. C., Schneider, M. D., Adelstein, R. S., Schmidt, L. S., Sadoshima, J. & Marston Linehan, W. 2014. Folliculin (Flcn) inactivation leads to murine cardiac hypertrophy through mTORC1 deregulation. *Hum Mol Genet*, 23, 5706-19.
- [5] Hoffmann, J. A. 2003. The Immune Response Of Drosophila. *Nature*, 426, 33-8.
- [6] Hong, S. B., Oh, H., Valera, V. A., Baba, M., Schmidt, L. S. & Linehan, W. M. 2010. Inactivation of the FLCN tumor suppressor gene induces TFE3 transcriptional activity by increasing its nuclear localization. *PLoS One*, 5, e15793.
- [7] Hoogewijs, D., Houthoofd, K., Matthijssens, F., Vandesompele, J. & Vanfleteren, J. R. 2008. Selection and validation of a set of reliable reference genes for quantitative sod gene expression analysis in C. elegans. *BMC Mol Biol*, 9, 9.
- [8] Irazoqui, J. E., Troemel, E. R., Feinbaum, R. L., Luhachack, L. G., Cezairliyan, B. O. & Ausubel, F. M. 2010a. Distinct pathogenesis and host responses during infection of C. elegans by P. aeruginosa and S. aureus. *PLoS Pathog*, 6, e1000982.
- [9] Irazoqui, J. E., Urbach, J. M. & Ausubel, F. M. 2010b. Evolution of host innate defence: insights from Caenorhabditis elegans and primitive invertebrates. *Nat Rev Immunol*, 10, 47-58.
- [10] Ishii, K. J., Koyama, S., Nakagawa, A., Coban, C. & Akira, S. 2008. Host Innate Immune Receptors And Beyond: Making Sense Of Microbial Infections. *Cell Host Microbe*, 3, 352-63.
- [11] Jiang, H., Liu, W., Zhan, S. K., Pan, Y. X., Bian, L. G., Sun, B., Sun, Q. F. & Pan, S. J. 2016. GSK621 Targets Glioma Cells via Activating AMP-Activated Protein Kinase Signalings. *PLoS One*, 11, e0161017.
- [12] Kamath, R. S., Martinez-Campos, M., Zipperlen, P., Fraser, A. G. & Ahringer, J. 2001. Effectiveness of specific RNA-mediated interference through ingested double-stranded RNA in Caenorhabditis elegans. *Genome Biology*, 2.
- [13] Karin, M. 2009. NF-kappaB as a critical link between inflammation and cancer. *Cold Spring Harb Perspect Biol*, 1, a000141.
- [14] Kato, M. 1972. Site of action of lipid A on mitochondria. *J Bacteriol*, 112, 268-75.
- [15] Kauffman, E. C., Ricketts, C. J., Rais-Bahrami, S., Yang, Y., Merino, M. J., Bottaro, D. P., Srinivasan, R. & Linehan, W. M. 2014. Molecular genetics and cellular features of TFE3 and TFEB fusion kidney cancers. *Nat Rev Urol*, 11, 465-75.
- [16] Lapierre, L. R., De Magalhaes Filho, C. D., Mcquary, P. R., Chu, C. C., Visvikis, O., Chang, J. T., Gelino, S., Ong, B., Davis, A. E., Irazoqui, J. E., Dillin, A. & Hansen, M. 2013. The TFEB orthologue HLH-30 regulates autophagy and modulates longevity in Caenorhabditis elegans. *Nat Commun*, 4, 2267.
- [17] Martina, J. A., Chen, Y., Gucek, M. & Puertollano, R. 2012. MTORC1 functions as a transcriptional regulator of autophagy by preventing nuclear transport of TFEB. *Autophagy*, 8, 903-14.
- [18] Martina, J. A., Diab, H. I., Lishu, L., Jeong, A. L., Patange, S., Raben, N. & Puertollano, R. 2014. The nutrient-responsive transcription factor TFE3 promotes autophagy, lysosomal biogenesis, and clearance of cellular debris. *Sci Signal*, 7, ra9.

- [19] Martina, J. A. & Puertollano, R. 2013. Rag GTPases mediate amino acid-dependent recruitment of TFEB and MITF to lysosomes. *J Cell Biol*, 200, 475-91.
- [20] Mcgivney, A. & Bradley, S. G. 1980. Action Of Bacterial Lipopolysaccharide On The Respiration Of Mouse Liver Mitochondria. *Infect Immun*, 27, 102-6.
- [21] Medzhitov, R. 2007. Recognition of microorganisms and activation of the immune response. *Nature*, 449, 819-26.
- [22] MEDZHITOV, R. 2009. Damage control in host-pathogen interactions. *Proc Natl Acad Sci U S A*, 106, 15525-6.
- [23] Najibi, M., Labed, S. A., Visvikis, O. & Irazoqui, J. E. 2016. An Evolutionarily Conserved PLC-PKD-TFEB Pathway for Host Defense. *Cell Rep*, 15, 1728-42.
- [24] O'rourke, D., Baban, D., Demidova, M., Mott, R. & Hodgkin, J. 2006. Genomic clusters, putative pathogen recognition molecules, and antimicrobial genes are induced by infection of C. elegans with M. nematophilum. *Genome Res*, 16, 1005-16.
- [25] Pastore, N., Brady, O. A., Diab, H. I., Martina, J. A., Sun, L., Huynh, T., Lim, J. A., Zare, H., Raben, N., Ballabio, A. & Puertollano, R. 2016. TFEB and TFE3 cooperate in the regulation of the innate immune response in activated macrophages. *Autophagy*, 12, 1240-58.
- [26] Peli-Gulli, M. P., Raucci, S., Hu, Z., Dengjel, J. & De Virgilio, C. 2017. Feedback Inhibition of the Rag GTPase GAP Complex Lst4-Lst7 Safeguards TORC1 from Hyperactivation by Amino Acid Signals. *Cell Rep.* 20, 281-288.
- [27] Petit, C. S., Roczniak-Ferguson, A. & Ferguson, S. M. 2013. Recruitment of folliculin to lysosomes supports the amino acid-dependent activation of Rag GTPases. *J Cell Biol*, 202, 1107-22.
- [28] Possik, E., Ajisebutu, A., Manteghi, S., Gingras, M. C., Vijayaraghavan, T., Flamand, M., Coull, B., Schmeisser, K., Duchaine, T., Van Steensel, M., Hall, D. H. & Pause, A. 2015. Flcn And Ampk Confer Resistance to Hyperosmotic Stress via Remodeling of Glycogen Stores. *PLoS Genet*, 11, e1005520.
- [29] Possik, E., Jalali, Z., Nouet, Y., Yan, M., Gingras, M. C., Schmeisser, K., Panaite, L., Dupuy, F., Kharitidi, D., Chotard, L., Jones, R. G., Hall, D. H. & Pause, A. 2014. Folliculin regulates ampk-dependent autophagy and metabolic stress survival. *PLoS Genet*, 10, e1004273.
- [30] Possik, E. & Pause, A. 2015. Measuring oxidative stress resistance of Caenorhabditis elegans in 96-well microtiter plates. *J Vis Exp*, e52746.
- [31] Possik, E. & Pause, A. 2016. Glycogen: A must have storage to survive stressful emergencies. *Worm*, 5, e1156831.
- [32] Powell, J. R. & Ausubel, F. M. 2008. Models of Caenorhabditis elegans infection by bacterial and fungal pathogens. *Methods Mol Biol*, 415, 403-27.
- [33] Prantner, D., Perkins, D. J. & Vogel, S. N. 2017. AMP-activated Kinase (AMPK) Promotes Innate Immunity and Antiviral Defense through Modulation of Stimulator of Interferon Genes (STING) Signaling. *J Biol Chem*, 292, 292-304.
- [34] Raben, N. & Puertollano, R. 2016. TFEB and TFE3: Linking Lysosomes to Cellular Adaptation to Stress. *Annu Rev Cell Dev Biol*, 32, 255-278.
- [35] Rehli, M., Den Elzen, N., Cassady, A. I., Ostrowski, M. C. & HumE, D. A. 1999. Cloning and characterization of the murine genes for bHLH-ZIP transcription factors TFEC and TFEB reveal a common gene organization for all MiT subfamily members. *Genomics*, 56, 111-20.

- [36] Roczniak-Ferguson, A., Petit, C. S., Froehlich, F., Qian, S., Ky, J., Angarola, B., Walther, T. C. & Ferguson, S. M. 2012. The transcription factor TFEB links mTORC1 signaling to transcriptional control of lysosome homeostasis. *Sci Signal*, 5, ra42.
- [37] Rohlfing, A. K., Miteva, Y., Hannenhalli, S. & Lamitina, T. 2010. Genetic and physiological activation of osmosensitive gene expression mimics transcriptional signatures of pathogen infection in C. elegans. *PLoS One*, 5, e9010.
- [38] Samie, M. & Cresswell, P. 2015. The transcription factor TFEB acts as a molecular switch that regulates exogenous antigen-presentation pathways. *Nat Immunol*, 16, 729-36.
- [39] Sardiello, M. 2016. Transcription factor EB: from master coordinator of lysosomal pathways to candidate therapeutic target in degenerative storage diseases. *Ann N Y Acad Sci*, 1371, 3-14.
- [40] Schmidt, L. S. & Linehan, W. M. 2015. Molecular genetics and clinical features of Birt-Hogg-Dube syndrome. *Nat Rev Urol*, 12, 558-69.
- [41] Settembre, C., De Cegli, R., Mansueto, G., Saha, P. K., Vetrini, F., Visvikis, O., Huynh, T., Carissimo, A., Palmer, D., Klisch, T. J., Wollenberg, A. C., Di Bernardo, D., Chan, L., Irazoqui, J. E. & Ballabio, A. 2013. TFEB controls cellular lipid metabolism through a starvation-induced autoregulatory loop. *Nat Cell Biol*, 15, 647-58.
- [42] Settembre, C., Di Malta, C., Polito, V. A., Garcia Arencibia, M., Vetrini, F., Erdin, S., Erdin, S. U., Huynh, T., Medina, D., Colella, P., Sardiello, M., Rubinsztein, D. C. & Ballabio, A. 2011. TFEB links autophagy to lysosomal biogenesis. *Science*, 332, 1429-33.
- [43] Settembre, C., Zoncu, R., Medina, D. L., Vetrini, F., Erdin, S., Erdin, S., Huynh, T., Ferron, M., Karsenty, G., Vellard, M. C., Facchinetti, V., Sabatini, D. M. & Ballabio, A. 2012. A lysosome-to-nucleus signalling mechanism senses and regulates the lysosome via mTOR and TFEB. *EMBO J*, 31, 1095-108.
- [44] Sinha, A., Rae, R., Iatsenko, I. & Sommer, R. J. 2012. System wide analysis of the evolution of innate immunity in the nematode model species Caenorhabditis elegans and Pristionchus pacificus. *PLoS One*, 7, e44255.
- [45] Takagi, Y., Kobayashi, T., Shiono, M., Wang, L., Piao, X., Sun, G., Zhang, D., Abe, M., Hagiwara, Y., Takahashi, K. & Hino, O. 2008. Interaction of folliculin (Birt-Hogg-Dube gene product) with a novel Fnip1-like (FnipL/Fnip2) protein. *Oncogene*, 27, 5339-47.
- [46] Tee, A. R. & Pause, A. 2013. Birt-Hogg-Dube: tumour suppressor function and signalling dynamics central to folliculin. *Fam Cancer*, 12, 367-72.
- [47] Troemel, E. R., Chu, S. W., Reinke, V., Lee, S. S., Ausubel, F. M. & Kim, D. H. 2006. p38 MAPK regulates expression of immune response genes and contributes to longevity in C. elegans. *PLoS Genet*, 2, e183.
- [48] Tsun, Z. Y., Bar-Peled, L., Chantranupong, L., Zoncu, R., Wang, T., Kim, C., Spooner, E. & Sabatini, D. M. 2013. The folliculin tumor suppressor is a GAP for the RagC/D GTPases that signal amino acid levels to mTORC1. *Mol Cell*, 52, 495-505.
- [49] Vincent, E. E., Coelho, P. P., Blagih, J., Griss, T., Viollet, B. & Jones, R. G. 2015. Differential effects of AMPK agonists on cell growth and metabolism. *Oncogene*, 34, 3627-39.
- [50] Visvikis, O., Ihuegbu, N., Labed, S. A., Luhachack, L. G., Alves, A. F., Wollenberg, A. C., Stuart, L. M., Stormo, G. D. & Irazoqui, J. E. 2014. Innate host defense requires TFEB-mediated transcription of cytoprotective and antimicrobial genes. *Immunity*, 40, 896-909.

- [51] Wada, S., Neinast, M., Jang, C., Ibrahim, Y. H., Lee, G., Babu, A., Li, J., Hoshino, A., Rowe, G. C., Rhee, J., Martina, J. A., Puertollano, R., Blenis, J., Morley, M., Baur, J. A., Seale, P. & Arany, Z. 2016. The tumor suppressor FLCN mediates an alternate mTOR pathway to regulate browning of adipose tissue. *Genes Dev*, 30, 2551-2564.
- [52] Yan, M., Audet-Walsh, E., Manteghi, S., Dufour, C. R., Walker, B., Baba, M., St-Pierre, J., Giguere, V. & Pause, A. 2016. Chronic AMPK activation via loss of FLCN induces functional beige adipose tissue through PGC-1alpha/ERRalpha. *Genes Dev*, 30, 1034-46.
- [53] Yan, M., Gingras, M. C., Dunlop, E. A., Nouet, Y., Dupuy, F., Jalali, Z., Possik, E., Coull, B. J., Kharitidi, D., Dydensborg, A. B., Faubert, B., Kamps, M., Sabourin, S., Preston, R. S., Davies, D. M., Roughead, T., Chotard, L., Van Steensel, M. A., Jones, R., Tee, A. R. & Pause, A. 2014. The tumor suppressor folliculin regulates AMPK-dependent metabolic transformation. *J Clin Invest*, 124, 2640-50.
- [54] Young, N. P., Kamireddy, A., Van Nostrand, J. L., Eichner, L. J., Shokhirev, M. N., Dayn, Y. & Shaw, R. J. 2016. AMPK governs lineage specification through Tfeb-dependent Regulation Of Lysosomes. *Genes Dev*, 30, 535-52.
- [55] ZHANG, B. B., ZHOU, G. & LI, C. 2009. AMPK: an emerging drug target for diabetes and the metabolic syndrome. *Cell Metab*, 9, 407-16.

CHAPTER 3	3 – Folliculin in ndent induction	npairs breast t n of the Warbu	umor growth irg effect and	by repressing angiogenesis	ГFE3-

Folliculin impairs breast tumor growth by repressing TFE3-dependent induction of the Warburg effect and angiogenesis

Leeanna El-Houjeiri^{1,2,5}, Marco Biondini^{1,5}, Mathieu Paquette^{1,2}, Helen Kuasne¹, Alain Pacis¹, Morag Park^{1,2,3,4}, Peter M. Siegel^{1,2,3}*, and Arnim Pause^{1,2}*

¹Goodman Cancer Research Institute, McGill University, Montréal, Canada. ²Department of Biochemistry, McGill University, Montréal, Canada. ³Department of Medicine, McGill University, Montréal, Canada. ⁴Department of Pathology, McGill University Montréal, Canada. ⁵Equal contribution, *Equal correspondence

Manuscript published in Journal of Clinical Investigation 131.22 (2021): e144871

*Corresponding Authors:

Arnim Pause Peter M. Siegel

3655 promenade Sir William Osler 1160 Pine Avenue West

Room 707B Room 513

Montréal, Québec, Canada Montréal, Québec, Canada

H3G 1Y6 H3A 1A3

Phone: (514) 398-1521 Phone: (514) 398-4259

Fax: (514) 398-3380 Fax: (514) 398-6769

Email: arnim.pause@mcgill.ca E-mail: peter.siegel@mcgill.ca

Keywords: Angiogenesis; Breast cancer; Cancer; Metabolism.

3.1. ABSTRACT

Growing tumors exist in metabolically compromised environments that require activation of multiple pathways to scavenge nutrients to support accelerated rates of growth. The folliculin (FLCN) tumor suppressor complex (FLCN, FNIP1, FNIP2) is implicated in the regulation of energy homeostasis via 2 metabolic master kinases: AMPK and mTORC1. Loss-of-function mutations of the FLCN tumor suppressor complex have only been reported in renal tumors in patients with the rare Birt-Hogg-Dube syndrome. Here, we revealed that FLCN, FNIP1, and FNIP2 are downregulated in many human cancers, including poor-prognosis invasive basal-like breast carcinomas where AMPK and TFE3 targets are activated compared with the luminal, less aggressive subtypes. FLCN loss in luminal breast cancer promoted tumor growth through TFE3 activation and subsequent induction of several pathways, including autophagy, lysosomal biogenesis, aerobic glycolysis, and angiogenesis. Strikingly, induction of aerobic glycolysis and angiogenesis in FLCN-deficient cells was dictated by the activation of the PGC-1α/HIF-1α pathway, which we showed to be TFE3 dependent, directly linking TFE3 to Warburg metabolic reprogramming and angiogenesis. Conversely, FLCN overexpression in invasive basal-like breast cancer models attenuated TFE3 nuclear localization, TFE3-dependent transcriptional activity, and tumor growth. These findings support a general role of a deregulated FLCN/TFE3 tumor suppressor pathway in human cancers.

3.2. INTRODUCTION

Breast cancer (BC) is the first leading cause of cancer deaths in women worldwide, with thousands dying from the disease each year [1]. Gene expression profiling classifies human breast cancers into different subtypes, including luminal, HER2+, and basal-like [2-4]. Around 10-20% of breast cancer patients are diagnosed with basal-like tumors, a high percentage of which are triple negative breast cancers (TNBC), an extremely heterogeneous disease lacking estrogen and progesterone receptors, as well as human epidermal growth factor receptor 2 [5]. The TNBC subtype lacks effective targeted therapy options, and hence is associated with the worst prognostic outcomes for breast cancer patients [6].

A general characteristic of cancer cells is the capability to obtain nutrients from a nutrient-deprived environment and to use these nutrients to sustain their transformed state and increase cell proliferation [7]. We have previously shown that folliculin (FLCN) plays an important role in mediating an AMPK-dependent resistance to several energy depleting stresses including; nutrient deprivation, oxidative stress, anoxia and hyperosmotic stresses [8-12]. FLCN is an AMPK binding partner [13, 14] identified as a tumor suppressor protein responsible for the Birt-Hogg-Dubé (BHD) syndrome in humans [15]. The interaction of FLCN with AMPK is mediated by two homologous FLCN-binding proteins, called FNIP1 and FNIP2; where at least FLCN and one of the FNIPs is required for the full function of the complex [13, 15]. We have previously shown that FLCN loss results in constitutive AMPK activation, which enhances survival to several metabolic stresses [8-11]. Metabolic changes following FLCN loss include enhanced ATP production and an increase in metabolic intermediates derived from induction of mitochondrial oxidative phosphorylation (OXPHOS) and aerobic glycolysis. Metabolic rewiring following FLCN loss is dependent on the AMPK-dependent activation of the peroxisome proliferator-activated receptor

gamma coactivator 1-alpha (PGC- 1α) and subsequently the hypoxia-inducible factor 1-alpha (HIF- 1α) [12].

HIF-1 α , a well-defined hypoxia responsive factor, activates diverse pathways that regulate cellular metabolism, angiogenesis, proliferation, and drug resistance [16, 17]. HIF pathway activation in tumor cells is an important stimulus for blood vessel growth, where it regulates the expression of multiple pro-angiogenic genes, primarily the vascular endothelial growth factor (*VEGF*) [18]. Interestingly, studies have shown that TNBC tumors express high levels of intratumoral VEGF [19], possess high microvessel density [20] and display VEGF gene amplification compared to non-TNBC tumors [21], suggesting a marked angiogenic dependency in TNBC tumorigenesis.

In addition to HIF-1 α activation, several studies support a role for FLCN in TFE3 regulation, where FLCN loss induces TFE3 nuclear translocation and subsequent transcriptional activation [22-25]. TFE3, a transcription factor belonging to the microphthalmia/transcription factor E (MiT/TFE) family of transcription factors, has recently emerged as a global regulator of cell survival and metabolic reprogramming [26, 27]. TFE3 regulates the expression of target genes involved in cellular processes ranging from cell-specific differentiation to basic cellular energy homeostasis including: autophagy, lysosomal biogenesis, lipid homeostasis [28]. Indeed, TFE3 activation and nuclear accumulation has been shown to be tightly regulated by cellular nutrient/energy status [28]. Under nutrient rich conditions, TFE3 is hyper-phosphorylated, predominantly by the mammalian target of rapamycin (mTOR) and remains inactive within the cytoplasm. Conversely, upon nutrient depletion, TFE3 becomes de-phosphorylated and translocates to the nucleus where it induces the expression of genes in the Coordinated Lysosomal Expression and Regulation (CLEAR) network [29]. Interestingly, the link between FLCN and

mTOR has been previously proposed, where FLCN was identified as a guanosine triphosphate (GTP)-activating protein (GAP) for Ras-related GTPase (Rag) C/D, which ultimately activates mTOR [30-32], implicating FLCN as a positive regulator of mTOR signaling pathway. TFE3 and other conserved family members (TFEB and MITF) can act as oncogenes in renal cancer, melanoma, and pancreatic cancer [26].

Given that loss of FLCN mediates resistance to energy depleting stresses encountered during tumor growth through several pathways, we investigated the previously unexplored role of FLCN in breast cancer. In this study, we report that FLCN and its binding partners FNIP1/2 are downregulated, while AMPK and TFE3 transcriptional targets are elevated in TNBCs when compared to less aggressive luminal breast cancer subtypes. We show that FLCN loss in luminal breast cancer cells enhances tumor growth in a TFE3-dependent manner. Conversely, FLCN overexpression in basal-like TNBC models attenuates the nuclear localization and transcriptional activity of TFE3 and leads to impaired tumor growth. We further show that, beyond its impact on autophagy and lysosomal biogenesis, FLCN loss or downregulation activates TFE3, which subsequently engages a PGC1-α/HIF-1α-dependent induction of OXPHOS, glycolysis, and angiogenesis pathways that promote aggressive tumor growth.

3.3. RESULTS

FLCN, FNIP1 and FNIP2 downregulation is recurrent in triple negative breast cancer when compared to luminal subtypes

FLCN was identified as a classic tumor suppressor gene when second hit mutations were identified in BHD-associated renal tumors [33]. Thus, we first investigated *FLCN* expression levels across different tumor types compared to their corresponding normal tissue. Using The

Cancer Genome Atlas (TCGA) dataset, we show that *FLCN* levels are substantially lower across several important human tumor types compared to their normal tissue counterparts (Figure S1A). Given that patients affected with BHD syndrome are at risk of developing renal, skin, and colon tumors [34], we were particularly interested in studying the unexplored role of FLCN in invasive breast carcinoma.

Using the invasive breast carcinoma TCGA dataset, we show that FLCN, FNIP1, and FNIP2 levels are all significantly downregulated in the TNBC compared the less aggressive luminal subtypes (Figure 1A and Figure S1B, C, D). Additionally, we show that the downstream targets of AMPK (PPARGC1A and PPARGC1B) and TFE3 (ATP6V0A4, ATP6V1F, ATG4B, ATG4D, ATG9B, ATG3, CTSC, CTSH) are upregulated in TNBC (Figure 1A). Analysis of RNAsequencing data from a panel of 37 breast cancer patient-derived xenografts (PDX) [35] revealed that the expression levels of FLCN, FNIP1, and FNIP2 are all significantly downregulated in basal-like samples when compared to normal breast tissue (Figure 1B). Moreover, immunoblot analysis of 12 representative basal-like PDX tumor lysates show reduced expression of at least one of the components of the FLCN, FNIP1, and FNIP2 complex across the tumor samples (Figure 1C). To determine the relevance of functional vs. deregulated FLCN/FNIPs complex, we assessed the localization and activity of TFE3 in the tumor samples. In a functional FLCN complex setting, such as Goodman Cancer Research Centre PDX samples 1738 and 1828 (GCRC1738 and GCRC1828), where at least FLCN and one of the FNIPs is highly expressed, we show by immunohistochemistry (IHC) that TFE3 is mainly localized in the cytoplasm, where it remains inactive (Figure 1D). In contrast, in tumors where the FLCN complex is deregulated (GCRC1868 and GCRC1882: loss/reduced expression of FLCN/FNIP1/2) we show that TFE3 is mainly localized to the nucleus (Figure 1D). Notably, higher magnification images demonstrate some

nuclear TFE3 staining in the functional FLCN complex setting, which we attribute to the tumor-infiltrating immune cells. Nuclear TFE3 is transcriptionally active, as evident by the upregulation of GPNMB, which is a well-known downstream TFE3 target [36] (Figure S1E and F). Finally, we examined *FLCN* expression across different breast cancer cell lines using a published dataset [37] representing luminal and basal-like subtypes, and show that *FLCN* levels are significantly downregulated in basal-like compared to luminal subtypes (Figure S1G). To identify breast cancer models for further functional studies, we selected a panel of cell lines representing luminal A (MCF7 and T47D) and basal-like TNBC subtypes (MDA-MB-436 and MDA-MB-157). In agreement with results from the TGCA dataset and PDX models, we show that FLCN, FNIP1 and FNIP2 are more highly expressed in luminal A versus TNBC cell lines (Figure 1E). AMPK activation (pThr172-AMPK) is associated with reduced FLCN/FNIP1/FNIP2 levels (Figure 1F). Immunofluorescence (IF) staining reveals that TFE3 is nuclear localized to a greater extent in TNBC subtypes compared to luminal subtypes (Figure 1F, Figure S1H).

Loss of FLCN in luminal breast cancer cell lines activates AMPK and induces TFE3 nuclear localization and activation

We next asked whether FLCN loss in luminal breast cancer cells (MCF7, T47D) impacts tumor growth. To investigate this, we knocked out FLCN using CRISPR/CAS9 genome editing approaches. For each of cell line, we employed two different guide RNAs targeting FLCN. Individual clones were selected, FLCN loss was verified by immunoblot and a reconstituted pool (n=4 clones) was generated to minimize the possibility of clonal effects (Figure 2A). Consistent with our previous studies [9-12], we show that loss of FLCN in both cell lines activates AMPK as shown by phosphorylation of AMPK (pThr172-AMPK) and its substrate ACC (pSer79-ACC).

Additionally, we show that GPNMB is induced upon FLCN loss, indicating transcriptional activation of TFE3 (Figure 2A). Notably, GPNMB is highly abundant in many tumors including TNBC and was shown to be implicated in tumor growth, angiogenesis, and poor prognosis of TNBC [38]. Immunofluorescence staining reveals that TFE3 is 100% localized within the nucleus of both MCF7 and T47D FLCNKO cells and re-expression of FLCN restored TFE3 cytoplasmic localization (Figure 2B, C). To further investigate TFE3 transcriptional activity, we used a luciferase reporter containing the TFE3 consensus promoter region (Coordinated Lysosomal Expression and Regulation; CLEAR), where we report a ~2-fold enhanced transcriptional activity in T47D and MCF7 FLCN-deficient luminal cell lines (Figure 2D). Given that one of the important readouts of TFE3 activation is the enhanced lysosomal activity [29], cells were assayed for their ability to process Dye Quenched-Bovine Serum Albumin (DQ-BSA). DQ-BSA is a self-quenched fluorescent substrate that enters the cell through endocytosis and fluoresces upon lysosomal degradation [39]. We show a significant ~10-fold increase in DQ-BSA fluorescence intensity indicating enhanced lysosomal activity in FLCN-deficient cells (Figure 2E, F). Furthermore, we assessed the expression of known TFE3 target genes involved in autophagy and lysosomal biogenesis (ATP6V0E1, ASAH1, TPP1, MCOLN1), all of which contain the CLEAR motif consensus sequence in their promoter regions and show a significant increase upon FLCN loss in both T47D and MCF7 cells (Figure 2G). To investigate whether this observed increase is TFE3dependent, we transiently reduced TFE3 expression using small interfering RNAs (siRNA) and show a significant decrease in the expression of all the assessed genes (Figure 2G).

Since many TFE3 target genes are also regulated by TFEB, we assessed the contribution of TFEB to the enhanced autophagy/lysosomal biogenesis responses observed upon FLCN loss using siRNAs targeting TFEB alone, TFE3 alone or both simultaneously. Interestingly,

downregulation of TFEB alone had no effect on the expression level of the assessed genes in FLCN-deficient cells, and TFEB/TFE3 double knockdown produced similar effects to downregulation of TFE3 alone (Figure 2G). It is worth noting that expression levels of TFEB are much lower than TFE3 in human breast cancer cell lines (http://www.proteinatlas.org). All together, these results suggest that TFE3 may be more dynamically involved in the FLCN-AMPK pathway than TFEB in this context. In light of these observations, we have focused specifically on the role of TFE3 in breast tumor phenotypes associated with loss of FLCN.

Loss of FLCN in MCF7 cells enhances cellular metabolism in a TFE3-dependent manner

A fundamental characteristic of cancer cells is to couple nutrient consumption to macromolecular biosynthesis and energy production to facilitate tumor growth and survival [40]. We have previously shown that FLCN loss induces an AMPK-dependent increase in resistance to several energy depleting stresses, and this is likely to contribute to cellular metabolic adaptation [8-10, 12]. However, the link between metabolic reprograming following FLCN loss and TFE3 activation has not been studied to date. We show a significant 1.7-fold increase in ATP levels in FLCN deficient MCF7 cell lines, which is abolished following transient knockdown of TFE3 (Figure 3A). In parallel, we show an increase in glucose consumption and lactate production (Figure 3B), an enhanced extracellular acidification rate (ECAR) (Figure 3C) and oxygen consumption rate (OCR) (Figure 3D) under basal culture conditions in FLCN-deficient MCF7 cell lines compared to EV controls. Notably, all of these metabolic changes were dependent on TFE3 activity, as TFE3 downregulation in FLCN^{KO} cells mitigated these effects (Figure 3B-D). Finally, we assessed the expression of common glycolytic genes (*HK2*, *SLCA1*, and *LDHA*) in MCF7 cells and show a significant increase in FLCN-deficient cells compared to EV, which was abolished

following TFE3 downregulation (Figure 3E). Taken together, we show that loss of FLCN in luminal breast cancer cells engages metabolic reprogramming toward increased cellular bioenergetics, which can provide a metabolic advantage to cells to facilitate growth and survival.

Loss of FLCN in luminal breast cancer cells enhances tumor growth

Next, we investigated the impact of FLCN loss on breast tumor growth. FLCN null MCF7 and T47D luminal breast cancer cells exhibited significantly increased tumor growth as compared to wild type control cells when injected into the mammary fat pads of NOD SCID gamma (NSG) mice (Figure 4A and B, Figure S2A). Importantly, re-expression of FLCN in MCF7 FLCN^{KO} cells restored tumor growth kinetics to those observed with parental MCF7 breast cancer cells (Figure 4A and B). In line with the *in vitro* data, characterization of these tumors following resection shows enhanced AMPK activity (pThr172-AMPK) upon FLCN loss, which occurs in both MCF7 and T47D cells (Figure 4C, Figure S2B). Again, elevated AMPK activity was abrogated upon reexpression of FLCN in MCF7 FLCN^{KO} cells (Figure 4C). Notably, we show that tumors 10 and 12 had higher expression of FLCN as evident by immunoblot analysis (Figure 4C), which was associated with lower tumor volumes (Figure 4B). Conversely, the weak FLCN expression achieved in tumor 11 (Figure 4C) was associated with a much greater tumor volume (Figure 4B).

IHC analysis demonstrates that TFE3 is localized to the nucleus in FLCN deficient MCF7 and T47D tumors and is transcriptionally active, as shown by an enhanced GPNMB expression (Figure 4D, Figure S2C). TFE3 localization reverted to the cytoplasm and GPNMB levels were reduced upon FLCN re-expression in MCF7 FLCN^{KO} cells (Figure 4D). In keeping with increased tumor growth, we report a significant increase in nuclear Ki67 staining in FLCN-deficient luminal breast tumors (Figure 4D, Figure S2C), which was suppressed following FLCN expression in the

MCF7 model (Figure 4D). IHC staining with cleaved caspase-3, a marker of apoptosis, failed to detect any significant differences in MCF7 or T47D cells as a result of FLCN loss (Figure S2D). These results indicate that loss of FLCN in luminal breast cancer tumors potentially enhances proliferation without altering apoptosis.

An angiogenic profile emerges following FLCN loss in luminal breast cancer cells

We have shown that FLCN loss induces the nuclear localization and activation of TFE3, which is shown to be involved in several cellular stress pathways [29], all of which could potentially contribute to the enhanced tumor growth observed in FLCN deficient luminal breast cancer cells. Hence, we wanted to elucidate the genes and pathways involved in the growth of FLCN-deficient tumors. We performed RNA-sequencing analysis on MCF7 WT and FLCNdeficient mammary tumors and report significant differences in the gene expression profile in both cohorts (Figure 5A). Specifically, Gene Ontology (GO) analysis following RNA-sequencing revealed enrichment in several pathways; many of which we have recently reported in FLCNdeficient cells [8], including autophagy, lysosomal biogenesis and innate immune responses (Figure 5B, Table S2). Importantly, regulation of angiogenesis pathway was one of the top hits in FLCN-deficient tumors compared to their controls (Figure 5B, Table S3). This was of interest since, to our knowledge, a direct link between FLCN, TFE3 and angiogenesis has yet to be reported. We show a significant increase in many angiogenesis genes in FLCN deficient tumors compared to their WT controls including: HIF1-α, EGLN1, SEMA, TMEM2, EPHA2, NOS3, VEGFA and VEGFB (Figure 5B), all of which have been shown to be involved in angiogenesis [18]. To further evaluate this angiogenic profile, we assessed a panel of secreted angiogenic factors by multiplex-ELISA in FLCN-proficient and deficient tumor lysates. We observed a multiple-fold

increase in several of these factors, including: EGF, Endoglin, IL-6 and VEGF-A in FLCN deficient compared to FLCN-expressing MCF7 cells (Figure 5C). IHC analyses of the resected MCF7 and T47D tumors confirmed a significant increase in VEGF-A staining in FLCN-deficient cells compared to their controls (Figure 5D, Figure S3A, B). FLCN re-expression in MCF7 FLCN^{KO} cells caused a reduction in VEGF-A levels (Figure 5D). We also show that the number of intra-tumoral vessels, as determined by mouse CD31 staining, is significantly increased in FLCN-deficient cells compared to their controls (Figure 5D, Figure S3A, C), which is also lost following FLCN re-expression in MCF7 FLCN^{KO} cells (Figure 5D).

Given that early initiation of tumor angiogenesis is required to support fast growing tumors [41], we performed a short-term *in vivo* experiment to assess the degree of angiogenesis at earlier time points during tumor growth. MCF7 EV and FLCN^{KO} tumors were resected 2 weeks post-injection in NSG mice. In agreement with our previous observations (Figure 4A), we show that tumor volumes are larger in FLCN^{KO} MCF7 cells (Figure S3D). Interestingly, FLCN^{KO} MCF7 tumors also exhibit a prominent red coloration (Figure S3D), which may reflect the increased vascularization we see in end-stage tumors. Indeed, IHC staining of these early tumors reveals a significant increase in VEGF-A and CD31 staining in FLCN-deficient cells compared to their control (Figure S3E, F, G).

Given that VEGF-A is a key player in tumor-associated angiogenesis, we validated VEGF-A expression and its dependence on FLCN and TFE3 in MCF7 breast cancer cells. Using RT-qPCR and ELISA, we show that *VEGF-A* is expressed at higher levels in MCF7 FLCN-deficient tumors compared to FLCN-expressing controls, and that VEGF-A levels are reduced following reexpression of FLCN (Figure 5E). Interestingly, we show that this increase in *VEGF-A* levels in MCF7 FLCN^{KO} cells is TFE3-dependent via transient TFE3 knockdown (Figure 5F). Thus, tumor-

derived VEGF-A is likely to contribute to the enhanced angiogenic response observed in FLCN null breast cancer cells.

Loss of FLCN in luminal breast cancer cells enhances tumor growth in a TFE3-dependent manner

We next investigated if the enhanced tumor growth in FLCN deficient cells was dependent on TFE3 transcriptional activity. Accordingly, we stably reduced TFE3 expression levels in MCF7 FLCN^{KO} cells by shRNA and show that the increase in tumor growth observed following FLCN loss is abolished by the concomitant reduction of TFE3 expression (Figure 6A). Characterization of these tumors following resection confirms loss of FLCN and reduced TFE3 expression (Figure 6B). The residual signal for TFE3 observed in whole tumor lysates likely represents stromal contamination, as no TFE3 expression was detected in the MCF7 FLCN-deficient cells expressing TFE3-targeting shRNAs *in vitro* (Figure S4). Additionally, our IHC analysis of the resected tumors shows that TFE3 is localized to the nucleus in FLCN deficient MCF7 cells compared to WT controls, which was ablated upon downregulation of TFE3 (Figure 6C). Moreover, we report an increase in VEGF-A and CD31 staining in FLCN-deficient cells compared to EV, both of which were significantly reduced upon downregulation of TFE3 (Figure 6C). These results indicate that loss of FLCN in luminal breast cancer tumors enhances tumor growth and angiogenesis in a TFE3-dependent manner.

Loss of FLCN in luminal breast cancer cells activates a HIF-1 α -dependent angiogenesis program in a TFE3-dependent manner

One of the main transcription factors involved in a glycolytic and angiogenic response is the hypoxia-induced factor-lalpha (HIF- 1α) [42]. HIF- 1α regulates several hundred genes, including numerous glycolytic genes and the vascular endothelial growth factors (VEGF). Interestingly, we have previously shown that loss of FLCN in cells provides energetic advantage due to metabolic reprograming that engages aerobic glycolysis, a process that we show to be dependent on the activation of peroxisome-proliferator-activated receptor-gamma coactivator-lalpha (PGC- 1α), a potent metabolic sensor upstream of HIF- 1α [12].

Our data suggest that FLCN loss induces a TFE3-dependent angiogenic program, including upregulation of VEGF-A. Given that HIF- 1α is one of the main transcription factors involved in VEGF-A expression, we next investigated the dependency of VEGF-A expression on the PGC- 1α /HIF- 1α axis, and whether it is linked to TFE3 activity. Our RNA-sequencing analyses revealed that TFE3, PGC- 1α , and HIF- 1α downstream targets are all upregulated in FLCN-deficient MCF7 tumors compared to FLCN-expressing controls (Figure 7A-C). To further corroborate these results and assess the role of TFE3 in PGC- 1α /HIF- 1α pathway induction, we show that the HIF- 1α transcriptional activity is elevated in FLCN deficient MCF7 cells and this is abrogated upon the downregulation of TFE3 (Figure 7D). We have previously shown that enhanced cellular reactive oxygen species (ROS) induced HIF transcriptional activity and drove Warburg metabolic reprogramming in an AMPK- and PGC- 1α -dependent manner [12]. We quantified the relative levels of cellular ROS using the CM-H2DCFDA general oxidative stress indicator. We observed that loss of FLCN is associated with a significant 1.7-fold increase of intracellular ROS levels, which we show to be TFE3-dependent (Figure 7E). We next verified the RNA-sequencing results

by qPCR, showing that loss of FLCN in MCF7 cells induces the upregulation of several TFE3, PGC-1 α and HIF-1 α target genes (Figure 7F). Importantly, downregulation of TFE3 in FLCN deficient cells significantly abrogated the observed induction of TFE3 (*ATPV1C1*, *ASAH1*), PGC-1 α (*ATP5J*, *PGC-1\beta*), and HIF-1 α (*ENO1*, *HK2*) target genes (Figure 7F), revealing an important role of TFE3 in controlling the PGC-1 α /HIF-1 α pathway. To investigate this pathway further, we downregulated PGC-1 α in FLCN-deficient cells and observed a significant decrease of both PGC-1 α and HIF-1 α target genes, but the levels of TFE3 target genes were unaffected (Figure 7G). Similarly, downregulation of HIF-1 α in FLCN deficient cells abrogated only the HIF-1 α target genes, but the levels of both PGC-1 α and TFE3 target genes were unaffected (Figure 7H). Together, these results indicate that loss of FLCN in luminal MCF7 cells induces TFE3 activity, which acts upstream of PGC-1 α /HIF-1 α pathway. Importantly, we have identified a novel oncogenic pathway where TFE3 acts as a master regulator of autophagy and lysosomal biogenesis on one hand, while controlling PGC1- α /HIF-1 α pathways involving OXPHOS, glycolysis and angiogenesis, all of which could be contributing to tumor growth.

FLCN overexpression in basal-like breast cancer cells restores TFE3 cytoplasmic localization and attenuates tumor growth

We have shown that loss of FLCN in luminal breast cancer cells, which typically express high levels of FLCN, enhances tumor growth in a TFE3-dependent manner. We next investigated the effect of increasing FLCN expression in basal-like triple negative breast cancer cell lines, which typically express lower FLCN levels when compared to luminal cell lines (Figure 1). Accordingly, we stably overexpressed FLCN in two basal-like triple negative breast cancer cell lines: MDA-MB-436 and Hs578T, both of which exhibit low FLCN levels and predominant TFE3

nuclear localization (Figure 8A and B). Interestingly, immunofluorescence staining revealed that TFE3 nuclear localization is significantly impaired in both MDA-MB-436 and Hs578T following FLCN overexpression (Figure 8B). To investigate the impact of FLCN overexpression on the angiogenic pathway, we assessed the relative expression of TFE3, PGC-1α, and HIF-1α target genes by qPCR and report a significant decrease in the levels of these genes in both MDA-MB-436 and Hs578T cell lines (Figure 8C). Reduced nuclear TFE3 localization and target gene activation was associated with a significant decrease in cellular proliferation *in vitro*, which was more profound in Hs578T FLCN overexpressing cells (Figure 8D).

Importantly, FLCN overexpression also impaired mammary tumor growth in vivo, inducing a more profound effect in the Hs578T cells when compared to the MDA-MB-436 model (Figure 8E and F). Interestingly, Hs578T breast cancer cells overexpressing FLCN can only be detected as residual cancer cells at the site of injection as compared to control cells (Figure S5A and B). In contrast, MDA-MB-436 cells that overexpress FLCN exhibit an early growth defect that is rapidly overcome, resulting in similar growth rates and tumor volumes as their empty vector controls at endpoint (Figure 8E). This likely reflects the fact that FLCN overexpression has a more modest effect in reducing the nuclear localization of TFE3, TFE3 downstream gene activation, and in vitro proliferation in MDA-MB-436 cells when compared to Hs578T cells (Figure 8B, C and D). Indeed, while expression is still detectable in end-stage MDA-MB-436 mammary tumors (Figure S5C), FLCN levels are significantly reduced in end-stage tumors when compared to the levels detected in MDA-MB-436 cells just prior to injection (Figure S5D). Notably, both MDA-MB-436 control and FLCN over-expressing tumors displayed a similar degree of nuclear TFE3 staining in end-stage mammary tumors (Figure S5E and F). These data suggest that there is strong selective pressure to maintain TFE3 nuclear localization in rapidly growing cancer cells.

Collectively, these results demonstrate that expression of exogenous FLCN in basal-like triple negative breast cancer cells impairs TFE3 nuclear localization and TFE3-dependent transcription, which results in impaired tumor growth.

3.4. DISCUSSION

TNBC remains the most challenging breast cancer subtype to treat, potentially due to a lack of targeted therapies that underscores the need to better understand the molecular pathways that contribute to the growth and metastatic progression of this aggressive disease. In this study, we report that the FLCN-TFE3 pathway is dysregulated in TNBC subtype; where FLCN and its binding partners FNIP1 and FNIP2 are downregulated, and AMPK and TFE3 downstream targets are elevated compared to the less aggressive luminal subtype. We show that loss of FLCN in luminal subtypes promotes tumor growth through the activation of several pathways that enhance tumor growth including; metabolic reprograming, autophagy, lysosomal biogenesis and engagement of an angiogenic program, all of which we report to be regulated by the MiT/TFE family member TFE3. Importantly, we show that FLCN overexpression in TNBC models attenuates TFE3 nuclear localization and transcriptional activity, leading to impaired tumor cell growth in vitro. Hs578T breast cancer cells overexpressing FLCN failed to grow into palpable tumors and could only be detected as residual deposits of cancer cells at endpoint. In contrast, FLCN overexpression in MDA-MB-436 cells only transiently exhibited impaired tumor growth. Notably, exogenous FLCN levels were reduced in end-stage MDA-MB-436 tumors, which correlated with increased nuclear TFE3 localization. Together, these data argue for a strong selective pressure to maintain TFE3 nuclear localization in rapidly growing TNBC cells.

Growing tumors exist in metabolically compromised environments and require activation of multiple pathways to scavenge nutrients to support accelerated rates of growth. We have previously shown that loss of FLCN increases the AMPK-dependent resistance to several energy depleting stresses including; nutrient deprivation, oxidative stress, heat, anoxia, hyperosmotic stresses, obesity and pathogen infection [8-12]. In line with our previous studies, we report here that loss of FLCN in luminal breast cancer cells prompts metabolic reprogramming that increases cellular bioenergetics. These metabolic changes encompass an increase in ATP production, enhanced glycolysis, mitochondrial respiration, elevated autophagic flux, and increased lysosomal biogenesis. Importantly, we show that all such changes, which improves the metabolic fitness of FLCN-deficient cells, is driven through TFE3 transcriptional activation.

In this work, we report several pathways affected by FLCN loss in luminal breast cancers, all of which have been independently linked to tumorigenesis. Indeed, TFE3 nuclear localization and activation [43], PGC1- α induction and mitochondrial biogenesis [44], ROS production [45] and HIF1- α activation [46] have all been described as steps leading to tumor development in different cellular systems.

The role of MiT/TFE family members in cancer has also been previously reported. For example, oncogenic TFEB and TFE3 gene fusions have been described in renal cell carcinoma [47]. TFEB and TFE3 have also been shown to play a crucial role in regulating autophagy-lysosome function, which promotes the growth of pancreatic ductal adenocarcinoma [26]. More recently, TFE3 was shown to exert pro-tumorigenic roles in a Kras-dependent, non-small-cell lung cancer model through activation of autophagy-lysosomes [48].

In addition to these well documented cellular phenotypes for TFE3 in cancer, we reveal a novel consequence of FLCN loss, which is the induction of multiple bioenergetic programs

including OXPHOS, glycolysis, and angiogenesis in breast cancers, which are controlled by PGC1- α /HIF-1 α downstream of TFE3. Moreover, knockdown of TFE3 in the context of FLCN loss impairs tumor growth and mitigates these responses.

HIF1- α is a key factor in regulation of VEGF and other angiogenic factors. IHC analysis of human tumor biopsies reveals that HIF-1 α overexpression is a common feature of many solid cancers [42] and associates with increased tumor VEGF expression and vascularization [49, 50]. Interestingly, a role for MiT/TFE factors in the regulation of angiogenesis was first hypothesized following the observation that TFEB knockout mice die prenatally due to a defect in placental vascularization [51]. Thus, our results demonstrate that FLCN loss causes the nuclear localization of TFE3, which in turn engages the PGC-1 α /HIF1- α axis to increase the expression of angiogenic factors such as VEGF-A.

The relative contributions of metabolic reprogramming, autophagy/lysosomal biogenesis, or increased angiogenesis to the pro-growth phenotype observed with FLCN-deficient luminal breast cancer cells remains to be elucidated. It is entirely possible that all three processes are required. One could speculate that during initial stages of tumor development, all solid tissues require a proper vasculature that grants oxygen, nutrients, and waste disposal. Hence, early activation of angiogenic processes is mandatory to sustain the deregulated proliferation of tumor cells. When nutrients become limiting, cancer cells may benefit from the enhanced metabolic flexibility (increased glycolysis and OXPHOS-dependent metabolism) observed in FLCN-null cancer cells. Moreover, metabolic stresses may be overcome through the utilization of nonconventional energy sources that are mobilized through activation of nutrient scavenging pathways involving autophagy and the lysosome, both of which are induced by TFE3. Thus, aggressive/metastatic cancers are highly reliant on constitutive activation of these pathways to

degrade and recycle cellular materials. Strikingly, we show that cellular metabolism, autophagy/lysosomal biogenesis, increased glycolysis, OXPHOS-dependent metabolism, and angiogenic pathways can be regulated by TFE3. It is likely that each of these processes will be differentially activated depending on the environmental cues and energetic demands of the growing tumor. FLCN-deficient breast cancer cells permanently activate each of these processes, and hence are provided with advantage over FLCN-proficient control cells, which contributes to increased tumor growth.

In the work presented here, we uncover a signaling pathway that links TFE3 activity to HIF/PGC-1α pathway via FLCN loss or downregulation. Interestingly, the components of the FLCN tumor suppressor complex are rarely mutated in sporadic human cancers with the exception of somatic mutations in rare cases of renal cell carcinoma, colorectal cancer, and thyroid oncocytoma [52-55]. In this study, we show that downregulation of FLCN is not only limited to breast cancer but is recurrent in many human cancers. The mechanism of FLCN/FNIP downregulation will be subject to further research. Collectively, these findings have wider implications for a general role of a deregulated FLCN tumor suppressor pathway in human cancers in which TFE3 or HIF activity is known to be induced.

3.5. METHODS

Cell Lines and Cell Culture

MCF7, T47D, MDA-MB-436, MDA-MB-157, and Hs578T breast cancer cells were obtained from the American Type Culture Collection (ATCC). Cell lines were maintained in Dulbecco's modified Eagle's medium (DMEM) (Wisent, 319-005CL) supplemented with 10% fetal bovine serum (FBS) (Wisent, 080-150), 100 U/mL penicillin plus 100 μg/mL streptomycin (Wisent, 450-201-EL), and 50 μg/mL gentamycin (Wisent, 450-135) in 5% CO2 at 37°C. For gene-silencing

experiments, breast cancer cells were seeded in 6-cm dishes and transfected with 10 nM siRNA duplexes using Lipofectamine RNAiMax (Invitrogen, 13778030) according to the manufacturer's instructions. The following siRNA SMARTpools were used: human TFEB (locus ID, 7942) (Dharmacon, L-009798-00-0005), human TFE3 (locus ID, 7030) (Dharmacon, L-00933-00-0005), human PPARGC1A (QIAGEN, GeneSolution, GS10891), human HIF-1α (locus ID, 3091) (Dharmacon, L-004018-00-0005) and siControl (Dharmacon, D-001810-10-05). Experiments were performed 48 to 72 hours after transfection. Stable knockdown of TFE3 in MCF7 FLCN-KO breast cancer cells was achieved using the Mission lentivirus shRNA empty vector (shEV), shTFE3 (Sigma-Aldrich, TRCN0000232151). For FLCN rescue or overexpression experiments, the human FLCN cDNA was cloned into pLenti CW57-MCS1-P2A-MCS2-BLAST (a gift from Adam Karpf, Addgene plasmid 80921).

Generation of knockout lines

CRISPR/Cas9 guide RNA targeting sequences for human FLCN were identified bioinformatically using the CRISPR Design Tool available at http://chopchop.cbu.uib.no/, Zhang Lab). Two different guide RNA sequences were used to target the first expressed exon in the gene. Targeting sequences used were TCGCACATGTCCGACTTTTT and GCGGGCTGCTGGACTCGACGC. Targeting sequences were cloned into the lentiCRISPR plasmid (http://www.addgene.org/49535/) as previously described (56). Lentivirus was produced for the FLCN targeting sequences as well as an empty lentiCRISPR vector for control lines. Lentiviral transfer plasmids were cotransfected along with VSV-G envelope (https://www.addgene.org/12259/) and packaging plasmids (https://www.addgene.org/12260/), into HEK293T cells using Lipofectamine LTX (Invitrogen, 15338-500). Media were changed after 24 hours and virus-containing media were collected and

centrifuged 72 hours after transfection. For the MCF7 and T47D cell lines, we performed single-cell cloning for each FLCN guide RNA, and once FLCN-KO cells were verified by immunoblotting, a pool of 4 clones was generated in an effort to eliminate clonal effects.

Reagents, Chemicals, and Antibodies

N-acetyl-L-cysteine (NAC) (Sigma-Aldrich, A7250) was dissolved in $1 \times PBS$ to a stock concentration of 1 M and pH adjusted to 7.4. NAC was used at a final concentration of 5 mM. β -Estradiol (Sigma-Aldrich, E8875) was dissolved in 100% ethanol to a final concentration of 3 mg/mL. This solution was then diluted in canola oil to 20 μ g/mL, which was then used to subcutaneously inject mice during the tumor growth experiments, once per week at 1 μ g per mouse.

Antibodies used for immunoblotting were against β-actin (Santa Cruz Biotechnology, sc-47778), AMPKα (Cell Signaling Technology, 2532), human FLCN (Cell Signaling Technology, 3967), human FNIP1 (Abcam, ab61395), human FNIP2 (Sigma-Aldrich, SAB3500010), p-AMPKα (Thr172) (Cell Signaling Technology, 2531), ACC (Cell Signaling Technology, 3676), p-ACC (S79) (Cell Signaling Technology, 3661), GPNMB (Cell Signaling Technology, 38313), and TFE3 (Cell Signaling Technology, 14779S; and Sigma-Aldrich, HPA023881). Antibodies used for IHC were against the following proteins: human GPNMB (Cell Signaling Technology, 38313), human TFE3 (Sigma-Aldrich, HPA023881), mouse F4/80 (Cell Signaling Technology, 70076), human cleaved caspase-3 (Cell Signaling Technology, 9661), mouse CD31 (Dianova, AF5149-01; and Cell Signaling Technology, 77699), human Ki67 (Cell Signaling Technology, 9449), and human VEGF-A (Dako Technology, M7273).

Luciferase reporter assays

Cells were seeded in 6-well plates and transfected for 6–8 hours with 1 µg of the 4XCLEAR-luciferase reporter plasmid (Addgene, 66800) or firefly luciferase HIF activity reporter pGL2-TK-HRE plasmid (gift from G. Melillo, NCI, Frederick, Maryland, USA) and 0.1 µg of CMV-Renilla Luciferase plasmid (Promega, E2261) using 5 µL of polyethylenimine (PEI) (Polysciences, 23966-1) at 1 mg/mL stock concentration. Proteins were extracted using 100 µL of Passive Lysis Buffer from the Dual-Luciferase reporter assay system (Promega, E1980) according to the manufacturer's instructions and assayed using FLUOstar Omega (BMG Labtech). Samples were normalized against nontransfected controls and CMV-Renilla values.

DQ-BSA assay

T47D and MCF7 cells were seeded at 500,000 cells per well. The next day, the cells were incubated with 5 μg/mL DQ Red BSA (Thermo Fisher Scientific, D12051) for 1 hour and washed twice with 37°C PBS. Cells were then fixed and stained with DAPI (0.1 μg/mL) in PBS for 15 minutes at room temperature. PBS-washed dishes were covered with coverslips and imaged with an Axioskop microscope (Zeiss). Gray pixels from pictures acquired were then quantified using ImageJ (NIH).

RT-qPCR in mammalian cells

MCF7 and T47D cells were seeded in triplicate in 6-well plates at 5 × 105 cells per well in DMEM supplemented with 10% FBS. After incubation for 24 hours at 37°C and 5% CO2, cells were collected, and total RNA was isolated and purified using a Total RNA Mini Kit (Geneaid) according to the manufacturer's instructions. For RT-qPCR analysis, 1 μg of total RNA was reverse transcribed using the SuperScript III kit (Invitrogen). SYBR Green reactions using the

SYBR Green qPCR supermix (Invitrogen) and specific primers (available upon request) were performed using an AriaMAX Real-time PCR system (Agilent Technologies). Relative expression of mRNAs was determined after normalization against housekeeping gene RPLP0 or B2M. Oligonucleotide sequences of the primers used for RT-qPCR can be found in Supplemental Table 1.

Protein Extraction and Immunoblotting

For AMPK immunoblotting, cells were washed twice with cold PBS, lysed in AMPK lysis buffer (10 mM Tris-HCl [pH 8.0], 0.5 mM CHAPS, 1.5 mM MgCl2, 1 mM EGTA, 10% glycerol, 5 mM NaF, 0.1 mM Na3VO4, 1 mM benzamidine, 5 mM NaPPi) supplemented with complete protease inhibitor (Roche) and DTT (1 mM), and cell lysates were cleared by centrifugation at 13,000g. For all other immunoblotting, cells were washed twice with cold PBS and lysed directly in RIPA light buffer (50 mM Tris-HCl [pH 8.8], 150 mM NaCl, 1% NP40, 0.1% SDS, 0.1% Triton X-100, 5 mM EDTA). Proteins were resolved in SDS-PAGE gels and revealed by Western blotting using the antibodies listed above.

Immunofluorescence

Cells were washed with PBS and fixed in Petri dishes with 3.7% formaldehyde at room temperature for 30 minutes. After fixation, cells were washed twice with PBS and then permeabilized with 0.3% Triton X-100 in PBS at room temperature for 15 minutes. Cells were incubated in 5% BSA in PBS for 1 hour and then with anti-TFE3 primary antibody in 1.5% BSA in PBS for 2 hours at 37°C. Cells were washed 3 times with PBS and incubated with the corresponding secondary antibodies conjugated to Alexa Fluor 488 in 1.5% BSA in PBS for 30 minutes at 37°C. Cells were washed 3 times with PBS and incubated with DAPI (0.1 μg/mL) in

PBS for 15 minutes at room temperature. PBS-washed dishes were coverslipped and observed with a Zeiss Axioskop microscope.

Metabolic Assays

Glucose production and lactate consumption were measured using a NOVA Bioanalysis flux analyzer or the Eton Bioscience kit (Eton Bioscience). Briefly, cells were plated at 500,000 cells/well in triplicate in 6-well plates in DMEM for 24 hours. Conditioned media were collected, spun down at 13,000g for 5 minutes, and transferred to new tubes in which the media were analyzed using the NOVA Bioanalysis flux analyzer. OCR and ECAR measurements were obtained using an XF96 Extracellular Flux Analyzer (Seahorse Bioscience). In brief, MCF7 EV, FLCN-KO, and FLCN-KO cells treated with TFE3 siRNA were plated at 10,000 cells/well in growth medium for 24 hours. After 24 hours, cells were incubated in nonbuffered DMEM containing 25 mM glucose and 2 mM glutamine in a CO₂-free incubator at 37°C for 2 hours to allow for temperature and pH equilibration before loading into the XF96 apparatus. XF assays consisted of sequential mix (3 minutes), pause (3 minutes), and measurement (5 minutes) cycles, allowing for determination of OCR/ECAR every 10 minutes.

ATP Quantification

Cells were plated in triplicate at 10,000 cells/well in 96-well plates. After 24h, cells were lysed and mixed for 10 min according to manufacturer's instructions (CellTiter-Glo luminescent cell viability assay, Promega). Luminescence was measured using Fluostar Omage (BMG Labtech) directly in plates.

Immunohistochemistry

Mammary tumors were fixed overnight in 4% paraformaldehyde at 4°C. After washing with 1× PBS, tumors were embedded in paraffin and sectioned by the GCRC Histology Core. Sections were stained using routine IHC protocols provided by the GCRC Histology Core using a Ventana BenchMark ULTRA system (Roche). Briefly, for Ventana: Sections were stained using routine IHC protocols provided by the GCRC Histology Core using a Ventana BenchMark ULTRA system (Roche). Slides were deparaffinized in EZ prep buffer for 8 minutes at 75°C. Antigen retrieval was performed by incubating slides in cell conditioning buffer 1 (CC1) at 95°C for 44 minutes. Slides were then blocked with the included Inhibitor CM at 37°C for 8 minutes. Incubation with primary antibody was conducted at 37°C for 32 minutes. Incubation with secondary antibody was performed by applying 1 drop of OmniMap anti-Rb HRP on slides for 16 minutes. Staining was revealed by adding one drop of DAB CM for 8 minutes. Slides were then incubated for 5 minutes with 1 drop of Copper CM followed by counterstain with hematoxylin for 8 minutes. Post counterstaining was performed for 8 minutes with Bluing Reagent. Slides were then dehydrated using increasing concentrations of ethanol, cleaned in xylene, and mounted using Acrytol mounting media. Staining was quantified with the Imagescope software (Aperio) using the positive pixel count algorithm (GPNMB, F4/80, CD31, and cleaved caspase-3) and nuclear algorithm (TFE3 and Ki67).

Quantification of soluble VEGF-A.

For in vitro studies, MCF7 cells were seeded in triplicate in 6-well plates at 5×10^5 cells per well in DMEM supplemented with 10% FBS. After incubation for 24 hours at 37°C and 5% CO₂, conditioned media were collected, spun down at 13,000g for 5 minutes. VEGF-A levels in

conditioned media were then assessed by employing a human VEGF-A quantikine ELISA kit (R&D Systems, DVE00) according to the manufacturer's instructions. For in vivo studies, 1 µg of tumor lysates from each condition was used to assess levels of VEGF-A by employing the same human VEGF-A quantikine ELISA kit according to the manufacturer's instructions.

Multiplex assay human angiogenesis array

The Discovery Assay simultaneously measures 17 angiogenic/growth factors in a single microwell. The multiplex assay was performed by using the Bio-Plex 200 system (Bio-Rad Laboratories, Inc.) and a Milliplex Mouse Cytokine/Chemokine kit (Millipore). The 32-plex consisted of angiopoietin-2, BMP-9, EGF, endoglin, endothelin-1, FGF-1, FGF-2, FLCN, G-CSF, HB-EGF, HGF, IL-8, leptin, PLGF, VEGF-A, VEGF-C, and VEGF-D. The change in the cytokine levels in FLCN-KO medium was normalized against their respective WT medium.

Mammary fat pad injections

For in vivo studies, 5×106 MCF7 cells were suspended in a 50:50 mixture of $1 \times$ PBS/Matrigel (Corning, 354248) and injected into the fourth mammary fat pads of 6- to 8-week-old NSG female mice (NOD.Cg-Prkdcscid Il2rgtm1Wjl/SzJ) (Jackson Laboratory, 005557). Forty-eight hours before tumor inoculation, mice were injected subcutaneously with 1 μ g of β -estradiol (Sigma-Aldrich, E8875) dissolved in corn oil and β -estradiol injections were repeated once per week until the experimental endpoint. Mammary tumors were monitored by palpation every few days and tumor volumes were calculated from weekly caliper measurements. Tumors were resected and

harvested when tumor volumes reached between 150 and 300 mm3. Mice were housed in the McGill Animal Care Facility in standard cages with food and water ad libitum. Mice were maintained at 22°C to 24°C on a 12-hour light/12-hour dark cycle.

ROS potential

Cellular ROS levels were determined using the general oxidative stress indicator CM-H2DCFDA (Invitrogen). Briefly, subconfluent adherent cells were incubated for 30 minutes at 37°C with CM-H2DCFDA dye. Cells were collected and analyzed using a BD FACSDiva analyzer. Cells not incubated with the dye or pretreated with 100 μ M H2O2 were used as negative and ROS-positive controls, respectively.

IncuCyte Cell Proliferation Assay

Cells were seeded at 1 × 104 per well in a 6-well plate, which was then incubated at 37°C with 5% CO2 and monitored on the IncuCyte Live Cell Analysis System (Sartorius). After incubation for the indicated times, live-cell images were obtained using a 10× objective lens (4 images per well) within the instrument and cell density was analyzed using the IncuCyte software.

RNA extraction for RNA-Sequencing Method

MCF7 EV and FLCN-KO mammary fat pad tumors were resected 6 weeks after injection, flash frozen, and stored in liquid nitrogen. RNA was extracted from 3 mammary tumors in each cohort using TRIzol and purified using QIAGEN RNeasy columns. RNA samples were processed for RNA-sequencing analysis at Genome Québec.

RNA-sequencing analysis

Adaptor sequences and low quality score bases (Phred score < 30) were first trimmed using Trimmomatic [57]. The resulting reads were aligned to the human genome reference sequence (GRCh38), using STAR [58]. Read counts are obtained using HTSeq [59] and are represented as a table that reports, for each sample (columns), the number of reads mapped to a given gene (rows). For all downstream analyses, lowly-expressed genes with an average read count lower than 10 across all samples were excluded, resulting in 19,133 genes in total. The R package limma [60] was used to identify differences in gene expression levels between wild-type (WT) and FLCN^{KO} samples. Nominal p-values were corrected for multiple testing using the Benjamini-Hochberg method. The complete list of differentially expressed genes is presented in Supplementary Table S2.

Gene set enrichment analysis

We used Enrichr [61] (https://amp.pharm.mssm.edu/Enrichr/) to test for enrichment of functionally annotated gene sets among the differentially expressed genes. The complete GO enrichment results are reported in Supplementary Table S3.

Data and Software Availability

he RNA-sequencing and microarray data are deposited in NCBI's Gene Expression Omnibus database (GEO GSE163791). PDX breast cancer RNAseq data was obtained from Savage et al. [32], GEO access number: GSE14276. Normal breast gene expression levels were obtained from GTEx Portal (https://gtexportal.org/home/). TCGA breast cancer data was obtained from Firehose Broad GDAC (illuminahiseq rnaseqv2-RSEM genes normalized -

http://gdac.broadinstitute.org/. Accessed 17 Mar 2019). The intrinsic molecular breast cancer subtyping were obtained according to Paquet and Hallett [62].

Statistics

Data are expressed as mean \pm SEM. Statistical analyses for all data were performed using 2-tailed Student's t test for comparisons between 2 groups, 1-way or 2-way ANOVA with Bonferroni's correction for comparisons between 3 or more groups, and log-rank Mantel-Cox test for survival plots, using GraphPad Prism 7 software. The data were assumed normal as tested by the Shapiro-Wilk normality test. Statistical significance is indicated in figures (*P < 0.05, **P < 0.01, ***P < 0.001, ****P < 0.0001) or included in the supplemental tables, with a P value of less than 0.05 considered significant. In vitro studies were biologically repeated at least 3 times in triplicate. The numbers of animals in each experiment are indicated in the figure legends.

Study approval

All mouse studies were approved by the Animal Resource Centre at McGill University and comply with guidelines set by the Canadian Council of Animal Care.

3.6. ACKNOWLEDGEMENTS

L.E-H. and M.B were supported by FRQS PhD and post-doctoral fellowships, respectively. Ma.P was supported by Canadian Institutes of Health Research (CIHR) PhD fellowship. Ar.P acknowledges that funding for this work was supported by grants from CIHR (PJT-165829) and the Cancer Research Society (CRS) (79664). P.M.S and Ar.P acknowledge funding from a Terry Fox New Frontiers Program Project Grant (TFRI-251427). P.M.S acknowledges funding from a CIHR grant (PJT-247494). P.M.S. is a McGill University William Dawson Scholar. We

acknowledge Dr. Matthew Annis and Dr. Sebastien Tabaries for help with animal work. Microscopy image processing and analysis for this manuscript was performed in the McGill University Life Sciences Complex Advanced BioImaging Facility (ABIF). We also thank McGill Core Flow Cytometry Facility (McGill University) for their technical support and expertise. We would like to thank the Canadian Centre for Computational Genomics, Genome Canada funded bioinformatics platform and the Goodman Cancer Research Centre Histology Core Facility (McGill University) for their services. PDXs banking was performed by the BCFGG breast tissue and data bank at the Goodman Cancer Research Centre-RI- MUHC in collaboration with the Réseau de Recherche sur le cancer (Fonds de la Recherche du Québec- Santé), which is affiliated with the Canadian Tumor Repository Network (CTRNet). We further acknowledge support from the Goodman Cancer Research Centre Metabolomics Core Facility (McGill University), which is supported by the Canada Foundation for Innovation, the Terry Fox Research Institute and the Quebec Breast Cancer Foundation.

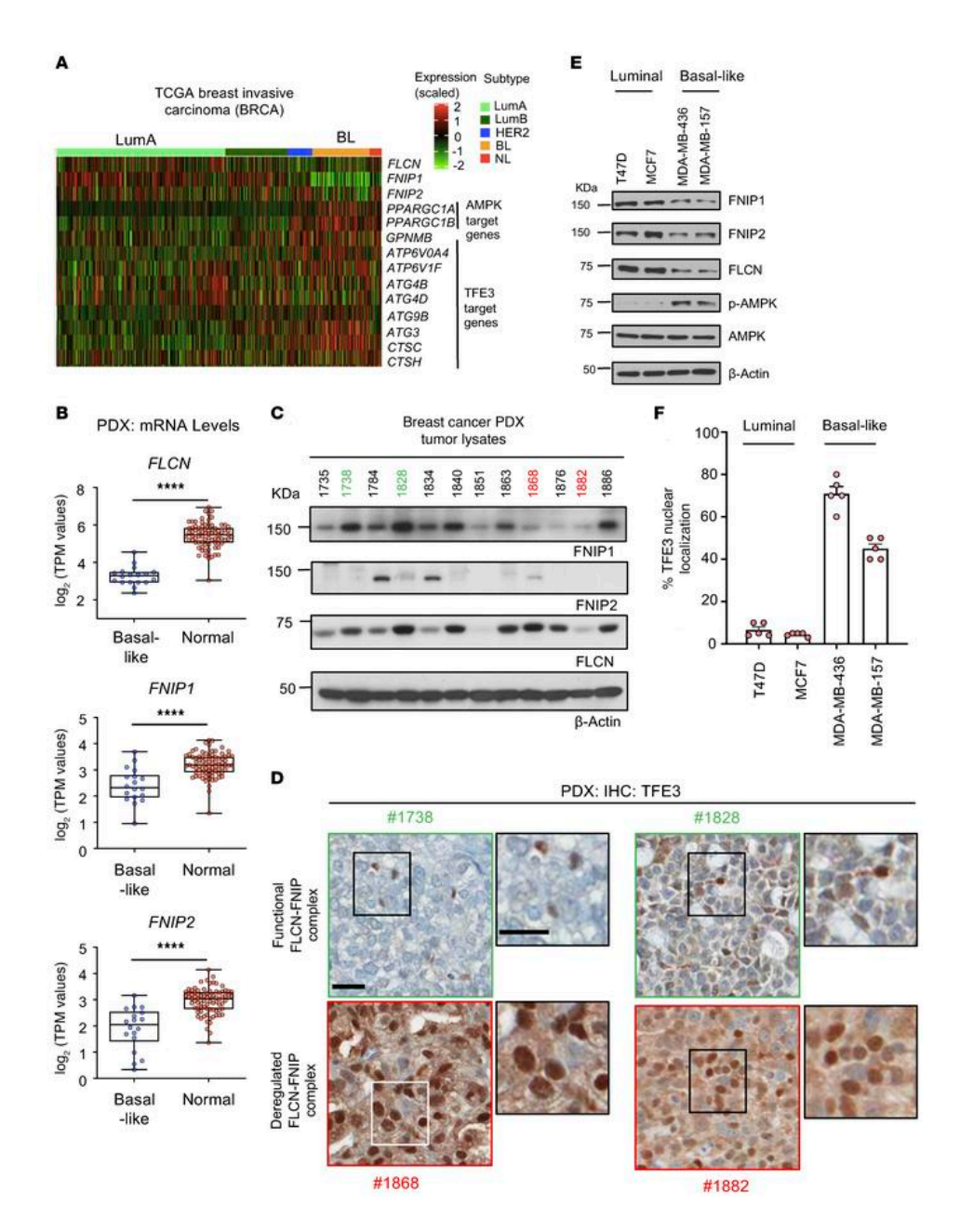
3.7. AUTHORS' CONTRIBUTIONS

LEH, MB, PMS, and A Pause conceived and designed the experiments. LEH, MB, M Paquette, A Pacis, and HK performed, collected, and assembled the experiments. LEH, MB, PMS, and A Pause wrote the manuscript. LEH, MB, M Paquette, HK, M Park, PMS, and A Pause revised the manuscript critically for important intellectual content.

CONFLICT OF INTEREST

The authors have no competing interest to report and have no potential or real conflicts of interest to declare.

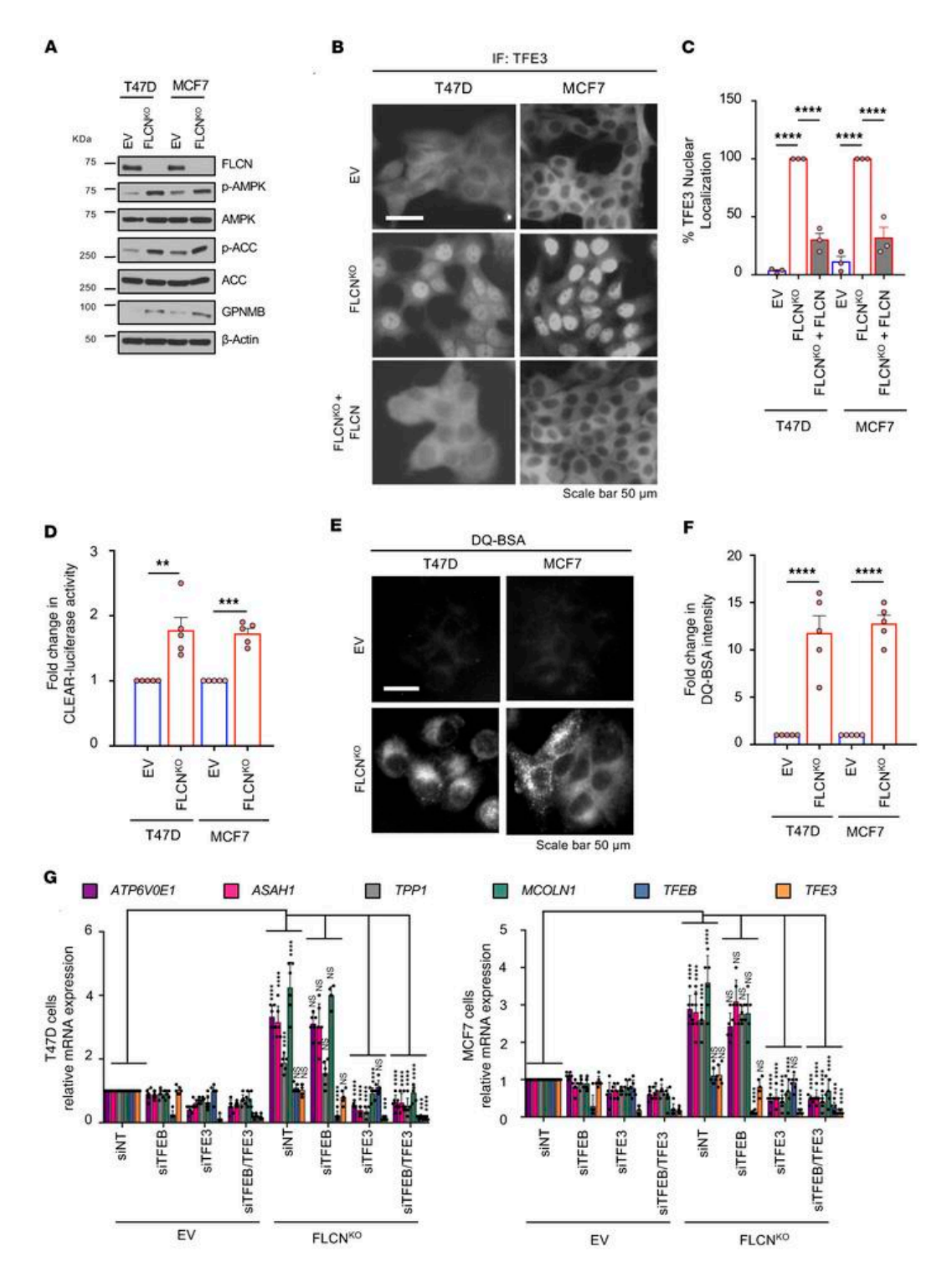
3.8. FIGURES AND FIGURE LEGENDS



¹³Figure 1. FLCN and its binding partners FNIP1 and FNIP2 are downregulated in basal-like breast cancer compared to luminal subtypes.

(A) TCGA analysis of invasive breast carcinoma comparing the expression of *FLCN*, *FNIP1*, *FNIP2*, and the downstream targets of AMPK and TFE3 in basal-like breast cancer (TNBC) compared with luminal subtypes. The different subtypes are color coded, where

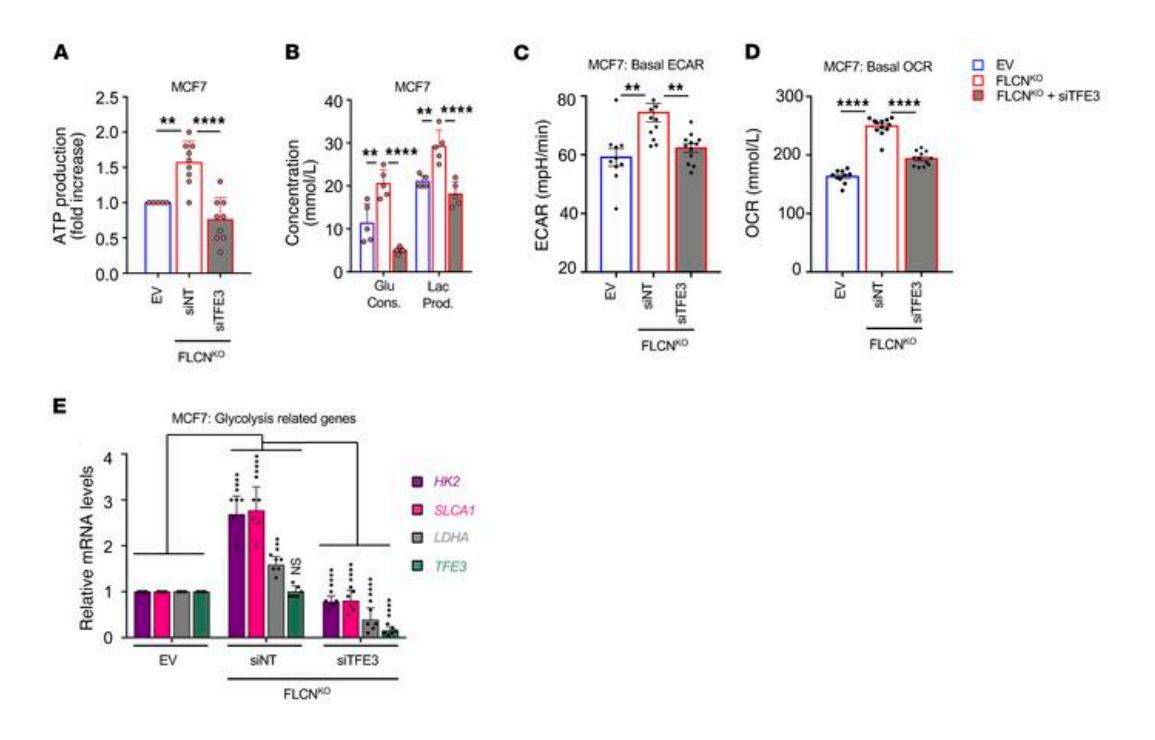
light green is luminal A, dark green is luminal B, dark blue is HER2⁺, orange is basal-like (BL), and red is normal-like (NL) subtype. (B) RNA expression of FLCN, FNIP1, and FNIP2 in basal patient-derived xenografts (PDXs) compared with normal GTEx breast tissue. Significance was determined using Student's t test. ****P < 0.0001. (C) Immunoblot analysis showing the expression levels of FNIP1, FNIP2, and FLCN in PDX tumor lysates from patients with TNBC. Each number represents a PDX model derived from a different breast cancer patient. The numbers highlighted in green (1738 and 1828) represent PDXs with a functional FLCN-FNIP1-FNIP2 complex, while those in red (1868 and 1882) represent PDXs with a deregulated complex. Actin was used as a loading control. (D) Immunohistochemistry analysis of TFE3 for the selected PDX models representing the deregulated FLCN-FNIP1-FNIP2 complex in red (1868 and 1868) and the functional complex in green (1738 and 1828). Scale bars: 20 µm. (E) Immunoblot analysis indicating expression levels of FNIP1, FNIP2, FLCN, p-Thr172-AMPK (representing the activated form of AMPK), and total AMPK in breast cancer cell lines representing luminal (T47D and MCF7) and TNBC (MDA-MB-436 and MDA-MB-157) cells. Actin was used as a loading control. Blots are representative of at least 3 independent experiments. (F) Immunofluorescence analysis showing the percentage nuclear localization of TFE3 in luminal (T47D and MCF7) compared with TNBC (MDA-MB-436 and MDA-MB-157) cells. Results represent the mean ± SEM from at least 3 independent experiments performed in triplicate.



¹⁴Figure 2. Loss of FLCN in luminal breast cancer cell lines activates AMPK and induces TFE3 nuclear localization and transcriptional activation.

(A) Immunoblot analysis of FLCN and downstream signaling molecules in empty vector (EV) control and CRISPR/Cas9-mediated FLCN-knockout (FLCN^{KO}) T47D and MCF7 cells. β-Actin

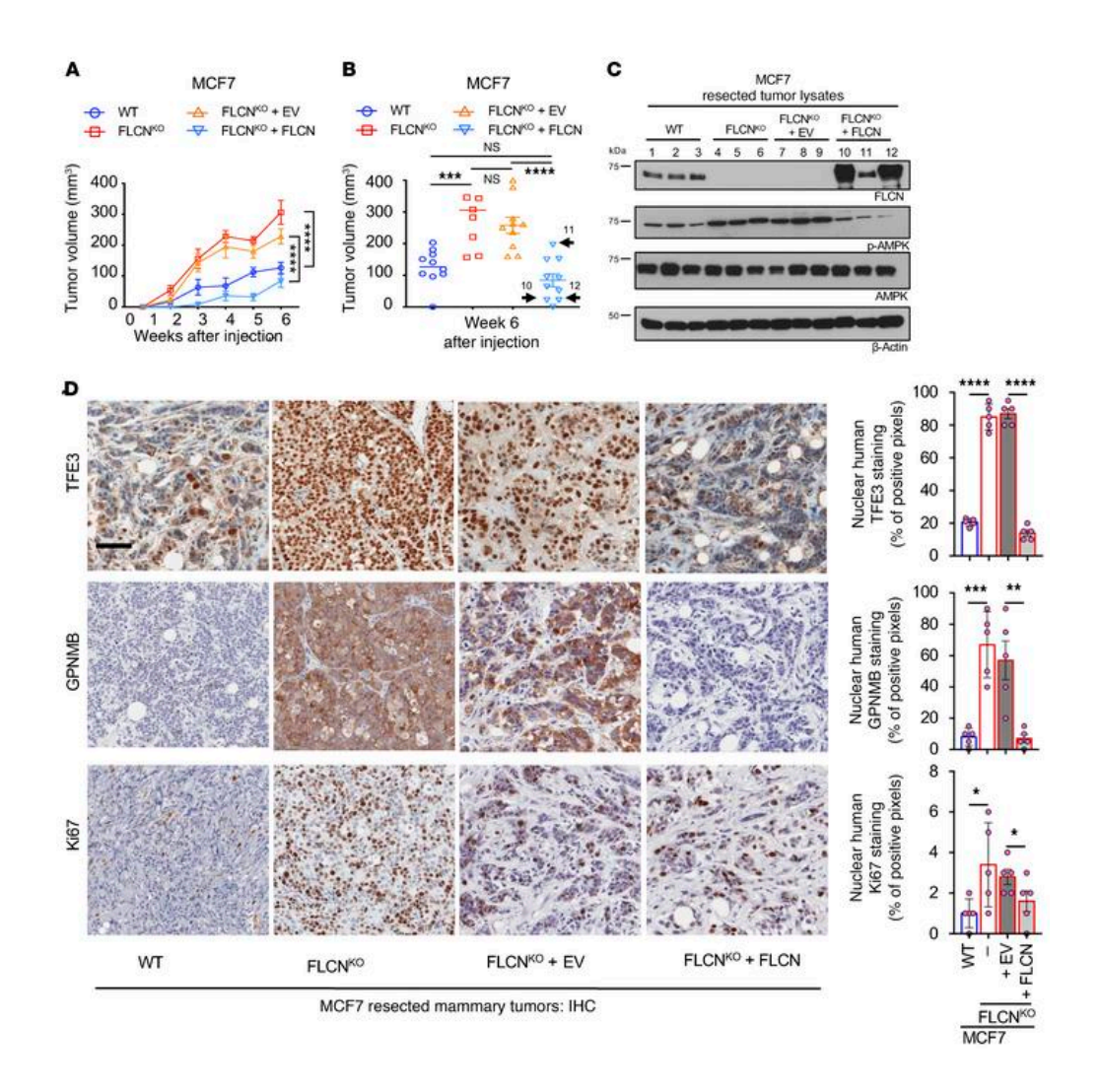
was used as a loading control. (B) Representative immunofluorescence images showing the localization of TFE3 in EV, FLCNKO, and reexpression of FLCN in T47D and MCF7 cells. Scale bar: 20 µm. (C) Quantitative analysis of the immunofluorescence results in **D** showing the percentage of TFE3 nuclear localization in EV, FLCNKO, and reexpression of FLCN inT47D and MCF7 cells. Results represent the mean ± SEM of at least 3 independent experiments, each performed in triplicate. Significance was determined using Student's t test. ****P < 0.0001. (**D**) Fold change in TFE3 transcriptional activity, as determined by CLEAR-luciferase promoter activity normalized against CMV-Renilla, in EV and FLCNKO T47D and MCF7 cells. Data represent the average ± SEM of 3 independent experiments, each performed in triplicate. Significance was determined using Student's t test. **P < 0.01, ***P < 0.001. (E) Representative images of EV and FLCNKO T47D and MCF7 cells after 1 hour of incubation with DQ-BSA-Red followed by a 2-hour chase in complete cellular media prior to fixation. Scale bar: 20 µm. Images are representative of at least 3 independent experiments. (F) Relative lysosomal activity, as determined by DQ-BSA assay, in EV and FLCNKO T47D and MCF7 cells upon treatment as indicated in E. Results represent the mean \pm SEM of at least 3 independent experiments, each performed in triplicate. Significance was determined using Student's t test. ****P < 0.0001. (G) Relative TFE3 and TFEB mRNA levels and their lysosomal and autophagy target gene mRNA levels measured by RT-qPCR in EV and FLCNKO T47D (left) and MCF7 (right) cells transfected with nontargeting (NT) siRNA control, or siRNA targeting TFEB or TFE3, or both. Data represent the average ± SEM of 3 independent experiments, each performed in triplicate. Statistical significance was determined using 2-way ANOVA with Bonferroni's multiple-comparison correction. ***P < 0.001; ****P < 0.0001. NS, not significant.



¹⁵Figure 3. Loss of FLCN in MCF7 enhances cellular metabolism in a TFE3-dependent manner.

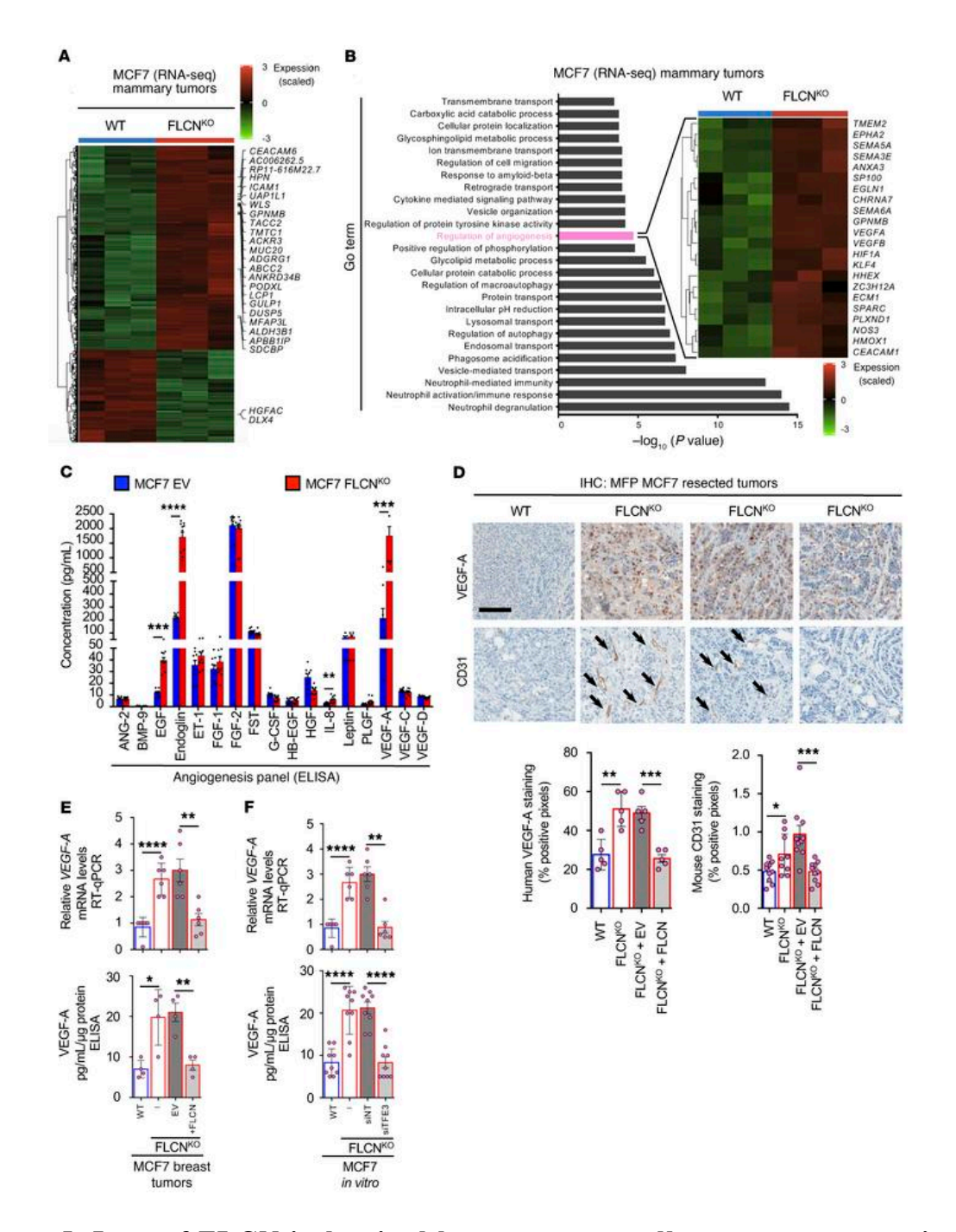
(A) Fold change in ATP levels in empty vector (EV) and FLCN-knockout (FLCN^{KO}) MCF7 cells transfected with nontargeting (NT) siRNA control or siRNA targeting TFE3, after 48 hours of transfection as measured by CellTiter-Glo Luminescent Cell Viability Assay. Data represent the average \pm SEM of at least n=3 independent experiments, each performed in triplicate. Statistical significance was determined using 2-way ANOVA with Bonferroni's multiple-comparison correction. **P < 0.01; ****P < 0.0001. (B) Glucose consumption and lactate production levels in the cellular media were measured using a NOVA Bioanalysis flux analyzer in EV and FLCN^{KO} MCF7 cells transfected with nontargeting (NT) control siRNA or siRNA targeting TFE3 after 48 hours of transfection. Data represent the average \pm SEM of at least n=3 independent experiments, each performed in triplicate. Statistical significance was determined using 2-way ANOVA with Bonferroni's multiple-comparison correction. **P < 0.01; ****P < 0.0001. (C and D) Basal extracellular acidification rate (ECAR) (C) and oxygen consumption rate (OCR) (D) in EV and FLCN^{KO} MCF7 cells transfected with NT control siRNA or siRNAs targeting TFE3,

after 48 hours of transfection, measured by Seahorse Bioscience XF96 extracellular flux analyzer. Data represent the average \pm SEM of at least n=3 independent experiments, each performed in triplicate. Statistical significance was determined using 2-way ANOVA with Bonferroni's multiple-comparison correction. **P < 0.01; ****P < 0.0001. (E) Relative mRNA levels of TFE3 and glycolysis-related genes measured by RT-qPCR in EV and FLCN^{KO} MCF7 cells transfected with nontargeting (NT) control siRNA or siRNA targeting TFE3. Data represent the average \pm SEM of n=6 independent experiments, each performed in triplicate, where each point represents the average of the triplicate. Statistical significance was determined using 2-way ANOVA with Bonferroni's multiple-comparison correction. ***P < 0.001; ****P < 0.0001. NS, not significant.



¹⁶Figure 4. Loss of FLCN in luminal breast cancer cells enhances tumor growth. (A) Growth curves of tumors of WT (blue), FLCN-knockout (FLCN^{KO}) (red), FLCN^{KO} plus EV (orange), and FLCN^{KO} FLCN-reexpressing (turquoise) MCF7 cells injected in mammary fat pads (MFP) of NSG mice over the course of 6 weeks. Data represent the mean volumes \pm SEM of each cohort measured each week (n = 10 mice in each cohort). Significance was determined using repeated-measures 1-way ANOVA. ****P < 0.0001. (B) Individual volumes of tumors as recorded 6 weeks after injection in cells indicated in A. Data represent the average volume \pm SEM of each cohort recorded 6 weeks after injection (n = 10 mice in each cohort). Statistical significance was determined using 2-way ANOVA with Bonferroni's multiple-comparison

correction. ***P < 0.001; ****P < 0.0001. NS, not significant. Samples 10 and 12 represent tumors with higher FLCN expression compared with sample 11, where FLCN expression was lower (refer to panel **C**). (**C**) Immunoblot analysis of WT, FLCN^{KO}, FLCN^{KO} plus EV, and FLCN^{KO} FLCN-reexpressing MCF7 tumors resected 6 weeks after injection. Three representative samples were run from each cohort. β -Actin was used as a loading control. (**D**) Representative images of immunohistochemistry (IHC) staining for human TFE3, GPNMB, and Ki67 in WT, FLCN^{KO}, FLCN^{KO} plus EV, and FLCN^{KO} FLCN-reexpressing MCF7 tumors resected 6 weeks after injection (left). Scale bar: 50 μ m. Quantification of IHC results showing the percentage of TFE3 nuclear localization, positive GPNMB staining, and positive Ki67 staining (right). Data represent mean quantifications \pm SEM of IHC images from at least 5 different mice. Statistical significance was determined using 2-way ANOVA with Bonferroni's multiple-comparison correction. *P < 0.05; **P < 0.01; ***P < 0.001; ****P < 0.0001.

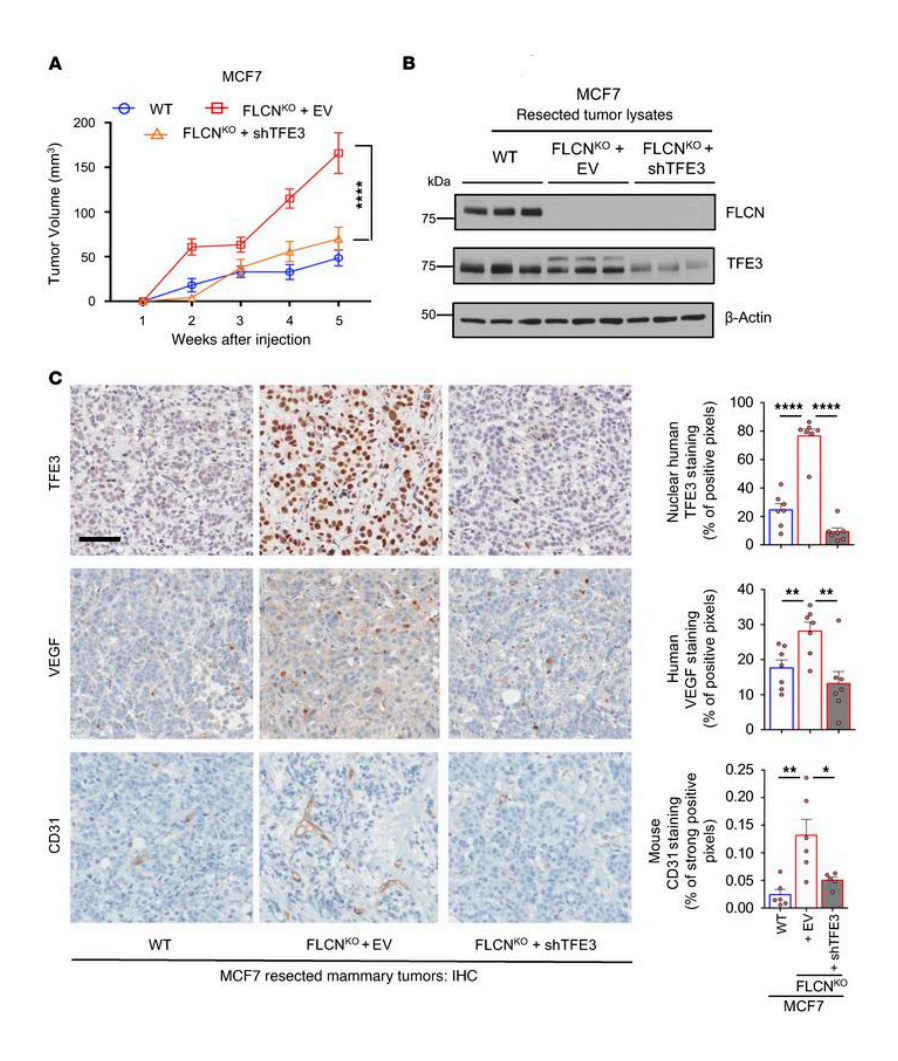


¹⁷Figure 5. Loss of FLCN in luminal breast cancer cells promotes an angiogenic profile.

(A) Heatmap representing differential gene expression in WT and FLCN-knockout (FLCN^{KO}) MCF7 tumors following RNA-sequencing analysis. Each column represents a different mouse from each cohort, where blue is WT and red is FLCN^{KO}. Fold increase was normalized against EV and color coded (dark red indicates 3-fold or more increase, light green indicates 3-fold or more

decrease, black indicates no change). (B) Gene enrichment scores for significantly upregulated pathways in FLCN^{KO} compared with WT MCF7 tumors highlighting regulation of angiogenesis as a differentially induced pathway, with the heatmap specifically showing the upregulation of angiogenesis-related genes. Each column represents a different mouse from each cohort, where blue is WT and red is FLCNKO. Fold increase was normalized against EV and color coded (dark red indicates 3-fold or more increase, light green indicates 3-fold or more decrease, black indicates no change). (C) Fold increase in 17 angiogenic/growth factors detected in WT and FLCN^{KO} MCF7 tumor lysates using human angiogenesis array. Data represent the average values of 10 mice in each of the indicated cohorts. Significance was determined using Student's t test. **P < 0.01, ***P < 0.001, ****P < 0.0001. (D) Representative images of immunohistochemistry (IHC) staining for human VEGF-A, mouse CD31, and mouse F4/80 of WT, FLCNKO, FLCNKO plus EV, and FLCN^{KO} FLCN-reexpressing MCF7 tumors resected 6 weeks after injection (top). Scale bar: 50 µm. Quantification of IHC results showing percentage positive VEGF-A staining, positive CD31 staining, and positive F4/80 staining (bottom). Data represent mean quantifications \pm SEM of IHC images from at least 5 different mice. Statistical significance was determined using 2-way ANOVA with Bonferroni's multiple-comparison correction. *P < 0.05; **P < 0.01; ***P < 0.01; *** < 0.001. (E) Relative human VEGFA mRNA levels measured by RT-qPCR in WT, FLCNKO, FLCN^{KO} plus EV, and FLCN^{KO} FLCN-reexpressing MCF7 tumors (top). Concentration of human VEGF-A in EV and FLCNKO cells transfected with siRNA targeting TFE3 in MCF7 cells, and FLCNKO FLCN-reexpressing MCF7 tumor lysates, as measured by ELISA (bottom). Data represent the average \pm SEM of at least 5 different mice from each cohort, performed in triplicate. Statistical significance was determined using 2-way ANOVA with Bonferroni's multiple-***P* < 0.01; *****P* < 0.0001. comparison correction. *P< 0.05; Relative

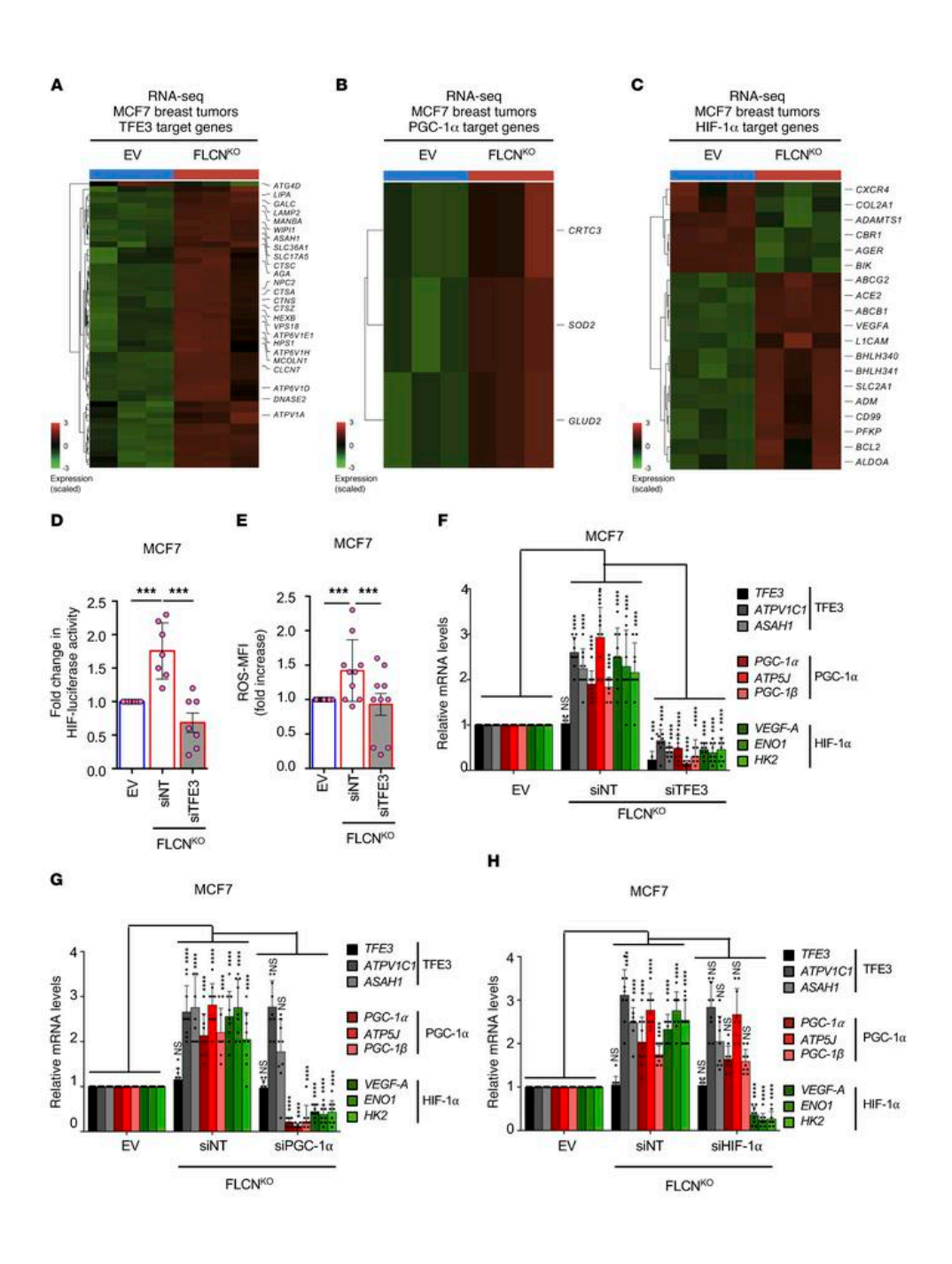
human VEGFA mRNA levels measured by RT-qPCR in EV, FLCN^{KO}, and FLCN^{KO} cells transfected with nontargeting (NT) control siRNA or siRNA targeting TFE3 in MCF7 cells (top). Concentration of human VEGF-A in EV and FLCN^{KO} cells transfected with siRNA targeting TFE3 in MCF7 cells, and FLCN^{KO} FLCN-reexpressing MCF7 tumor lysates, as measured by ELISA (bottom). Data represent the average \pm SEM of at least n=3, each performed in triplicate. Statistical significance was determined using 2-way ANOVA with Bonferroni's multiple-comparison correction. **P < 0.01; ****P < 0.0001.



¹⁸Figure 6. Loss of FLCN in luminal breast cancer cells enhances tumor growth and promotes angiogenesis in a TFE3-dependent manner.

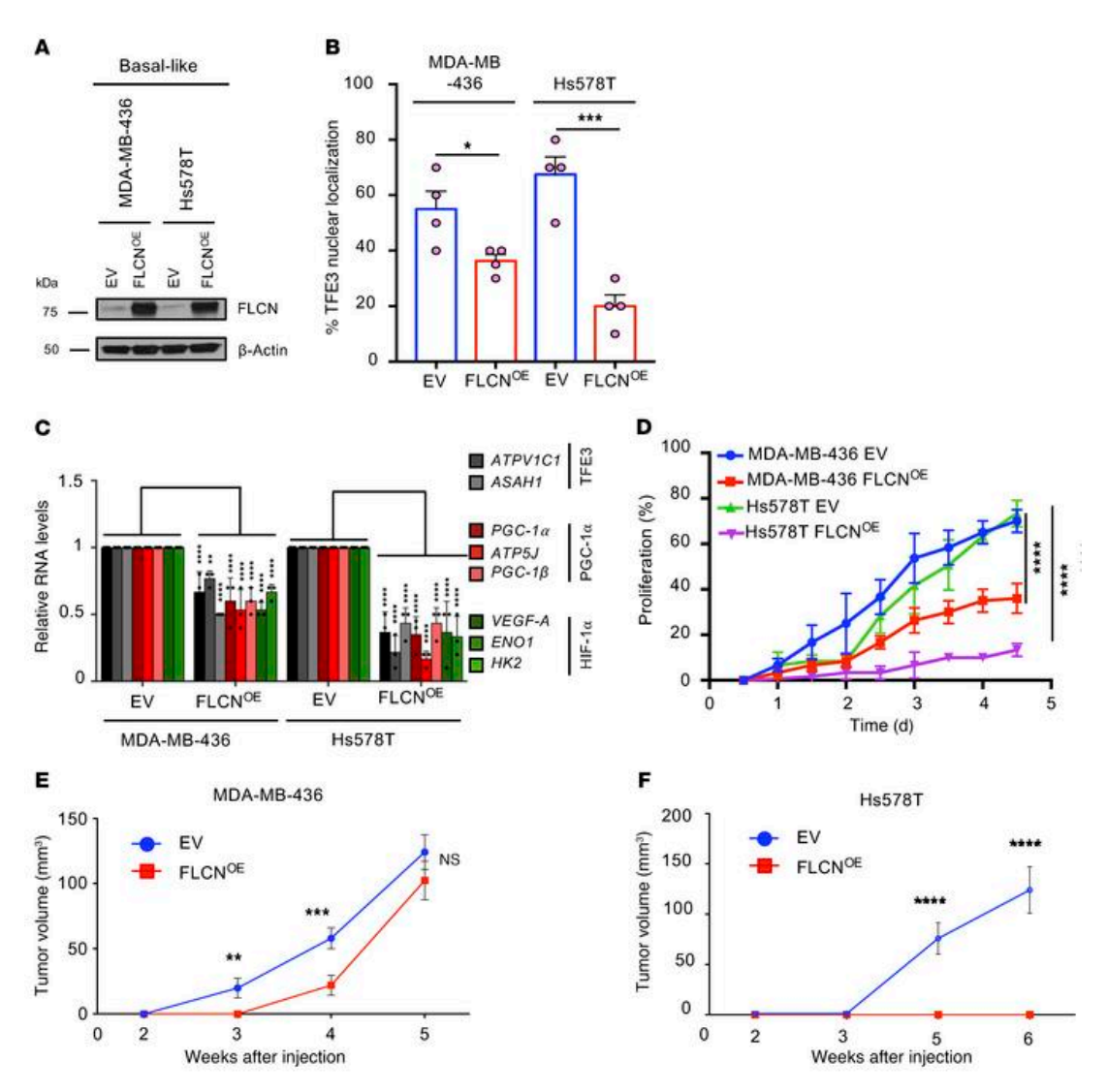
A) Growth of mammary tumors in mice injected with WT (blue), FLCN-knockout (FLCN^{KO}) (red), and FLCN^{KO} plus shTFE3 (orange) MCF7 cells over the course of 5 weeks. Data represent the mean tumor volumes \pm SEM of each cohort measured each week (n = 10 mice in each cohort). Significance was determined using repeated-measures 1-way ANOVA. ****P < 0.0001. (B) Immunoblot analysis of WT, FLCN^{KO}, and FLCN^{KO} plus shTFE3 MCF7 tumors resected 5 weeks after injection. Three representative samples were run from each cohort. β-Actin was used as a loading control. (C) Left: Representative images of the immunohistochemistry (IHC) staining for human TFE3, human VEGF-A, and mouse CD31 in WT, FLCN^{KO}, and FLCN^{KO} plus shTFE3 MCF7 tumors resected 6 weeks after injection. Scale bar: 50 μm. Right: Quantification of IHC

results showing the percentage TFE3 nuclear localization, VEGF-A staining, and CD31 staining in the indicated cohorts. Data represent the mean quantifications \pm SEM of IHC images from at least 5 different mice. Statistical significance was determined using 2-way ANOVA with Bonferroni's multiple-comparison correction. *P < 0.05; **P < 0.01; ****P < 0.0001.



 19 Figure 7. Loss of FLCN in luminal breast cancer cells activates a HIF-1 α -dependent angiogenic program in a TFE3-dependent manner.

(A–C) Heatmaps representing the differential TFE3 (A), PGC-1 α (B), and HIF-1 α (C) target gene expression in WT and FLCN-knockout (FLCNKO) MCF7 tumors following RNA-sequencing analysis. Each column represents gene expression from a different mouse from each cohort, where blue indicates WT and red indicates FLCNKO tumors. Fold increase was normalized against EV and color coded (dark red indicates 3-fold or more increase, light green indicates 3-fold or more decrease, black indicates no change). (D) Fold change in HIF-1a transcriptional activity, as determined by HIF-1a luciferase promoter activity normalized to CMV-Renilla, in EV and FLCN^{KO} MCF7 cells transfected with nontargeting (NT) control siRNA or siRNA targeting TFE3. Data represent the average \pm SEM of n=7 independent experiments. Statistical significance was determined using 2-way ANOVA with Bonferroni's multiple-comparison correction. ***P < 0.001. (E) Relative mean fluorescence intensity of the total cellular reactive oxygen species (ROS) in EV and FLCN^{KO} MCF7 cells transfected with NT control siRNA or siRNA targeting TFE3, as measured by flow cytometry. Data represent the average \pm SEM of at least n=3independent experiments, each performed in triplicate. Significance was determined using Student's t test. ***P < 0.001. (F–H) Relative TFE3, PGC-1 α , and HIF-1 α downstream target gene mRNA levels measured by RT-qPCR in EV and FLCNKO MCF7 cells transfected with NT control siRNA or siRNA targeting TFE3 (F), PGC-1\alpha (G), or HIF-1\alpha (H). Data represent the average \pm SEM of at least n=3 independent experiments, each performed in triplicate. Statistical significance was determined using 2-way ANOVA with Bonferroni's multiple-comparison correction. ***P < 0.001; ****P < 0.0001. NS, not significant.

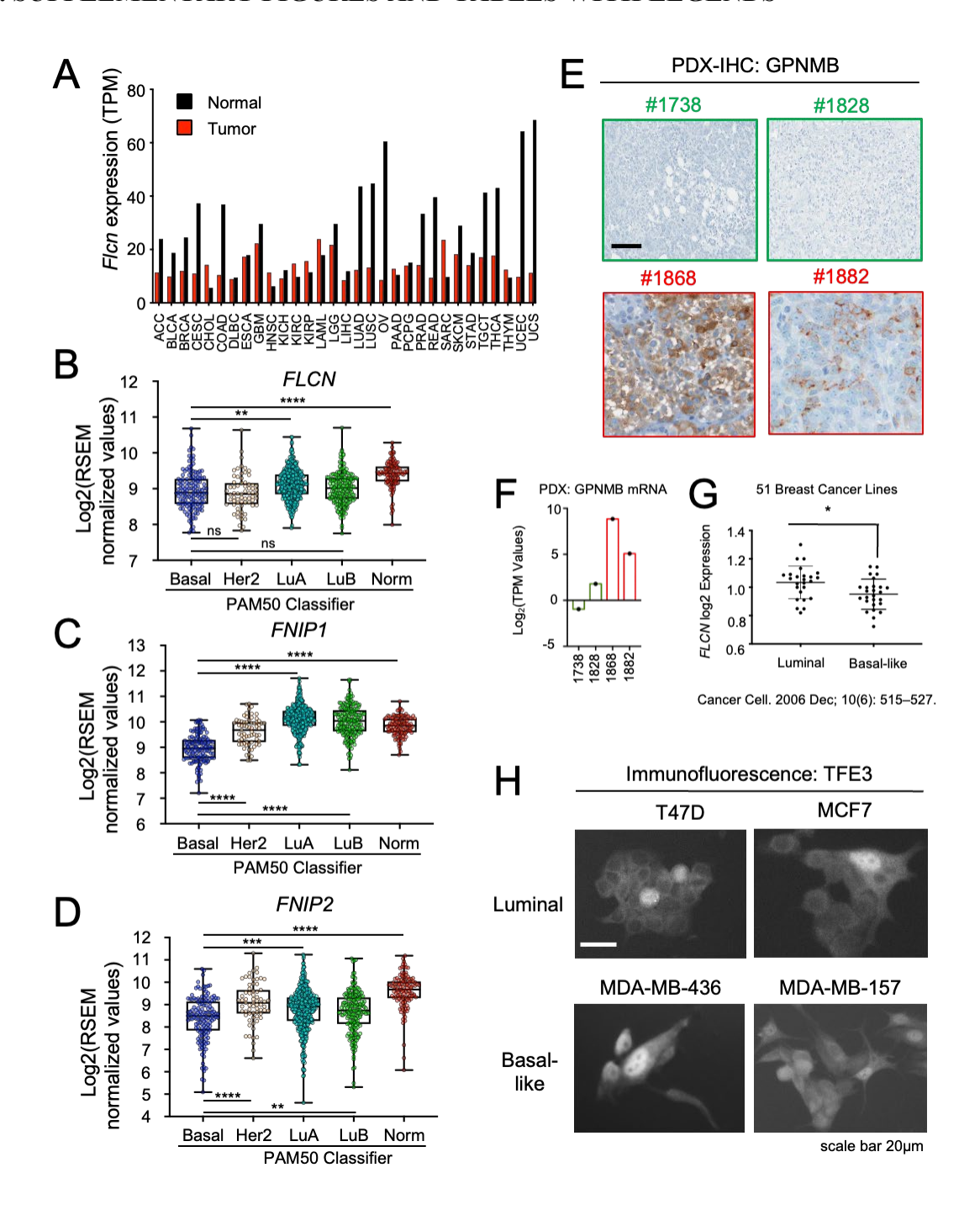


²⁰Figure 8. FLCN overexpression in basal-like breast cancer cells restores TFE3 cytoplasmic localization and attenuates tumor growth.

(A) Immunoblot analysis of empty vector (EV) and FLCN-overexpressing (FLCN^{OE}) MDA-MB-436 and Hs578T basal-like breast cancer cells. β -Actin was used as a loading control. (B) Quantitative analysis of the immunofluorescence data showing the percentage of TFE3 nuclear localization in EV and FLCN^{OE} MDA-MB-436 and Hs578T cells. Data represent the average \pm SEM of n=4 independent experiments. Statistical significance was determined using 2-way ANOVA with Bonferroni's multiple-comparison correction. *P < 0.05; ***P < 0.001. (C) Relative TFE3, PGC-1 α , and HIF-1 α downstream target gene mRNA levels measured by RT-

qPCR in EV and FLCN^{OE} MDA-MB-436 and Hs578T cells. Data represent the average \pm SEM of at least n=3 independent experiments, each performed in triplicate. Statistical significance was determined using 2-way ANOVA with Bonferroni's multiple-comparison correction. **P < 0.001; ****P < 0.0001. (**D**) The percentage proliferation of EV and FLCN^{OE} MDA-MB-436 and Hs578T cells over 5 days, as monitored and analyzed by an IncuCyte Live Cell Analysis System. Data represent the average \pm SEM of at least n=3 independent experiments, each performed in triplicate. Significance was determined using repeated-measures 1-way ANOVA. ****P < 0.0001. (E and F) Growth of mammary tumors in mice injected with WT (EV) (blue) or FLCN^{OE} cells (red) in MDA-MB-436 (E) and Hs578T (F) cell models over the course of 5 to 6 weeks. Data represent the mean tumor volumes \pm SEM of each cohort measured each week (n=10 mice in each cohort). Significance was determined using repeated-measures 1-way ANOVA. **P < 0.001, ***P < 0.001, ***P < 0.001, ***P < 0.0001, ***P < 0.0001

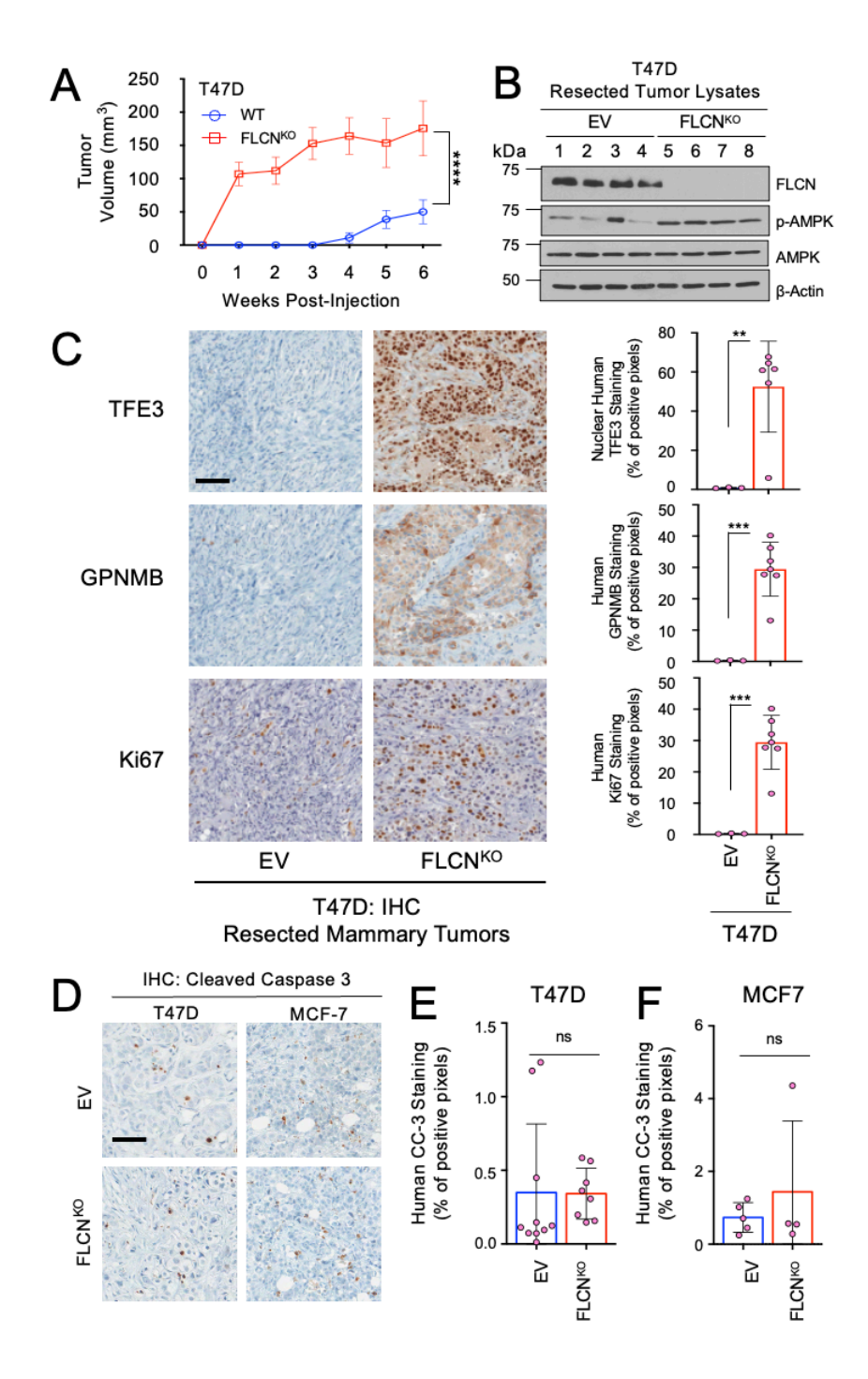
3.9. SUPPLEMENTARY FIGURES AND TABLES WITH LEGENDS



²¹Supplemental Figure 1 (related to Figure 1). FLCN, FNIP1 and FNIP2 are downregulated in basal-like breast cancer models compared to luminal subtypes.

(A) FLCN gene expression profile across different tumor samples and paired normal tissues from TCGA dataset (http://gepia2.cancer-pku.cn/#general). The height of each bar represents the

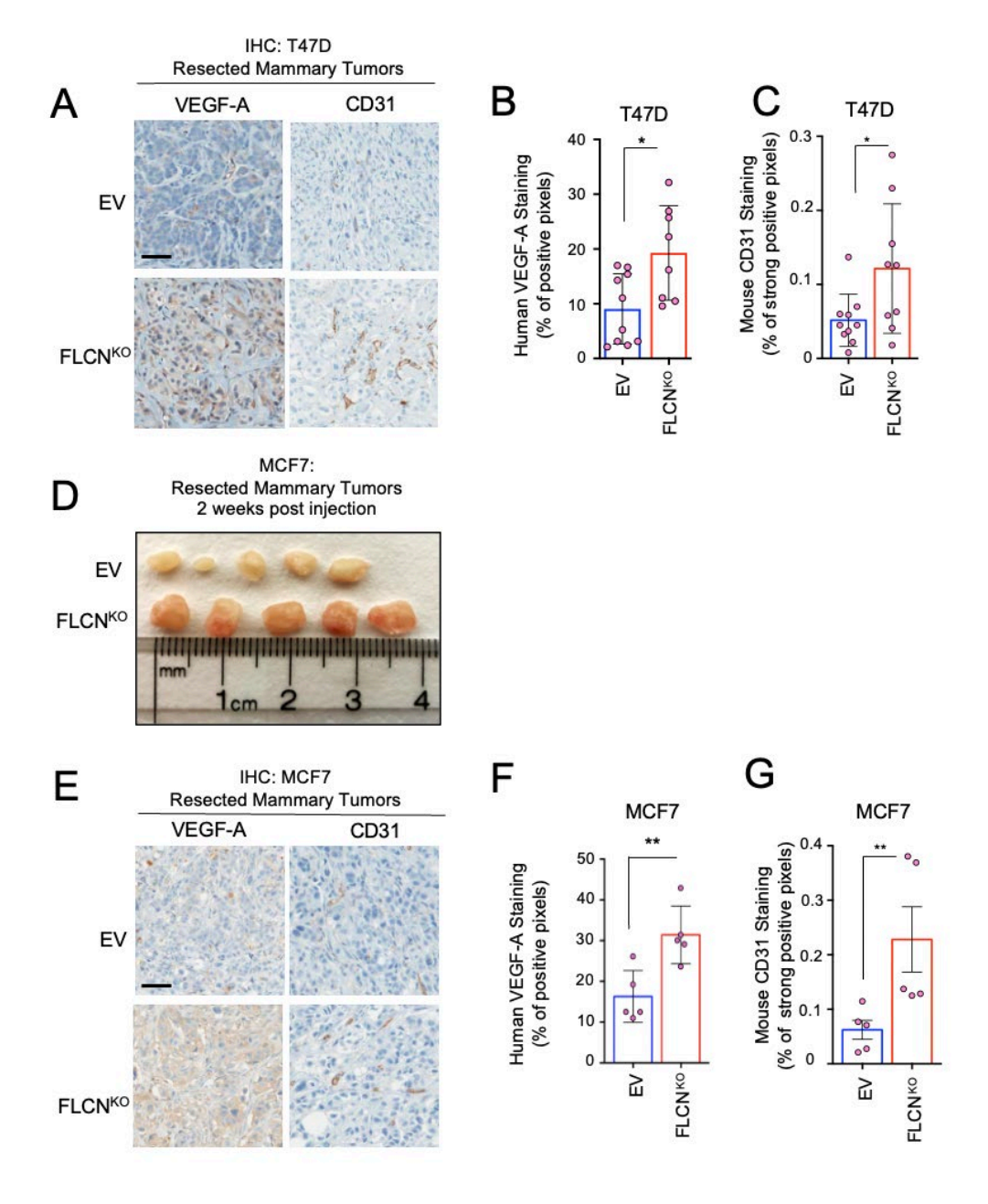
median expression in the specified tumor types or normal tissue. ACC: Adrenocortical carcinoma; BLCA: Bladder Urothelial Carcinoma; BRCA: Breast invasive carcinoma; CESC: Cervical squamous cell carcinoma and endocervical adenocarcinoma; CHOL: Cholangiocarcinoma; LCML: Chronic Myelogenous Leukemia; COAD: Colon adenocarcinoma; CNTL: Controls; ESCA: Esophageal carcinoma; FPPP: FFPE Pilot Phase II; GBM: Glioblastoma multiform, HNSC: Head and Neck squamous cell carcinoma; KICH: Kidney Chromophobe; KIRC: Kidney renal clear cell carcinoma; KIRP: Kidney renal papillary cell carcinoma; LGG: Brain Lower; Grade Glioma; LIHC: Liver hepatocellular carcinoma; LUAD: Lung adenocarcinoma; LUSC: Lung squamous cell carcinoma; DLBC: Lymphoid Neoplasm Diffuse Large B-cell Lymphoma; MESO: Mesothelioma; MISC: Miscellaneous; OV: Ovarian serous cystadenocarcinoma; PAAD: Pancreatic adenocarcinoma; PCPG: Pheochromocytoma and Paraganglioma; PRAD: Prostate adenocarcinoma; READ: Rectum adenocarcinoma; SARC: Sarcoma; SKCM: Skin Cutaneous Melanoma; STAD: Stomach adenocarcinoma; TGCT: Testicular Germ Cell Tumors; THYM: Thymoma; THCA: Thyroid carcinoma; UCS: Uterine Carcinosarcoma. (B-D) Expression levels 22 of FLCN (B), FNIP1 (C) and FNIP2 (D) in the different molecular subtypes of breast cancer in the TCGA dataset, as defined by the PAM50/AIMS (prediction analysis of microarray 50) gene signature. Significance was determined using one-way ANOVA with application of the Bonferroni correction (**p<0.01, ***p<0.001, ****p<0.0001). (E) Immunohistochemistry analysis of human GPNMB for the selected patient derived xenografts (PDXs) representing the functional FLCN/FNIP1/2 complex in green (1738 and 1828) and the deregulated FLCN-FNIP1/2 complex in red (1868 and 1882). Scale bar represents 50 µm. (F) Transcript levels of human GPNMB in the selected patient-derived xenografts (PDXs) indicated in (E). (G) FLCN expression levels in 51 different breast cancer cell lines stratified into luminal and basal subtypes, data was obtained and analyzed from Cancer Cell. 2006 Dec; 10(6): 515–527. (H) Representative immunofluorescence images showing the localization of TFE3 in luminal (T47D and MCF7) and Triple negative breast cancer (TNBC) (MDA-MB-436 and MD-MB-157) cells. Scale bar represents 20μm.



²²Supplemental Figure 2 (related to Figure 4). Loss of FLCN in luminal breast cancer cells enhances tumor growth.

(A) Growth curves of tumors of empty vector (EV) (blue) and FLCN knock out (FLCN^{KO}) (red) T47D cells injected in mammary fat pad (MFP) of NSG mice over the course of 7 weeks. Data represents the mean volumes of mice in each cohort measured each week (n=10 in each cohort) \pm

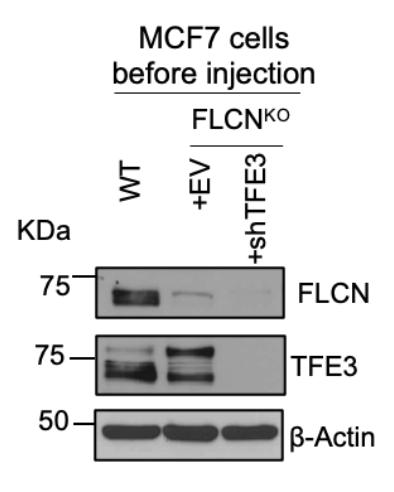
SEM. Significance was determined using repeated measures one-way Anova on prism (****p<0.0001). (B) Immunoblot analysis of EV and FLCN^{KO} T47D tumor lysates resected 7 weeks post-injection. Four representative samples were run from each cohort. Actin was used as a loading control. (C) Representative images of the immunohistochemistry (IHC) staining for TFE3, GPNMB and Ki67 of EV and FLCNKO re-expressing FLCN T47D tumors resected 7 weeks postinjection. Scale bar represents 50 µm (left). Quantification of IHC results showing the percentage TFE3 nuclear localization, positive GPNMB staining and positive Ki67 staining, in the EV and FLCNKO T47D tumors (right). Data represents mean quantifications of IHC images from at least 3 different mice ± SEM. Significance was determined using Student's t-test (***p<0.001, **p<0.01). (D) Representative IHC of cleaved caspase-3 staining in EV and FLCN^{KO} tumors resected from mice injected with T47D or MCF7 cells on week 6 and 5, respectively. Scale bar represents 50 µm. Quantification of IHC results showing the positive cleaved caspase-3 staining in T47D and MCF7 cells, in the EV and FLCNKO tumors. Data represents mean quantifications of IHC images from at least 3 different mice \pm SEM. Significance was determined using Student's ttest (ns=non-significant).



²³Supplemental Figure 3 (related to Figure 5). Loss of FLCN in luminal breast cancer cells induces an angiogenic response.

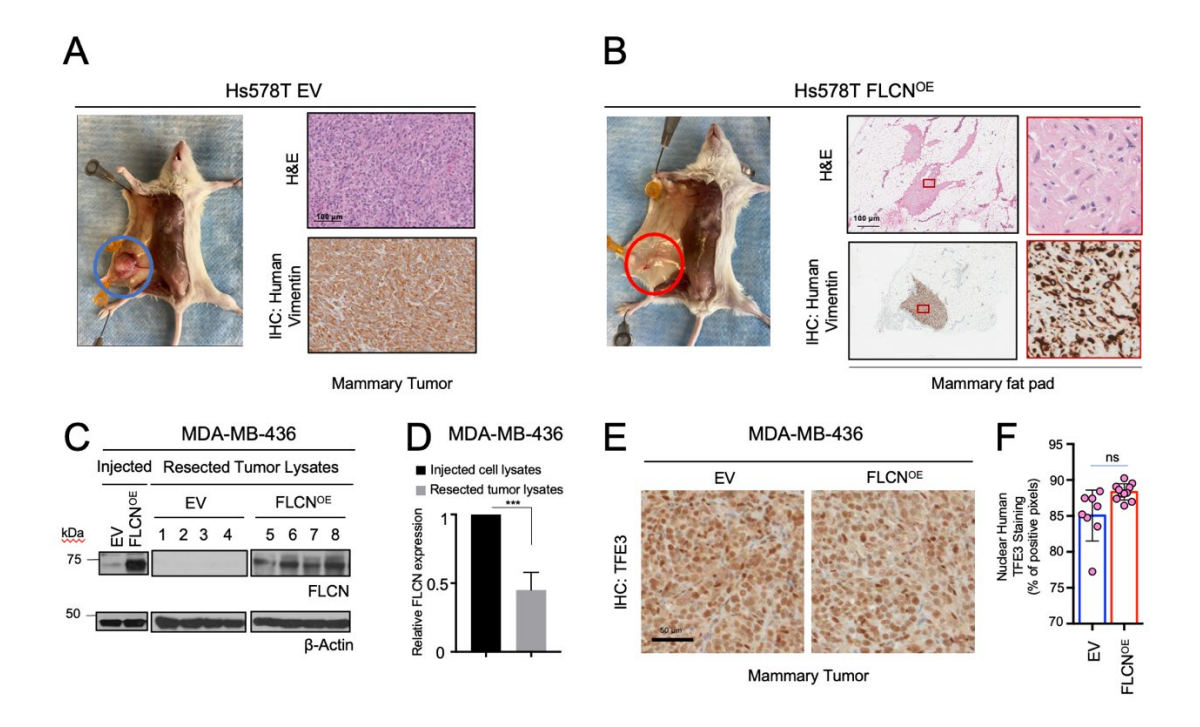
(A) Representative images of the immunohistochemistry (IHC) staining for human VEGF-A and mouse CD31 of empty vector (EV) and FLCN knock out (FLCN^{KO}) T47D tumors resected 7 weeks post-injection. Scale bar represents 50 μm. (B, C) Quantification of IHC results in (A) showing % positive VEGF-A staining (B) and positive CD31 staining (C) in EV and FLCN^{KO} T47D tumors.

Data represents mean quantifications of IHC images from at least 9 different mice ± SEM. Significance was determined using Student's t-test (**p<0.01). (D) Photograph image of MCF7 EV and FLCN^{KO} mammary fat pad tumors resected 2 weeks post-injection. (E) Representative images of the immunohistochemistry (IHC) staining for human VEGF-A of EV and mouse CD31 and FLCN^{KO} tumors resected 2 weeks post-injection. Scale bar represents 50 μm. (F) Quantification of IHC results in (E) showing % positive VEGF-A staining (F) and positive CD31 staining (G) in EV and FLCN^{KO} MCF7 tumors. Data represents mean quantifications of IHC images from at least 5 different mice ± SEM. Significance was determined using Student's t-test **p<0.01). Heatmap representing differential gene expression of tumor secreted chemoattractants in WT and FLCN^{KO} MCF7 tumors following RNA-sequencing analysis. Each column represents a different mouse from each cohort, where blue is WT and red is FLCN^{KO}. Fold increase was normalized against EV and color-coded (dark red indicates 3-fold or more increase, light green indicates 3-fold or more decrease, black indicates no change).



²⁴Supplemental Figure 4 (related to Figure 6). Validation of TFE3 and FLCN levels in MCF7 breast cancer cells prior to injection.

(A) Immunoblot analysis of TFE3 and FLCN levels in wild type (WT), FLCN KO (FLCN^{KO}) +EV, and FLCN KO +shTFE3 MCF7 cells before injection. Actin was used as a loading control.



²⁵Supplemental Figure 5 (related to Figure 8). FLCN overexpression in basal-like breast cancer cells.

(A) Representative images of mice injected with Hs578T empty vector (EV) cells, highlighting the tumor in the mammary fat pad (blue circle, left image). Representative images of H&E and immunohistochemistry (IHC) staining for human vimentin in Hs578T EV cells tumors resected 6 weeks post-injection (right). Scale bar represents 100 μm. (B) Representative images of mice injected with Hs578T FLCN overexpressing (FLCN^{OE}) cells, highlighting the mammary fat pad containing residual cancer cells (red circle, left image). Representative images of H&E and IHC staining for human vimentin, revealing residual cancer cells, in the mammary fat pad of the mice injected with Hs578T FLCN^{OE} cells resected 6 weeks post-injection (right). Scale bar represents 100 μm. (C) Immunoblot analysis of EV and FLCN^{OE} MDA-MB-436 cells prior to injection and in end-stage tumors. Four representative samples were run from the FLCN^{OE} MDA-MB-436 tumors. β-Actin was used as a loading control. (D) Relative FLCN expression in samples indicated in (C) as quantified by ImageJ. Significance was determined using Student's t-test (***p<0.001).

(E) Representative images of IHC staining for human TFE3 in EV and FLCN^{OE} MDA-MB-436 tumors in end-stage tumors (left). Scale bar represents 50 μ m. (F) Quantitative analysis of the IHC results in (E), showing the % of TFE3 nuclear localization in EV and FLCN^{OE} MDA-MB-436 cells. Results represent the mean of the results from at least 7 mice \pm SEM. Significance was determined using Student's t-test (ns=non-significant).

Supplemental Table 1 (related to Figures 2, 3, 5, and 7): Oligonucleotide sequences of the human primers used for qPCR

Gene	Forward primer	Reverse primer	
ATP6V0E1	CTCACTGTGCCTCTCATTGTG	CACCAACATGGTAATGATAACTCC	
ASAH1	AGTTGCGTCGCCTTAGTCCT	TGCACCTCTGTACGTTGGTC	
TPP1	GGGAGGACCAGGAGCAT	GGGCCTAGAGAGCTCAGAAT	
MCOLIN1	TAGCGACTGCCTTCGACCC	GCCCTTTTCTCCACCGTGA	
TFEB	CGGACAGATTGACCTTCAGAG	GCTGCTGCTGTTGCATATAAT	
TFE3	CCGTGTTCGTGCTGTTGGA	CTCGTAGAAGCTGTCAGGAT	
SLCA1	GAAGCAGTGGCAGCGGTGTTTATT	ATGTGGCCGTGATACTGATGGTGA	
LDHA	CTCCAAGCTGGTCATTATCACG	AGTTCGGGCTGTATTTTACAACA	
НК-2	GAGCCACCACTCACCCTACT	ACCCAAAGCACACGGAAGTT	
ATPV1C1	ATTGCATGCGGCAACTTCAA	CCAAGACATCCAACGTGCCA	
PGC1-α	GTGTGTGCTGTGTG TCAGAGTGG	GAGTCTTGGCTGCACATGTCCC	
ATP5J	TCAGCCGTCTCAGTCCATTT	CCAAACATTTGCTTGAGCTT	
PGC1-β	CTCTTCACCCTGCCACTCC	ACCTCGCACTCCTCAATCTC	
VEGF-α	AGGCCAGCACATAGGAGAGA	TACCGGGATTTCTTGCGCTT	

ENO1	CTGGTGCCGTTGAGAAGGG	GGTTGTGGTAAACCTCTGCTC
TBP	AGGGTTTCTGGTTTGCCAAGA	CTGAATAGGCTGTGGGGTCA

Supplemental Table S2 (related to Figure 5). RNA-sequencing results of the complete list of differentially expressed genes in wild type (WT) compared to FLCN knock out (FLCN^{KO}) MCF7 cells. (attached)

Supplemental Table S3 (related to Figure 5). Complete GO enrichment list in FLCN knock out (FLCN^{KO}) MCF7 cells through enrichment of functionally annotated gene sets among the differentially expressed genes. (attached)

4.0. REFERENCES ASSOCIATED WITH CHAPTER 3

- [1] Siegel RL, Miller KD, Jemal A. Cancer statistics, 2020. CA: A Cancer Journal for Clinicians. 2020;70:7-30.
- [2] Perou CM, Sorlie T, Eisen MB, van de Rijn M, Jeffrey SS, Rees CA, et al. Molecular portraits of human breast tumours. Nature. 2000;406:747-52.
- [3] Sorlie T, Perou CM, Tibshirani R, Aas T, Geisler S, Johnsen H, et al. Gene expression patterns of breast carcinomas distinguish tumor subclasses with clinical implications. Proc Natl Acad Sci U S A. 2001;98:10869-74.
- [4] Sorlie T, Tibshirani R, Parker J, Hastie T, Marron JS, Nobel A, et al. Repeated observation of breast tumor subtypes in independent gene expression data sets. Proc Natl Acad Sci U S A. 2003;100:8418-23.
- [5] Foulkes WD, Smith IE, Reis-Filho JS. Triple-negative breast cancer. New England journal of medicine. 2010;363:1938-48.
- [6] DeBerardinis RJ, Lum JJ, Hatzivassiliou G, Thompson CB. The biology of cancer: metabolic reprogramming fuels cell growth and proliferation. Cell metabolism. 2008;7:11-20.
- [7] Hanahan D, Weinberg RA. Hallmarks of cancer: the next generation. cell. 2011;144:646-74.
- [8] El-Houjeiri L, Possik E, Vijayaraghavan T, Paquette M, Martina JA, Kazan JM, et al. The transcription factors TFEB and TFE3 link the FLCN-AMPK signaling axis to innate immune response and pathogen resistance. Cell reports. 2019;26:3613-28. e6.
- [9] Possik E, Ajisebutu A, Manteghi S, Gingras MC, Vijayaraghavan T, Flamand M, et al. FLCN and AMPK Confer Resistance to Hyperosmotic Stress via Remodeling of Glycogen Stores. PLoS Genet. 2015;11:e1005520.
- [10] Possik E, Jalali Z, Nouet Y, Yan M, Gingras MC, Schmeisser K, et al. Folliculin regulates ampk-dependent autophagy and metabolic stress survival. PLoS Genet. 2014;10:e1004273.
- [11] Yan M, Audet-Walsh E, Manteghi S, Dufour CR, Walker B, Baba M, et al. Chronic AMPK activation via loss of FLCN induces functional beige adipose tissue through PGC-1alpha/ERRalpha. Genes Dev. 2016;30:1034-46.
- [12] Yan M, Gingras MC, Dunlop EA, Nouet Y, Dupuy F, Jalali Z, et al. The tumor suppressor folliculin regulates AMPK-dependent metabolic transformation. J Clin Invest. 2014;124:2640-50.
- [13] Baba M, Hong SB, Sharma N, Warren MB, Nickerson ML, Iwamatsu A, et al. Folliculin encoded by the BHD gene interacts with a binding protein, FNIP1, and AMPK, and is involved in AMPK and mTOR signaling. Proc Natl Acad Sci U S A. 2006;103:15552-7.
- [14] Takagi Y, Kobayashi T, Shiono M, Wang L, Piao X, Sun G, et al. Interaction of folliculin (Birt-Hogg-Dube gene product) with a novel Fnip1-like (FnipL/Fnip2) protein. Oncogene. 2008:27:5339-47.
- [15] Tee AR, Pause A. Birt-Hogg-Dube: tumour suppressor function and signalling dynamics central to folliculin. Fam Cancer. 2013;12:367-72.
- [16] Wilson GK, Tennant DA, McKeating JA. Hypoxia inducible factors in liver disease and hepatocellular carcinoma: current understanding and future directions. Journal of hepatology. 2014;61:1397-406.

- [17] Keith B, Johnson RS, Simon MC. HIF1α and HIF2α: sibling rivalry in hypoxic tumour growth and progression. Nature Reviews Cancer. 2012;12:9-22.
- [18] Krock BL, Skuli N, Simon MC. Hypoxia-induced angiogenesis: good and evil. Genes & cancer. 2011;2:1117-33.
- [19] Linderholm B, Hellborg H, Johansson U, Elmberger G, Skoog L, Lehtiö J, et al. Significantly higher levels of vascular endothelial growth factor (VEGF) and shorter survival times for patients with primary operable triple-negative breast cancer. Annals of oncology. 2009;20:1639-46.
- [20] Mohammed RA, Ellis IO, Mahmmod AM, Hawkes EC, Green AR, Rakha EA, et al. Lymphatic and blood vessels in basal and triple-negative breast cancers: characteristics and prognostic significance. Modern Pathology. 2011;24:774-85.
- [21] Andre F, Zielinski C. Optimal strategies for the treatment of metastatic triple-negative breast cancer with currently approved agents. Annals of oncology. 2012;23:vi46-vi51.
- [22] Betschinger J, Nichols J, Dietmann S, Corrin PD, Paddison PJ, Smith A. Exit from pluripotency is gated by intracellular redistribution of the bHLH transcription factor Tfe3. Cell. 2013;153:335-47.
- [23] Martina JA, Puertollano R. Rag GTPases mediate amino acid-dependent recruitment of TFEB and MITF to lysosomes. J Cell Biol. 2013;200:475-91.
- [24] Petit CS, Roczniak-Ferguson A, Ferguson SM. Recruitment of folliculin to lysosomes supports the amino acid-dependent activation of Rag GTPases. J Cell Biol. 2013;202:1107-22.
- [25] Wada S, Neinast M, Jang C, Ibrahim YH, Lee G, Babu A, et al. The tumor suppressor FLCN mediates an alternate mTOR pathway to regulate browning of adipose tissue. Genes Dev. 2016;30:2551-64.
- [26] Perera RM, Stoykova S, Nicolay BN, Ross KN, Fitamant J, Boukhali M, et al. Transcriptional control of autophagy-lysosome function drives pancreatic cancer metabolism. Nature. 2015;524:361-5.
- [27] Pastore N, Vainshtein A, Herz NJ, Huynh T, Brunetti L, Klisch TJ, et al. Nutrient-sensitive transcription factors TFEB and TFE 3 couple autophagy and metabolism to the peripheral clock. The EMBO journal. 2019;38:e101347.
- [28] Martina JA, Diab HI, Li H, Puertollano R. Novel roles for the MiTF/TFE family of transcription factors in organelle biogenesis, nutrient sensing, and energy homeostasis. Cellular and molecular life sciences. 2014;71:2483-97.
- [29] Raben N, Puertollano R. TFEB and TFE3: linking lysosomes to cellular adaptation to stress. Annual review of cell and developmental biology. 2016;32:255-78.
- [30] Shen K, Rogala KB, Chou H-T, Huang RK, Yu Z, Sabatini DM. Cryo-EM structure of the human FLCN-FNIP2-Rag-ragulator complex. Cell. 2019;179:1319-29. e8.
- [31] Lawrence RE, Fromm SA, Fu Y, Yokom AL, Thelen AM, Young LN, et al. Structural mechanism of a Rag GTPase activation checkpoint by the lysosomal folliculin complex. Science. 2019;366:971-7.
- [32] Petit CS, Roczniak-Ferguson A, Ferguson SM. Recruitment of folliculin to lysosomes supports the amino acid—dependent activation of Rag GTPases. Journal of Cell Biology. 2013;202:1107-22.
- [33] Vocke CD, Yang Y, Pavlovich CP, Schmidt LS, Nickerson ML, Torres-Cabala CA, et al. High frequency of somatic frameshift BHD gene mutations in Birt-Hogg-Dube—associated renal tumors. Journal of the National Cancer Institute. 2005;97:931-5.

- [34] Schmidt LS, Linehan WM. Molecular genetics and clinical features of Birt-Hogg-Dube syndrome. Nat Rev Urol. 2015;12:558-69.
- [35] Savage P, Pacis A, Kuasne H, Liu L, Lai D, Wan A, et al. Chemogenomic profiling of breast cancer patient-derived xenografts reveals targetable vulnerabilities for difficult-to-treat tumors. Communications biology. 2020;3:1-15.
- [36] Hong S-B, Oh H, Valera VA, Baba M, Schmidt LS, Linehan WM. Inactivation of the FLCN tumor suppressor gene induces TFE3 transcriptional activity by increasing its nuclear localization. PloS one. 2010;5.
- [37] Neve RM, Chin K, Fridlyand J, Yeh J, Baehner FL, Fevr T, et al. A collection of breast cancer cell lines for the study of functionally distinct cancer subtypes. Cancer cell. 2006;10:515-27.
- [38] Maric G, Rose AA, Annis MG, Siegel PM. Glycoprotein non-metastatic b (GPNMB): A metastatic mediator and emerging therapeutic target in cancer. OncoTargets and therapy. 2013;6:839.
- [39] Vázquez CL, Colombo MI. Assays to assess autophagy induction and fusion of autophagic vacuoles with a degradative compartment, using monodansylcadaverine (MDC) and DQ-BSA. Methods in enzymology. 2009;452:85-95.
- [40] Cairns RA, Harris IS, Mak TW. Regulation of cancer cell metabolism. Nature Reviews Cancer. 2011;11:85-95.
- [41] Lugano R, Ramachandran M, Dimberg A. Tumor angiogenesis: Causes, consequences, challenges and opportunities. Cellular and Molecular Life Sciences. 2020;77:1745-70.
- [42] Talks KL, Turley H, Gatter KC, Maxwell PH, Pugh CW, Ratcliffe PJ, et al. The expression and distribution of the hypoxia-inducible factors HIF-1α and HIF-2α in normal human tissues, cancers, and tumor-associated macrophages. The American journal of pathology. 2000;157:411-21.
- [43] Perera RM, Di Malta C, Ballabio A. MiT/TFE family of transcription factors, lysosomes, and cancer. Annual review of cancer biology. 2019;3:203-22.
- [44] Bost F, Kaminski L. The metabolic modulator PGC-1α in cancer. American journal of cancer research. 2019;9:198.
- [45] Aggarwal V, Tuli HS, Varol A, Thakral F, Yerer MB, Sak K, et al. Role of reactive oxygen species in cancer progression: Molecular mechanisms and recent advancements. Biomolecules. 2019;9:735.
- [46] Semenza GL. HIF-1: upstream and downstream of cancer metabolism. Current opinion in genetics & development. 2010;20:51-6.
- [47] Kauffman EC, Ricketts CJ, Rais-Bahrami S, Yang Y, Merino MJ, Bottaro DP, et al. Molecular genetics and cellular features of TFE3 and TFEB fusion kidney cancers. Nat Rev Urol. 2014;11:465-75.
- [48] Eichner LJ, Brun SN, Herzig S, Young NP, Curtis SD, Shackelford DB, et al. Genetic analysis reveals AMPK is required to support tumor growth in murine Kras-dependent lung cancer models. Cell metabolism. 2019;29:285-302. e7.
- [49] Bos R, Zhong H, Hanrahan CF, Mommers EC, Semenza GL, Pinedo HM, et al. Levels of hypoxia-inducible factor-1α during breast carcinogenesis. Journal of the national cancer institute. 2001;93:309-14.
- [50] Giatromanolaki A, Koukourakis M, Sivridis E, Turley H, Talks K, Pezzella F, et al. Relation of hypoxia inducible factor 1 α and 2 α in operable non-small cell lung cancer to angiogenic/molecular profile of tumours and survival. British journal of cancer. 2001;85:881-90.

- [51] Steingrímsson E, Tessarollo L, Reid SW, Jenkins NA, Copeland NG. The bHLH-Zip transcription factor Tfeb is essential for placental vascularization. Development. 1998;125:4607-16.
- [52] Gad S, Lefevre S, Khoo S, Giraud S, Vieillefond A, Vasiliu V, et al. Mutations in BHD and TP53 genes, but not in HNF1β gene, in a large series of sporadic chromophobe renal cell carcinoma. British journal of cancer. 2007;96:336-40.
- [53] Khoo SK, Kahnoski K, Sugimura J, Petillo D, Chen J, Shockley K, et al. Inactivation of BHD in sporadic renal tumors. Cancer research. 2003;63:4583-7.
- [54] Schmidt LS, Linehan WM. FLCN: The causative gene for Birt-Hogg-Dubé syndrome. Gene. 2018;640:28-42.
- [55] Pradella LM, Lang M, Kurelac I, Mariani E, Guerra F, Zuntini R, et al. Where Birt–Hogg–Dube meets Cowden Syndrome: mirrored genetic defects in two cases of syndromic oncocytic tumours. European Journal of Human Genetics. 2013;21:1169-72.
- [56] Shalem O, Sanjana NE, Hartenian E, Shi X, Scott DA, Mikkelsen TS, et al. Genome-scale CRISPR-Cas9 knockout screening in human cells. Science. 2014;343:84-7.
- [57] Bolger AM, Lohse M, Usadel B. Trimmomatic: a flexible trimmer for Illumina sequence data. Bioinformatics. 2014;30:2114-20.
- [58] Dobin A, Davis CA, Schlesinger F, Drenkow J, Zaleski C, Jha S, et al. STAR: ultrafast universal RNA-seq aligner. Bioinformatics. 2013;29:15-21.
- [59] Anders S, Pyl PT, Huber W. HTSeq—a Python framework to work with high-throughput sequencing data. Bioinformatics. 2015;31:166-9.
- [60] Ritchie ME, Phipson B, Wu D, Hu Y, Law CW, Shi W, et al. limma powers differential expression analyses for RNA-sequencing and microarray studies. Nucleic acids research. 2015;43:e47-e.
- [61] Chen EY, Tan CM, Kou Y, Duan Q, Wang Z, Meirelles GV, et al. Enrichr: interactive and collaborative HTML5 gene list enrichment analysis tool. BMC bioinformatics. 2013;14:128.
- [62] Paquet ER, Hallett MT. Absolute assignment of breast cancer intrinsic molecular subtype. Journal of the National Cancer Institute. 2015;107:dju357.

CHAPTER 4 – Identification and	d functional isoforms	characterizati	on of the two TFE3

Identification and functional characterization of the two TFE3 isoforms

Leeanna El-Houjeiri^{1,2*}, Rafael Cuesta*, Hyeonju Jeong, Mathieu Paquette, Peter. M. Siegel[#], and Arnim Pause[#].

¹Goodman Cancer Research Institute, McGill University, Montréal, Canada. ²Department of Biochemistry, McGill University, Montréal, Canada. ³Department of Medicine, McGill University, Montréal, Canada. ⁴Department of Pathology, McGill University Montréal, Canada. *Equal contribution, *Equal correspondence

Manuscript in preparation

*Corresponding Authors:

Arnim Pause Peter M. Siegel

3655 promenade Sir William Osler 1160 Pine Avenue West

Room 707B Room 513

Montréal, Québec, Canada Montréal, Québec, Canada

H3G 1Y6 H3A 1A3

Phone: (514) 398-1521 Phone: (514) 398-4259

Fax: (514) 398-3380 Fax: (514) 398-6769

Email: arnim.pause@mcgill.ca E-mail: peter.siegel@mcgill.ca

Keywords: TFE3 isoforms, mTORC1, AMPK, Skp2, proteasomal degradation

4.1. ABSTRACT

The transcription factor TFE3 plays a central role in autophagy, lysosomal biogenesis, and more recently in the immune response. To date, two isoforms of human TFE3 protein have been identified: the full-length TFE3 (TFE3-L: 575aa) and an alternatively spliced, N-terminal truncated, isoform (with alternative exon 3, TFE3-S: 470aa). However, the functional characterization of each isoform has not been described to date. Here, we provide evidence that both TFE3 isoforms have distinct expression patterns in different cellular models and under distinct cell stress conditions. We show that under normal growth conditions, the TFE3-S form is more abundant when compared to TFE3-L. In contrast, TFE3-L expression is increased in cells that are experiencing stress, such as starvation, mTOR inhibition, AMPK activation or depletion of FLCN. We show that TFE3-L accumulation is post-translationally controlled by proteasomal degradation. Moreover, we identify Skp2-containing SCF (SKP1-cullin1-F-box protein) E3 ubiquitin ligase as a potential ligase controlling TFE3-L stability. Interestingly, we demonstrate that protein levels of TFE3-L are associated with breast cancer disease aggressiveness. Based on these findings, we aim herein to further explore the mechanisms controlling TFE3-L protein stability and decipher the different functional roles played by each TFE3 isoform, which will provide new insights into their aberrant expression in human cancers.

4.2. INTRODUCTION

The human genome encodes over 2,000 different transcription factors (TFs). TFs are DNA-binding proteins that control chromatin structure and gene transcription by influencing the formation or activity of the transcriptional machinery. Many TFs are deregulated as a consequence of activating or inactivating mutations, where both mutational status or altered expression can promote tumorigenesis by sustaining oncogenic programs (Bradner et al., 2017; Garraway and Lander, 2013). In addition to cancer-associated mutations, RNA sequencing clearly showed that TFs display aberrant splicing patterns in cancer cells that result from deregulated RNA splicing. These splice variants influence the initiation, growth and progression to therapy-resistant tumors (Biamonti et al., 2019; David and Manley, 2010; Dong and Chen, 2020; Escobar-Hoyos et al., 2019; Sveen et al., 2016). Alternative splicing of transcription factors has critical roles in diverse biological processes including cell-fate determination, and its deregulation is associated with numerous diseases including cancer (Daguenet et al., 2015; Jangi and Sharp, 2014; Kalsotra and Cooper, 2011).

TFE3, a transcription factor belonging to the MiT/TFE family of transcription factors, has recently emerged as a global regulator of cell survival and metabolic reprogramming. TFE3 regulates the expression of target genes involved in cellular processes ranging from cell-specific differentiation to basic cellular energy homeostasis including: autophagy, lysosomal biogenesis, immune response, and lipid homeostasis (El-Houjeiri et al., 2019; Martina et al., 2014, 2016, Pastore et al., 2016, 2017; Perera et al., 2015). Indeed, TFE3 activation and nuclear accumulation has been shown to be tightly regulated by cellular nutrient and energy status, where in nutrient replete conditions, TFE3 is phosphorylated, predominantly by the mammalian target of rapamycin complex 1 (mTORC1) and remains inactive within the cytoplasm (Martina et al., 2014, Roczniak-

Ferguson et al., 2012,). Conversely, upon nutrient depletion, repressive phosphorylation events are lifted and TFE3 translocates to the nucleus where it induces the expression of genes belonging to the Coordinated Lysosomal Expression and Regulation (CLEAR) network (Raben and Puertollano, 2016). Other MiT/TFE family members include *MiTF*, *TFEB*, and *TFEC* (Hemesath et al., 1994) that share structural similarities, consisting of a basic helix-loop-helix (bHLH) leucine zipper (LZ) dimerization motif, a transactivation domain, and an identical DNA binding regions (Beckmann et al., 1990; Sato et al., 1997; Steingrímsson et al., 2004). All four MiT/TFE members are conserved in vertebrates (Bouché et al., 2016) and can form homo- or hetero-dimers through their HLH-LZ motif with other family members, but not with other related bHLH proteins (Hemesath et al., 1994; Pogenberg et al., 2012).

Beyond the individual levels of each MiTF/TFE family member, their relative expression, one to the other, may also be important. Indeed, their expression levels differ considerably between cell types (Rehli et al., 1999; Takemoto et al., 2002; Zhao et al., 1993), which suggests a model where the ratio of MiTF/TFE family member expression dictates specific dimerization patterns and, subsequently, the expression of target genes. While chromosomal translocations involving the TFE3 and TFEB genes have been implicated in subtypes of renal cell carcinomas, and TFE3 rearrangements were found in alveolar soft part sarcomas (Kauffman et al., 2014; Lazar et al., 2007; Perera et al., 2015), very little is known regarding how the expression levels or alternatively spliced forms of these transcription factors are coordinately regulated to impart their biological roles in different cellular contexts and human diseases.

Of all the MiTF/TFE family members, the *MiTF* gene has been shown to encode different isoforms that are under the control of distinct promoters (Hallsson et al., 2000; Udono et al., 2000). Currently, at least eight major MiTF isoforms have been identified that are differentially expressed

in a variety of tissues, including melanocytes, heart and mast cells (Amae et al., 1998; Fuse et al., 1999; Hodgkinson et al., 1993; Oboki et al., 2002; Takeda et al., 2002; Takemoto et al., 2002; Udono et al., 2000). These isoforms share the important functional domains of MiTF, including the transactivation domain, basic region, helix—loop—helix and leucine zipper, but differ in their N-termini. These N-termini may contribute to the cell type-specific properties of the various isoforms, for example by recruiting cofactors to the transcription apparatus. However, thus far, little is known about the tissue distribution and splice variants of the other MiTF/TFE family members, including TFE3, TFEB and TFEC.

To date, two isoforms of human TFE3 protein have been identified: the full length TFE3 (herein, TFE3-L) protein and an alternatively spliced, N-terminally truncated, variant (with alternative exon 3; herein, TFE3-S). However, the function of each isoform has not yet been fully described. In this study, we provide evidence that both TFE3 isoforms have different stabilities and gene activation potentials, and we explore the mechanisms controlling TFE3-L stability in cancer cells that may provide new insights for their aberrant expression in human cancers.

4.3. RESULTS

TFE3 exists in two different isoforms with differential expression patterns

We have previously shown that TFE3 is more active in the triple negative breast cancer (TNBC) as compared to the less aggressive luminal subtypes (El-Houjeiri et. al 2021, under revision). In these cells, the tumor suppressor FLCN-FNIP complex is disrupted and TFE3 activity was enhanced, as assessed by nuclear localization and downstream target gene expression. Interestingly, immunoblot analysis revealed the existence of two TFE isoforms with different molecular weights (\sim 72 and 89 kDa, respectively). Of particular interest was the observation that the upper band was present at higher levels in TNBC when compared to luminal subtypes (Figure 1A). To expand our observation to additional cancer types, we assessed the expression of TFE3 in several leukemia, pancreatic, ovarian, and renal cancer cell lines, and we observe differential expression of the two TFE3 osoforms (Figure 1B). Investigating this further, we found that TFE3 exists as two mRNA variants produced by alternative RNA splicing within exon 3. Transcript variant 1 encodes the full length TFE3 isoform (575 aa) and transcript variant 2 encodes the Nterminally truncated TFE3 isoform (470 aa) (Figure 1C) as a consequence of translation initiation at a downstream in-frame start codon. The resulting proteins possess distinct amino termini, but share transactivation, DNA binding and dimerization motifs. To date, these two isoforms have not been functionally characterized.

Interestingly, loss of FLCN induced the permanent expression of the upper TFE3 isoform in T47D, MCF7 and 293T cells (Figure 1D). This was of interest since our lab and others have shown that loss of FLCN induces the constitutive nuclear localization and activation of TFE3 (Betschinger et al., 2013; El-Houjeiri et al., 2019; Hong et al., 2010; Martina and Puertollano, 2013; Paquette et al., 2021; Petit et al., 2013; Wada et al., 2016). To validate that both isoforms

correspond to TFE3, we transiently knocked down TFE3 in MCF7 FLCN^{KO} cells using siRNA and confirm a reduction of both isoforms (Figure E, left panels). Additionally, using CRISPR/CAS9, we targeted the coding sequence for the TFE3-L isoform within exon 1 and specifically downregulated the full-length isoform. These results indicate that upper band corresponds to the TFE3-L isoform and lower band corresponds to TFE3-S isoform. Although other groups detected the expression of two TFE3 bands, we are the first to identify them as two distinct isoforms instead of post-translationally modified forms of TFE3, as previously proposed (Hong et al., 2010; Martina and Puertollano, 2013).

We next generated an antibody that recognizes a peptide present within the N-terminal region of TFE3-L that is missing in TFE3-S. To evaluate the specificity of this anti-TFE3-L antibody, we ectopically expressed Flag-tagged TFE3-L or TFE3-S in 293T cells. We next assessed isoform expression in whole cell lysates or Flag IPs by immunoblotting with our TFE3-L specific antibody or a commercially available anti-TFE3 antibody that recognizes the C-terminal region of TFE3 that is shared by both isoforms (Figure 1F). The anti-TFE3-L antibody specifically detected Flag-TFE3-L protein while the commercial anti-TFE3 recognized both Flag-TFE3-L and Flag-TFE3-S. Importantly, in FLCN^{KO} 293T cells that constitutively express the long TFE3 isoform, the anti-TFE3-L antibody exclusively detects the higher molecular weight isoform, while the commercial anti-TFE3 antibody detects both TFE3 isoforms (Figure 1F). As expected, the commercial anti-TFE3 antibody recognizes TFE3-S in 293T cells.

Collectively, these results validate the existence of two TFE3 isoforms: TFE3-L and TFE3-S, where the latter is constitutively expressed and the former is induced in certain cellular contexts.

TFE3 Long isoform expression is post-translationally regulated

We next asked how TFE3-L expression is controlled in cells. For this, we designed specific primers for each variant, and assessed their mRNA levels by qPCR in MCF7 empty vector (EV) cells that predominantly express the TFE3-S form and MCF7 FLCN^{KO} cells that constitutively express both isoforms. We show that there are no significant differences in the mRNA levels of *TFE3-L* and *TFE3-S* in both cells, indicating a post-translational regulation of the long isoform (Figure 2A). In light of this result, we hypothesized that TFE3-L might be constitutively translated under normal cellular conditions but targeted for rapid degradation. To test this, we treated MCF7 and 293T cells with a 26S proteosome inhibitor (MG-132) for 5 hrs to impair proteasomal degradation and observed an increase in TFE3-L isoform accumulation in both cell lines (Figure 2B). To determine the protein stability of each isoform, we treated the cells with cycloheximide that inhibits protein synthesis and then chased protein expression for over 8 hours in MCF7 EV and FLCN^{KO} cells. The short isoform is relatively stable in both cell lines; however, TFE3-L expression is stable in FLCN^{KO} cells, but possessed a half-life of approximately 3.5 hrs in EV cells (Figure 2C and D).

We next assessed the stability of both isoforms in a TNBC cell line (MDA-MD-436) in which FLCN levels are low, both TFE3 isoforms are expressed and TFE3 is mostly nuclear and active (Figure 1A; El-Houjeiri et. al 2021, under revision). We observed that TFE3-L is more stable in MDA-MB-436 cells when compared to MCF7 cells (11.4 hrs versus 3.5 hrs, respectively), while the stability of TFE3-S is similar. Increased TFE3-L stability may account for the higher expression levels observed in MDA-MB-436 cells and FLCN^{KO} MCF7 cells (Figure 2E and F). Together, these results indicate that TFE3-L isoform expression is controlled post-translationally through proteasomal degradation.

Expression of TFE3-L is dependent on cellular nutrient status

Thus far, our data suggests that TFE3-L levels are stabilized in FLCNKO cells. We next sought to investigate mechanisms regulating TFE3-L expression under additional conditions that induce TFE3 nuclear translocation and transcriptional activation. TFE3 activity is mainly controlled by its phosphorylation status at Ser 321 by mTORC1, which enforces TFE3 cytoplasmic localization under nutrient rich condition (Martina et al., 2014; Roczniak-Ferguson et al., 2012). Accordingly, we assessed whether the nutritional status, dictated by mTORC1 activity, modulates the expression of the TFE3 isoforms. Amino acid or glucose starvation, both of which inhibit mTORC1 activity as indicated by reduced phosphorylation of its immediate downstream target S6K or the S6K target S6, induce the accumulation of TFE3-L as early as 15 and 45 min, respectively (Figure 3 A and B). This observation was confirmed in both MCF7 and 293T cells (Figure S1A and B). Although nutrient deprivation induces TFE3-L expression, only amino acid starvation revealed a clear correlation between mTORC1 inhibition and upregulation of TFE3-L. In agreement with the amino acid starvation results, direct inhibition of mTORC1 by Torin1 induces the accumulation of TFE3-L as early as 15 min (Figure 3C). Previous studies suggest that, following glucose withdrawal, AMPK activation on lysosomal membranes regulates the inactivation of lysosomal-associated mTORC1 (Zhang et al., 2014). We observe early AMPK activation, as determined by its phosphorylation at T172 or phosphorylation of its target ACC upon glucose starvation, which could explain the early TFE3-L accumulation detected under these conditions (Figure S1C). Interestingly, acute activation of AMPK using GSK-621 enhances the accumulation of TFE3-L isoform (Figure S1D). However, whether this accumulation is due to mTORC1 inactivation is still to be investigated. A direct effect of AMPK on TFE3-L expression cannot be ruled out since we have recently reported additional regulation of TFE3 by AMPK-mediated phosphorylation (Paquette et al., 2021).

To assess if TFE3-L accumulation is dictated by cellular nutrient status in an mTORC1-dependent manner, we cultured MCF7 cells in amino acid- or glucose-free media for 6 h and detected an increase in TFE3-L isoform with a concomitant decrease in p-S6 levels, indicating inhibition of mTORC1 (Figure 3D and E). Interestingly, amino acid or glucose refeeding for 4 h following starvation caused a reduction in TFE3-L expression ,which was prevented by pretreating the cells for 30 min with Torin1 before refeeding (Figure 3D and E). This data suggests that mTORC1 pathway (through direct or indirect mechanisms) regulates TFE3-L levels in cells.

Expression of TFE3-L is regulated through its binding to active Rag GTPases

It has been previously reported that the interaction between TFE3 and mTORC1 occurs at the lysosome when both mTORC1 and TFE3 are bound to the active Rag GTPases. Notably, TFE3 contains Rag binding sites that facilitate binding to active RagC/D (GDP-bound) at the lysosome (Martina and Puertollano, 2013). Under nutrient rich conditions, the RagC/D GTPases are in a GDP-bound/active state and can bind TFE3 at the lysosomal surface, which places it in close proximity with activated mTORC1, facilitating TFE3 phosphorylation and 14-3-3-mediated cytoplasmic retention (Martina and Puertollano, 2013; Napolitano et al., 2020). Interestingly, this Rag binding site is shared between the two TFE3 isoforms. To assess the role of Rag GTPases in the differential expression of the TFE3 isoforms, we transiently co-overexpressed an active form of RagB (permanently in GTP-bound form) and RagD (permanently in GDP-bound form). A decrease TFE3-L expression was observed in both wild-type and FLCN^{KO} 293T cells, which coincided with an increase in mTORC1 activity as shown by increased phosphorylation of S6 and

an upward TFE3-S mobility shift (Figure 4A). Conversely, transient overexpression of the inactive Rag GTPases slightly increased TFE3-L isoform expression in wild-type cells (Figure 4B).

FLCN is a GAP for RagC/D, converting RagC/D from the inactive (GTP)-bound to the active (GDP)-bound form, thereby facilitating the recruitment of TFE3 to the surface of the lysosome where it can be phosphorylated by mTORC1 (Napolitano et al., 2020). We have shown that loss of FLCN induces the expression of TFE3-L (Figures 1, 2, and 4) in a manner similar to that observed in cells transiently overexpressing inactive Rag GTPases. Interestingly, we show that overexpression of wild-type FLCN in FLCN-deficient cells decreases TFE3-L expression and induces a mobility shift of TFE3-S, whereas overexpression of a FLCN-R164A mutant lacking its GAP activity has no effect on TFE3-L isoform levels or TFE3-S mobility (Figure 4B). To check whether the expression of TFE3 isoforms is modulated by their Rag binding ability, we mutated the Rag binding sites in TFE3-L and -S isoforms (Figure 4C). We then treated transfected 293T cells with cycloheximide and chased HA-tagged TFE3 isoform protein levels for over 8 hours (Figure 4D). Mutation of the Rag binding site stabilized the expression of TFE3-L isoform but had no effect on TFE3-S isoform, which remained stable in both cases (Figure 4D and E).

Collectively, these results indicate that the binding of TFE3-L to active RagC/D on the lysosome induces its degradation, while any condition that prevents its interaction with RagC/D stabilizes TFE3-L expression.

Identification of Skp2 as a potential E3 ligase regulating TFE3 Long isoform stability

We have shown that TFE3-L expression is post-translationally controlled by proteasomal degradation, and this regulatory mechanism involves TFE3-L binding to active Rag GTPases and, plausibly, its phosphorylation by mTORC1. To further characterize this mechanism, we first

attempted to identify the E3 ubiquitin ligase responsible for TFE3-L isoform ubiquitination and degradation. Given that TFE3-L is stabilized in FLCN^{KO} cells, we utilized our previously published RNA-sequencing data (GEO: GSE163791) to check for potential E3 ligases that are uniquely downregulated in FLCN^{KO} tumors when compared to their wild-type counterparts. Interestingly, from the F-box proteins assessed, we found *Skp2* mRNA levels to be significantly downregulated in MCF7 FLCN^{KO} cells (Figure 5A). Notably, Skp2 has been previously shown to control the activity of the TFE3 family member; TFEB, through degradation of its co-activator CARM1 (Shin et al., 2016). Interestingly, in line with our RNA seq data (Figure 5A), we show that in MCF7 FLCN-deficient cells, Skp2 levels are lower compared to wild-type cells (Figure 5B) and transient downregulation of Skp2 using two different shRNAs resulted in higher expression of the TFE3-L isoform in wild-type MCF7 cells (Figure 5B), implying a potential role of Skp2 in mediating TFE3-L stability.

F-box proteins, such as Skp2, are subunits within the SCF E3 ubiquitin ligase complex that are responsible for the recognition of specific "degron" motifs within their substrates, leading to target ubiquitination (Asmamaw et al., 2020). Thus, we next investigated whether Skp2 specifically interacted with TFE3-L. We transfected 293T cells with constructs expressing HA-tagged TFE3-L, -TFE3-S or C-terminal truncated TFE3-L products (Figure 5C) in conjunction with Flag-tagged Skp2. Immunoprecipitation assays with either anti-HA or anti-Flag antibodies revealed that Skp2 binds specifically to TFE3-L but not TFE3-S via the N-terminal region (1-145aa) of TFE3-L (Figure 5D and E). It is important to note that the 145 amino acid region contains the Rag binding site identified in both TFE3-L and TFE3-S isoforms. We included this site within the N-terminal TFE3-L product because binding of TFE3 to active Rag GTPase contributed to TFE3-L degradation (Figure 4). However, we observed that Skp2 efficiently binds to a smaller

105aa N-terminal region of TFE3-L (Figure 5F). These results suggest that the interaction of TFE3-L with the Rag GTPases enhances the binding of Skp2 to the N-terminal region of TFE3-L, potentially through mTORC1-mediated phosphorylation of the TFE3-L degron motif. It has been extensively reported that phosphorylation or glycosylation of degron motifs promotes the interaction of F-box proteins with their substrates (Asmamaw et al., 2020). A well-characterized example is Skp2-mediated degradation of the Cyclin-dependent Kinase (CDK) inhibitor p27kip1, whose phosphorylation at T187 by cyclin E-cdk2 is required for Skp2 binding (Carrano et al., 1999). Interestingly, we determined that the interaction of TFE3-L to Skp2 decreases in FLCN-depleted 293T cells compared to control 293T cells, which correlates with TFE3-L stabilization observed in cells lacking FLCN(Figure 5G).

To further investigate the potential role of Skp2 as the ubiquitin ligase targeting TFE3-L, we performed an *in vivo* ubiquitination assay. 293T cells were transfected with constructs expressing HA-tagged ubiquitin, either HA-GST-tagged TFE3-L or TFE3-S, and either Flagtagged wild-type Skp2 or a dominant-negative Skp2 ΔF mutant (Figure 5H). TFE3-L, but not TFE3-S, undergoes ubiquitination in Skp2-overexpressing 293T cells, as evident by a ubiquitin smear. Conversely, expression of the dominant-negative Skp2ΔF mutant (lacking the F-box domains and hence able to bind the substrate but not to form a Skp2-SCF-complex), attenuated the ubiquitination smear in TFE3-L isoform (Figure 5H).

These results suggest that Skp2 functions as a E3 ubiquitin ligase, which is responsible for regulating the stability of TFE3-L. As part of Skp2-SCF E3 ubiquitin ligase complex, Skp2 binds to the N-terminal region that is unique to the TFE3-L isoform to promote its ubiquitination and subsequent degradation. Further experiments with other F-box containing ubiquitin ligases will be

important to determine the specificity of Skp2 ligase in mediating TFE3-L ubiquitination and degradation.

mTORC1 and AMPK signaling pathways regulate Skp2-mediated TFE3-L degradation.

Nutritional deprivation, FLCN knockout or pharmacological compounds that inhibit mTORC1 and/or activate AMPK signalling pathways lead to increased expression of TFE3-L (Figure 1, 3, and S1). Skp2 acts as the potential substrate recognition subunit of the SCF E3 ubiquitin ligase complex responsible for controlling TFE3-L stability. Interestingly, Skp2 expression is reported to be oppositely regulated by both mTORC1 and AMPK pathways. AMPK-mediated phosphorylation of the transcriptional repressor FOXO3a leads to reduced expression of Skp2 upon glucose starvation (Shin et al., 2016). By contrast, phosphorylation of Skp2 at Ser64 by mTORC1 promotes Skp2 accumulation by preventing its degradation by the proteasome (Geng et al., 2017). Thus, we investigated whether these signaling pathways control TFE3-L stability through the regulation of Skp2 levels and/or activity.

We first assessed the levels of Skp2 in 293T CRISPR/CAS9 AMPK alpha1/alpha2 double knockout (AMPK^{DKO}) cells. We verified that Skp2 protein and mRNA levels are increased in AMPK^{DKO} compared to control 293T cells by immunoblot assays and qPCR, respectively (Figure 6A and B). This prompted us to assess changes in Skp2 protein levels after short- (2 h) or long-term (24h) treatment with Torin (mTORC1 inhibitor) or GSK-621 (AMPK activator) and evaluate the effect on TFE3-L stability. Interestingly, no changes in Skp2 levels were detected after 2h of treatment, although TFE3-L levels increased (Figure 6C). However, long-term treatments resulted in the reduction in Skp2 levels, which was accompanied by further increases in TFE3-L protein levels (Figure 6C). Conversely, increased expression of Skp2 in AMPK^{DKO} MCF7 cells results in

delayed accumulation of TFE3-L compared to control cells following amino acid starvation (Figure 6D). These results suggest that long-term inhibition of mTORC1 and/or activation of AMPK contributes to TFE3-L accumulation by reducing Skp2 levels. However, this mechanism does not account for the changes in TFE3-L levels observed following short-term treatments.

Phosphorylation of degrons is a frequent modification that promotes substrate recruitment by F-box proteins (Skaar et al., 2013). Since binding to active Rag GTPase and active mTORC1 induced TFE3-L degradation, we speculated that mTORC1-mediated phosphorylation of TFE3-L may contribute to its recognition by Skp2. To assess this, 293T cells expressing HA-tagged TFE3-L or an N-terminal portion of TFE3-L (TFE3-L (1-145)) plus Flag-tagged Skp2 were treated with DMSO or Torin for 2h. Next, we evaluated the binding of Skp2 to TFE3-L by coimmunoprecipitation assays and observed that their interaction is reduced in Torin-treated cells compared to controls (Figure 6E). These results suggest that mTORC1-mediated phosphorylation of TFE3-L promotes TFE3-L recruitment by Skp2, which could explain the accumulation of TFE3-L observed at early time points following torin treatment. This prompted us to analyze the N-terminal region of TFE3-L for potential mTOR phosphorylation sites. Using Phosphonet Kinase Predictor tool (www.phosphonet.ca), we identified Ser93 and Ser95 as putative mTOR phosphorylation sites (Figure S2A). These two sites were conserved in mammals. To investigate the importance of these serine residues for the interaction between Skp2 and TFE3-L, we first generated TFE3-L mutants that substituted S93, 95, 96, and 96 for alanine residues (S4A). Similar substitutions were done in other evolutionary well-conserved serine residues within the N-terminal region of TFE3-L (S34A, S39A, and S47A). HA-GST-tagged wild-type TFE3-L or phosphomutants were expressed in 293T cells and isolated by GST pulldown (Figure S2B). Interestingly, reduced TFE3-L S4A binding to Skp2 was observed when compared to wild-type TFE3-L or the

other phospho-mutants. We further characterized the impact of S93 and S95 phosphorylation on TFE3-L binding to Skp2. To accomplish this, phosphorylation-defective (S93A or S95A) or phospho-mimetic (S93D, S93E, S95D, or S95E) TFE3-L mutants were generated. Using GST pulldown assays, we showed that TFE3-L phospho-mimetic mutants showed stronger binding to Skp2 when compared to wild-type or phosphorylation-defective mutants (Figure 6F). These results support the notion that phosphorylation at S93 and/or S95 serve as post-translational modifications that promote recognition of TFE3-L by Skp2.

Functional characterization of TFE3-L

To assess the physiological significance of each isoform, we specifically knocked out TFE3-L in MCF7 cells and confirmed efficient reduction of TFE3-L levels (Figure 7A). We then assessed expression of TFE-3 targets that encode components of the lysosomal biogenesis pathway. Interestingly, MCF7 TFE3-L^{KO} cells exhibited a higher level of gene expression compared to WT cells following amino acid withdrawal (Figure 7B). We did not detect any differential effects on proliferation between MCF7 TFE3-L^{KO} or MCF7 TFE3-L^{WT} cells under normal culture conditions (Figure 7C). However, we speculate that further characterization of the proliferation status under different energy stressed conditions would be more informative, which represent the conditions under which TFE3-L levels are the highest. The functional difference between both isoforms with respect to modulating tumor growth is currently under investigation in several breast cancer models.

4.4. DISCUSSION

The full-length human TFE3 protein consists of 575 amino acids (NCBI protein accession number: NP_006512.2 and UNIPROT protein accession number: P19532-1). It is 96% identical to the mouse TFE3 protein (NCBI protein accession number: NP_766060.2 and UNIPROT protein accession number: Q64092-1) and shares the conserved bHLH-LZ and transactivation domains found in the other MiT-TFE family members (Kauffman et al., 2014). In the NCBI database, an additional TFE3 isoform has been identified, termed transcription factor E3 isoform 2 (NP_001269071.1), which encodes a 470-residue protein. Even though TFE3 is usually referred to as the full-length (575 aa) protein in literature, it is typically not expressed at basal conditions. To date, no distinctions are made between the two isoforms, and they haven't been functionally characterized.

Here we provide evidence that the protein levels of both isoforms are differentially regulated in a variety of human cancer cell lines and under diverse cellular conditions. The short isoform, which we referred to as TFE3-S, is more ubiquitously expressed among all cancer types and under all conditions, including nutrient replete and nutrient-depleted conditions. However, we show that the expression of full-length isoform, which we refer to as TFE3-L, is elevated in specific cancer cell lines and under certain cellular stressed conditions, such as nutrient starvation. Importantly, we report that TFE3-L accumulates to higher levels in the more aggressive basal-like breast cancer subtypes when compared to the luminal subtypes, which predominantly expressed TFE3-S.

We found that TFE3-L levels are post-translationally regulated by the ubiquitinproteasome system. We identify the F-box protein Skp2 as the recognition subunit of SFC complex that specifically interacts with TFE3-L to promote its ubiquitination and subsequent degradation. Mechanistically, we propose that, under genetic or nutritional conditions that lead to activation of lysosomal Rag GTPases (RagA/B-GTP and RagC/D-GDP), the binding of TFE3-L to RagC/D facilitates mTORC1-mediated phosphorylation of TFE3-L in the N-terminal region, which enhances its recruitment of Skp2. Alternatively, active mTORC1 may recruit Skp2 to active Rags and facilitate its interaction with TFE3-L. Supporting this model, the association of Skp2 with active Rag GTPases has been described (Jin et al., 2015). On the other hand, genetic or nutritional conditions that lead to the inactivation of the Rag GTPases or inhibition of mTORC1 might affect the binding of Skp2 to TFE3-L and, therefore, facilitate its accumulation, nuclear translocation, and activation. Interestingly, the expression of TFEB and MiTF is also regulated by the ubiquitinproteasome system. For TFEB, the STUB1 E3 ubiquitin ligase is responsible for the degradation of inactive TFEB phosphorylated at S142 and/or S211, which reduces its ability to dimerize with the non-phosphorylated form under starvation conditions. Thus, this active TFEB translocates to the nucleus and activated its transcriptional program (Sha et al., 2017). Similarly, for MiTF, c-kit induces its MAPK- and RSK1-dependent phosphorylation at S73 and S409, respectively, which activates its transcriptional activity and induces its degradation by the proteasome. This activation/degradation mechanism may prevent long-term MiTF activity (Wu et al., 2000).

Other well-characterized examples of genes that encode multiple TF isoforms with a regulatory role are p63 and p73, two members of the p53 gene family. Both genes produce splice variants as well as N-terminally truncated forms that originate from internal promoters (Pozniak et al., 2000; Yang et al., 1999). These studies report a dominant-negative role of these isoforms by forming heteromeric complexes with p63, p73, and p53 (Fillippovich et al., 2001; Nakagawa et al., 2002; Yang et al., 1998). The N-truncated isoforms were found to be essential for normal growth and development and provide a regulatory system for modulating cell survival and cell

death (Pozniak et al., 2000; Yang et al., 1999). Based on our finding, we hypothesize that the TFE3-S isoform may be vital for normal cell function, which might explain its ubiquitous expression. The TFE3-L isoform seems to be more important under stressful conditions. One could speculate that TFE3-L forms heterodimers with TFE3-S and, thereby, modulates the ability of the complex to regulate downstream target gene expression, either by preventing DNA binding, changing the DNA-binding specificity, or altering the binding capacities of transcriptional cofactors. Alternatively, increased TFE3-L levels may contribute to enhanced TFE3 transcriptional activity under stress conditions. We cannot rule out the possibility that each TFE3 isoform controls a different set of target genes, and their differential expression allows cancer cells to adapt to new environmental or nutritional conditions.

In this study, we assessed the differential expression of TFE3 isoforms in various cancer models. However, since TFE3 is a major regulator of cellular development and differentiation (Steingrimsson et al., 2002; Steingrimsson et al., 2004), the identification of isoform-specific activities is likely to provide key insights pertinent to developmental decisions. Further analysis of the mechanistic basis of this activity will thus be of importance.

4.5. METHODS

Cell Lines and Cell Culture

MCF7, T47D, MDA-MB-436, MDA-MB-157, 293T, K562, MOLT-4, RPMI-8226, SR, Capan-1, Capan-2, MIAPACA-2, BxPC-3, IGR-OV1, OVCAR-3, OVCAR-4, OVCAR-5, 786-0, A498, ACHN and CAKI-1 cells were obtained from the American Type Culture Collection (ATCC). Cell lines were maintained in Dulbecco's modified Eagle's medium (DMEM) or RPMI (Wisent, cat# 319-005CL) supplemented with 10% fetal bovine serum (FBS) (Wisent, cat# 080-150), 100 U/ml

penicillin+100 μg/ml streptomycin (Wisent, cat# 450-201-EL), and 50 μg/mL gentamycin (Wisent, cat# 450-135) in 5% CO₂ at 37°C. For gene-silencing experiments, breast cancer cells were seeded in 6cm dishes and transfected with 10nM siRNA duplexes using Lipofectamine RNAiMax (Invitrogen, cat# 13778030) according to manufacturer's instructions. The following siRNA SMARTpools was used: human TFE3 (7030) (Dharmacon, L-00933-00-0005). Stable knockdown of Skp2 in MCF7 breast cancer cells was achieved using the Mission lentivirus shRNA empty vector (shEV), shSkp2 (Sigma-Aldrich, TRCN00000007530 and TRCN00000007531).

Generation of knockout lines

CRISPR-Cas9 guide RNA targeting sequences for human FLCN, AMPK alpha1, AMPK alpha2, TFE3 Long isoform (targeting exon 1; sequence encoding N-terminal region of TFE3-L) and TFE3 (targeting exon 3 that is shared between both isoforms), were designed using the CRISPR Design Tool available at http://chopchop.cbu.uib.no/, Zhang Lab). MCF7 FLCN^{KO} cells were described in (El-Houjeiri et. al, JCI, under revision, 2021). 293T FLCN^{KO} and AMPK^{DKO} cells were described in (Paquette et al., 2021). The two guide RNA sequences targeting TFE3-L were: ACAGCACGACACACGGCTCGA and AACAGCACGAACACGGCTCG. The guide RNA sequences targeting both TFE3 isoforms were: CCTGTTCCCGACGCTCACGCCTC and CCTGCGCCTGGGCCCGCATTAGC. Targeting sequences were cloned into the lentiCRISPR plasmid (http://www.addgene.org/49535/) that has been previously described (Shalem et al., 2014). Lentivirus was produced for the TFE3-L and TFE3-L/S targeting sequences as well as an empty lentiCRISPR vector for control lines. Lentiviral transfer plasmids were co-transfected, along with VSV-G envelope (https://www.addgene.org/12259/) and packaging plasmids (https://www.addgene.org/12260/), into HEK293T cells using Lipofectamine LTX (Invitrogen,

cat# 15338–500). Media was changed after 24h and virus-containing media was collected and centrifuged 72h post-transfection. We performed single cell cloning for each guide RNA, and once knockout cells were verified by immunoblotting, a pool of 4 clones was generated in an effort to eliminate clonal effects.

Reagents, Chemicals, and Antibodies

Antibodies used for immunoblotting include: β-Actin (SC-47778; Santa Cruz Biotechnology), AMPKα (2532; Cell Signaling Technology), human FLCN (3697; Cell Signaling Technology), p-AMPKα (Thr172) (2531; Cell Signaling Technology), ACC (3676; Cell Signaling Technology), p-ACC (S79) (3661; Cell Signaling Technology), p70S6K (2708; Cell Signaling Technology), p-P0S6K (9205; Cell Signaling Technology), S6 (2217; Cell Signaling Technology), p-S6 (4858; Cell Signaling Technology), Skp2 (4358; Cell Signaling Technology), Flag M2 (F1804; Sigma-Aldrich), HA.11 (MMS-101R; Covance), FNIP1 (ab134969; abcam), FNIP2 (HPA042779; Sigma-Aldrich) and TFE3 (14779S; Cell Signaling Technology and HPA023881; Sigma-Aldrich). The antibody against the N-terminal region (EERRPADSAQLLSLNSL) of TFE3-L was generated by Yenzym Antibodies, LLC. MG-132 (474790; Sigma-Aldrich) was used at a final concentration of 5 mg/ml. Cycloheximide (239763; Sigma-Aldrich) was used at a final concentration of 100 ugml. Torin (4247; Tocris Bioscience) was used at a final concentration of 1 uM. GSK-621 (S7898; Selleckchem) was used at a final concentration of 30uM.

Quantitative Real-Time RT-PCR in Mammalian Cells

Cells were seeded in triplicate in 6-well plates at 5×10^5 cells per well in DMEM medium supplemented with 10% FBS. After incubation for 24h at 37°C, 5% CO2, cells were collected, and

total RNA was isolated using a Total RNA Mini Kit (Geneaid) according to the manufacturer's instructions. For quantitative real-time PCR analysis, 1 µg of total RNA was reverse-transcribed using the SuperScript III kit (Invitrogen). SYBR Green reactions using the SYBR Green qPCR supermix (Invitrogen) and specific primers (available upon request) were performed using an AriaMAX Real-time PCR system (Agilent Technologies). Relative expression of mRNAs was determined after normalization against the housekeeping gene *RPLP0* or *B2M*.

Protein Extraction and Immunoblotting

For AMPK immunoblotting, cells were washed twice with cold PBS, lysed in AMPK lysis buffer (10 mM Tris-HCl (pH 8.0), 0.5 mM CHAPS, 1.5 mM MgCl2, 1 mM EGTA, 10% glycerol, 5 mM NaF, 0.1 mM Na3VO4, 1 mM benzamidine, 5 mM NaPPi), supplemented with complete protease inhibitor (Roche) and DTT (1 mM), and cell lysates were cleared by centrifugation at 13000 x g. For all other immunoblotting, cells were washed twice with cold PBS and lysed directly in RIPA light buffer (50 mM Tris-HCl (pH 8.8), 150 mM NaCl, 1% NP40, 0.1% SDS, 0.1% Triton x-100, 5mM EDTA). Proteins were separated on SDS-PAGE gels and subjected to immunoblotting using the antibodies listed above. For immunoprecipitations (IPs), cells were lysed in: 50 mM Tris-HCl (pH 7.5), 150 mM NaCl, 1% Sodium deoxycholate, 1% Triton X-100, 2mM EDTA, 5 mM NaPPi, 50 mM NaF, 0.1 mM Na₂VO₄, Protease inhibitors (11697498001; Sigma-Aldrich). For perform IPs, cell lysates were incubated with 10 ml of anti-HA magnetic beads (88836; Sigma-Aldrich), 10 ul of anti-Flag M2 magnetic beads (M8823; Sigma-Aldrich), or 25 ul of GST Sepharose 4B (GE17-0756-01; Sigma-Aldrich) overnight at 4°C. Beads were washed five times with 1 ml of lysis buffer and complexes were separated on SDS-PAGE gels and revealed by western blot using the antibodies listed above.

Ubiquitination assay in live cells

Cells were transfected with HA-tagged Ubiquitin, HA-GST-tagged TFE3-L or TFE3-S, and Flagtagged Flag-Skp2 or a dominant-negative Skp2ΔF mutant. After incubation for 36 h, cells were treated with vehicle (DMSO) or MG-132 (5ml/ml) for 4 h, lysed with lysis buffer described above, and lysates were incubated with 25 ul of GST Sepharose 4B overnight at 4°C. GST beads were washed five times with 1 ml of lysis buffer and subjected to immunoblot analysis.

IncuCyte Cell Proliferation Assay

Cells were seeded at 1×10^4 cells per well in a 6-well plate, which were then incubated at 37° C with 5% CO₂ and monitored on the IncuCyte[®] Live Cell Analysis System (Sartorius, USA). After incubation for the indicated times, live-cell images were obtained using a $10\times$ objective lens (four images per well) within the instrument, and cell density was analyzed using the IncuCyte software.

Quantification and Statistical Analysis

Data are expressed as mean \pm SEM. Statistical analyses for all data were performed using Student's t test for comparisons between 2 groups, one-way ANOVA for comparisons between 3 or more groups, using GraphPad Prism 7 software. The data is assumed normal as tested by the Shapiro and Wilk normality test. Statistical significance is indicated in figures (*p < 0.05, **p < 0.01, ***p < 0.001, ****p < 0.0001). *In vitro* studies were biologically repeated at least three times in triplicates.

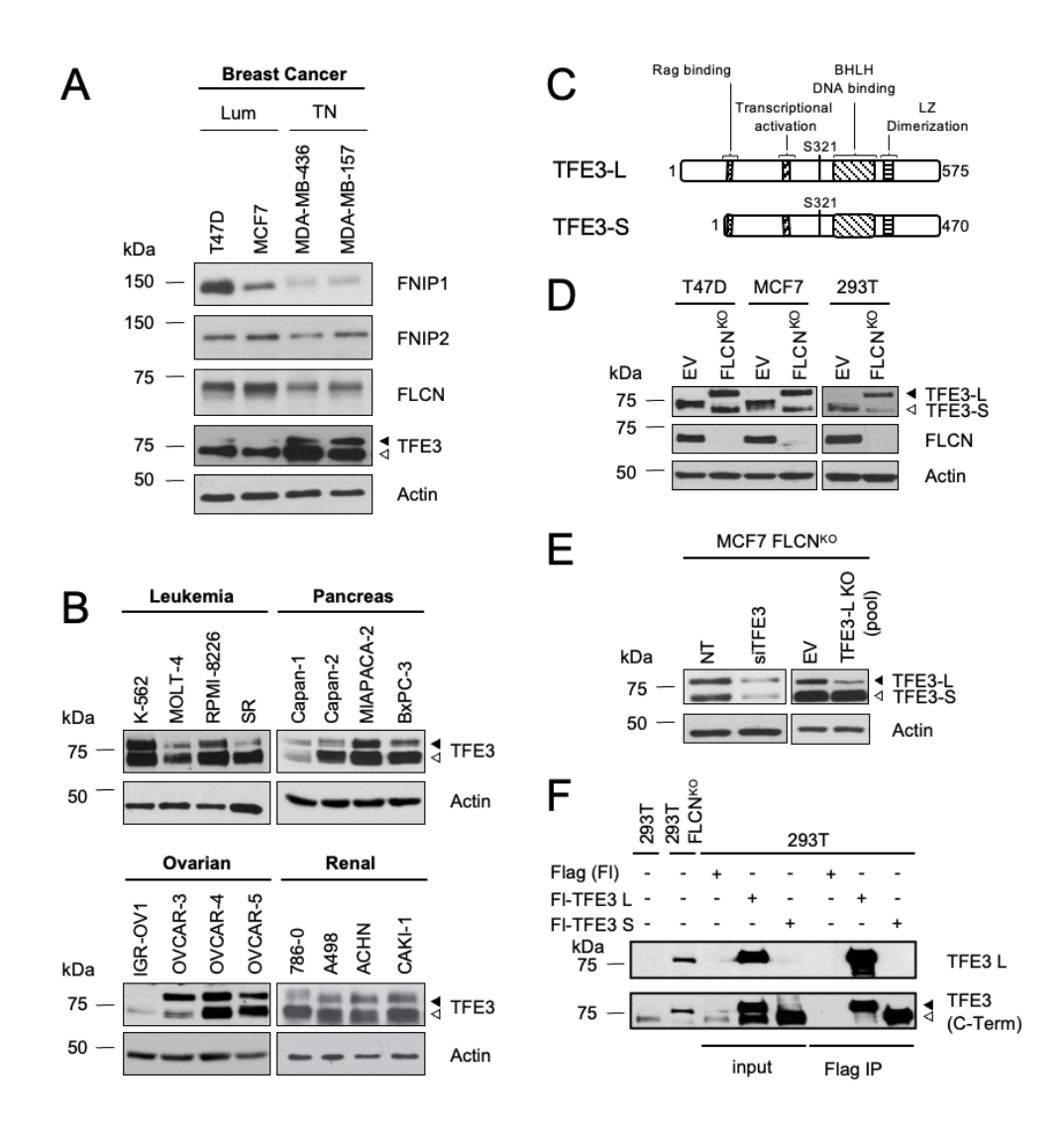
4.6. ACKNOWLEDGEMENTS

We thank Jose Teodoro, Isabelle Gamache, and Mohamed Moustafa-Kamal for kindly providing reagents used in this study. L.E-H. was supported by the Doctoral Training Scholarship from the Fonds de Recherche du Québec – Santé. A.P acknowledges that funding for this work was supported by grants from CIHR (PJT-165829) and the Cancer Research Society (CRS) (79664). P.M.S and A.P acknowledge funding from a Terry Fox New Frontiers Program Project Grant (TFRI-251427). P.M.S acknowledges funding from a CIHR grant (PJT-247494). P.M.S. is a McGill University William Dawson Scholar.

4.7. AUTHORS' CONTRIBUTIONS

L.E.-H., R.C., P.M.S., and A.P. conceived and designed the experiments. L.E.-H., R.C., H.J., M.P., M.B., performed, collected, and assembled the experiments. L.E.-H., R.C., P.M.S., and A.P., wrote the manuscript. L.E.-H., R.C., P.M.S., and A.P revised the manuscript critically for important intellectual content.

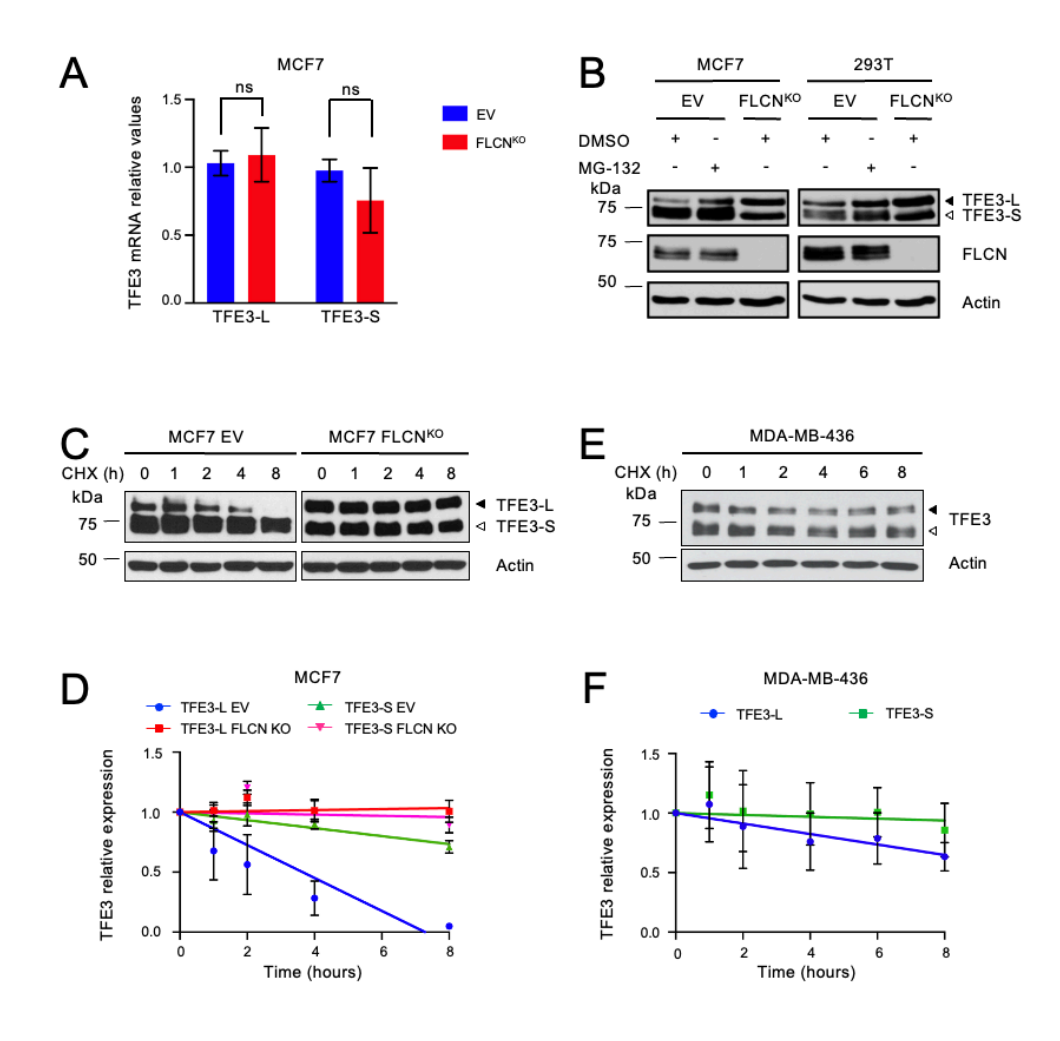
4.8. FIGURES AND FIGURE LEGENDS



²⁶Figure 1. TFE3 exists as two different isoforms with distinct expression patterns

(A) Immunoblot analysis indicating expression levels of FNIP1, FNIP2, FLCN and TFE3 in breast cancer cell lines representing luminal (T47D, MCF7) and TNBC (MDA-MB-436 and MDA-MB-157) cells. Actin was used as a loading control. (B) Immunoblot analysis indicating expression levels of two TFE3 forms with different migration patterns in several cancer cell lines representing

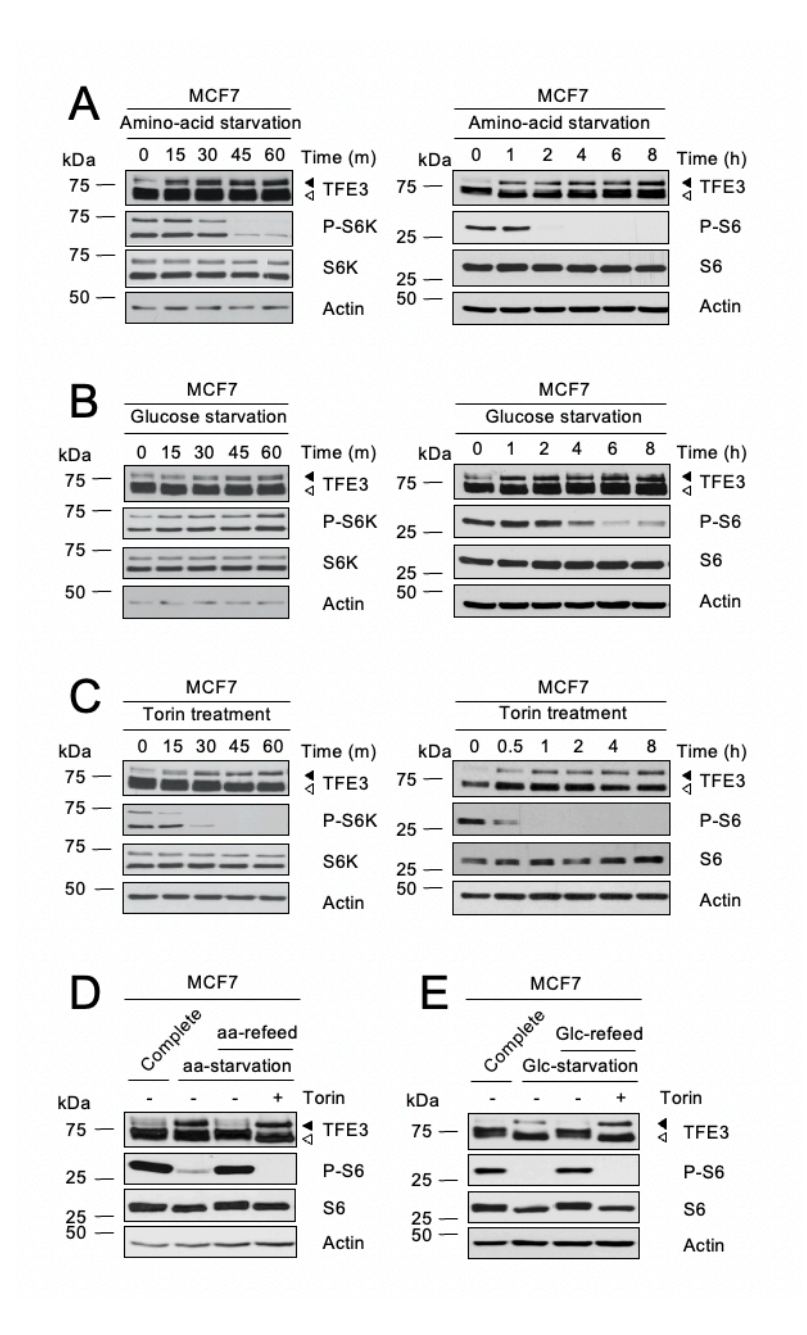
leukemia (K-562, MOLT-4, RPMI-8226, SR), pancreas (Capan-1, Capan-2, MIAPACA-2, BxPC), ovarian (IGR-OV1, OVCAR-3, OVICAR-4, OVICAR-5), and renal (786-0, A498, ACHN, CAKI-1). Actin was used as a loading control. (C) Schematic representation of the two TFE3 isoforms generated by alternative splicing in human cells, indicating the important functional domains. (D) Immunoblot analysis indicating expression levels of the two different TFE3 isoforms in empty vector (EV) control and CRISPR/CAS9-mediated FLCN knock out (FLCN^{KO}) T47D, MCF7 and 293T cells. Actin was used as a loading control. (E) Immunoblot analysis indicating expression levels of the two different TFE3 isoforms in MCF7 FLCN^{KO} cells transfected with non-targeting (NT) siRNA control or siRNA targeting TFE3 or CRISPR/CAS9-mediated TFE3-L knock out (TFE3-L^{KO}). Actin was used as a loading control. (F) Immunoblot analysis indicating expression levels of the two different TFE3 isoforms in FLCN KO or EV 293T cells, or 293T cells transfected with Flag-EV (Flag), Flag-TFE3-L or Flag-TFE3-S) constructs, as indicated. Anti-TFE3-L and commercial anti-TFE3 antibodies (TFE3 (C-Term)) produced against common C-terminal region of TFE3 were assessed.



²⁷Figure 2. TFE3-L expression is post-translationally regulated

(A) Relative *TFE3-L* and *TFE3-S mRNA* levels measured by RT-qPCR in empty vector (EV) and FLCN knock out (FLCN^{KO}) MCF7 cells. Data represent the average of three independent experiments, each performed in triplicate ± SEM. Significance was determined using Student's t-test (ns=non-significant). (B) Immunoblot analysis indicating expression levels of the two different TFE3 isoforms in EV control and FLCN^{KO} MCF7 and 293T cells treated with or without the proteasomal inhibitor MG-132 for 5 hrs. Actin was used as a loading control. (C) Immunoblot analysis indicating expression levels of the two different TFE3 isoforms in EV control and FLCN^{KO} MCF7 cells treated with cycloheximide and chased for 8 hours. Actin was used as a

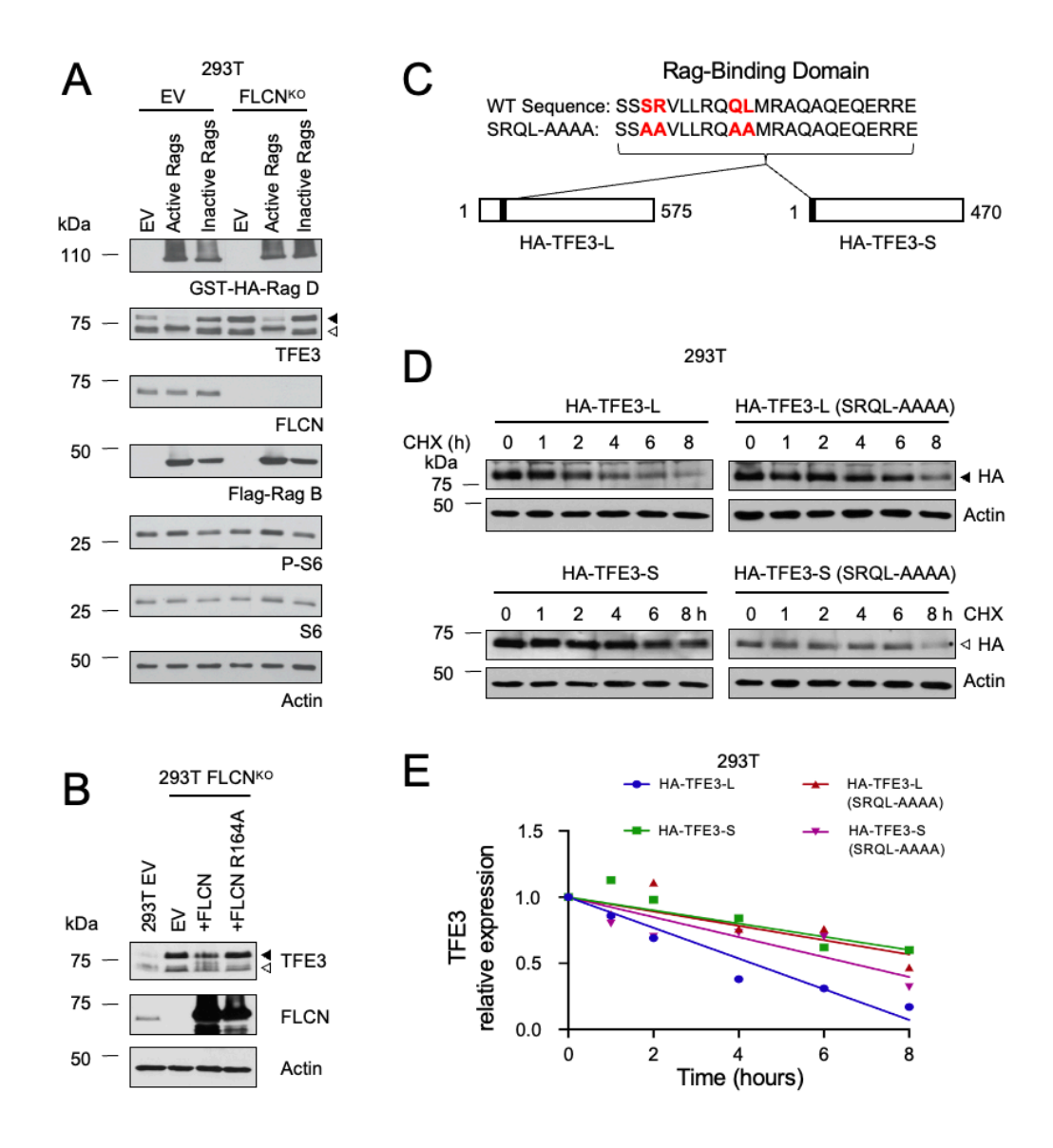
loading control. (D) Quantification of TFE3-L and TFE3-S expression levels in (C) relative to actin. Analysis was performed using ImageJ. Data represent the average of three independent experiments, each performed in triplicate \pm SEM. (E) Immunoblot analysis indicating levels of the two different TFE3 isoforms in MDA-MB-436 cells treated with cycloheximide and chased for 8 hours. Actin was used as a loading control. (F) Quantification of TFE3-L and TFE3-S expression levels in (E) relative to actin. Analysis was performed using ImageJ. Data represent the average of three independent experiments, each performed in triplicate \pm SEM.



²⁸Figure 3. Expression of TFE3-L is dependent on cellular nutrient status

(A, B) Immunoblot analysis indicating expression levels of the two TFE3 isoforms in MCF7 cells cultured in amino acid (A) or glucose (B) depleted media for up to 8 hrs. mTOR activity was measured by p-S6K (early time points) or p-S6 (late time points) levels. Actin was used as a loading control. (C) Immunoblot analysis indicating expression levels of the two TFE3 isoforms in MCF7 treated with the mTORC1 inhibitor (Torin1) for up to 8 hrs. mTORC1 activity was

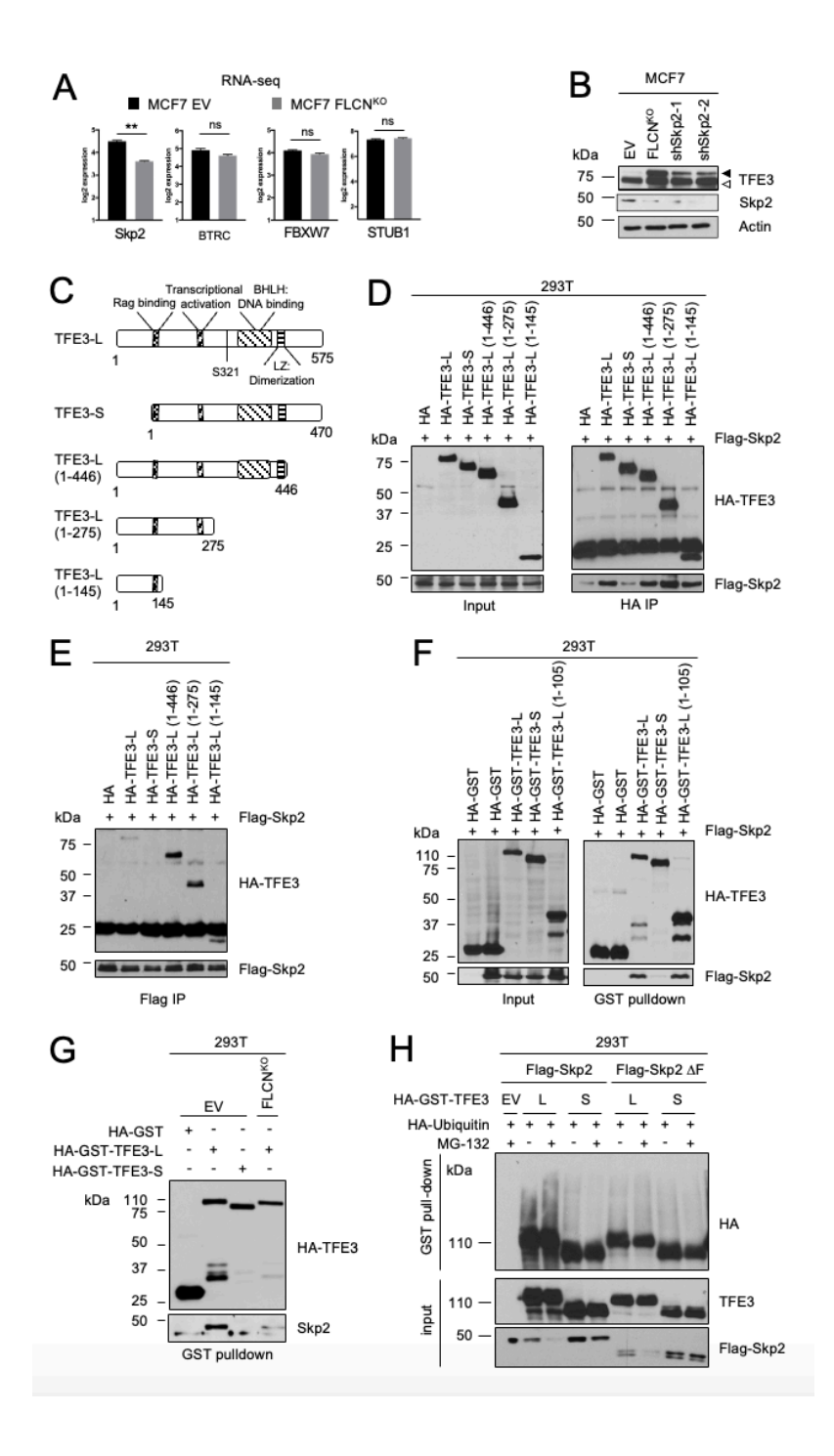
measured by p-S6K (early time points) and p-S6 (late time points) levels. Actin was used as a loading control. (D, E) Immunoblot analysis indicating expression levels of the two TFE3 isoforms in MCF7 cells cultured in amino acid (D) or glucose (E) depleted media for 6 hrs, treated with vehicle (DMSO) or Torin for 30 min, and refed with either amino acids (D) or glucose (E) for 4 hrs, as indicated. mTORC1 activity was measured by of p-S6 levels. Actin was used as a loading control.



²⁹ Figure 4. Expression of TFE3-L is regulated through its binding to active Rag GTPases.

(A) Immunoblot analysis indicating expression levels of the two TFE3 isoforms in empty vector (EV) and FLCN knock out (FLCN^{KO}) 293T cells transfected with active or inactive Rag GTPases. mTORC1 activity was measured by p-S6 levels. Actin was used as a loading control. (B) Immunoblot analysis indicating expression levels of the two TFE3 isoforms in EV and FLCN^{KO} 293T cells transfected with wild-type FLCN or FLCN R164A mutant. Actin was used as a loading

control. (C) Schematic representation of the HA-tagged TFE3 constructs indicating the Rag binding sites as either wild-type or mutated proteins. (D) Immunoblot analysis indicating expression levels of the two TFE3 isoforms in EV 293T cells over-expressing HA-TFE3 constructs indicated in (C) treated with cycloheximide and chased for 8 hours. Actin was used as a loading control.

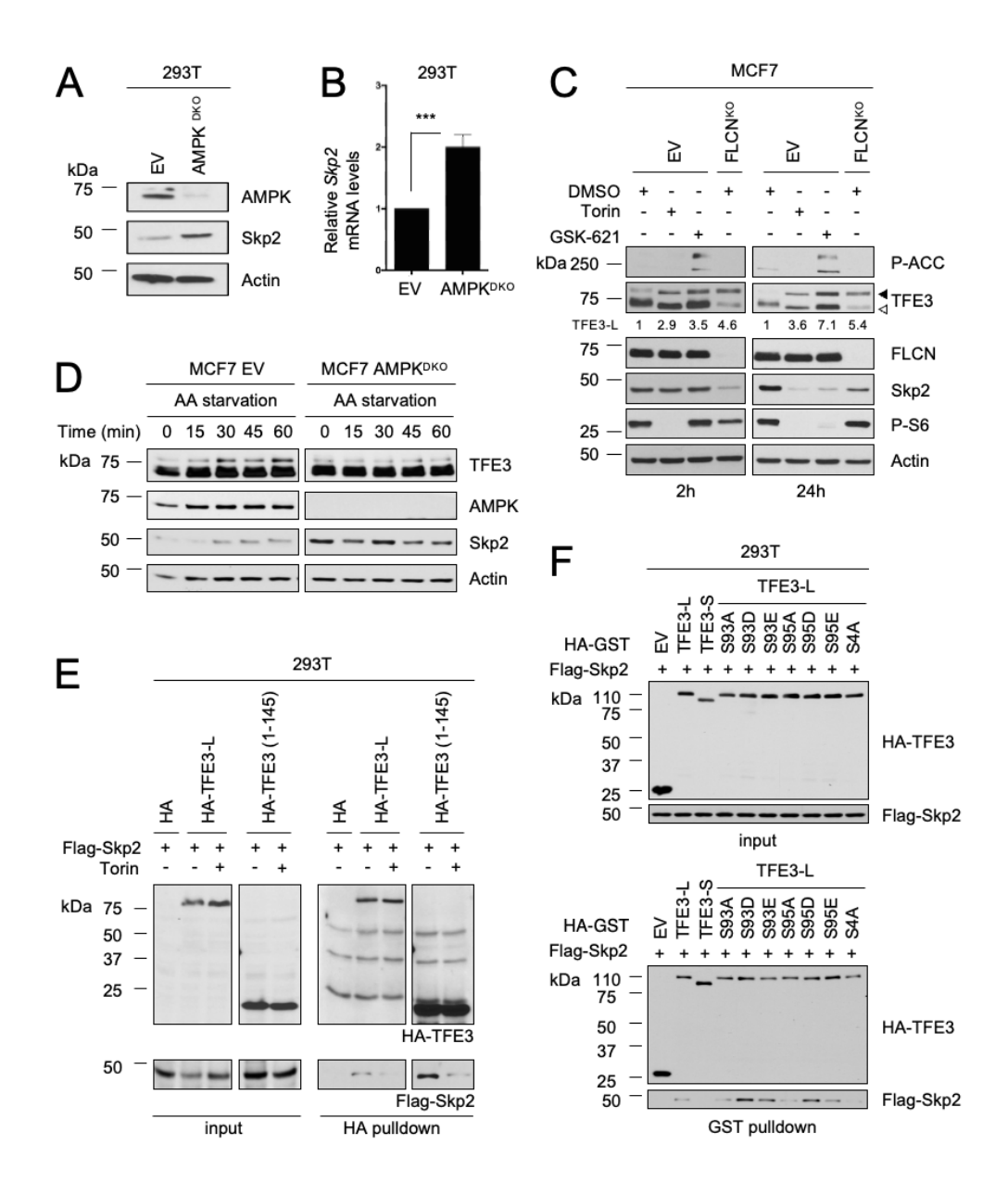


³⁰Figure 5. Identification of Skp2 as a potential E3 ligase regulating TFE3-L stability.

(A) RNA-expression of *Skp2*, *BTRC*, *FBXW7* and *STUB1* ubiquitin ligases in empty vector (EV) and FLCN knock out (FLCN^{KO}) MCF7 cells. Expression data was obtained from GSE163791.

Significance was determined using Student's t-test (ns=non-significant, **p<0.01). (B) Immunoblot analysis indicating expression levels of the two TFE3 isoforms in EV and FLCN^{KO} MCF7 cells. Skp2 was downregulated in MCF7 EV cells using two different shRNAs. Actin was used as a loading control. (C) Schematic representation of the HA-tagged TFE3-L, TFE3-S and C-terminal truncated TFE3-L constructs used in D and E. (D) Binding of Skp2 to TFE3-L isoform. 293T cells were transfected with Flag-tagged Skp2 and TFE3 constructs described in C. Levels of ectopically expressed TFE3 and Skp2 proteins were evaluated by immunoblotting (D, left panels). HA-tagged TFE3 proteins were immunoprecipitated with anti-HA conjugated magnetic beads and immunocomplexes were analyzed by immunoblotting with anti-HA or anti-Flag antibodies (D, right panels). Cells were treated with proteasome inhibitor MG-132 for 4 h before preparing the lysates to preserve the complex. (E) Lysates from D were incubated with anti-Flag conjugated magnetic beads to isolated Flag-Skp2 immunocomplexes. HA-TFE3 and Flag-Skp2 levels were analyzed by immunoblotting with anti-HA or anti-Flag antibodies. (F) Binding of Skp2 to Nterminal region of TFE3-L. 293T cells were transfected with Flag-tagged Skp2 and empty vector (HA-GST), HA-GST-tagged TFE3-L, TFE3-S, or an N-terminal region of TFE3-L (HA-GST-TFE3-L (1-105)). Levels of ectopically expressed TFE3 and Skp2 proteins were evaluated by immunoblotting (F, left panels). HA-GST-tagged TFE3 proteins were purified with GST beads and complexes were analyzed by immunoblotting with anti-HA or anti-Flag antibodies (F, right panels). Cells were treated with proteasome inhibitor MG-132 for 4 h before preparing the lysates to preserve the complex. (G) Binding of Skp2 to TFE3-L in 293T and FLCN knock out 293T cells. Cells were transfected with HA-GST-tagged TFE3 constructs as indicated and ectopically expressed TFE3 proteins were pulled down with GST beads. Levels of TFE3 and Skp2 were determined by immunoblot analysis. (H) Ubiquitination assay of TFE3 isoforms in live cells. 293T

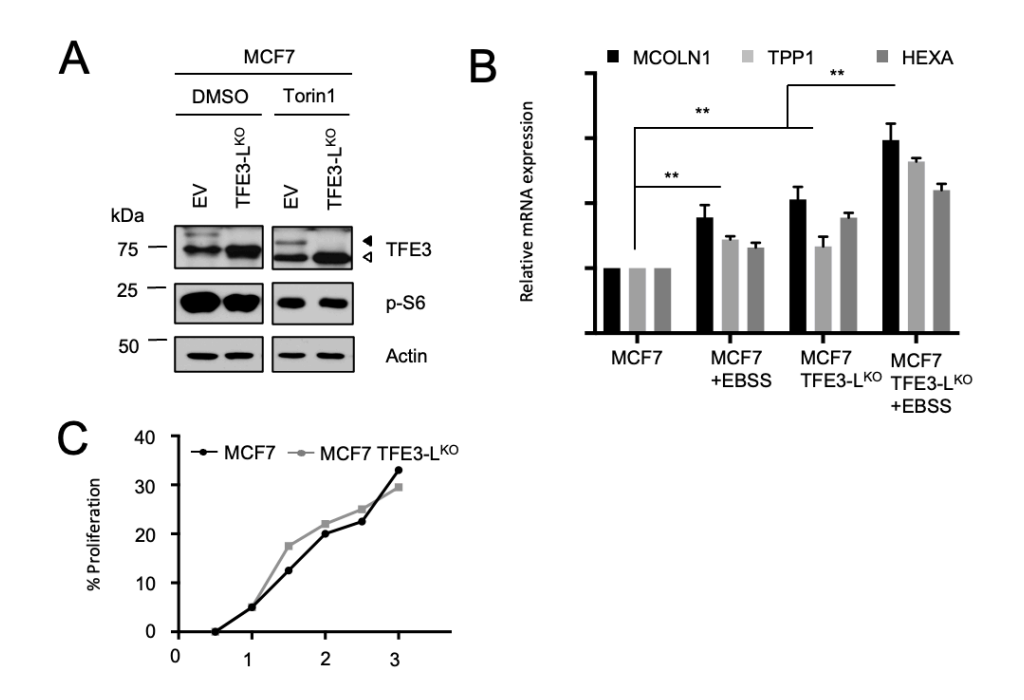
cells were co-transfected with HA-tagged ubiquitin, either Flag-tagged wild-type Skp2 or an inactive Skp2 ΔF mutant, and either HA-GST-tagged TFE3-L or -TFE3-S constructs. TFE3 isoforms were isolated by GST-bead pulldown and ubiquitinated forms detected by immunoblotting with anti-HA antibody. Expression of TFE3 isoforms and Skp2 proteins was analyzed by immunoblotting.



³¹Figure 6. Contribution of mTORC1 and AMPK signaling pathways to Skp2-mediated TFE3-L degradation.

(A) Immunoblot analysis indicating expression levels of AMPK and Skp2 in CRISPR/CAS9-mediated AMPK alpha1/alpha2 double knockout (AMPK^{DKO}) 293T cells. Actin was used as a loading control. (B) Relative *Skp2* mRNA levels measured by RT-qPCR in EV and AMPK^{DKO} cells. Data represent the average of three independent experiments, each performed in triplicate ±

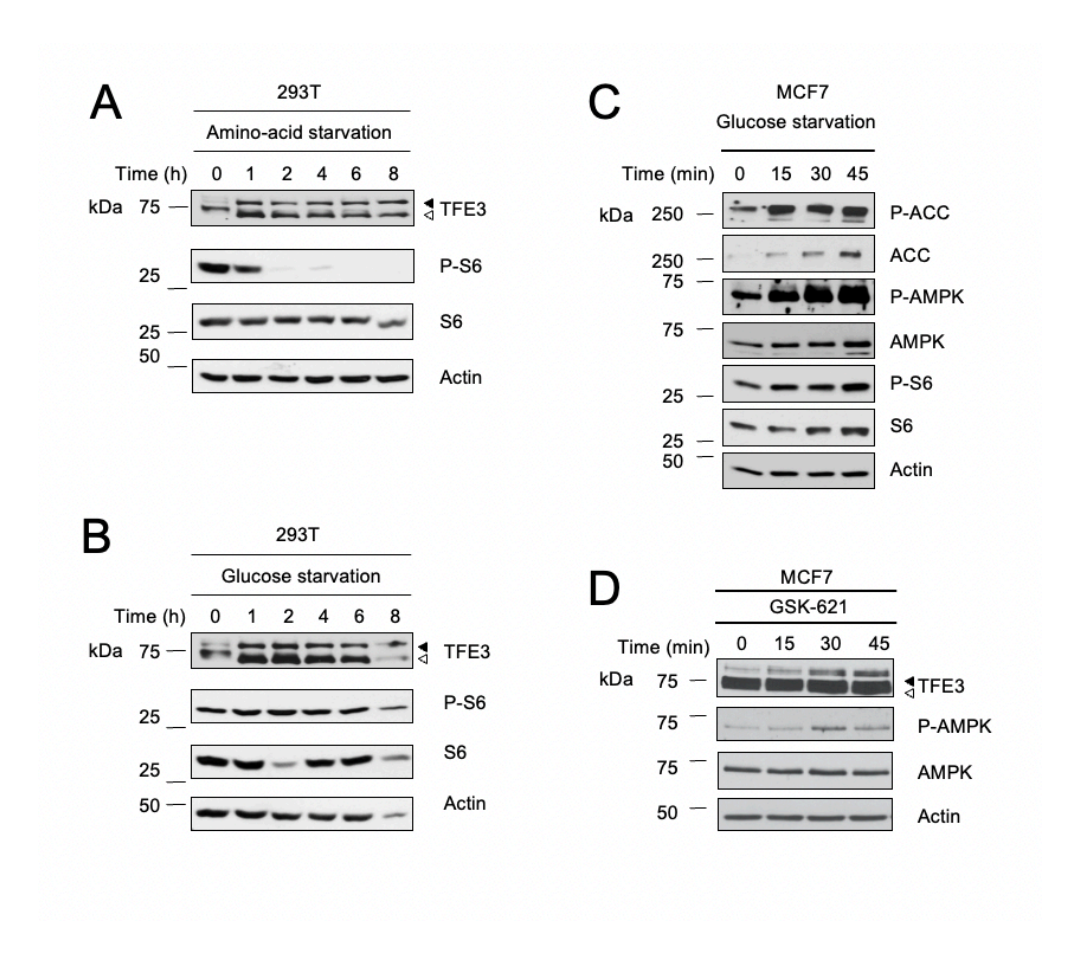
SEM. Significance was determined using Student's t-test (***p<0.001). (C) Immunoblot analysis indicating expression levels of the two different TFE3 isoforms and Skp2 in EV and FLCN^{KO} MCF7 cells, treated with DMSO, Torin1, or GSK-621 for 2 or 24h hours, as indicated. Actin was used as a loading control. (D) Immunoblot analysis indicating expression levels of the two different TFE3 isoforms and Skp2 in EV and AMPK^{DKO} MCF7 cells in response to amino acid starvation for the indicated times. Actin was used as a loading control. (E) Effect of mTORC1 inhibition on the binding of Skp2 to TFE3-L. 293T cells were transfected with empty vector (HA), or constructs expressing HA-tagged TFE3-L or TFE3-L (1-145) and Flag-tagged Skp2 and treated with vehicle (DMSO) or Torin for 3 hours. TFE3-L proteins were pulled down by immunoprecipitation with anti-HA antibody and levels of TFE3-L and Skp2 proteins were determined by immunoblot analysis using anti-HA and anti-Flag antibodies, respectively. Cells were treated with proteasome inhibitor MG-132 for 4 h before preparing the lysates to preserve the complex. (F) Binding of TFE3-L S93 or S95 mutants to Skp2. 293T cells were transfected with constructs expressing HA-GST (EV), HA-GST-tagged TFE3 L, TFE3-S, or TFE3-L mutants at S93 or S95 to A, D, or E, and Flag-tagged Skp2 as indicated. TFE3 proteins were pulled down with GST beads and levels of TFE3 and Skp2 proteins were determined by immunoblot analysis using anti-HA and anti-Flag antibodies, respectively. Cells were treated with proteasome inhibitor MG-132 for 4 h before preparing the lysates to preserve the complex.



³²Figure 7. Functional characterization of TFE3-L

(A) Immunoblot analysis indicating expression levels of TFE3 in the CRISPR/CAS9-mediated TFE3-long form knock out (TFE3-L^{KO}) MCF7 cells. Cells were treated with Torin1 for 4 hrs and p-S6 was used as measure of mTORC1 activity. Actin was used as a loading control. (C) Relative TFE3 target gene mRNA levels measured by RT-qPCR in EV and TFE3-L^{KO} MCF7 cells treated with or without Torin1 for 4 hours. Data represent the average of three independent experiments, each performed in triplicate ± SEM. Significance was determined using Student's t-test (**p<0.01). (D) % Proliferation of MCF7 and MCF7 TFE3-L^{KO} cells as measured by incucyte.

4.9. SUPPLEMENTAL FIGURES AND LEGENDS

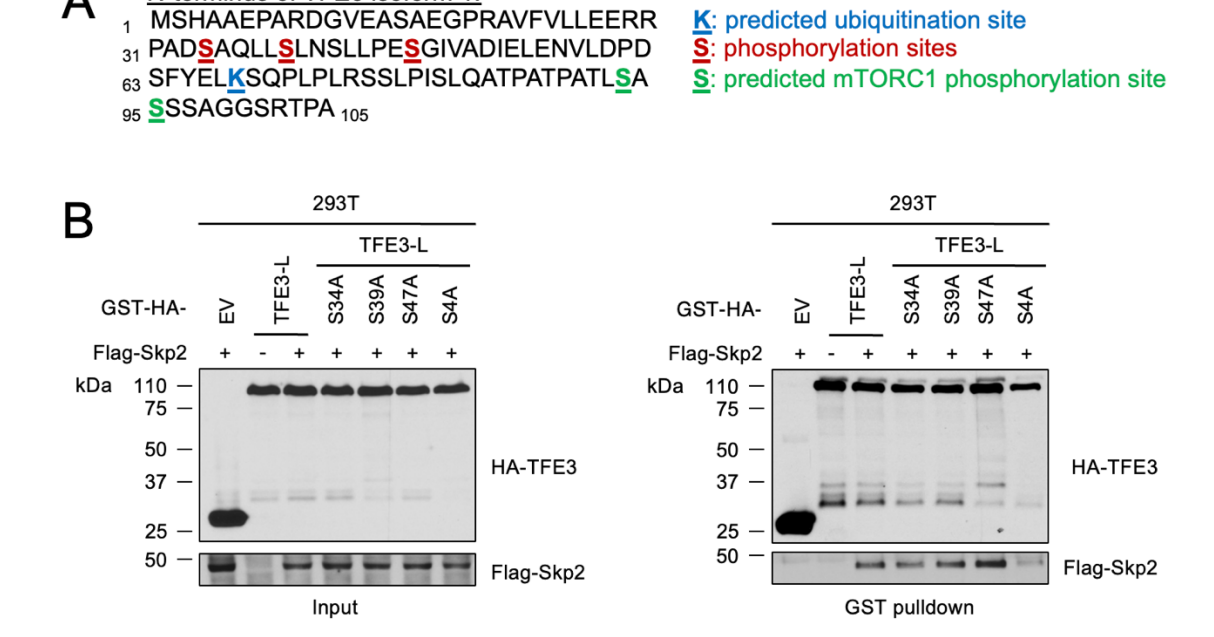


³³Supplemental Figure S1 (related to Figure 3). Expression of TFE3-L is dependent on cellular nutrient status

(A, B) Immunoblot analysis indicating expression levels of the two TFE3 isoforms in 293T cells cultured in amino acid (A) or glucose (B) depleted media at the indicated intervals. mTOR activity was determined by p-S6 levels. Actin was used as a loading control. (C, D) Immunoblot analysis indicating mTORC1 and AMPK activities in MCF7 cells upon glucose starvation for the indicated times. mTOR activity was determined by p-S6 levels and AMPK activity was analyzed by p-AMPK and p-ACC. Actin was used as a loading control. (D) Immunoblot analysis indicating expression levels of the two TFE3 isoforms in MCF7 cells treated with the AMPK activator (GSK-

621) for the indicated times. AMPK activity was measured by immunoblot analysis with anti-p-AMPK antibodies. Actin was used as a loading control.

N-terminus of TFE3 isoform 1:



³⁴Supplemental Figure S2 (related to Figure 6). Amino acid sequence of the N-terminal region of TFE3-L and Binding of TFE3-L mutants to Skp2.

(A) Amino acid sequence of the N-terminal region of TFE3-L, indicating the predicted ubiquitination, phosphorylation and mTORC1 phosphorylation sites. (B) Binding of TFE3-L mutants to Skp2. 293T cells were transfected with constructs expressing HA-GST (EV), HA-GST-tagged TFE3 L or -TFE3-L =S34, S39, S47, or S93/95/96/97 (S4) to A, D, or E, mutants and Flag or Flag-tagged Skp2 as indicated. TFE3 proteins were purified with GST beads and the levels of TFE3 and Skp2 proteins were determined by immunoblot analysis using anti-HA and anti-Flag antibodies, respectively. Cells were treated with proteasome inhibitor MG-132 for 4 h before preparing the lysates to preserve the complex.

4.10. REFERENCES ASSOCIATED WITH CHAPTER 4

- [1] Amae, S., Fuse, N., Yasumoto, K., Sato, S., Yajima, I., Yamamoto, H., Udono, T., Durlu, Y.K., Tamai, M., Takahashi, K., et al. (1998). Identification of a novel isoform of microphthalmia-associated transcription factor that is enriched in retinal pigment epithelium. Biochem. Biophys. Res. Commun. 247, 710–715.
- [2] Asmamaw, M.D., Liu, Y., Zheng, Y.-C., Shi, X.-J., and Liu, H.-M. (2020). Skp2 in the ubiquitin-proteasome system: A comprehensive review. Med Res Rev 40, 1920–1949.
- [3] Beckmann, H., Su, L.K., and Kadesch, T. (1990). TFE3: a helix-loop-helix protein that activates transcription through the immunoglobulin enhancer muE3 motif. Genes Dev. 4, 167–179.
- [4] Betschinger, J., Nichols, J., Dietmann, S., Corrin, P.D., Paddison, P.J., and Smith, A. (2013). Exit from pluripotency is gated by intracellular redistribution of the bHLH transcription factor Tfe3. Cell *153*, 335–347.
- [5] Biamonti, G., Infantino, L., Gaglio, D., and Amato, A. (2019). An Intricate Connection between Alternative Splicing and Phenotypic Plasticity in Development and Cancer. Cells 9.
- [6] Bouché, V., Espinosa, A.P., Leone, L., Sardiello, M., Ballabio, A., and Botas, J. (2016). Drosophila Mitf regulates the V-ATPase and the lysosomal-autophagic pathway. Autophagy 12, 484–498.
- [7] Bradner, J.E., Hnisz, D., and Young, R.A. (2017). Transcriptional addiction in cancer. Cell *168*, 629–643.
- [8] Carrano, A.C., Eytan, E., Hershko, A., and Pagano, M. (1999). SKP2 is required for ubiquitin-mediated degradation of the CDK inhibitor p27. Nat. Cell Biol. *1*, 193–199.
- [9] Daguenet, E., Dujardin, G., and Valcárcel, J. (2015). The pathogenicity of splicing defects: mechanistic insights into pre-mRNA processing inform novel therapeutic approaches. EMBO Rep. 16, 1640–1655.
- [10] David, C.J., and Manley, J.L. (2010). Alternative pre-mRNA splicing regulation in cancer: pathways and programs unhinged. Genes Dev. 24, 2343–2364.
- [11] Dong, X., and Chen, R. (2020). Understanding aberrant RNA splicing to facilitate cancer diagnosis and therapy. Oncogene *39*, 2231–2242.
- [12] El-Houjeiri, L., Possik, E., Vijayaraghavan, T., Paquette, M., Martina, J.A., Kazan, J.M., Ma, E.H., Jones, R., Blanchette, P., Puertollano, R., et al. (2019). The Transcription Factors TFEB and TFE3 Link the FLCN-AMPK Signaling Axis to Innate Immune Response and Pathogen Resistance. Cell Rep. *26*, 3613–3628.e6.
- [13] Escobar-Hoyos, L., Knorr, K., and Abdel-Wahab, O. (2019). Aberrant RNA splicing in cancer. Annu. Rev. Cancer Biol. *3*, 167–185.
- [14] Fillippovich, I., Sorokina, N., Gatei, M., Haupt, Y., Hobson, K., Moallem, E., Spring, K., Mould, M., McGuckin, M.A., Lavin, M.F., et al. (2001). Transactivation-deficient p73alpha (p73Deltaexon2) inhibits apoptosis and competes with p53. Oncogene 20, 514–522.
- [15] Fuse, N., Yasumoto, K. i, Takeda, K., Amae, S., Yoshizawa, M., Udono, T., Takahashi, K., Tamai, M., Tomita, Y., Tachibana, M., et al. (1999). Molecular cloning of cDNA encoding a novel microphthalmia-associated transcription factor isoform with a distinct amino-terminus. J. Biochem. *126*, 1043–1051.
- [16] Garraway, L.A., and Lander, E.S. (2013). Lessons from the cancer genome. Cell *153*, 17–37.

- [17] Geng, Q., Liu, J., Gong, Z., Chen, S., Chen, S., Li, X., Lu, Y., Zhu, X., Lin, H.-K., and Xu, D. (2017). Phosphorylation by mTORC1 stablizes Skp2 and regulates its oncogenic function in gastric cancer. Mol. Cancer *16*, 83.
- [18] Hallsson, J.H., Favor, J., Hodgkinson, C., Glaser, T., Lamoreux, M.L., Magnúsdóttir, R., Gunnarsson, G.J., Sweet, H.O., Copeland, N.G., Jenkins, N.A., et al. (2000). Genomic, transcriptional and mutational analysis of the mouse microphthalmia locus. Genetics *155*, 291–300.
- [19] Hemesath, T.J., Steingrímsson, E., McGill, G., Hansen, M.J., Vaught, J., Hodgkinson, C.A., Arnheiter, H., Copeland, N.G., Jenkins, N.A., and Fisher, D.E. (1994). microphthalmia, a critical factor in melanocyte development, defines a discrete transcription factor family. Genes Dev. *8*, 2770–2780.
- [20] Hodgkinson, C.A., Moore, K.J., Nakayama, A., Steingrímsson, E., Copeland, N.G., Jenkins, N.A., and Arnheiter, H. (1993). Mutations at the mouse microphthalmia locus are associated with defects in a gene encoding a novel basic-helix-loop-helix-zipper protein. Cell 74, 395–404.
- [21] Hong, S.-B., Oh, H., Valera, V.A., Baba, M., Schmidt, L.S., and Linehan, W.M. (2010). Inactivation of the FLCN tumor suppressor gene induces TFE3 transcriptional activity by increasing its nuclear localization. PLoS One *5*, e15793.
- [22] Jangi, M., and Sharp, P.A. (2014). Building robust transcriptomes with master splicing factors. Cell 159, 487–498.
- [23] Jin, G., Lee, S.-W., Zhang, X., Cai, Z., Gao, Y., Chou, P.-C., Rezaeian, A.H., Han, F., Wang, C.-Y., Yao, J.-C., et al. (2015). Skp2-Mediated RagA Ubiquitination Elicits a Negative Feedback to Prevent Amino-Acid-Dependent mTORC1 Hyperactivation by Recruiting GATOR1. Mol. Cell *58*, 989–1000.
- [24] Kalsotra, A., and Cooper, T.A. (2011). Functional consequences of developmentally regulated alternative splicing. Nat. Rev. Genet. 12, 715–729.
- [25] Kauffman, E.C., Ricketts, C.J., Rais-Bahrami, S., Yang, Y., Merino, M.J., Bottaro, D.P., Srinivasan, R., and Linehan, W.M. (2014). Molecular genetics and cellular features of TFE3 and TFEB fusion kidney cancers. Nat. Rev. Urol. *11*, 465–475.
- [26] Lazar, A.J.F., Das, P., Tuvin, D., Korchin, B., Zhu, Q., Jin, Z., Warneke, C.L., Zhang, P.S., Hernandez, V., Lopez-Terrada, D., et al. (2007). Angiogenesis-promoting gene patterns in alveolar soft part sarcoma. Clin. Cancer Res. *13*, 7314–7321.
- [27] Martina, J.A., and Puertollano, R. (2013). Rag GTPases mediate amino acid-dependent recruitment of TFEB and MITF to lysosomes. J. Cell Biol. 200, 475–491.
- [28] Martina, J.A., Diab, H.I., Lishu, L., Jeong-A, L., Patange, S., Raben, N., and Puertollano, R. (2014). The nutrient-responsive transcription factor TFE3 promotes autophagy, lysosomal biogenesis, and clearance of cellular debris. Sci. Signal. 7, ra9.
- [29] Martina, J.A., Diab, H.I., Brady, O.A., and Puertollano, R. (2016). TFEB and TFE3 are novel components of the integrated stress response. EMBO J. 35, 479–495.
- [30] Nakagawa, T., Takahashi, M., Ozaki, T., Watanabe Ki, K., Todo, S., Mizuguchi, H., Hayakawa, T., and Nakagawara, A. (2002). Autoinhibitory regulation of p73 by Delta Np73 to modulate cell survival and death through a p73-specific target element within the Delta Np73 promoter. Mol. Cell. Biol. 22, 2575–2585.
- [31] Napolitano, G., Di Malta, C., Esposito, A., de Araujo, M.E.G., Pece, S., Bertalot, G., Matarese, M., Benedetti, V., Zampelli, A., Stasyk, T., et al. (2020). A substrate-specific mTORC1 pathway underlies Birt-Hogg-Dubé syndrome. Nature *585*, 597–602.

- [32] Oboki, K., Morii, E., Kataoka, T.R., Jippo, T., and Kitamura, Y. (2002). Isoforms of mi transcription factor preferentially expressed in cultured mast cells of mice. Biochem. Biophys. Res. Commun. 290, 1250–1254.
- [33] Paquette, M., El-Houjeiri, L., C Zirden, L., Puustinen, P., Blanchette, P., Jeong, H., Dejgaard, K., Siegel, P.M., and Pause, A. (2021). AMPK-dependent phosphorylation is required for transcriptional activation of TFEB and TFE3. Autophagy 1–19.
- [34] Pastore, N., Brady, O.A., Diab, H.I., Martina, J.A., Sun, L., Huynh, T., Lim, J.-A., Zare, H., Raben, N., Ballabio, A., et al. (2016). TFEB and TFE3 cooperate in the regulation of the innate immune response in activated macrophages. Autophagy *12*, 1240–1258.
- [35] Pastore, N., Vainshtein, A., Klisch, T.J., Armani, A., Huynh, T., Herz, N.J., Polishchuk, E.V., Sandri, M., and Ballabio, A. (2017). TFE3 regulates whole-body energy metabolism in cooperation with TFEB. EMBO Mol. Med. 9, 605–621.
- [36] Perera, R.M., Stoykova, S., Nicolay, B.N., Ross, K.N., Fitamant, J., Boukhali, M., Lengrand, J., Deshpande, V., Selig, M.K., Ferrone, C.R., et al. (2015). Transcriptional control of autophagy-lysosome function drives pancreatic cancer metabolism. Nature *524*, 361–365.
- [37] Petit, C.S., Roczniak-Ferguson, A., and Ferguson, S.M. (2013). Recruitment of folliculin to lysosomes supports the amino acid-dependent activation of Rag GTPases. J. Cell Biol. 202, 1107–1122.
- [38] Pogenberg, V., Ogmundsdóttir, M.H., Bergsteinsdóttir, K., Schepsky, A., Phung, B., Deineko, V., Milewski, M., Steingrímsson, E., and Wilmanns, M. (2012). Restricted leucine zipper dimerization and specificity of DNA recognition of the melanocyte master regulator MITF. Genes Dev. 26, 2647–2658.
- [39] Pozniak, C.D., Radinovic, S., Yang, A., McKeon, F., Kaplan, D.R., and Miller, F.D. (2000). An anti-apoptotic role for the p53 family member, p73, during developmental neuron death. Science 289, 304–306.
- [40] Raben, N., and Puertollano, R. (2016). TFEB and TFE3: linking lysosomes to cellular adaptation to stress. Annu. Rev. Cell Dev. Biol. *32*, 255–278.
- [41] Rehli, M., Lichanska, A., Cassady, A.I., Ostrowski, M.C., and Hume, D.A. (1999). TFEC is a macrophage-restricted member of the microphthalmia-TFE subfamily of basic helix-loophelix leucine zipper transcription factors. J. Immunol. *162*, 1559–1565.
- [42] Roczniak-Ferguson, A., Petit, C.S., Froehlich, F., Qian, S., Ky, J., Angarola, B., Walther, T.C., and Ferguson, S.M. (2012). The transcription factor TFEB links mTORC1 signaling to transcriptional control of lysosome homeostasis. Sci. Signal. *5*, ra42.
- [43] Sato, S., Roberts, K., Gambino, G., Cook, A., Kouzarides, T., and Goding, C.R. (1997). CBP/p300 as a co-factor for the Microphthalmia transcription factor. Oncogene *14*, 3083–3092.
- [44] Sha, Y., Rao, L., Settembre, C., Ballabio, A., and Eissa, N.T. (2017). STUB1 regulates TFEB-induced autophagy-lysosome pathway. EMBO J. *36*, 2544–2552.
- [45] Shalem, O., Sanjana, N.E., Hartenian, E., Shi, X., Scott, D.A., Mikkelson, T., Heckl, D., Ebert, B.L., Root, D.E., Doench, J.G., et al. (2014). Genome-scale CRISPR-Cas9 knockout screening in human cells. Science *343*, 84–87.
- [46] Shin, H.-J.R., Kim, H., Oh, S., Lee, J.-G., Kee, M., Ko, H.-J., Kweon, M.-N., Won, K.-J., and Baek, S.H. (2016). AMPK-SKP2-CARM1 signalling cascade in transcriptional regulation of autophagy. Nature *534*, 553–557.
- [47] Skaar, J.R., Pagan, J.K., and Pagano, M. (2013). Mechanisms and function of substrate recruitment by F-box proteins. Nat. Rev. Mol. Cell Biol. *14*, 369–381.
- [48] Steingrimsson, E., Tessarollo, L., Pathak, B., Hou, L., Arnheiter, H., Copeland, N.G., and

- Jenkins, N.A. (2002). Mitf and Tfe3, two members of the Mitf-Tfe family of bHLH-Zip transcription factors, have important but functionally redundant roles in osteoclast development. Proc. Natl. Acad. Sci. USA 99, 4477–4482.
- [49] Steingrímsson, E., Copeland, N.G., and Jenkins, N.A. (2004). Melanocytes and the microphthalmia transcription factor network. Annu. Rev. Genet. 38, 365–411.
- [50] Sveen, A., Kilpinen, S., Ruusulehto, A., Lothe, R.A., and Skotheim, R.I. (2016). Aberrant RNA splicing in cancer; expression changes and driver mutations of splicing factor genes. Oncogene *35*, 2413–2427.
- [51] Takeda, K., Yasumoto, K., Kawaguchi, N., Udono, T., Watanabe, K., Saito, H., Takahashi, K., Noda, M., and Shibahara, S. (2002). Mitf-D, a newly identified isoform, expressed in the retinal pigment epithelium and monocyte-lineage cells affected by Mitf mutations. Biochimica et Biophysica Acta (BBA) Gene Structure and Expression *1574*, 15–23.
- [52] Takemoto, C.M., Yoon, Y.-J., and Fisher, D.E. (2002). The identification and functional characterization of a novel mast cell isoform of the microphthalmia-associated transcription factor. J. Biol. Chem. 277, 30244–30252.
- [53] Udono, T., Yasumoto, K., Takeda, K., Amae, S., Watanabe, K., Saito, H., Fuse, N., Tachibana, M., Takahashi, K., Tamai, M., et al. (2000). Structural organization of the human microphthalmia-associated transcription factor gene containing four alternative promoters. Biochimica et Biophysica Acta (BBA) Gene Structure and Expression *1491*, 205–219.
- [54] Wada, S., Neinast, M., Jang, C., Ibrahim, Y.H., Lee, G., Babu, A., Li, J., Hoshino, A., Rowe, G.C., Rhee, J., et al. (2016). The tumor suppressor FLCN mediates an alternate mTOR pathway to regulate browning of adipose tissue. Genes Dev. 30, 2551–2564.
- [55] Wu, M., Hemesath, T.J., Takemoto, C.M., Horstmann, M.A., Wells, A.G., Price, E.R., Fisher, D.Z., and Fisher, D.E. (2000). c-Kit triggers dual phosphorylations, which couple activation and degradation of the essential melanocyte factor Mi. Genes Dev. 14, 301–312.
- [56] Yang, A., Kaghad, M., Wang, Y., Gillett, E., Fleming, M.D., Dötsch, V., Andrews, N.C., Caput, D., and McKeon, F. (1998). p63, a p53 homolog at 3q27-29, encodes multiple products with transactivating, death-inducing, and dominant-negative activities. Mol. Cell 2, 305–316.
- [57] Yang, A., Schweitzer, R., Sun, D., Kaghad, M., Walker, N., Bronson, R.T., Tabin, C., Sharpe, A., Caput, D., Crum, C., et al. (1999). p63 is essential for regenerative proliferation in limb, craniofacial and epithelial development. Nature *398*, 714–718.
- [58] Zhang, C.-S., Jiang, B., Li, M., Zhu, M., Peng, Y., Zhang, Y.-L., Wu, Y.-Q., Li, T.Y., Liang, Y., Lu, Z., et al. (2014). The lysosomal v-ATPase-Ragulator complex is a common activator for AMPK and mTORC1, acting as a switch between catabolism and anabolism. Cell Metab. *20*, 526–540.
- [59] Zhao, G.Q., Zhao, Q., Zhou, X., Mattei, M.G., and de Crombrugghe, B. (1993). TFEC, a basic helix-loop-helix protein, forms heterodimers with TFE3 and inhibits TFE3-dependent transcription activation. Mol. Cell. Biol. *13*, 4505–4512.

CHAPTER 5 – General Discussion

5.1. Potential roles for FLCN in regulating important metabolic and cellular processes

We have previously shown that FLCN loss activates AMPK, increasing the resistance to oxidative stress, heat, anoxia, hyperosmotic stresses and obesity in *C. elegans* and mammalian models (Possik et al., 2014, 2015, Yan et al., 2014, 2016). In this thesis, several potential roles for FLCN in regulating the immune response, breast tumor growth and regulation of TFE3 isoforms stability have been described.

5.1.1. TFEB and TFE3 link the FLCN-AMPK signaling axis to innate immune responses

In our studies, we show that AMPK and FLCN act upstream of TFEB and TFE3 in regulation of the innate immune response in C. elegans and mammalian cells (El-Houjeiri et al., 2019). We report that FLCN loss constitutively activates AMPK and induces TFEB and TFE3dependent antimicrobial gene expression, in an mTOR independent manner. Similar results were obtained upon expression of a constitutively active AMPK mutant in nematodes or through pharmacological AMPK activation in mammalian cells. Moreover, treatment of macrophages with lipopolysaccharide (LPS) triggers an acute energy stress that activates AMPK. These signaling responses ultimately enhance TFEB and TFE3 activation, thereby promoting inflammatory cytokine secretion and phagocytosis. Ablation of AMPK abolished TFEB and TFE3 translocation and transcriptional activation. Importantly, we have recently shown that AMPK can directly phosphorylate TFEB and TFE3 on a highly conserved cluster of serine residues near the c-terminus region further enhancing their transcriptional activation (Paquette et al., 2021). These data support the idea that AMPK lies upstream of TFEB and TFE3 and propose novel role of the FLCN/AMPK axis in the regulation of innate immune response via TFEB/TFE3, shedding the light on the potential use of AMPK activators in the stimulation of the immune response and defense against pathogens.

Interestingly, another contemporaneous study showed that LPS stimulation in bone marrow derived macrophages (BMDMs) caused a decrease in FLCN protein expression (compared to control cells), concomitant with increased TFE3 nuclear translocation (Li et al., 2019). Moreover, myeloid-specific deletion of *Flcn* (*Flcn*^{ΔLysM}) resulted in constitutive TFE3 nuclear localization in BMDMs, lysosomal gene induction and lysosomal expansion (LAMP2 immunofluorescence) relative to controls (Li et al., 2019). *In vivo, Flcn*^{ΔLysM} mice exhibited spontaneous alopecia, anemia, splenomegaly and hepatomegaly. Moreover, whole blood analysis and cell sorting showed expansion of the monocyte precursor and neutrophil populations.

Therefore, FLCN has been proposed as a negative regulator of TFE3 that can dampen inflammation in macrophages, although more studies are required to determine the exact molecular mechanisms of TFE3 control by FLCN and how AMPK acts as a mediator in this signaling cascade.

5.1.1.2 BHD disease and inflammation

Patients affected with the rare Birt-Hogg-Dube syndrome (BHD) syndrome are at risk of developing cutaneous fibrofolliculomas, pulmonary cysts, renal cell carcinoma and recurrent pneumothoraxes (Schmidt and Linehan, 2018). In addition, chromosomal translocations leading to TFE3 or TFEB over-activation were reported in sporadic juvenile and advanced renal cell carcinoma (RCC) (Kauffman et al., 2014). Hence, it is tempting to speculate that FLCN loss, and subsequent AMPK activation, induces a chronic inflammatory response that results in the symptoms reported in BHD patients. Of particular interest is the formation and progression of cancers associated with BHD that may parallel cancer cases where innate immune response pathways, such as NF-κB, are over-activated (Karin, 2009). Interestingly, Peutz-Jeghers syndrome (PJS) is another inherited rare condition that is phenotypically very similar to BHD disease, which

is associated with an increased risk for developing hamartomatous polyps in the digestive tract and the predisposition of patients to several types of cancer (Westerman and Wilson, 1999). The development of hamartomatous polyps in PJS patients has been attributed to cell-intrinsic tumor suppressor functions for Stk11in epithelial and/or stromal tissue cells in the gastrointestinal tract (Katajisto et al., 2008). Recently, immune-mediated inflammation was reported as a hallmark of PJS disease (Poffenberger et al., 2018). Given the role of FLCN in the immune response (El-Houjeiri et al., 2019; Li et al., 2019), comparably, our data argue for a more complex role for FLCN in BHD disease development, raising the possibility that inflammatory events reported in FLCN downregulated cells may trigger chronic inflammation, stimulating skin lesions, pulmonary cysts and predisposition to cancer. Hence, locally targeting this chronic inflammation may present a novel approach to reducing disease incidence and cancer predisposition in BHD patients.

5.1.2 Role of the FLCN-TFE3-AMPK signaling pathway in Breast Cancer tumor growth

The FLCN-TFE3-AMPK pathway is involved in regulating important cellular pathways, which provides resistance to several energy depleting stresses. However, the significance of this pathway in cancer setting is poorly described. Loss-of-function mutations of the FLCN/FNIP tumor suppressor complex have only been reported in renal tumors in patients with the BHD syndrome (Vocke et al., 2005). Here we reveal that FLCN, FNIP1 and FNIP2 are downregulated in many human cancers including poor prognosis invasive basal-like triple negative breast carcinomas (TNBC) where AMPK and TFE3 targets are activated compared to the luminal, less aggressive subtypes. Given that TNBC remains the most challenging breast cancer subtype to treat due to its heterogeneity, it is crucial to understand the molecular pathways that contribute to the growth and metastatic progression of this aggressive disease. We show that FLCN loss in luminal breast cancer promotes tumor growth through TFE3 activation and subsequent induction of several

pathways including autophagy, lysosomal biogenesis, aerobic glycolysis and angiogenesis. Importantly, induction of aerobic glycolysis and angiogenesis in FLCN deficient cells was dictated by the activation of PGC-1α/HIF-1α pathway, which we show to be TFE3-dependent, directly linking TFE3 to Warburg metabolic reprogramming and angiogenesis. Conversely, we report that FLCN overexpression in invasive basal-like breast cancer models attenuates TFE3 nuclear localization, TFE3-dependent transcriptional activity and tumor growth. These findings support a general role of a deregulated FLCN/TFE3 tumor suppressor pathway in human cancers.

5.1.2.1. Autophagy, angiogenesis and cancer: is TFE3 the link?

Today, FLCN is listed in a panel of seven genes that can cause renal cancer when mutated (Linehan, 2012). Each of the seven known kidney cancer genes VHL, MET, FLCN, TSC1, TSC2, FH and SDH are all involved in nutrient stimulation and/or metabolic stress pathways, classifying renal cancer as a metabolic disease (Linehan, 2012; Linehan et al., 2010). For example, the VHL protein is a component of the oxygen and iron sensing pathway that regulates HIF levels in the cell, MET signaling affects the LKB1/AMPK energy sensing pathway, TSC1/TSC2 are downstream of AMPK and negatively regulate mTOR in response to cellular energy scarcity and the FLCN/FNIP complex interacts with AMPK and therefore may affect cellular energy and nutrient sensing pathways (Linehan, 2012; Linehan et al., 2010). Some of the diseases caused by mutations in those genes present similar clinical manifestations, hinting at a potential integrated signaling pathway response (Linehan, 2012; Linehan et al., 2010; Schmidt and Linehan, 2018). We have recently shown that in addition to AMPK activation, loss of FLCN in cells induces TFE3 activation leading to induction of multiple bioenergetic programs including glycolysis, and angiogenesis, which are controlled by PGC1- α /HIF-1 α downstream of TFE3. Interestingly, the link between MiT/TFE factors and angiogenesis was first hypothesized following the observation

that TFEB knockout mice die prenatally due to a defect in placental vascularization (Steingrímsson et al., 1998). In addition, MITF was also shown to positively regulate angiogenesis through direct transcriptional control of HIF (Buscà et al., 2005). Finally, ASPSCR1-TFE3-driven alveolar soft part sarcomas are highly vascularized tumors, which responds to antiangiogenic therapy (Lazar et al., 2007; Zhou et al., 2017). Hence, it might be relevant to understand whether renal cancer subtypes with FLCN mutations and TFE3 nuclear localization and activation are associated with high vascularization status and to assess their response rate to antiangiogenic therapy combined with autophagy inhibitors.

5.1.2.2 Potential Role of the FLCN-TFE3-AMPK pathway in TNBC inflammatory phenotype

Given the proposed role of FLCN in mediating an immune response, as described in Chapter 2, it is plausible that FLCN downregulation reported in the aggressive TNBC subtypes can additionally modulate the immune microenvironment of these tumors. The link between inflammation and cancer was first suggested in 1863 (Virchow, 1989), yet, whether inflammation aggravates or resolves cancer remains a matter of debate. Interestingly, in our RNA-seq gene enrichment analysis, we report stimulation of multiple pathways involving the immune response including upregulation in cytokine mediated pathways, phagosome acidification, neutrophil mediated immunity, neutrophil activation/immune response and neutrophil degranulation (Chapter 3, Figure 5B). Among BC subtypes, TNBC is characterized by a greater degree of tumor-infiltrating lymphocytes (TILs) (Cocco et al., 2020). TILs are present both intratumorally and in adjacent stromal tissues and are composed mainly of cytotoxic CD8⁺ lymphocytes, and, to a lesser extent, CD4⁺ T-helper cells, T-regulatory cells, macrophages, mast cells, and plasma-cells. Interestingly, the presence of intra-tumoral and stromal TILs was reported to have predictive and prognostic role. In TNBC increased TILs at diagnosis have been associated with pathologic

complete responses with neoadjuvant chemotherapy and improved survival after adjuvant chemotherapy (García-Teijido et al., 2016; Loi et al., 2019a; Mao et al., 2016). Interestingly, there is an association between high number of stromal TILs and more favorable survival outcomes and response to chemotherapy. These results underscore the prognostic and predictive value of TILs and immune activity in aggressive breast cancer subtypes. This also suggests that the effect of chemotherapy may be partially mediated by the immune system, making the investigation of immunotherapy in TNBC particularly interesting (Borcherding et al., 2018; Loi et al., 2019b, 2019a). In our studies, we show that FLCN is downregulated in TNBC and is associated with enhanced inflammation and cytokine secretion. It would be worthwhile to examine levels of intertumoral and stromal TILS in TNBC models, where FLCN levels are downregulated. If the levels of FLCN correlate with the tumor infiltrates, then it can potentially act as a prognostic and predictive tool in response to chemotherapy.

5.1.3. Role of FLCN in stabilizing TFE3-L

The role for FLCN in the cytoplasmic retention and negative regulation of TFE3 and TFEB has been well established (Betschinger et al., 2013; El-Houjeiri et al., 2019; Martina and Puertollano, 2013; Paquette et al., 2021; Petit et al., 2013; Wada et al., 2016). Herein, we add an additional layer of regulation through which FLCN not only controls TFE3 activity, but also its stability. We characterized two TFE3 isoforms the full-length (TFE3-L) and the alternatively spliced shorter (TFE3-S) isoform. We show that both isoforms are differentially expressed in different human cancer cell lines and under diverse cellular conditions; TFE3-L levels being elevated in specific cancer cell lines or under certain conditions such as nutrient starvation or FLCN-deficient conditions. Upon nutrient rich settings, FLCN acts as a GAP on the Rag C/D activating them and promoting TFE3 binding at the lysosomal surface, which facilitates its

phosphorylation and cytoplasmic retention (Martina and Puertollano, 2013; Napolitano et al., 2020). Interestingly, the Rag binding site is shared between the two TFE3 isoforms, where we speculate that under genetic or nutritional conditions that lead to activation of lysosomal Rag GTPases (RagA/B-GTP and RagC/D-GDP), the binding of TFE3-L to Rag C/D facilitates mTORC1-mediated recruitment of E3 ubiquitin ligase to its N-terminal region, promoting its degradation. From these results it seems that under normal conditions, the cells need to maintain a low level of TFE3-L through engagement of multiple mechanisms to ensure its constant degradation. We proposed a chronic vs. acute response to stress through which TFE3-L levels are manipulated by AMPK and mTORC1, respectively. AMPK seems to play an indirect role during energy stress through repressing Skp2 transcription and hence promoting the accumulation of TFE3-L isoform. Conversely, our data supports the idea that mTORC1 might directly phosphorylate the unique N-terminal region in TFE3-L, promoting Skp2 binding and proteasomal degradation. Both mechanisms propose an immensely controlled regulation of TFE3-L levels in the cells, which suggests its potential importance in diverse cellular processes. Hence, characterizing the distinct functions of both TFE3 isoforms in different cellular systems can uncover additional modes of regulation that is of interest in health and disease.

The differential functions of TFE3 isoforms are still under investigation. It would be interesting to utilize a cellular model where both isoforms are ubiquitously expressed (e.g., FLCN-deficient cells or TNBC cells), knock out TFE3-L isoform, then assess the effect on *in vitro* and *in vivo* proliferation and examine the downstream target gene regulation and expression. Another important experiment would be to knock out the two TFE3 isoforms, stably express each isoform individually, then assess the resulting consequences including ability to form heterodimers with other MiTF family members, downstream target gene regulation, DNA binding, DNA-binding

specificity, and binding potential to transcriptional cofactors or co-repressors. One might also speculate that the relative levels of each isoform might be dictating their function. Hence, further analysis of their expression ratio in different cellular conditions can be very informative.

5.2. Controversial role of FLCN/FNIP complex on mTORC1-explained

The mechanisms through which TFEB and TFE3 are regulated have been well characterized. Most studies to date suggest that mTORC1-dependent phosphorylation of TFEB and TFE3 causes cytoplasmic retention of these transcription factors under nutrient-rich conditions. Inhibition of mTORC1 activity upon nutrient starvation has been associated with nuclear accumulation of TFEB and TFE3 inducing the up-regulation of genes involved in autophagy and lysosomal biogenesis, which favors cell survival and adaption to stress (Martina and Puertollano, 2013; Martina et al., 2012; Petit et al., 2013; Roczniak-Ferguson et al., 2012; Settembre et al., 2012). However, in the second chapter of this thesis, we report normal mTOR activity in FLCN-deficient cellular models and propose that, under these conditions, TFEB and TFE3 activation status is mTOR independent (El-Houjeiri et al., 2019). This controversial role of FLCN/FNIP complex as a positive modulator of mTORC1 activity is well documented. While depletion of FLCN in certain cell lines impairs mTORC1 activity (Petit et al., 2013; Tsun et al., 2013), FLCN loss does not affect mTORC1 activity in cells or in BHD-derived kidney tumors (Baba et al., 2008; El-Houjeiri et al., 2019; Hasumi et al., 2009; Napolitano et al., 2020; Wada et al., 2016). Recent studies provide an explanation for this controversy through a substrate-specific effect of FLCN GAP activity on mTORC1. Accordingly, mTORC1 substrates containing a "TOR signaling" (TOS) motif such as S6K and 4E-BP1 require GTP-Rheb, but not GDP-bound Rag C/D, to be phosphorylated on the lysosome. However, mTORC1 substrates without a TOS motif such as the transcription factors TFE3 and TFEB require FLCN GAP activity to activate the Rags to be

phosphorylated (Napolitano et al., 2020). Consequently, FLCN loss fails to activate the Rags, and promotes the nuclear translocation and activation of TFEB/TFE3. Recent studies revealed that TFEB and TFE3 are in turn able to reciprocally regulate mTORCl activity through inducing the expression of *RRAGD* and *RRAGC*, the genes encoding RagD and RagC, respectively (Di Malta et al., 2017; Li et al., 2019). Consequently, transcriptional induction of RagC/D promotes Rag assembly on the lysosomal surface, enabling mTORCl recruitment once nutrients become available. Thus, TFEB, TFE3 and mTORCl are involved in a feedback loop through which mTORCl inhibits their nuclear localization and function, and in turn, they regulate mTORCl lysosomal recruitment and activity through the RagC/D GTPase (Di Malta et al., 2017; Li et al., 2019). Hence, increased expression of these Rags may explain enhanced activation of mTORCl associated with FLCN loss in BHD-derived renal tumors (Napolitano et al., 2020).

From these studies, it is becoming clear that the regulatory role of FLCN, mTOR and AMPK on TFEB and TFE3 is part of the complex and tightly regulated metabolic program. TFEB and TFE3 are deactivated by mTORC1 under conditions of high nutrient availability but also control mTORC1 lysosomal recruitment, which is required for its activation, creating a mechanism for transducing the information of the cell energy environment into the switch between anabolic and catabolic pathways (Di Malta et al., 2017; Li et al., 2019; Perera et al., 2015).

5.3. Lysosomal and autophagy disfunction as a recurrent feature in cancer

Immune disorders and other pathological conditions linked with excessive inflammation, such as neurodegenerative diseases, obesity and cancer, have long been linked with dysregulation of lysosomal and autophagic pathways. Several studies have implicated excessive lysosomal activity and autophagy as a recurrent feature in cancer. First, cancer cells have higher metabolic

demands than normal cells and thus may rely on induction of the autophagy-lysosome machinery for survival (Rabinowitz and White, 2010). Second, cancer patients experience muscle atrophy, a syndrome known as cachexia, which is due to excessive muscle protein breakdown via activation of ubiquitin ligases, upregulation of proteasome-mediated degradation and induction of the autophagy-lysosome system. In fact, lung and pancreatic ductal adenocarcinoma (PDA) tumors appear to be reliant on constitutive activation of autophagy for supplying essential nutrients and for removing damaged mitochondria (Guo et al., 2011; Karsli-Uzunbas et al., 2014; Perera et al., 2015; Rao et al., 2014; Strohecker et al., 2013; White and DiPaola, 2009). Several other cancers, including melanoma, breast and prostate cancer, show context- and stage-specific reliance on autophagy during tumor initiation and progression (Huo et al., 2013; Lock et al., 2011; Santanam et al., 2016; Wei et al., 2011; Xie and Klionsky, 2007). In fact, in our studies, we report that the FLCN-TFE3 pathway is dysregulated in TNBC subtype; where FLCN and its binding partners FNIP1 and FNIP2 are downregulated, and AMPK and TFE3 downstream targets (including autophagy and lysosomal genes) are elevated compared to the less aggressive luminal subtypes. Our data supports the idea of "context-specific reliance" on autophagy, where the less aggressive luminal breast cancer subtype types don't rely on autophagy and lysosomal biogenesis for survival to the same extent as the triple negative breast cancer subtypes. We show that FLCN overexpression in TNBC models attenuates TFE3 nuclear localization and significantly decreases autophagy and lysosomal gene transcription, leading to impaired tumor growth. Although it is still unclear how TFE3 may help promote the oncogenic state, the emerging evidence suggests that cancer cells may exploit the TFE3-mediated transcriptional activation for their survival. The discovery that TFE3 regulates autophagy, lysosome biogenesis, and mTORCl activation suggests that this transcription factor may be broadly implicated in a wider array of cancers than previously

anticipated. Further defining the full cohort of interacting partners and transcriptional targets of TFE3 may help pinpoint the specific gene programs activated in different tissues and states. Similarly, continued characterization of upstream signaling cascades that control TFE3 levels, stability, localization and activity may contribute to the discovery of novel therapeutic strategies to switch off TFE3 in cancer cells.

5.4. Therapeutic Implications

The diverse roles of TFEB and TFE3 transcription factors in promoting inflammation and tumorigenesis make them and their downstream pathways important targets for generating antiinflammatory or anticancer agents. However, activation of these transcription factors seems beneficial in many neurological and lysosomal disorders but may confer an adaptive advantage to cancer cells. To date, several studies using in vitro and in vivo tumor models have shown that targeting autophagy and lysosome function significantly impaired tumor growth (White, 2015). For example, over 50 currently ongoing clinical trials integrate the lysosomal inhibitor hydroxychloroquine (HCQ) in the treatment of a diverse array of tumor types (Perera and Bardeesy, 2015). Results from ongoing trials of HCQ in combination with chemotherapy (gemcitabine/Abraxane and FOLFIRINOX) in PDA are currently ongoing and highly anticipated. Most recently, treatment of 31 preoperative PDA patients with HCQ and gemcitabine resulted in a significant increase in overall survival (Boone et al., 2015). The success of autophagy-lysosome inhibition against an array of tumor types including glioblastoma, myeloma, prostate cancer and breast cancer highlights the broader importance of this pathway in promoting tumorigenesis (Mahalingam et al., 2014; Rangwala et al., 2014; Vogl et al., 2014).

Even though mTOR inhibitors were effective in reducing the number and size of renal tumors and cysts in *FLCN*-deficient mouse models (Baba et al., 2008; Chen et al., 2015; Wu et al.,

2015), they have not been successful in treating BHD-associated fibrofolliculomas (Gijezen et al., 2014) and a limited survival advantage was observed in BHD patients (Nakamura et al., 2013). These results are corroborated by the recent studies showing that TFEB and TFE3 act upstream of mTORC1 and stimulate its activity through a feedback mechanism where these tumors may confer resistance to mTOR inhibitors (Li et al., 2019; Napolitano et al., 2020). Thus, simultaneous suppression of several pathways downstream of MiT/TFE factors with next-generation inhibitors, such as the recently described mTOR RapaLink compound (Rodrik-Outmezguine et al., 2016), and more potent lysosome inhibitors (McAfee et al., 2012; Rebecca et al., 2017), could confer enhanced efficacy in MiT/TFE-dependent cancers.

5.5. Concluding remarks

We have only recently begun to understand the contribution of the FLCN-AMPK pathway to cellular response to stress through the activation of the MiT/TFE transcription factors. The role of these transcription factors in cellular adaptation to a wide variety of internal stresses and environmental fluctuations is intricately linked to their unique ability to globally regulate the multiple metabolic components including autophagic/lysosomal system, inflammation, glycolysis and angiogenesis. The development of small molecules that modulate TFEB/TFE3 activity in an accurate temporal- and tissue-specific manner is a rewarding area for future studies. These molecules have the potential to be used for a plethora of human diseases, including metabolic, immune, neurological, and oncogenic disorders, and would no doubt improve our understanding of the complex regulation of cellular adaptation to stress.

5.6. References associated with Chapter 5

- [1] Baba, M., Furihata, M., Hong, S.-B., Tessarollo, L., Haines, D.C., Southon, E., Patel, V., Igarashi, P., Alvord, W.G., Leighty, R., et al. (2008). Kidney-targeted Birt-Hogg-Dube gene inactivation in a mouse model: Erk1/2 and Akt-mTOR activation, cell hyperproliferation, and polycystic kidneys. J. Natl. Cancer Inst. *100*, 140–154.
- [2] Betschinger, J., Nichols, J., Dietmann, S., Corrin, P.D., Paddison, P.J., and Smith, A. (2013). Exit from pluripotency is gated by intracellular redistribution of the bHLH transcription factor Tfe3. Cell *153*, 335–347.
- [3] Boone, B.A., Bahary, N., Zureikat, A.H., Moser, A.J., Normolle, D.P., Wu, W.-C., Singhi, A.D., Bao, P., Bartlett, D.L., Liotta, L.A., et al. (2015). Safety and Biologic Response of Preoperative Autophagy Inhibition in Combination with Gemcitabine in Patients with Pancreatic Adenocarcinoma. Ann. Surg. Oncol. 22, 4402–4410.
- [4] Borcherding, N., Kolb, R., Gullicksrud, J., Vikas, P., Zhu, Y., and Zhang, W. (2018). Keeping tumors in check: A mechanistic review of clinical response and resistance to immune checkpoint blockade in cancer. J. Mol. Biol. *430*, 2014–2029.
- [5] Buscà, R., Berra, E., Gaggioli, C., Khaled, M., Bille, K., Marchetti, B., Thyss, R., Fitsialos, G., Larribère, L., Bertolotto, C., et al. (2005). Hypoxia-inducible factor 1{alpha} is a new target of microphthalmia-associated transcription factor (MITF) in melanoma cells. J. Cell Biol. *170*, 49–59.
- [6] Chen, J., Huang, D., Rubera, I., Futami, K., Wang, P., Zickert, P., Khoo, S.-K., Dykema, K., Zhao, P., Petillo, D., et al. (2015). Disruption of tubular Flcn expression as a mouse model for renal tumor induction. Kidney Int. 88, 1057–1069.
- [7] Cocco, S., Piezzo, M., Calabrese, A., Cianniello, D., Caputo, R., Lauro, V.D., Fusco, G., Gioia, G. di, Licenziato, M., and De Laurentiis, M. (2020). Biomarkers in Triple-Negative Breast Cancer: State-of-the-Art and Future Perspectives. Int. J. Mol. Sci. 21.
- [8] Di Malta, C., Siciliano, D., Calcagni, A., Monfregola, J., Punzi, S., Pastore, N., Eastes, A.N., Davis, O., De Cegli, R., Zampelli, A., et al. (2017). Transcriptional activation of RagD GTPase controls mTORC1 and promotes cancer growth. Science *356*, 1188–1192.
- [9] El-Houjeiri, L., Possik, E., Vijayaraghavan, T., Paquette, M., Martina, J.A., Kazan, J.M., Ma, E.H., Jones, R., Blanchette, P., Puertollano, R., et al. (2019). The Transcription Factors TFEB and TFE3 Link the FLCN-AMPK Signaling Axis to Innate Immune Response and Pathogen Resistance. Cell Rep. 26, 3613–3628.e6.
- [10] García-Teijido, P., Cabal, M.L., Fernández, I.P., and Pérez, Y.F. (2016). Tumor-Infiltrating Lymphocytes in Triple Negative Breast Cancer: The Future of Immune Targeting. Clin Med Insights Oncol 10, 31–39.
- [11] Gijezen, L.M.C., Vernooij, M., Martens, H., Oduber, C.E.U., Henquet, C.J.M., Starink, T.M., Prins, M.H., Menko, F.H., Nelemans, P.J., and van Steensel, M.A.M. (2014). Topical rapamycin as a treatment for fibrofolliculomas in Birt-Hogg-Dubé syndrome: a double-blind placebo-controlled randomized split-face trial. PLoS One *9*, e99071.
- [12] Guo, J.Y., Chen, H.-Y., Mathew, R., Fan, J., Strohecker, A.M., Karsli-Uzunbas, G., Kamphorst, J.J., Chen, G., Lemons, J.M.S., Karantza, V., et al. (2011). Activated Ras requires autophagy to maintain oxidative metabolism and tumorigenesis. Genes Dev. 25, 460–470.
- [13] Hasumi, Y., Baba, M., Ajima, R., Hasumi, H., Valera, V.A., Klein, M.E., Haines, D.C., Merino, M.J., Hong, S.-B., Yamaguchi, T.P., et al. (2009). Homozygous loss of BHD causes early

- embryonic lethality and kidney tumor development with activation of mTORC1 and mTORC2. Proc. Natl. Acad. Sci. USA *106*, 18722–18727.
- [14] Huo, Y., Cai, H., Teplova, I., Bowman-Colin, C., Chen, G., Price, S., Barnard, N., Ganesan, S., Karantza, V., White, E., et al. (2013). Autophagy opposes p53-mediated tumor barrier to facilitate tumorigenesis in a model of PALB2-associated hereditary breast cancer. Cancer Discov. *3*, 894–907.
- [15] Karsli-Uzunbas, G., Guo, J.Y., Price, S., Teng, X., Laddha, S.V., Khor, S., Kalaany, N.Y., Jacks, T., Chan, C.S., Rabinowitz, J.D., et al. (2014). Autophagy is required for glucose homeostasis and lung tumor maintenance. Cancer Discov. 4, 914–927.
- [16] Katajisto, P., Vaahtomeri, K., Ekman, N., Ventelä, E., Ristimäki, A., Bardeesy, N., Feil, R., DePinho, R.A., and Mäkelä, T.P. (2008). LKB1 signaling in mesenchymal cells required for suppression of gastrointestinal polyposis. Nat. Genet. 40, 455–459.
- [17] Lazar, A.J.F., Das, P., Tuvin, D., Korchin, B., Zhu, Q., Jin, Z., Warneke, C.L., Zhang, P.S., Hernandez, V., Lopez-Terrada, D., et al. (2007). Angiogenesis-promoting gene patterns in alveolar soft part sarcoma. Clin. Cancer Res. *13*, 7314–7321.
- [18] Li, J., Wada, S., Weaver, L.K., Biswas, C., Behrens, E.M., and Arany, Z. (2019). Myeloid Folliculin balances mTOR activation to maintain innate immunity homeostasis. JCI Insight 5.
- [19] Linehan, W.M. (2012). Genetic basis of kidney cancer: role of genomics for the development of disease-based therapeutics. Genome Res. 22, 2089–2100.
- [20] Linehan, W.M., Srinivasan, R., and Schmidt, L.S. (2010). The genetic basis of kidney cancer: a metabolic disease. Nat. Rev. Urol. 7, 277–285.
- [21] Lock, R., Roy, S., Kenific, C.M., Su, J.S., Salas, E., Ronen, S.M., and Debnath, J. (2011). Autophagy facilitates glycolysis during Ras-mediated oncogenic transformation. Mol. Biol. Cell 22, 165–178.
- [22] Loi, S., Drubay, D., Adams, S., Pruneri, G., Francis, P.A., Lacroix-Triki, M., Joensuu, H., Dieci, M.V., Badve, S., Demaria, S., et al. (2019a). Tumor-Infiltrating Lymphocytes and Prognosis: A Pooled Individual Patient Analysis of Early-Stage Triple-Negative Breast Cancers. J. Clin. Oncol. *37*, 559–569.
- [23] Loi, S., Schmid, P., Aktan, G., Karantza, V., and Salgado, R. (2019b). Relationship between tumor infiltrating lymphocytes (TILs) and response to pembrolizumab (pembro)+chemotherapy (CT) as neoadjuvant treatment (NAT) for triple-negative breast cancer (TNBC): Phase Ib KEYNOTE-173 trial. Ann. Oncol. 30, iii2.
- [24] Mahalingam, D., Mita, M., Sarantopoulos, J., Wood, L., Amaravadi, R.K., Davis, L.E., Mita, A.C., Curiel, T.J., Espitia, C.M., Nawrocki, S.T., et al. (2014). Combined autophagy and HDAC inhibition: a phase I safety, tolerability, pharmacokinetic, and pharmacodynamic analysis of hydroxychloroquine in combination with the HDAC inhibitor vorinostat in patients with advanced solid tumors. Autophagy *10*, 1403–1414.
- [25] Mao, Y., Qu, Q., Chen, X., Huang, O., Wu, J., and Shen, K. (2016). The Prognostic Value of Tumor-Infiltrating Lymphocytes in Breast Cancer: A Systematic Review and Meta-Analysis. PLoS One 11, e0152500.
- [26] Martina, J.A., and Puertollano, R. (2013). Rag GTPases mediate amino acid-dependent recruitment of TFEB and MITF to lysosomes. J. Cell Biol. 200, 475–491.
- [27] Martina, J.A., Chen, Y., Gucek, M., and Puertollano, R. (2012). MTORC1 functions as a transcriptional regulator of autophagy by preventing nuclear transport of TFEB. Autophagy 8, 903–914.
- [28] McAfee, Q., Zhang, Z., Samanta, A., Levi, S.M., Ma, X.-H., Piao, S., Lynch, J.P., Uehara,

- T., Sepulveda, A.R., Davis, L.E., et al. (2012). Autophagy inhibitor Lys05 has single-agent antitumor activity and reproduces the phenotype of a genetic autophagy deficiency. Proc. Natl. Acad. Sci. USA 109, 8253–8258.
- [29] Nakamura, M., Yao, M., Sano, F., Sakata, R., Tatenuma, T., Makiyama, K., Nakaigawa, N., and Kubota, Y. (2013). [A case of metastatic renal cell carcinoma associated with Birt-Hogg-Dubé syndrome treated with molecular-targeting agents]. Hinyokika Kiyo *59*, 503–506.
- [30] Napolitano, G., Di Malta, C., Esposito, A., de Araujo, M.E.G., Pece, S., Bertalot, G., Matarese, M., Benedetti, V., Zampelli, A., Stasyk, T., et al. (2020). A substrate-specific mTORC1 pathway underlies Birt-Hogg-Dubé syndrome. Nature *585*, 597–602.
- [31] Paquette, M., El-Houjeiri, L., C Zirden, L., Puustinen, P., Blanchette, P., Jeong, H., Dejgaard, K., Siegel, P.M., and Pause, A. (2021). AMPK-dependent phosphorylation is required for transcriptional activation of TFEB and TFE3. Autophagy 1–19.
- [32] Perera, R.M., and Bardeesy, N. (2015). Pancreatic cancer metabolism: breaking it down to build it back up. Cancer Discov. 5, 1247–1261.
- [33] Perera, R.M., Stoykova, S., Nicolay, B.N., Ross, K.N., Fitamant, J., Boukhali, M., Lengrand, J., Deshpande, V., Selig, M.K., Ferrone, C.R., et al. (2015). Transcriptional control of autophagy-lysosome function drives pancreatic cancer metabolism. Nature *524*, 361–365.
- [34] Petit, C.S., Roczniak-Ferguson, A., and Ferguson, S.M. (2013). Recruitment of folliculin to lysosomes supports the amino acid-dependent activation of Rag GTPases. J. Cell Biol. 202, 1107–1122.
- [35] Poffenberger, M.C., Metcalfe-Roach, A., Aguilar, E., Chen, J., Hsu, B.E., Wong, A.H., Johnson, R.M., Flynn, B., Samborska, B., Ma, E.H., et al. (2018). LKB1 deficiency in T cells promotes the development of gastrointestinal polyposis. Science *361*, 406–411.
- [36] Possik, E., Jalali, Z., Nouët, Y., Yan, M., Gingras, M.-C., Schmeisser, K., Panaite, L., Dupuy, F., Kharitidi, D., Chotard, L., et al. (2014). Folliculin regulates ampk-dependent autophagy and metabolic stress survival. PLoS Genet. *10*, e1004273.
- [37] Possik, E., Ajisebutu, A., Manteghi, S., Gingras, M.-C., Vijayaraghavan, T., Flamand, M., Coull, B., Schmeisser, K., Duchaine, T., van Steensel, M., et al. (2015). FLCN and AMPK confer resistance to hyperosmotic stress via remodeling of glycogen stores. PLoS Genet. 11, e1005520.
- [38] Rabinowitz, J.D., and White, E. (2010). Autophagy and metabolism. Science 330, 1344–1348.
- [39] Rangwala, R., Leone, R., Chang, Y.C., Fecher, L.A., Schuchter, L.M., Kramer, A., Tan, K.-S., Heitjan, D.F., Rodgers, G., Gallagher, M., et al. (2014). Phase I trial of hydroxychloroquine with dose-intense temozolomide in patients with advanced solid tumors and melanoma. Autophagy *10*, 1369–1379.
- [40] Rao, S., Tortola, L., Perlot, T., Wirnsberger, G., Novatchkova, M., Nitsch, R., Sykacek, P., Frank, L., Schramek, D., Komnenovic, V., et al. (2014). A dual role for autophagy in a murine model of lung cancer. Nat. Commun. *5*, 3056.
- [41] Rebecca, V.W., Nicastri, M.C., McLaughlin, N., Fennelly, C., McAfee, Q., Ronghe, A., Nofal, M., Lim, C.-Y., Witze, E., Chude, C.I., et al. (2017). A unified approach to targeting the lysosome's degradative and growth signaling roles. Cancer Discov. 7, 1266–1283.
- [42] Roczniak-Ferguson, A., Petit, C.S., Froehlich, F., Qian, S., Ky, J., Angarola, B., Walther, T.C., and Ferguson, S.M. (2012). The transcription factor TFEB links mTORC1 signaling to transcriptional control of lysosome homeostasis. Sci. Signal. 5, ra42.
- [43] Rodrik-Outmezguine, V.S., Okaniwa, M., Yao, Z., Novotny, C.J., McWhirter, C., Banaji, A., Won, H., Wong, W., Berger, M., de Stanchina, E., et al. (2016). Overcoming mTOR resistance

- mutations with a new-generation mTOR inhibitor. Nature 534, 272–276.
- [44] Santanam, U., Banach-Petrosky, W., Abate-Shen, C., Shen, M.M., White, E., and DiPaola, R.S. (2016). Atg7 cooperates with Pten loss to drive prostate cancer tumor growth. Genes Dev. *30*, 399–407.
- [45] Schmidt, L.S., and Linehan, W.M. (2018). FLCN: The causative gene for Birt-Hogg-Dubé syndrome. Gene *640*, 28–42.
- [46] Settembre, C., Zoncu, R., Medina, D.L., Vetrini, F., Erdin, S., Erdin, S., Huynh, T., Ferron, M., Karsenty, G., Vellard, M.C., et al. (2012). A lysosome-to-nucleus signalling mechanism senses and regulates the lysosome via mTOR and TFEB. EMBO J. 31, 1095–1108.
- [47] Steingrímsson, E., Tessarollo, L., Reid, S.W., Jenkins, N.A., and Copeland, N.G. (1998). The bHLH-Zip transcription factor Tfeb is essential for placental vascularization. Development *125*, 4607–4616.
- [48] Strohecker, A.M., Guo, J.Y., Karsli-Uzunbas, G., Price, S.M., Chen, G.J., Mathew, R., McMahon, M., and White, E. (2013). Autophagy sustains mitochondrial glutamine metabolism and growth of BrafV600E-driven lung tumors. Cancer Discov. *3*, 1272–1285.
- [49] Tsun, Z.-Y., Bar-Peled, L., Chantranupong, L., Zoncu, R., Wang, T., Kim, C., Spooner, E., and Sabatini, D.M. (2013). The folliculin tumor suppressor is a GAP for the RagC/D GTPases that signal amino acid levels to mTORC1. Mol. Cell *52*, 495–505.
- [50] Virchow, R. (1989). Cellular pathology. As based upon physiological and pathological histology. Lecture XVI--Atheromatous affection of arteries. 1858. Nutr. Rev. 47, 23–25.
- [51] Vocke, C.D., Yang, Y., Pavlovich, C.P., Schmidt, L.S., Nickerson, M.L., Torres-Cabala, C.A., Merino, M.J., Walther, M.M., Zbar, B., and Linehan, W.M. (2005). High frequency of somatic frameshift BHD gene mutations in Birt-Hogg-Dubé-associated renal tumors. J. Natl. Cancer Inst. 97, 931–935.
- [52] Vogl, D.T., Stadtmauer, E.A., Tan, K.-S., Heitjan, D.F., Davis, L.E., Pontiggia, L., Rangwala, R., Piao, S., Chang, Y.C., Scott, E.C., et al. (2014). Combined autophagy and proteasome inhibition: a phase 1 trial of hydroxychloroquine and bortezomib in patients with relapsed/refractory myeloma. Autophagy *10*, 1380–1390.
- [53] Wada, S., Neinast, M., Jang, C., Ibrahim, Y.H., Lee, G., Babu, A., Li, J., Hoshino, A., Rowe, G.C., Rhee, J., et al. (2016). The tumor suppressor FLCN mediates an alternate mTOR pathway to regulate browning of adipose tissue. Genes Dev. 30, 2551–2564.
- [54] Wei, H., Wei, S., Gan, B., Peng, X., Zou, W., and Guan, J.-L. (2011). Suppression of autophagy by FIP200 deletion inhibits mammary tumorigenesis. Genes Dev. 25, 1510–1527.
- [55] Westerman, A.M., and Wilson, J.H. (1999). Peutz-Jeghers syndrome: risks of a hereditary condition. Scand. J. Gastroenterol. Suppl. 230, 64–70.
- [56] White, E. (2015). The role for autophagy in cancer. J. Clin. Invest. 125, 42–46.
- [57] White, E., and DiPaola, R.S. (2009). The double-edged sword of autophagy modulation in cancer. Clin. Cancer Res. *15*, 5308–5316.
- [58] Wu, M., Si, S., Li, Y., Schoen, S., Xiao, G.-Q., Li, X., Teh, B.T., Wu, G., and Chen, J. (2015). Flcn-deficient renal cells are tumorigenic and sensitive to mTOR suppression. Oncotarget *6*, 32761–32773.
- [59] Xie, Z., and Klionsky, D.J. (2007). Autophagosome formation: core machinery and adaptations. Nat. Cell Biol. 9, 1102–1109.
- [60] Yan, M., Gingras, M.-C., Dunlop, E.A., Nouët, Y., Dupuy, F., Jalali, Z., Possik, E., Coull, B.J., Kharitidi, D., Dydensborg, A.B., et al. (2014). The tumor suppressor folliculin regulates AMPK-dependent metabolic transformation. J. Clin. Invest. *124*, 2640–2650.

- [61] Yan, M., Audet-Walsh, É., Manteghi, S., Dufour, C.R., Walker, B., Baba, M., St-Pierre, J., Giguère, V., and Pause, A. (2016). Chronic AMPK activation via loss of FLCN induces functional beige adipose tissue through PGC-1α/ERRα. Genes Dev. *30*, 1034–1046.
- [62] Zhou, Y., Tang, F., Wang, Y., Min, L., Luo, Y., Zhang, W., Shi, R., Duan, H., and Tu, C. (2017). Advanced alveolar soft part sarcoma responds to apatinib. Oncotarget 8, 50314–50322.